SOLVENT MEDIATED ELECTRON TRANSFER IN C-CLAMP SHAPED MOLECULES

by

Ian Anthony Read

BS, Chemistry, University of Pittsburgh, 1993

Submitted to the Graduate Faculty of

Graduate School of Arts and Sciences in partial fulfillment

of the requirements for the degree of
Doctor of Philosophy

University of Pittsburgh

2009

UNIVERSITY OF PITTSBURGH

COLLEGE OF ARTS AND SCIENCES

This thesis was presented

by

Ian Anthony Read

It was defended on

February 17, 2009

and approved by

David W. Pratt, Professor, Chemistry

Sunil Saxena, Associate Professor, Chemistry

Maria Kurnikova, Assistant Professor, Chemistry, Carnegie Mellon University

Thesis Advisor: David H. Waldeck, Professor, Chemistry

SOLVENT MEDIATED ELECTRON TRANSFER IN C-CLAMP SHAPED MOLECULES

Ian Anthony Read, PhD

University of Pittsburgh, 2009

The role of solvent in mediating the electronic coupling between an electron donor and acceptor is investigated. The temperature dependent electron transfer rate constants in two C-clamp shaped Donor-Bridge-Acceptor (DBA) molecules are used to evaluate the electronic coupling between the donor and acceptor sites. By varying the solvent, it is demonstrated that the donor-acceptor electronic couping is strongly dependent on both the electronic nature and the position of the intervening medium. An experimental strategy that utilizes the semiclassical treatment of electron transfer together with a molecular based solvation model is introduced and shown to be a reliable way of determining the magnitude of the electronic coupling. The results demonstrate a strong dependence of the electronic coupling on the relative energy between the donor excited state energy and the intervening structure's LUMO energy. An observation consistent with electron mediated 'superexchange.' In addition, the dependence of the electron transfer rate on solvent position is evaluated. These results are consistent with a temperature dependent electronic coupling mechanism.

Acknowledgements

I would like to thank several people that have made this work possible. First, I thank Professor David H. Waldeck for his constructive ideas, passion for science, and unyielding patience. Without his guidance, I would not be where I am in my professional life. Also, Dr. Andrew Napper deserves my gratitude for bringing me through some rough patches during this process. Dr. Napper has always been a good friend and an outstanding researcher. I also cannot forget, although I have never met, Professor Matthew B. Zimmt, Brown University. The majority of this work was reviewed by Prof. Zimmt. I have no doubt that without his keen eye for detail, the solvation calculations presented here would have taken much more time.

TABLE OF CONTENTS

LIST OF TABLES

LIST OF FIGURES

LIST OF CHARTS

LIST OF SCHEMES

Chapter 1 Introduction

1.1 Overview

Electron transfer (eT) processes have been the subject of numerous studies in chemistry, biology, and physics. The interaction between an electron donor (D) and electron acceptor (A) is a fundamental element in key natural processes. Most notably, plant physiology relies on photoinduced electron transfer to convert light energy into chemical energy. This energy is harnessed and used to drive vital physiological processes. There has also been a renewed interest in photovoltaics (i.e. solar power) - the process of using light energy to generate electricity. The development of materials capable of converting absorbed light into electrical energy is critical to fulfilling the energy requirements of the future. Given the significant impact electron transfer processes have on our everyday life, there is much interest in developing a detailed understanding of this fundamental process.

In proteins, electron transfer has been shown to occur over considerably long distances[1,2] and across different intervening structures. It is well known that electron transfer across protein sub-structures plays an important physiological role. For instance, α-helices exhibit faster electron transfer rate constants than β-sheets. In nature, a carefully designed combination of pathways will determine the kinetics and/or efficiency for a particular process. In chemistry and physics, long range eT has been observed to occur through several intervening structures (i.e. vacuum, covalent bonds, solvent). The primary focus of this thesis is the study of long range eT occurring 'through-solvent' using specifically designed 'model' systems. Using these systems, the

long range electron transfer event can be well characterized both experimentally and theoretically.

Over the past few decades, several model systems have been designed to study specific parameters influencing the electron transfer event (i.e. solvation, electronic structure). Among the first model systems used for this purpose are the donor-bridge-acceptor molecules designed by Paddon-Row and co-workers. These molecules consist of a substituted naphthalene donor subunit and a substituted ethylene acceptor covalently attached by a norbornyl bridge. The length of the bridge is systematically lengthened without introducing significant changes in geometry. Their results showed that the electron transfer rate depends exponentially on the D-A separation distance. Empirically, the eT rate constant can be written as,

$$k_{ET} \propto e^{-\beta d} \tag{1.1}$$

where d is the distance between the donor and acceptor, and β is an attenuation factor. Using these systems it was possible to reliably determine the attenuation factor and compare the results with modern eT rate theories. Several authors have measured the value of β for several different structures. Its value ranges from ~3$Å^{-1}$ in vacuum to <0.04 $Å^{-1}$ in highly conjugated bridge structures[3].

This thesis investigates solvent effects on the measured eT rate constants in two model systems. First, the highly curved Donor-Bridge-Acceptor (DBA) molecule A9DCE (Figure 1) that consists of a dimethoxyanthracene donor and a cyclobutene acceptor subunit connected by a covalent bridge. This molecule's geometry allows for one or more solvent molecules to occupy the space between the D-A pair, thus allowing for a systematic investigation and characterization of 'through-solvent' electron transfer. The

D-A subunits have been chosen such that direct electron transfer is 'symmetry forbidden[4] so that contributions from eT mediated through the covalent bridge are minimized.

In Chapters 2 and 3, the rate constants are measured in a homologous series of alkyl-substituted aromatic solvents. For these experiments, the ability of A9DCE to form a molecular complex with the aromatic solvent and its effect on the electron transfer rate is examined. The geometry of the molecular complex is controlled by increasing the size and number of alkyl substituents. The eT rate constant is measured as a function of solvent size and shows that a particular solute-solvent configuration can mediate electron transfer. These data are discussed within the framework of modern eT theory.

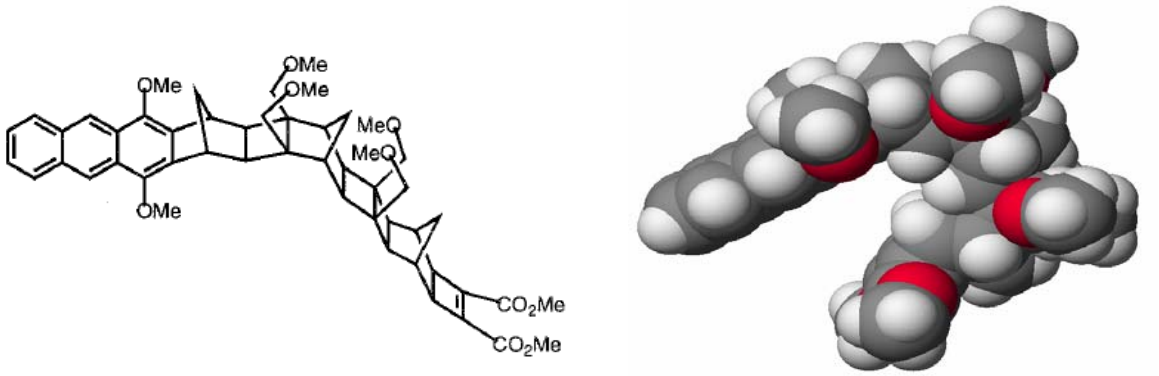

Figure 1.1 Model System A9DCE used in this thesis. The three dimensional rendering shows how the intramolecular cleft can accommodate one or more solvent molecules. Taken from Read, I.; Napper, A.; Kaplan, R.; Zimmt, M. B.; Waldeck, D. H.; *J. Am. Chem. Soc.;* 1999; 121(47); 10976-10986.

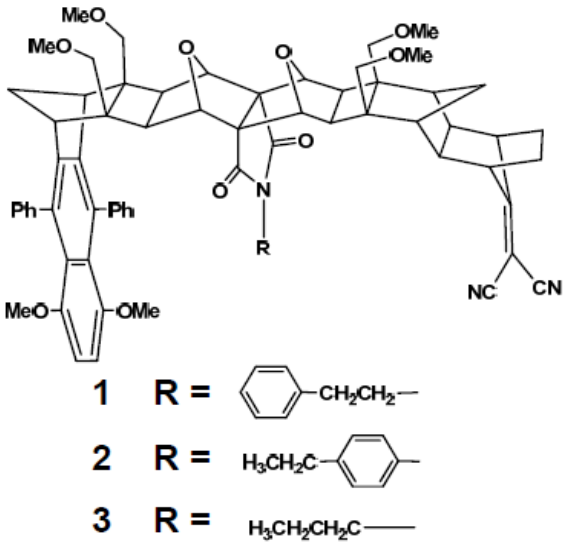

Figure 1.2 Model Systems used in this thesis. The pendant group (R) places a phenyl group in direct 'line-of-sight' 1 or slightly outside LOS 2 between the D-A pair. Molecule 3 is used as a control. Taken from Read, I.; Napper, A.; Zimmt, M. B.; Waldeck, D. H.; *J. Phys. Chem. A.;* 2000; 104(4 1); 93 85-9394.

Chapter 4 summarizes experiments using a DBA system (designed by Paddon-Row) to determine, unequivocally, the role played by nonbonded contacts that mediate the eT event. These molecules (Figure 2) have a similar structure to the 'C-clamp' molecules. However, the intervening 'solvent' molecule is covalently attached to the bridge by one or more methylene linkages. This allows for well defined placement of the intervening structure relative to the D-A pair and removes any ambiguity resulting from solvent association. The eT rate constants are evaluated as a function of solvent so that the electronic interaction between the D-A pair can be separated from solvation effects.

Chapter 5 summarizes results of temperature dependent experiments of A9DCE in solvents of varying electron affinity. The goal of this work is to understand how the reaction rate depends upon the orbital energetics of the intervening solvent molecule. A series of similarly sized aromatic solvents were chosen with EA values in the -1.1 - 0.25

eV range. These experiments show the enhancement of the eT rate with increasingly positive EA. Using Eq 1, this behavior is rationalized in terms of an increased electronic coupling between the D-A pair.

Chapter 6 uses A9DCE to evaluate the unusual temperature dependence of the experimental rate constants observed in bulky aromatic solvents. This behavior is most apparent in the aromatic solvent 1,3-diisopropylbenzene where the two isopropyl groups restrict the solvent's access to the molecular cleft. Several explanations are explored including the possibility of a temperature dependent electronic coupling. In general, the electronic coupling is assumed temperature independent, however, the conclusions drawn from this work favor the former explanation.

Chapter 7 demonstrates how the experimental strategy outlined in this work can be applied. An extenstion of the molecular systems studied in Chapter 4 were used to determine the electron transfer rate constants. The intervening structure is covalently linked to the bridge. Computational chemistry was used to determine which intramolecular geometry changes occur as a result of eT. This information is used to determine the internal reorganization energy. The accuracy of the results were corroborated using steady state charge transfer spectra. These results solidify the fundamental conclusion proposed in this work: solvent mediated electron transfer is most efficient in aromatic solvents. The orbital energetics of the intervening structure enhance the electronic coupling between the D-A pair.

1.2 Experimental Strategy

The experimental strategy is to first determine the electron transfer rate constants using time-resolved fluorescence. Chapter 2 describes the rate laws used to determine the forward and (when measurable) reverse eT rate constants. These data are then analyzed using modern electron transfer theory to extract values for the electronic coupling. Several parameters are necessary before |V| can be reliably determined. First, the reaction Gibbs energy must be known. For the systems used in this work, $\Delta_r G$ is determined directly from the measured rate constants in nonpolar solvents. In solvents where $\Delta_r G$ cannot be extracted from the rate data, a molecular based solvation model is used to calculate these values and their temperature dependence. In Chapter 3, we outline a strategy for these calculations which involves extrapolation of results from those measured in nonpolar solvents. The calibrated molecular based model is used to calculate the solvent reorganization energy, λ_o and its temperature dependence. The remaining parameters λ_i and ν have been determined previously[5] through evaluation of charge-transfer spectra. These analyses produce several best fit parameters producing similar quality fits. Therefore, theoretical calculations are used to determine the most physically relevant values. The details of this procedure are explained in the next sections.

1.3 Classical Theory of Electron Transfer

Marcus theory is widely accepted as a reliable desrcription of eT reactions in the classical limit. The reaction rate is defined in terms of a Gibbs energy of activation, ΔG^* as,

$$k = \rho(r) Z e^{-\frac{\Delta G^*}{RT}} \tag{1.2}$$

where Z represents the collisional frequency of the solute with the surrounding medium, ΔG^* is the activation energy, and $\rho(r)$ represents the electron transmission probability once an appropriate nuclear configuration is reached. In solution, this configuration is reached through the exchange of energy with the surrounding solvent. Traditionally, the Marcus free energy model is depicted as two intersecting parabolas (Figure 1.3).

The reaction coordinate is commonly defined as the free energy of the initial (left) and final states relative to the activation energy. The vertical distance between the curve minima defines the reaction free energy, $\Delta_r G$. The crossing point defines the activation barrier and is related to the reorganization energy through,

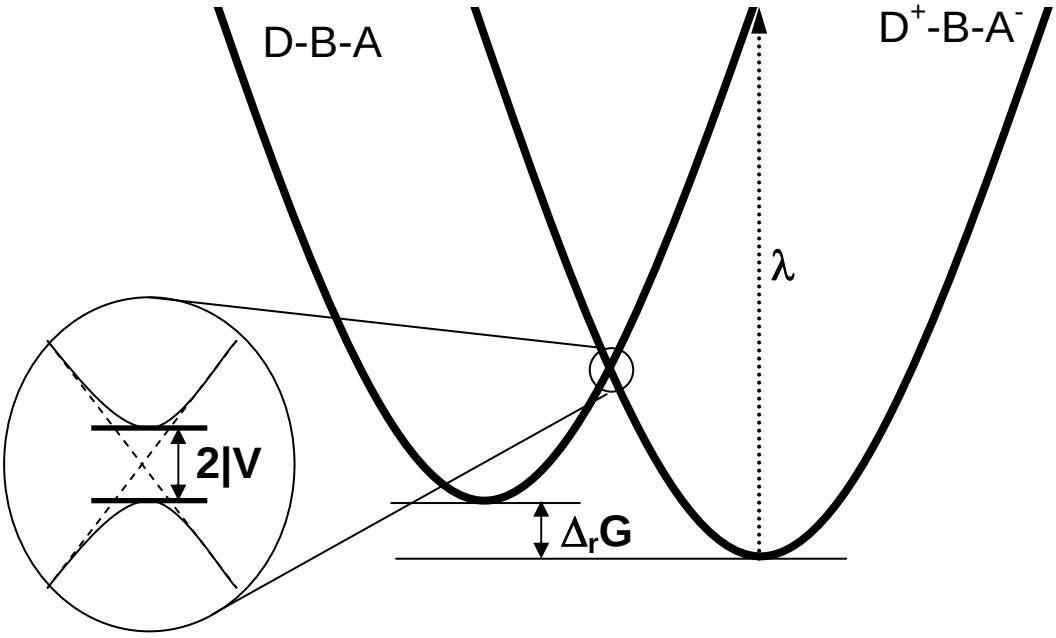

Figure 1.3 Free energy curves used to describe electron transfer. In the non-adiabatic limit, the magnitude of the avoided crossing (2 |V|) is small.

$$\Delta G^{*} = \left(\frac{\lambda + \Delta_r G}{4\lambda} \right)^2 \qquad (1.3)$$

where λ is the energy required to reorganize the reactants and the surrounding solvent molecules to the newly formed configuration of the products. In the classical (adiabatic) limit, the reaction rate is controlled by the probability of reaching the crossing point. *For nonadiabatic electron transfer, the interaction between the reactant electronic states is weak and a more sophisticated treatment is necessary (vide infra).* Using this definition, eq. 2 predicts that the reaction rate will increase as $\Delta_r G$ becomes more exoergic. However, according to Figure 1.4, in the limit when $\Delta_r G$ becomes exceedingly large, the reaction rate will decrease. This feature, termed the Marcus 'inverted region', has been demonstrated by several researchers[6].

Experimentally, Closs and Miller[7] studied the eT rate as a function of reaction driving force in substituted steroid molecules with an attached biphenyl donor. A series of acceptor subunits with varying electron affinities were used to modulate the reaction free energy. A snapshot of the eT rate data is shown in Figure 1.5 as a function of $\Delta_r G$. These data clearly show the 'turnover' in the rate constant at increasingly negative reaction free energy. In Chapter 6, we present results for A9DCE which exhibit similar behavior.

The reorganization energy λ includes both solute, λ_i, and solvent, λ_s contributions. Figure 1.3 shows that the total reorganization energy is equal to the vertical distance between the final state minimum and the initial state free energy surface less $\Delta_r G$. Qualitatively, the internal reorganization energy is the energy required

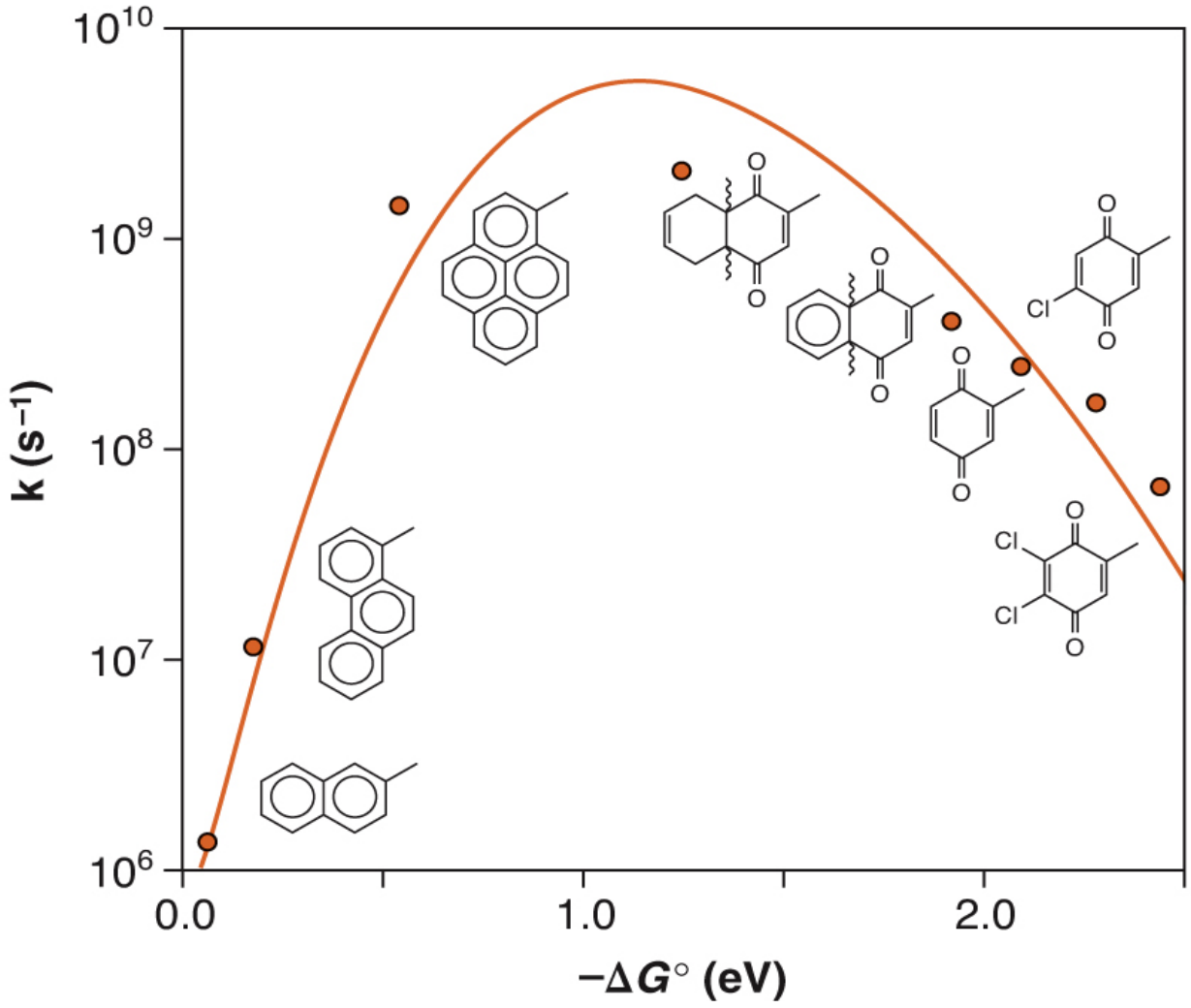

Figure 1.4 Experimental eT rate constants measured as a function of $\Delta_r G$. These data demonstrate the 'turnover' characteristic of the Marcus 'inverted region.'

for the reactant species to adopt the nuclear configuration of the product(s). Because the electronic transition occurs instantaneously relative to the nuclear motions, following eT, the solvent is no longer at equilibrium with the solute charge distribution. The outer sphere reorganization energy is the energy required for the solvent to reach equilibrium

with the newly formed charge separated species. This energy can be correlated to the dielectric properties of the solvent.

1.4 Quantum Mechanical Theory of Electron Transfer

Quantum mechanics treats the electron transfer event as the probability of an electron transition occurring between two electronic states. In the framework of the previous model, these states are defined by nuclear and electronic configurations of the reactant and product species at the crossing point. Similar to optically driven transitions, the transition can be effectively modeled using the 'Golden Rule' formulation[8]. The rate of the electron transfer is written as

$$k_{ET} = \frac{2\pi}{\hbar}|V|^2 FCWDS \qquad (1.4)$$

where FCWDS is the Franck-Condon weighted density of states, and |V| is the electronic coupling magnitude between the donor-acceptor pair. In accord with the Born-Oppenheimer approximation, the electronic (V) and nuclear (FCWDS) degrees of freedom are separated. This equation is useful in the nonadiabatic limit – the magnitude of the electronic coupling is small (Figure 1.3) compared to the reciprocal time spent in the transition state region.

A pure quantum mechanical treatment accounts for changes in electronic and nuclear configurations of both the solute and solvent molecules. For the supramolecular model systems employed in this work, a rigorous solution is not possible and approximations are necessary. Therefore, the semiclassical approximation is employed. In general, the approximation simplifies the problem by treating the solute vibrational modes quantum mechanically. The solvent is treated classically. Typically,

the problem is further simplified by reducing the solute degrees of freedom to a single vibrational mode. The appropriate mode frequency is chosen by calculating the most probable nuclear configurations involved in the electron transfer event. In this limit, the semiclassical rate equation becomes,

$$k_{ET} = \frac{2\pi|V|^2}{\hbar\sqrt{4\pi k_B T \lambda_0}} \sum_{n=0}^{\infty} e^{-S}\left(\frac{S^n}{n!}\right)\exp\left[\frac{-\left(\Delta_r G + \lambda_0 + nh\nu\right)}{4\lambda_0 k_B T}\right] \qquad (1.5)$$

Here the |V| is the electronic coupling magnitude, $\Delta_r G$ is the reaction free energy, λ_0 is the outer sphere reorganization energy, k_B is Boltzmann's constant and ν is the frequency of the vibrational mode active during the electron transfer event. S is the electron-phonon coupling which characterizes how the solute vibrations are coupled to the electron transition. It is the ratio of the inner sphere reorganization energy, λ_i, to the mode frequency. Typically, the summation converges rapidly and is rarely evaluated beyond the sixth term. Because the goal of this work is to extract values for the electronic coupling magnitude, |V|, in various solvents, it is necessary to adopt a reliable strategy for extracting the remaining parameters shown in equation 1.5. In the following sections, this strategy is described in detail.

1.5 Electronic Coupling

The electronic coupling is defined by the overlap between the reactant, product, and intermediate electronic states of the species involved in the electron transfer reaction. When D and A in the D-A pair are in close proximity, the overlap between the initial and final state wavefunctions controls |V|. In the case of long range electron

transfer, the direct orbital overlap is negligible because of their distance, yet significant electron transfer can be observed. The intervening structure must play a role in 'mediating' the electron transfer reaction. The first observation of such an effect was published by McConnell in 1960[9] where unusual EPR splitting patterns were observed in diphenylalkane systems. The patterns were explained as the interaction between the two species formed following redistribution of the 'injected' electron via intramolecular electron transfer. The mechanism of redistribution was explained as electron 'superexchange' - a process whereby the electronic orbitals of the intervening structure mix with those of the D-A pair to facilitate or 'mediate' electron transfer. Theoretically, superexchange is an extension of perturbation theory where new wavefunctions are

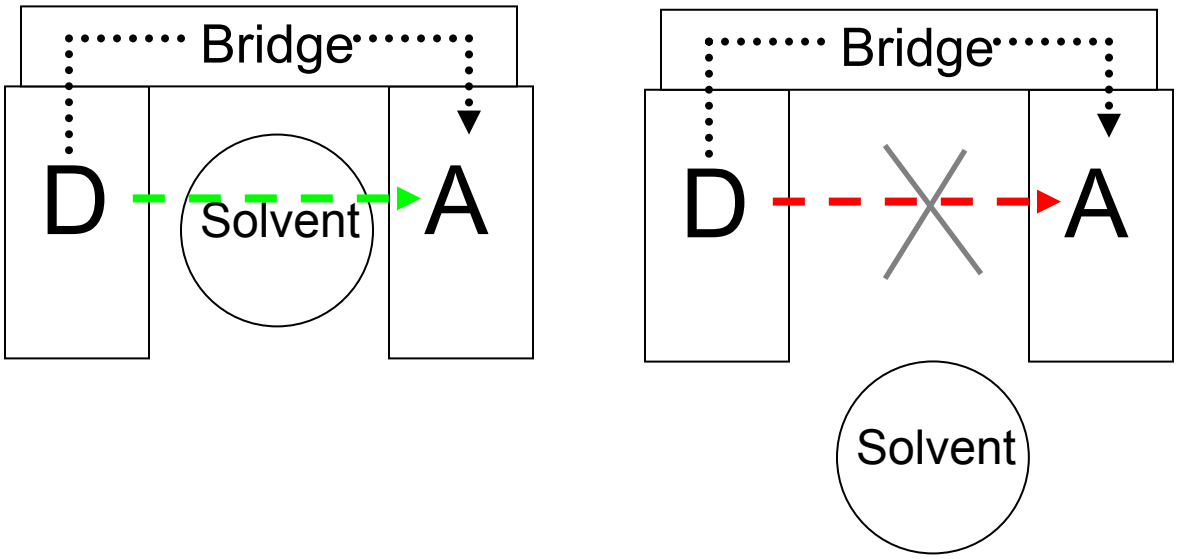

Figure 1.5 Schematic diagram showing possible eT pathways. For A9DCE, the 'through-space' mechanism (when no solvent lies between the D-A pair), and 'through-bridge' path have been effectively shut-off.

derived from the existing orbitals of the D-A pair and the intervening structure. The new wavefunctions create an intermediate electronic state through which the electron can travel. The process is shown schematically in figure 1.6 where the relevant eT paths between donor-acceptor subunits are shown. For A9DCE, the through-space pathway is unlikely since the D-A distance is large. eT through the covalent bridge is less likely due to the symmetry of the D-A orbitals. In both molecules, the 'through-solvent' path is the most likely mechanism.

Figure 1.6 depicts two possible superexchange mechanisms: hole-mediated and electron mediated. The hole-mediated process is one where the electron vacancy

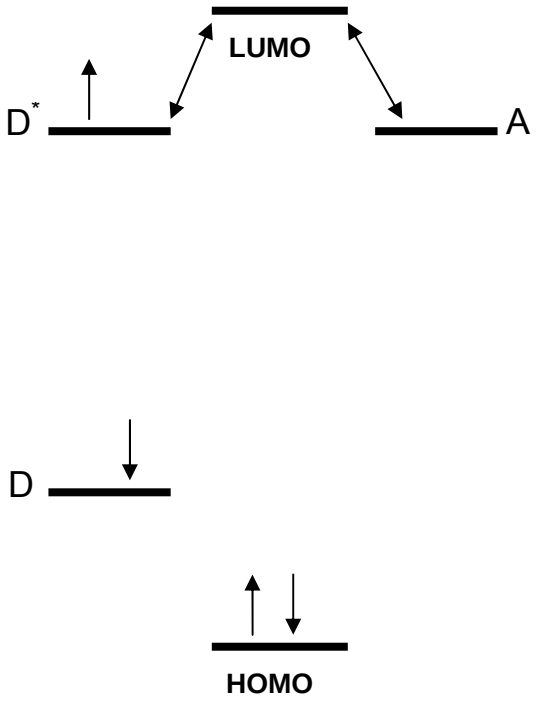

Figure 1.6 Energy level diagram describing photoinduced electron transfer occurring through superexchange. The frontier orbitals of the intervening structure interact with the D-A pair to facilitate the electron transfer.

migrates through the occupied orbitals of the bridge from the acceptor to the donor. Electron mediated process occurs when the electron migrates through the unoccupied orbitals. The interaction between the donor-acceptor pair and the 'solvent' is shown for the systems studied in this work. The 'bridging' unit is either the solvent molecule lying between the D-A pair or the pendant group. Mathematically, the electronic coupling is written as,

$$V = \frac{H_{D1}H_{1A}}{\varepsilon_t - \varepsilon_1} \tag{1.6}$$

where H_{D1} is the exchange energy between the donor-bridge, H_{1A} is the exchange energy between the bridge and the acceptor, ε_t is the electron tunneling energy and ε_1 is the energy of the bridge site. In chapter 7, the eT rate constant is studied as a function of solvent electron affinity. This solvent property effectively defines a value for ε_1.

1.6 Photoinduced Electron Transfer (PET)

The electron transfer processes are often facilitated through photon absorption to generate a higher energy excited singlet state. Because the electron is less tightly bound to the nuclear frame, it is more likely to transfer to an electron acceptor. There are several experimental advantages for using PET to study model systems. First, the reaction conditions are readily controlled. The reaction is initiated by photon absorption. For the experiments presented in this thesis, an ultrafast laser pulse of only a few picoseconds is used. Because this time scale is much faster than the electron transfer event, a straight-forward observation of the reaction is possible via fluorescence or transient absorption spectroscopies. Second, systems that undergo PET may give

measurable charge transfer absorption / emission spectra. In the present case, these spectra are used to determine λ_i and ν (vide infra).

Fluorescence lifetime data are measured using Time-Correlated Single Photon Counting (TCSPC). A complete description of the technique can be found elsewhere[10]. Briefly, the samples are prepared in an oxygen free environment. The optical density is kept at low levels to minimize contributions from intermolecular effects (i.e. energy transfer, exciplex formation, fluorescence quenching, etc.) The sample is excited with UV pulses of ~10 ps duration. Following absorption, the molecule emits a fluorescence photon that is detected using a fast PMT (microchannel plate, Hammamatsu). Repeated measurement (3 kHz) of the relative timing between the excitation (start) and emission (stop) photons provides a histogram of emission events from which the fluorescence lifetime can be extracted.

The time-resolved fluorescence measurements used in this work are a reliable way of measuring the electron transfer rate. These experiments monitor the transient concentration of the locally excited singlet state with picosecond time resolution. Throughout this work, the electron transfer rate data is extracted from the measured fluorescence lifetime using the kinetic scheme in Chapter 2. Here, the ground state absorbs a UV photon to form the locally excited state (LE). Following vibrational relaxation to the curve minimum, two processes can take place: relaxation to the ground state via fluorescence and formation of a charge separated state. *It is important to note that the curves shown in Figure 1.3 are free energy (not potential energy) surfaces. Therefore, the vibrational manifold corresponding to the semiclassical, single mode approximation is not shown. In addition, the electron transfer initial and final states are*

influenced by the surrounding medium. The energy difference between the curve minima represent the reaction free energy and not the orbital energetics of the electron transfer event. An interesting feature of the rate data observed for both systems studied is that in nonpolar solvents, the reaction free energy can be determined from the fluorescence lifetime data. This observation is explained as an excited state equilibrium between LE and CT states. Because the charge separated species is destabilized in nonpolar solvents, repopulation of the LE state occurs and manifests as nonexponential fluorescence decay law. As the solvent polarity increases, the CT state is stabilized which disfavors the reverse electron transfer process. Experimental measurement of $\Delta_r G$ and its temperature dependence provides a powerful way to interpret the results. In cases where experimental measurements are not possible, thermodynamic solvation models can be used. Chapter 2 and 3 outline these findings.

1.7 Charge Transfer Spectra

A widely used method for the analysis of experimental eT rate data is through charge transfer spectra. Using this approach, the steady-state absorption and/or emission data, I(ΔE) is fit to the following equation.

$$I(\Delta E) = \exp(-S)\sum_{n=0}^{\infty}\frac{S^n}{n!}\exp\left[-\frac{(\Delta_r G + \Delta E + nh\upsilon + \lambda_0)^2}{4\lambda_0 k_B T}\right] \qquad (1.7)$$

Similar to equation 1, the result contains the electronic coupling, reaction free energy, and reorganization energy. The parameters extracted from this procedure can be used to determine the electronic coupling. However, the fitting procedure typically does not lead to a unique solution. There is significant parameter coupling and many parameter combinations lead to similar quality fits. As a result, secondary methods must be used

to improve the reliability of the extracted results. For this work, the geometry changes associated with the eT event are determined by comparing the minimized geometries of the neutral and charge separated species. Careful analysis reveals the active vibrational mode which is used to determine λ_i.

This approach is used throughout this thesis to determine values for both λ_i and ν. However, for the systems studied, neither charge transfer absorption nor emission is observed. To determine these parameters, two model systems were designed that incorporate a shorter bridge were used. These molecules are shown in Figure 1.7.

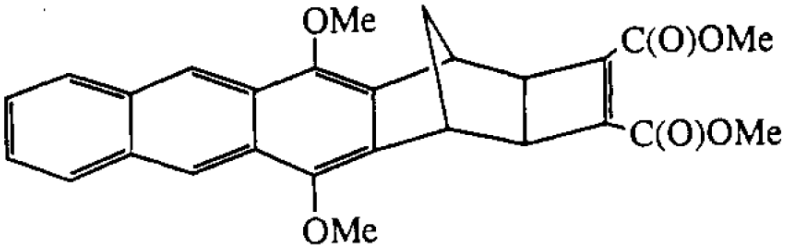

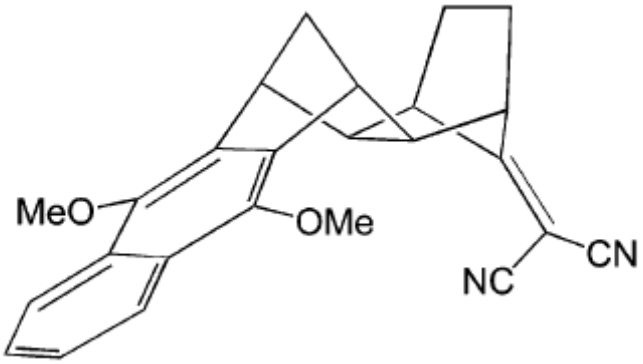

Figure 1.7 Model Systems used to determine λ_i and $h\nu$ from charge transfer spectra. The close proximity of the D-A pair favors enhanced emission from the charge separated state.

Enhancement of the CT emission is achieved by reducing the D-A separation. The reduced separation increases the electronic coupling and leads to the observed fluorescence. The resulting spectra are fit to equation 1.6. The remaining parameters necessary to extract |V| can be calculated using solvation theory. A brief description of the model's employed are presented in the next section.

1.8 Continuum Solvation Theory

The simplest approach to calculating solvation energies is continuum theory. The approach treats the solute as a point dipole immersed in a dielectric medium. Only long range interactions are considered in the calculation. Local solvent structure is neglected. Molecular mechanics calculations are used to determine the molecular size

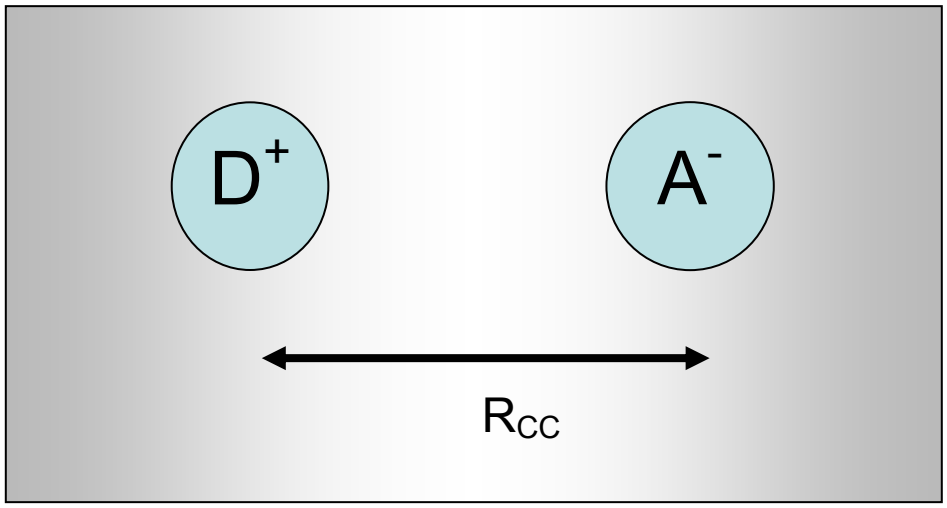

Figure 1.8 Schematic representation of continuum solvation theory. The reactant species are modeled as spheres separated by distance R_{CC}. The continuum properties are determined by the solvent bulk properties: the high, ε_∞, and low ε_S frequency dielectric constant.

and magnitude for the dipole moment and bulk solvent properties are used to determine the solvation energy. The model uses the following physical picture. Here, each species is depicted as a sphere of radius, r_i. The distance between the reactants, R_{CC}, is important since its value determines the magnitude of the dipole moment created by the charge transfer process. It is the interaction of this dipole moment with the surrounding medium that determines both $\Delta_r G$ and λ_0. Continuum models give the solvent response as a function of the bulk properties of the medium: dielectric constant and refractive index. Rehm and Weller formulated the following expression for a solvent separated ion pair,

$$\Delta_r G = -E_{00} + E_{OX} - E_{RED} + \frac{e^2}{2}\left(\frac{1}{r_A} + \frac{1}{r_D} - \frac{2}{R_{CC}}\right)\left(\frac{1}{\varepsilon(T)} - \frac{1}{\varepsilon_{REF}}\right) - \frac{e^2}{\varepsilon_{REF} R_{CC}} \qquad (1.8)$$

Here, E_{00} represents the optical transition energy, E_{OX} is the oxidation potential of the donor, E_{RED} is the reduction potential for the acceptor. $\varepsilon(T)$ is the static dielectric constant, and ε_∞ is the high-frequency dielectric constant. This equation has been successfully utilized to calculate free energies in polar solvents. A similar calculation has been employed for the outer sphere reorganization energy. λ_0 can be calculated as,

$$\lambda_0 = \frac{e^2}{2}\left(\frac{1}{r_A} + \frac{1}{r_D} - \frac{2}{R_{CC}}\right)\left(\frac{1}{\varepsilon(T)} - \frac{1}{\varepsilon_{REF}}\right) \qquad (1.9)$$

Continuum theory provides a useful means of calculating both $\Delta_r G$ and λ_0 in polar solvents. However, there are several limitations of the theory. First, its application requires correction factors in nonpolar solvents. These corrections are mainly due to

the relatively low and equal magnitudes of ε_s and ε_∞. Therefore, the calculated results for $\Delta_r G$ and λ_0 are unrealistically low since most nonpolar solvents are capable of significant solvation energies. There is also little variation in the calculated values as a function of solvent. In nonpolar solvents, experimental eT rate constants can be very sensitive to solvent properties. In particular, contributions from higher electrical moments can become significant. Another deficiency of the continuum models is their inability to predict correct values for the temperature dependence of λ_0 in polar solvents. Throughout this thesis, a molecular solvation model is employed to determine values for $\Delta_r G$ and λ_0. Its application to solvents across a wide range of polarity is evaluated and the results are compared to experimental results. In chapter 3, a careful analysis of these results is presented.

1.9 Molecular Solvation Model

A simple molecular approach to solvation treats the solvent molecules as dipolar hard spheres. In this case, the interaction between the solute and solvent is more realistic since the interaction potential gives rise to solvent structure. This structure develops from short range interactions with adjacent spheres. Each sphere realigns its dipole moment to maximize the stabilization energy. In contrast with continuum theory, the solvent experiences interactions that take place on a molecular scale. These interactions are not limited to adjacent spheres. Large dipole moments can influence the solvent structure on length scales many times the solvent diameter. The solvent structure is typically represented in statistical mechanics as g(r), the solute-solvent pair distribution function. Its functional form is shown in figure 1.10. As seen in the figure,

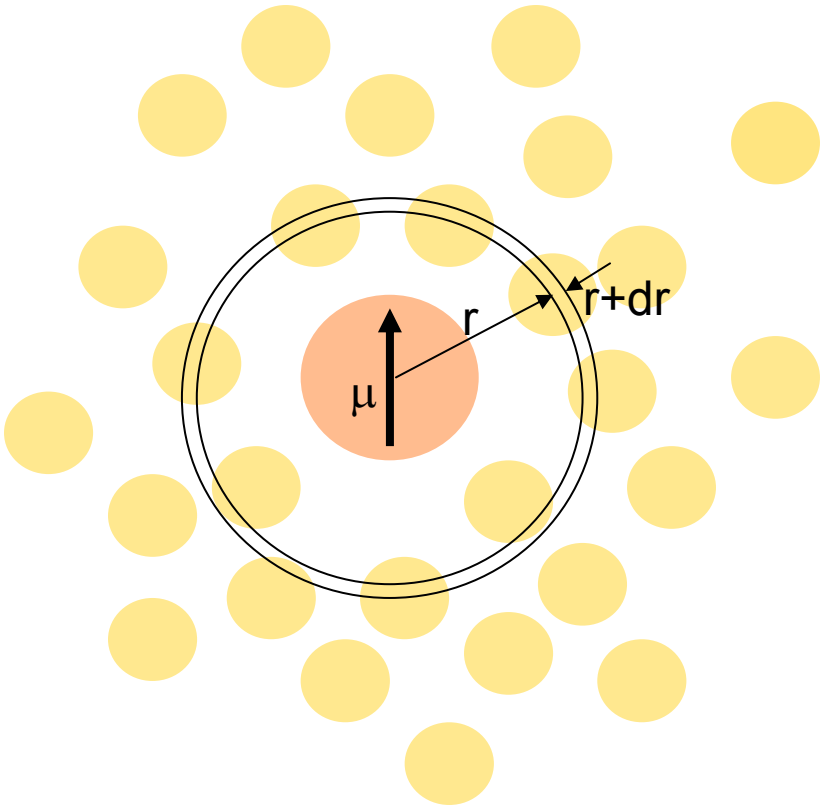

Figure 1.9 Schematic representation of the radial distribution function, g(r) which gives the probability of finding a particle at a distance, r, from a reference particle.

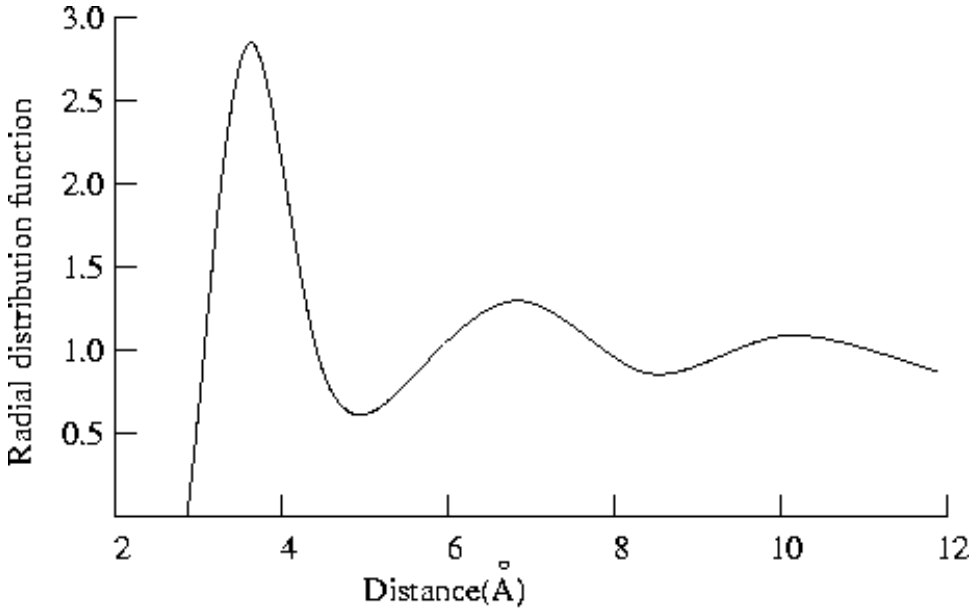

Figure 1.10 Plot of radial distribution function. Each peak represents the 1,2,nth solvation shell.

the maxima of g(r) represent the solvent structure. The curve represents the probability of finding a sovent molecule a distance, r from an arbitrary reference particle. The stabilizing interactions between adjacent particles lead to solvent structure. Figure 1.9 a graphical representation showing the 1,2,3,…,n^{th} solvation shell. The shape of g(r) is dictated by the solvent molecular size and the magnitude of the intermolecular interactions. Solvent polarizability, density, and polarity each play a significant role in determining the behavior of g(r). Because local interactions are explicitly accounted for, this solvation model provides a more realistic description of the molecular environment and will predict more accurate results.

In reality, solvent molecules are not hard spheres. In fact, a molecule has a more detailed shape and this shape can be influenced by the magnitude of the forces the solvent experiences (i.e. polarizability). A more realistic description of solvation should include shape, polarizability, and higher-order electrical moments. All of these properties have an influence on the interaction with the solute as well as on adjacent solvent molecules. Unfortunately, a rigorous treatment of solvation that includes all of these features is complicated. Matyushov[11] developed a molecular based theory that accounts for several of the key parameters. The model uses dipolar, polarizable hard spheres to describe the solvent. Each solvent molecule has a dipole moment and polarizability, as well as the bulk properties that influence how the solvent system will behave (i.e. density, size, dielectric constant, etc.) The solute-solvent, solvent-solvent, solute-solvent-solvent distribution functions are determined by molecular dynamics simulations of entire system. Their functional form is then determined using Pade

approximants. The solution to the interaction integrals are written as polynomial expressions.

Using this method, Matyushov derives an expression for $\Delta_r G$ as,

$$\Delta_r G = \Delta G_{\text{vacuum}} + \Delta G_{\text{dipole}} + \Delta G_{\text{dispersion}} \tag{1.10}$$

where $\Delta_{vac}G$ is the free energy of the reaction in vacuum, $\Delta_{dipole}G$ describes contributions from the solute-solvent dipole moments including their polarizability, $\Delta_{dispersion}G$ arises from dispersion interactions. Similarly, λ_0 is calculated as the sum of three contributions,

$$\lambda_o = \lambda_{\text{dipole}} + \lambda_{\text{dispersion}} + \lambda_{\text{induction}} \tag{1.11}$$

where λ_{dipole} is the dipolar contribution to the reorganization energy, $\lambda_{dispersion}$ is the dispersion contribution, and $\lambda_{induction}$ is the induction contribution.

Inclusion of higher order electrical moments can be important in aromatic solvents mainly because these solvents possess virtually no permanent dipole moment. Matyushov[12] has shown that interactions of the solvent quadrupole moment are greater than dipole interactions. Therefore, in solvents where little or no dipole moment exists, the quadrupolar contribution should be the dominant contributor to the overall free energy. When higher order interactions are accounted for the free energy expression becomes,

$$\Delta_r G = \Delta_{vac} G + \Delta_{dq,i} G^{(1)} + \Delta_{disp} G + \Delta_i G^{(2)} \tag{1.12}$$

where $\Delta_{dq,i}G^{(1)}$ is the dipolar-quadrupolar contribution and second-order induction interactions are given by the $\Delta_{dq,i}G^{(2)}$ term . A similar expression is written for the solvent reorganization energy. This model and its limitations are evaluated in detail in chapters 2 and 3.

In the following chapters, a reliable strategy for determining the electronic coupling is summarized. The results of this analysis provide convincing evidence of solvent mediated electron transfer. For the DBA systems studied, the results show significant enhancement of the electron transfer rate when an aromatic ring is positioned in direct line-of-sight between the donor acceptor subunits. The electron transfer rate can be correlated to the electron affinity of the intervening structure. This observation is consistent with a electron mediated 'superexchange' mechanism. In summary, the following work provides a solid foundation upon which future experiments can be designed. Evidenced in Chapters 6 and 7 are the possible directions this work can take. The possibility of a temperature dependent electronic coupling is explored in Chapter 6. Overall, these results present a careful and convincing example of how electron transfer model systems can be used to develop and explore the strengths and weaknesses of modern electron rate theories

1.10 References

1. Beratan, D. N.; Betts, J. N.; Onuchic, J. N. *Science* 1991, 252, 1285.

2. Onuchic, J. N.; Beratan, D. N.; Winkler, J. R.; Gray, H. B. *Annu. Rev. Biophys. Biomol. Struct*. 1992, 21, 349.

3. Davis, W.B.; Ratner, M.A.; Wasielewski, M.R. *J. Am. Chem. Soc.*, 2001, 123 (32), 7877.

4. Zeng, Y., Zimmt, M.B.; *J. Am. Chem. Soc.*, 1991, 113 (13), 5107–5109.

5. Zeng, Y., Zimmt, M.B.; *J. Phys. Chem., 1992*, 96 (21), 8395.

6. Gould, I.R.; Moody, R.; Farid, S.; *J. Am. Chem. Soc*. 1988, 110,1242

7. Closs, G.L.; Miller, J.R. *Science* 1988, 240, 440.

8. Dirac, P.A.M. *Proc. Roy. Soc.* 1972, 114 (767):243.

9. McConnell, H. M. *J. Chem. Phys*. 1961, 35, 508.

10. O'Connor, D.V.; Phillips, D. Time *Correlated Single Photon Counting*; Academic press: New York, 1984.

11. Matyushov, D.V.; Schmid, R.; *J. Chem. Phys.* 1996, 105, 4729.

12. Matyushov, D. V.; Voth, G. A.; *J. Chem.. Phys*. 1999, 111, 3630.

Chapter 2 Solvent-Mediated Electronic Coupling: The Role of Solvent Placement

The role of solvent location in mediating electronic coupling between electron donor and acceptor groups is investigated. The temperature-dependent electron-transfer rate constant in a C-clamp shaped donor-bridge-acceptor (DBA) molecule with a 7-Å donor-to-acceptor separation is used to evaluate the solvent reorganization energy and the electronic interaction between the donor and acceptor sites. By studying the reaction in an homologous series of alkylbenzene solvents, it is demonstrated that the donor-acceptor electronic interaction is greatly reduced in solvents that are too bulky for their aromatic ring to position itself between the donor and acceptor groups. The temperature dependence of the reaction free energy for charge separation, $\Delta_r G$, is directly determined from the experimental data. This allows parametrization of a molecular-based solvation model and provides a means to estimate the outer-sphere reorganization energy and its temperature dependence in aromatic solvents.[1]

2.1 Introduction

Electronic coupling between donor and acceptor sites is a prerequisite for electron- transfer reactions. Covalent bond "mediation" of this coupling is very important for intramolecular electron-transfer reactions, although alternate coupling pathways have been proposed. For example, hydrogen bonds and van der Waals contacts are believed to be important in mediating the electronic coupling for

[1] This chapter was previously published as: Read, I.; Napper, A.; Kaplan, R.; Zimmt, M. B.; Waldeck, D. H.; *J. Am. Chem. Soc.;* **1999**; 121(47); 10976-10986.

electron-transfer reactions in biomolecules.[1] Recent studies[2,3,4] have exploited the dependence of bond-mediated coupling magnitudes on the topology of donor-bridge-acceptor (D-B-A) molecules to quantify the relative importance of coupling pathways involving solvent molecules. Although the latter pathways are usually less important than bond-mediated coupling pathways for electron transfer across linear spacers, pathways involving solvents are expected to be important in intermolecular electron-transfer reactions and for intramolecular electron-transfer reactions involving highly curved spacers.

By studying the kinetics of electron transfer across highly curved donor-bridge-acceptor molecules in strongly polar solvents, it has been possible to demonstrate the participation of solvent in mediating the D-A electronic interaction, a phenomenon referred to as "solvent- mediated superexchange".[2,3] Detailed analyses of the temperature dependence of the electron- transfer rate constants were used to extract the electronic coupling matrix element, $|V|$, as a function of spacer topology and solvent. These analyses demonstrated a significant enhancement of D-A coupling for the "C-clamp" system **2** in the aromatic solvent benzonitrile, whereas no solvent dependence was found for the "linear" D-B-A molecule **1** (Chart 2.1). Additional evidence for solvent-mediated superexchange in electron transfer across U-shaped intramolecular systems was found by Paddon-Row and co-workers.[4] Solvent-mediated superexchange coupling in intermolecular electron-transfer reactions has also been identified in fluid solutions by Gould and Farid[5] and in frozen glasses by Miller.[6]

A deficiency in the earlier studies of **2** is the absence of experimental information that identifies the spatial placement of the solvent molecules most effective at mediating the electronic coupling. Prior theoretical studies indicated that the solvent molecule must lie within the cleft of **2** to produce significant coupling.[7] Unfortunately, experimental efforts to prove the presence and importance of solvent within the cleft were not successful. As an alternative, this study compares the electronic coupling in solvents that can position an

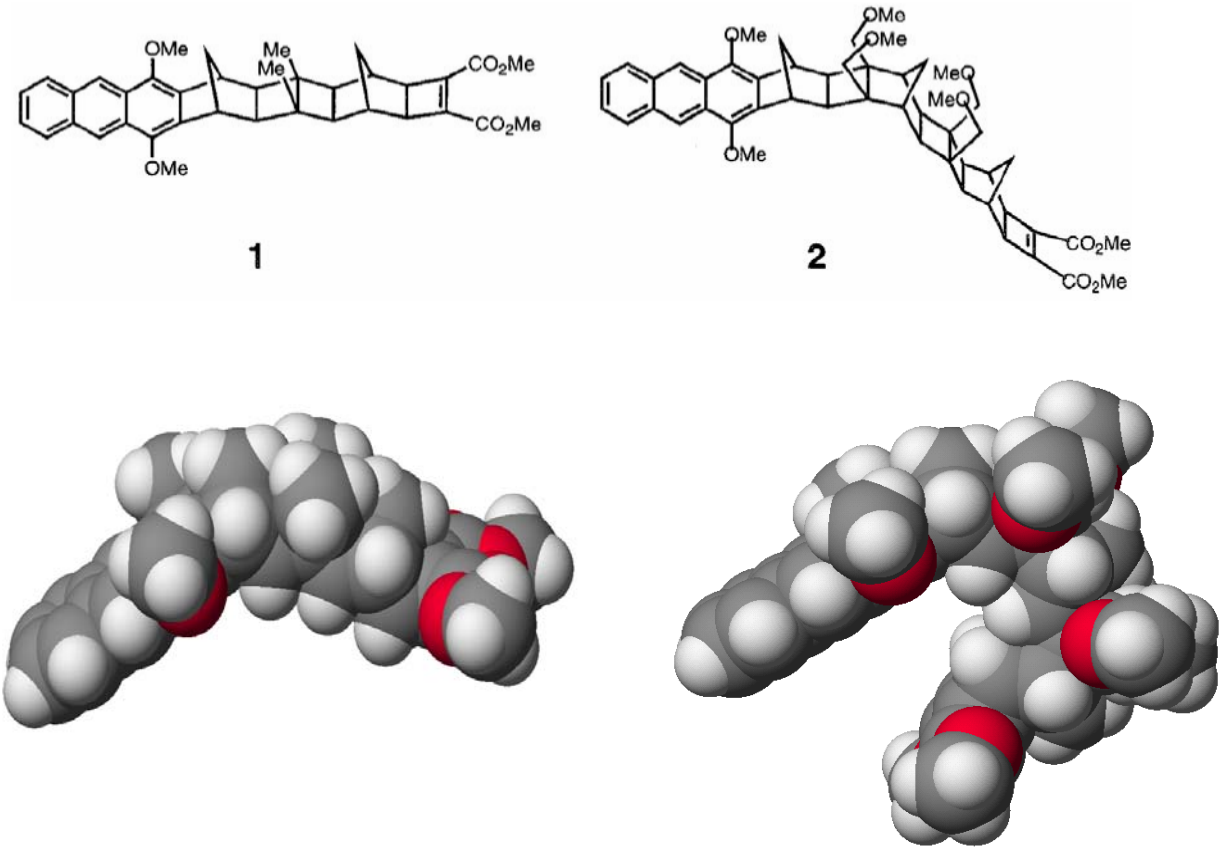

Chart 2.1 Chemical Structures of Donor-Bridge-Acceptor Molecules. A7DCE (1) and A9DCE (2), are shown with their CPK Renderings

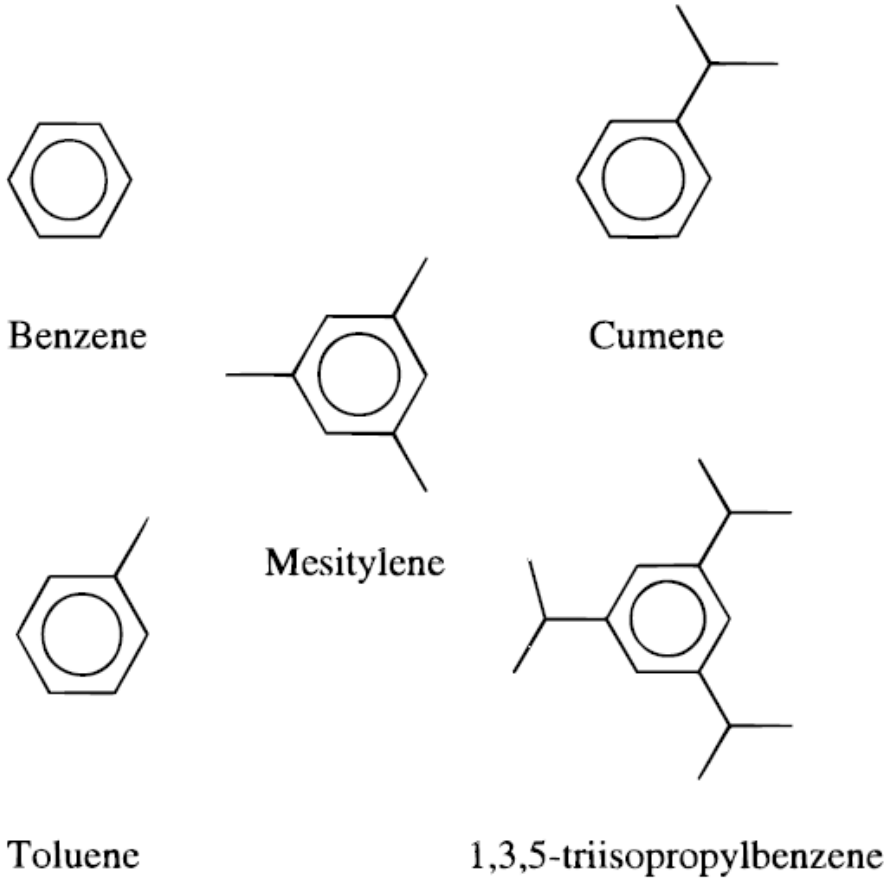

Chart 2.2 Chemical Structures of the Solvents Used in This Work

aromatic ring within the cleft interior with those that cannot. To this end, electron-transfer rate constants have been determined for **2** in a series of increasingly bulky alkylbenzene solvents (Chart 2.2). Consideration of van der Waals radii and molecular mechanics calculations indicate that benzene and the monoalkylated benzenes can access geometries in which their aromatic core achieves overlap with both the donor and acceptor π-functions of **2**. The steric bulk provided by the isopropyl groups prohibits such simultaneous overlap for 1,3,5-triisopropylbenzene (TIP). The lowest energy conformation of the isopropyl group projects a methyl group above and below the ring plane. The thickness of the molecule is increased in the vicinity of the isopropyl

group and this affects the placement of the solvent's aromatic core within the cleft of **2**. Chart 2.3 displays the results of molecular mechanics energy minimizations for **2** with cumene (A) or TIP (B and C). The heavy line connects the 9-position of the anthracene with the acceptor alkene carbon. When the isopropyl group of cumene

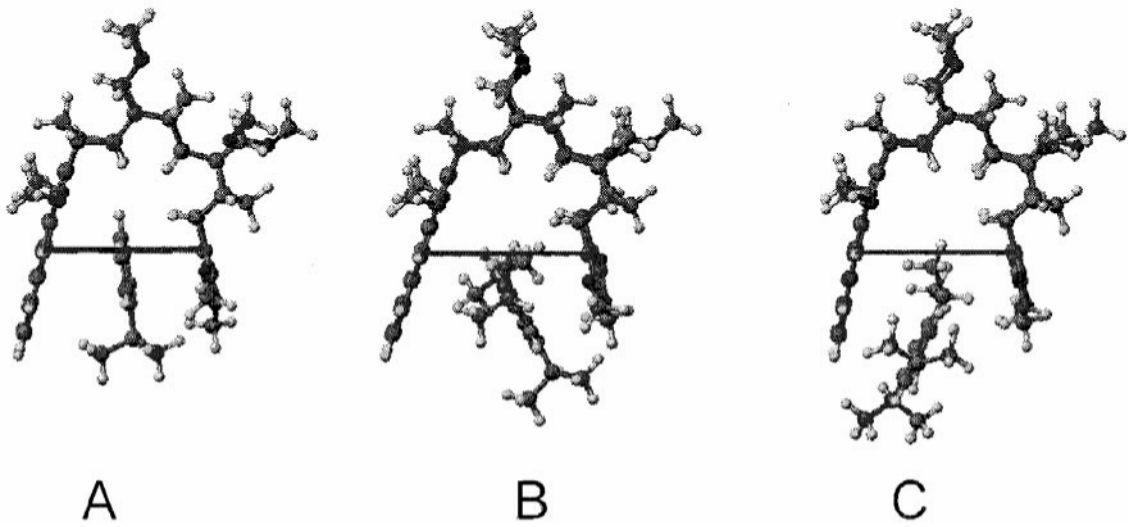

Chart 2.3 Results of Molecular Mechanics Energy Minimizations for 2 with Cumene (A) or TIP (B, C). Compound 2 and TIP are displayed as ball and stick renderings. The heavy line connects the anthracene 9 position and the acceptor alkene C.

projects down (Chart 2.3A), the aromatic ring is simultaneously in close proximity to both the anthracene and the alkene acceptor. With TIP, either one isopropyl group (C) or two isopropyl groups (B) must project into the cleft. Although the cleft appears to widen slightly to accommodate this solvent, its aromatic core is significantly further down in the cleft (Chart 2.3B,C) and farther from either the D or A group. If solvent-mediated coupling in **2** requires the solvent's aromatic core to be simultaneously proximate to both the D and A group, the experimentally determined coupling magnitude should decrease with increasing steric bulk of the solvent molecules. This effect has been experimentally observed.

Although the fluorescence decays from **2** in polar solvents[2,3] exhibited single exponential kinetics, the kinetics observed in these weakly polar aromatic solvents are not single exponential. Instead, they are well fit using biexponential rate expressions. This feature allows determination of both the forward $k_{for}(T)$ and reverse $k_{for}(T)$ electron- transfer rates and, consequently, the free energy of the charge separation reaction, $\Delta_r G(T)$. Direct knowledge of $\Delta_r G(T)$ restricts the number of adjustable parameters in the semiclassical model (eq 2.6) and allows robust conclusions to be drawn concerning the solvent dependence of the electronic coupling. In addition, the experimental $\Delta_r G(T)$ data is used to calibrate a molecular-based model for the solvation energy and the reorganization energy λ_0 in weakly polar and nonpolar solvents.[8] This sophisticated treatment of the outer-sphere reorganization energy produces values that are in reasonable agreement with those extracted from the rate constant data, $k_{ET}(T)$, assuming temperature independent values of λ_0 and the electronic coupling $|V|$.

The paper is organized as follows. Experimental and computational details as well as a general summary of the observations are provided in section 2.2. In section 2.3, the need for temperature-dependent outer-sphere reorganization energy and electronic coupling parameters is evaluated through analysis of the $k_{ET}(T)$ data with the semiclassical model (eq 2.6) and the experimentally determined $\Delta_r G(T)$. Section 2.4 describes the parametrization of a molecular solvation model using the $\Delta_r G(T)$ data. In section 2.5, the parametrized model is then used to predict the temperature dependence of the outer-sphere reorganization energy and to estimate the electronic coupling. The final section summarizes the findings and draws conclusions.

2.2 Experimental Section

2.2.1 Materials and Equipment

The preparation of compounds **1** and **2** has been reported elsewhere.[9] The compounds were stored in a refrigerated desiccator. The optical density of the samples was ~0.05 at the excitation wavelength. All solvents were purified in the following manner. First, the solvent was thoroughly washed with concentrated H_2SO_4 until the acid layer remained colorless upon vigorous shaking. Next, the solvent was washed several times with deionized water and dried over MgSO4. Finally, the solvent was fractionally distilled over sodium. In each case, the solvent was freshly distilled for sample preparation. The samples were then freeze-thaw-degassed three times to prevent oxygen quenching of the long lifetime component of the decay law. At higher temperatures, a positive argon (Matheson Inc., 99.99%) pressure was applied to the sample to prevent evaporation of the solvent from the heated section.

The time-correlated single photon counting method was used to measure the fluorescence intensity decays from the locally excited state of the anthracene. The sample was excited by 375-nm radiation from a frequency-doubled 750-nm dye laser pulse. The dye laser pulse train had a repetition rate of ~ 300 kHz and was generated by a cavity-dumped and synchronously pumped Coherent CR-599 dye laser. The pulse energies were kept below 1 nJ, and the count rates were kept below 4 kHz. All fluorescence measurements were made at the magic angle. Other particulars of the apparatus have been reported elsewhere.[10] The temperature cell was constructed from aluminum and controlled using a NESLAB RTE-110 chiller. Temperature

measurements were taken at the sample using a Type-K thermocouple (Fisher-Scientific) accurate to within 0.5 °C.

The fluorescence decays were fit to a sum of two exponential terms using the Marquardt-Levenberg nonlinear least squares algorithm. In each case the decay law was convolved with the instrument response function, measured by scattering from a BaSO4 colloid, and compared to the observed decay. Fitting to the semiclassical rate equation and the molecular based model calculations of the reorganization energies and reaction free energies were performed using Microsoft Excel 7.0. The FCWDS sum in eq 2.6 converges rapidly and was not evaluated beyond the sixth term.

2.2.2 Kinetic and Thermodynamic Analyses

In prior studies involving polar solvents,[2,3] the time evolution of the anthracene's lowest excited state (LE) fluorescence was adequately described by a single-exponential decay law. This indicated irreversible electron transfer to the acceptor; i.e., generation of the charge transfer state (CT). By contrast, in nonpolar solvents, the decay of the LE state is found to exhibit a double exponential decay law.[11] Figure 1 shows a fluorescence decay for **2** in mesitylene at 50°C. The best fit parameters are τ_1=0.909 ns (51.7%) and τ_2=19.3 ns (48.3%). The anthracene fluorescence data in the alkylated aromatic solvents was analyzed assuming interconversion of the lowest energy singlet excited states, LE and CT (Figure 2).

Table 2.1 displays lifetime parameters determined at selected temperatures in the alkylated benzene solvents. For the aromatic solvents other than TIP, increasing the number or size of the alkyl groups on the benzene core, or increasing the sample temperature, generates an increase in the value of the fast component lifetime and a

decrease in the fast component amplitude, A_1. Qualitatively, this suggests that the charge separation rate constant decreases with increasing temperature or with increasing alkyl substitution of the benzene ring. To quantify these variations, the solvent and temperature dependence of the decay parameters were interpreted using the kinetic scheme illustrated in Figure 2.2, where k_{for} is the forward (charge separation) electron-transfer rate constant (LE → CT), k_{back} is the reverse electron-

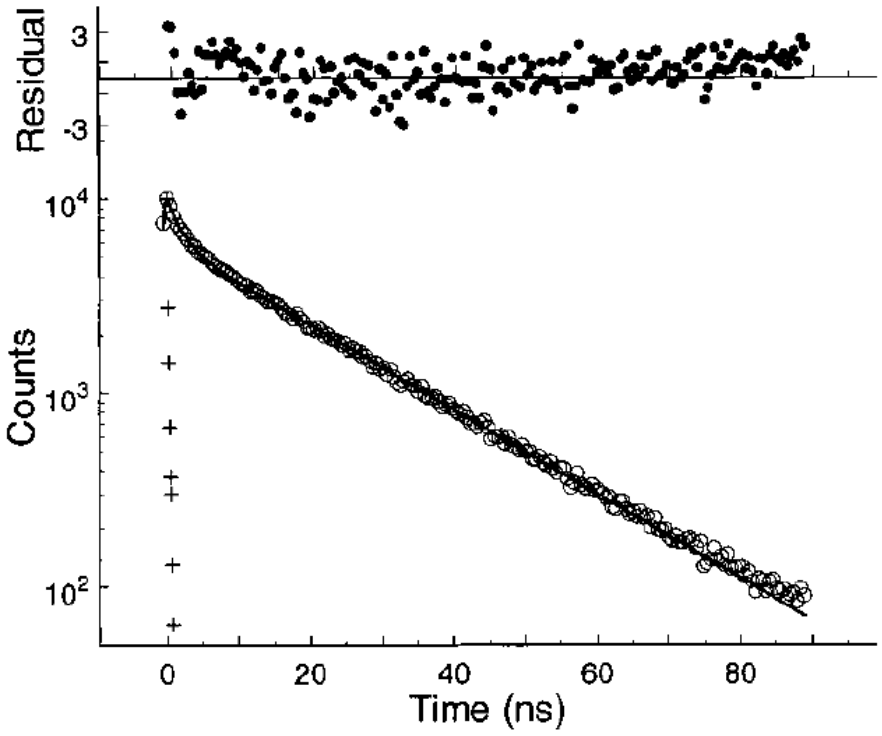

Figure 2.1 A fluorescence decay profile (circles) is shown for A9DCE in mesitylene at 50°C. The instrument function (+) is also shown. The best fit to a double exponential (line) gives τ_1 = 0.909 ns (51.7%); τ_2 = 19.3 ps (48.3%); and a χ^2 = 1.5. The residuals for the fit are also shown.

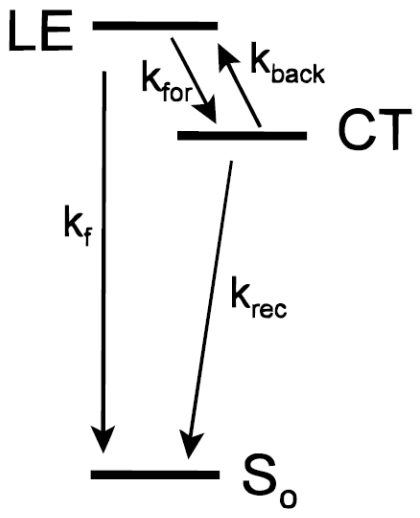

Figure 2.2 This diagram shows the kinetic scheme used to interpret the fluorescence intensity decay from 2 in the alkylated benzene solvents.

Table 2.1 Kinetic Parameters for 2 in Different Solvents as a Function of Solvent Polarity[a]

solvent	τ_1, ps (A_1)	T, K	V, Å^3	ϵ_S	n^2
benzene	325 (99%)	296	148	2.27	2.25
benzene	409 (90%)	342	148	2.19	2.18
toluene	371 (97%)	296	176	2.38	2.24
toluene	463 (69%)	347	176	2.26	2.15
cumene	586 (90%)	296	232	2.38	2.22
cumene	746 (47%)	345	232	2.28	2.13
mesitylene	678 (82%)	296	231	2.27	2.25
mesitylene	909 (52%)	323	231	2.27	2.25
TIP	3260 (68%)	260	397	2.29[c]	2.26[d]
TIP[b]	1720 (51%)	283	397	2.27[c]	2.23

[a] The long component time constant is 15−25 ns in each case. [b] TIP is 1,3,5-triisopropylbenzene. [c] The static dielectric constant for triisopropylbenzene could not be found in the literature. The value given here is that of triethylbenzene. [d] Experimentally determined.

transfer rate constant (CT → LE), k_{rec} is the sum of the rate constants for irreversible recombination to lower energy electronic states (CT → S_0, T_1) and k_f is the observed decay rate of the LE state in the absence of an electron acceptor. With the reasonable assumption that light excitation populates only the locally excited state and that only emission from this state is observed, one obtains a double exponential decay law for the fluorescence I(t) given by

$$I(t) = a_+ \exp(-k_+ t) + (1 - a_+) \exp(-k_- t) \tag{2.1}$$

where a_+ is the fraction of the fluorescence decaying with the fast rate constant k_+ and where k_- is the rate constant of the slow fluorescence decay. These parameters are related to the fundamental molecular rate constants by the following relations:

$$k_{for} = a_+(k_+ - k_-) + k_- - k_f \tag{2.2}$$

$$k_{back} = \frac{(k_+ - k_-)^2 - [2(k_{for} + k_f) - (k_+ + k_-)]^2}{4k_{for}} \tag{2.3}$$

and

$$k_{rec} = k_+ + k_- - k_f - k_{for} - k_{back} \tag{2.4}$$

The value of k is obtained from measurements of the donor-bridge compound and is very close to 5×10^{-7} s^{-1} in all the solvents at every temperature. The value of k_- (see footnote a to Table 2.1) was found to vary by as much as 50%, depending on the concentration of trace impurities in the solution. Fortunately, the values of k_{for} and k_{back}

depend only weakly on the slow rate constant (as it is much smaller than k_+). The scatter in k_- does generate considerable uncertainty in k_{rec}, however. For this reason, only the rate constants k_{for} and k_{back} are compared with the electron transfer rate theory.

The temperature dependence of the rate constants for the forward (filled symbols) and backward (open symbols) excited-state electron-transfer reactions are plotted in Figure 2.3. Figure 2.3A displays the data for the methyl-substituted benzenes, and Figure 2.3B displays the data for the isopropyl-substituted benzenes. The lines drawn in the graph represent fits to the semiclassical electron-transfer rate equation (vide infra). In the unsubstituted and singly substituted benzene solvents, the charge separation rate constants, k_{for} exhibit an apparent negative activation energy, whereas the excited-state charge recombination rate constants, k_{back} exhibit an apparent positive activation energy. In the trisubstituted solvents, the temperature dependence of k_{for} and k_{back} are more complex. In mesitylene, the slope $d(\ln k_{for})/dT$ becomes increasingly negative with increasing temperature. At low temperatures, k_{back} increases with increasing temperature, but at higher temperature, k_{back} becomes temperature independent. In triisopropylbenzene, both k_{for} and k_{back} increase with temperature. This observation of apparent positive activation energies for both the charge separation and recombination steps is unique among the five aromatic solvents investigated. The amount of scatter in the TIP data is greater than in the other solvents because the two rate constants for the fluorescence decay are more similar in magnitude, making it more difficult to extract the rate constants reliably. The two decay components are similar because the values of k_{for} and k_{back} are smaller in TIP

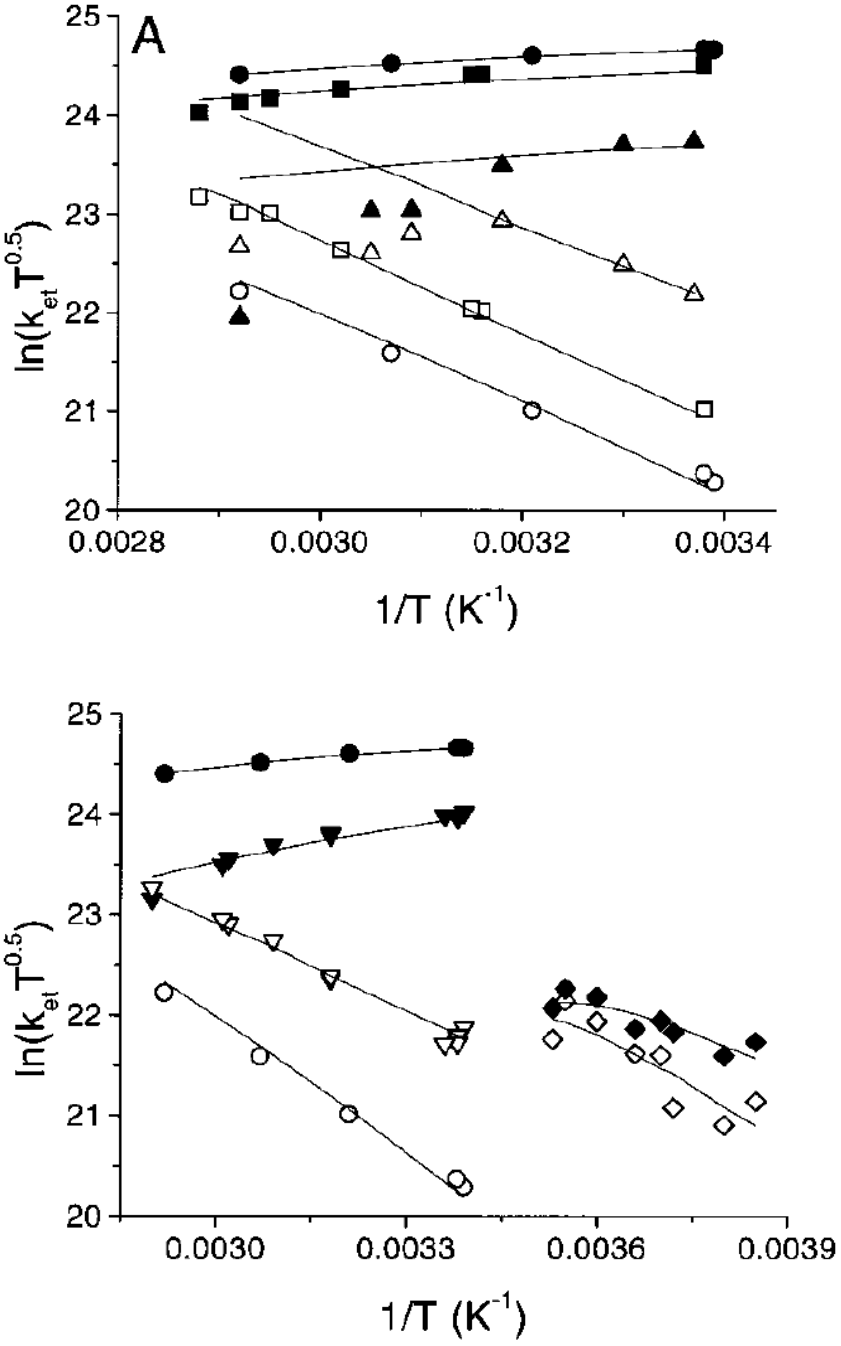

Figure 2.3 The temperature dependence of the forward (filled symbols) and backward (open symbol) electron-transfer rate constants are shown. Panel A shows the data for benzene (●,○), toluene (■,□), and mesitylene (▲, △). Panel B shows the data for benzene (●,○), cumene (▼,▽), and triisopropylbenzene (♦, ◊). The lines are fits to the data using the Matyushov model for $\Delta_r G(T)$ and $d\lambda_o(T)/dT$.

as compared to the other solvents (Table 2.1). Nonmonotonic and "negative" temperature dependence of electron-transfer rate constants of DBA systems in nonpolar and weakly polar solvents have been reported by other workers.[11] These observations may be explained, in part, by consideration of the temperature dependence of the LE → CT free energy difference.

The value of $\Delta_r G$ (LE → CT) at each temperature was computed from the ratio k_{for}/k_{back} (Figure 2.4). In each solvent, $\Delta_r G$ increases with increasing temperature; i.e., the charge transfer state is destabilized upon increasing the temperature. The entropy change upon charge separation, $\Delta_r S$ is quite negative, e.g. -22 and -26 cal/(mol K) in benzene and in cumene, respectively. Continuum models (Born, Onsager)[12] and molecular models of solvation[8] both predict the negative sign of $\Delta_r S$. However, simple continuum models predict that $\Delta_r G$ in benzene should be more positive than in either toluene or cumene, in contrast to the experimental results. This contradiction is one of numerous examples[13] that highlight the inability of simple continuum models to predict or rationalize solvation in nonpolar solvents. In an effort to view these results within the framework of a reasonable theory, a molecular model for solvation, developed by Matyushov[8] for dipolar, polarizable, hard-sphere solvents, is employed. As will be described in section 2.4, this theory reproduces the solvent and temperature variations of $\Delta_r G$ and provides some guidance as to the temperature dependence of the outer-sphere reorganization energy.

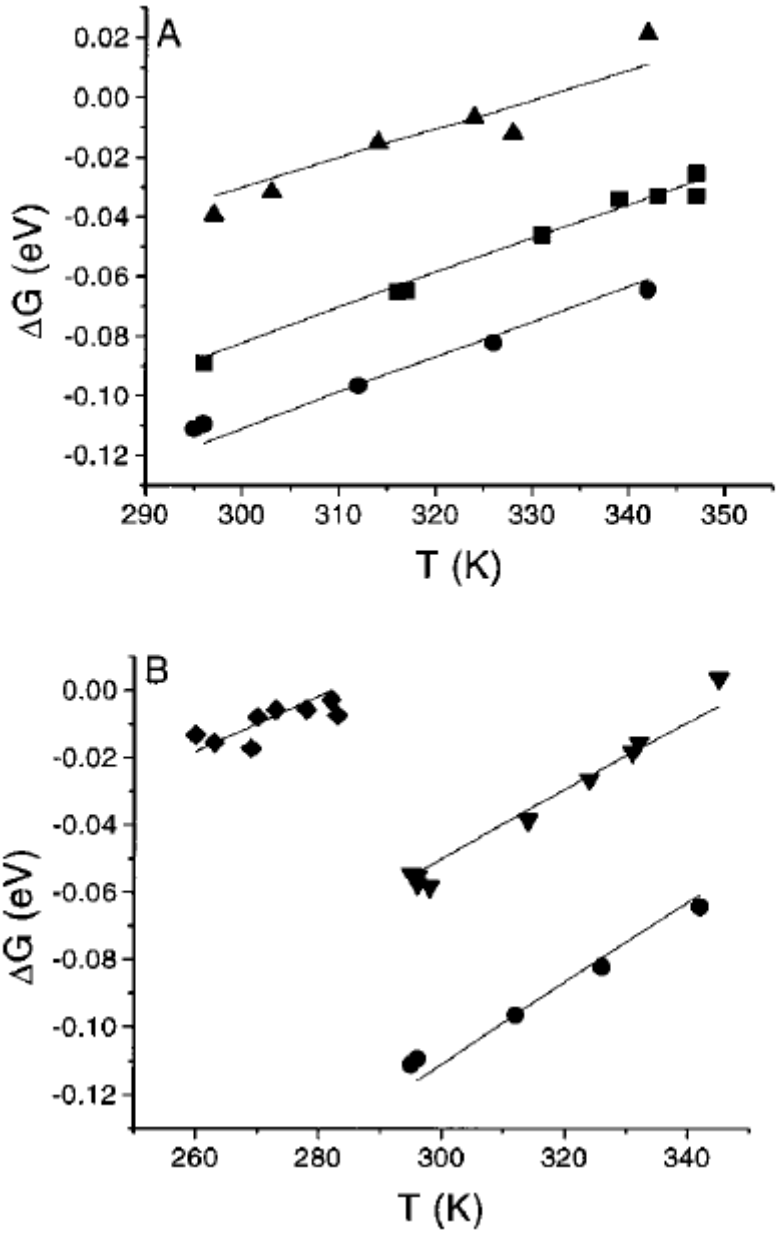

Figure 2.4 The temperature dependence of $\Delta_r G$ for the electron-transfer reaction is shown. Panel A shows the data for benzene(●), toluene(■), and mesitylene(▲). Panel B shows the data for benzene(●), cumene(▼), and triisopropylbenzene(♦).

2.3 Analyses

2.3.1 Kinetic Models

The donor-acceptor electronic coupling for **2** in the aromatic solvents is much smaller than *kT* and lies in the nonadiabatic, or weak, coupling regime.[14] In this case, the electron-transfer rate constant may be expressed in terms of the Golden Rule formula:

$$k_{\mathrm{ET}} = \frac{2\pi}{\hbar}|V|^2 \mathrm{FCWDS} \tag{2.5}$$

where |V| is the magnitude of the electronic coupling between the donor and acceptor groups and *FCWDS* is the Franck-Condon Weighted Density of States. The *FCWDS* factor accounts for the impact of nuclear coordinates on the electron-transfer rate. As discussed for this DBA system[3] and related ones[2,4] a semiclassical expression with a single quantized mode provides an adequate description of the rate constant. In particular,

$$k_{\mathrm{ET}} = \frac{2\pi|V|^2}{\hbar\sqrt{4\lambda_{\mathrm{o}}\pi k_{\mathrm{B}}T}} \sum_{n=0}^{\infty} \mathrm{e}^{-S}\left(\frac{S^n}{n!}\right) \exp\left[\frac{-(\Delta_{\mathrm{r}}G + \lambda_{\mathrm{o}} + nh\nu)^2}{4\lambda_{\mathrm{o}}k_{\mathrm{B}}T}\right] \tag{2.6}$$

where k_B is Boltzmann's constant, λ_0 is the outer-sphere (or solvent) reorganization energy, ν is the frequency of the effective quantized vibrational mode, $\Delta_r G$ is the reaction free energy, and *S* is the Huang-Rhys factor defined by

$$S = \frac{\lambda_{\mathrm{v}}}{h\nu} \tag{2.7}$$

in which λ_v is the inner-sphere reorganization energy. The total reorganization energy $\lambda = \lambda_v + \lambda_0$ represents the change in energy if the reactant were to change to the equilibrium configuration of the product without transferring an electron. This model for the rate constant has been widely successful in describing intramolecular electron-transfer processes.[15,16]

The rate expression in eq 2.6 has five parameters: $\Delta_r G$, λ_v, λ_0, ν and |V|. As noted above, the value of $\Delta_r G$ at each temperature can be obtained directly from the data. The inner-sphere reorganization energy λ_v and the characteristic vibrational frequency ν were previously determined by fitting charge-transfer spectra for a related system (same donor and acceptor units but a shorter bridge unit) and by quantum chemical calculations.[3] Those studies found that λ_v = 0.39 eV and $h\nu$= 0.175 eV were reasonable parameter values. These two quantities reflect the changes in the nuclear arrangement of the anthracene upon oxidation and of the acceptor upon reduction. As such, one expects the two parameters to remain nearly constant with changes in the bridge that are remote from the D or A group, or with changes in the solvent.[3] One potential caveat is raised by the recent computational work of Paddon-Row[17] which suggests that the D-A separation (in vacuo) changes significantly in the Coulomb field of the charge separated state. For **2**, such distortions could result in different $\Delta_r G$, λ_v, λ_0 and |V| for the forward and back electron-transfer steps. We have found no particular evidence supporting this behavior in these solvents. Thus, two parameters, |V| and λ_0 remain to be determined from the electron-transfer rate constants and their temperature dependence.

Considerable "parameter coupling" arises between the best fit values of the fitting parameters when analyzing temperature-dependent data. This issue has been discussed at length for these DBA systems in other solvents.[3] The availability of the "correct" value of $\Delta_r G$ from the ratio of k_{for}/k_{back} at each temperature greatly simplifies the task of extracting accurate values of |V| and λ_0. Nevertheless, a parametric relationship exists between the remaining two parameters, |V| and λ_0, at each temperature. This relationship is exhibited in Figure 2.5 for benzene, cumene, and triisopropylbenzene at selected temperatures. This figure shows that the value of |V| that is required to reproduce k_{for} varies nonlinearly with the assumed value of the outer-sphere reorganization energy. For these solvents, the parametric relationship varies only slightly with temperature (vide infra). The curves in Figure 2.5 support two limiting conclusions: (1) if λ_0 is relatively constant in all three solvents, |V| in benzene and cumene are nearly equal but |V| in TIP is at least three times smaller or (2) if |V| in TIP is the same magnitude as |V| in benzene, λ_0 must be ~ 0.1 eV (30-50%) larger in TIP than in benzene. Some combination of these explanations is also possible.

If one makes the conventional assumption that the electronic coupling |V| is temperature independent, it is possible to determine the temperature dependence of the outer-sphere reorganization energy from k_{for}[18]. However, it is possible that solvent-mediated electronic coupling (in contrast to bond-mediated electronic coupling) is temperature-dependent. Consequently, the analysis of the k_{ET} data proceeds in stages. First, the rate constant data are analyzed with the assumption that |V| is temperature-independent. This allows the apparent temperature dependence of the reorganization energy to be extracted from $k_{for}(T)$. For the

solvents in which λ_0 changes little over a reasonable range of temperatures, the rate constant data can be fit to eq 2.6 with |V| and λ_0 as temperature-independent fitting parameters. Next, a molecular model for solvation is parametrized using the $\Delta_r G(T)$ data. This model is used to predict the temperature dependence of the solvent reorganization energy. The kinetic data are then analyzed using the parametrized model in two ways. Initially, the model is used to predict the $\Delta_r G(T)$and $d\lambda_0/dT$ values so that |V| and $\lambda_0(295)$ are the adjustable fitting parameters. Finally, the model is more stringently tested by using the predicted $\Delta_r G(T)$and $\lambda_0(T)$ values with |V| as the only adjustable fitting parameter.

2.3.2. Is λ_0 Temperature-Dependent?

With values of 0.39 eV for λ_v, 0.175 eV for $h\nu$ and $\Delta_r G(T)$ available from the data, it is possible to obtain $\lambda_0(T)$ if a value for the electronic coupling |V| can be found. As one goal of this study is to learn more about the temperature dependence of λ_0 we proceed by assuming a reasonable value for |V| and then extract $\lambda_0(T)$ from the data using eq 2.6. Figure 2.6 displays the outer-sphere reorganization energies $\lambda_0(T)$ required to reproduce the $k_{for}(T)$ data for two different assumed values of the electronic coupling in the different methylbenzene (panel A) and isopropylbenzene (panel B) solvents. As was evident in Figure 2.5, larger values of |V| produce larger values of λ_0. For both assumed values of |V| , the required $\lambda_0(T)$ values in benzene decrease very slightly with temperature. The required $\lambda_0(T)$ values in toluene exhibit a similar magnitude and temperature dependence as the benzene values for the same assumed |*V*|. This result is

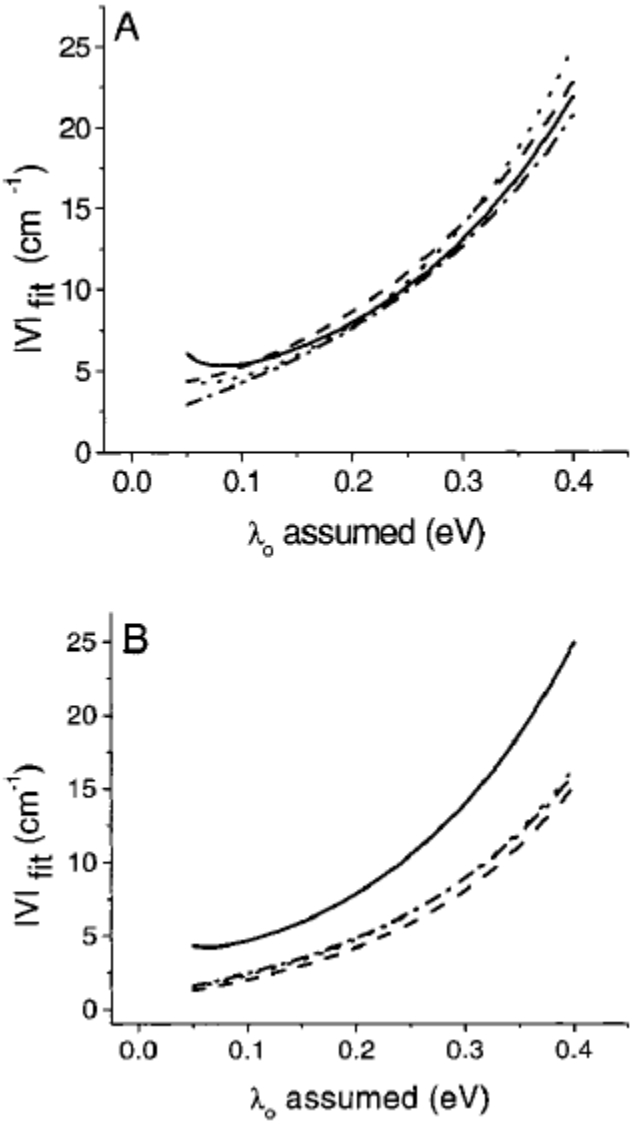

Figure 2.5 This figure illustrates the parameter coupling between |V| and λ_0. Panel A shows the data for benzene (295 K, solid line), benzene (342 K, dashed line), cumene (270 K, dotted line), cumene (345 K, dash-dot line). Panel B shows the data for cumene (270 K, solid line), triisopropylbenzene (260 K, dashed line), triisopropylbenzene (270 K, dotted line), triisopropylbenzene (283 K, dash-dot line). The 270 and 283 K curves overlap in panel B.

consistent with the similar electron-transfer rate constants in benzene and toluene, and these solvents' similar properties. Below 320 K, the required λ_0 in mesitylene is within 0.02 eV of that in benzene, for the same |V|. However, above 320 K, the λ_0 generated by this analysis rises steeply. In clear contrast to benzene and toluene, some property of mesitylene varies strongly with temperature. Comparing the open symbols (|V| = 10 cm^{-1}) and the solid symbols (|V| = 6 cm^{-1}), the absolute value of the reorganization energy is rescaled, but its temperature dependence is not affected. Panel B shows that the required values of λ_0 in cumene are also within 0.02 eV of those for benzene and, as seen in Figure 2.5, appear to increase slightly above 330 K. For the case of |V| = 6 cm^{-1}, the required λ_0 in TIP is almost double that of benzene and exhibits a steep, negative temperature dependence. Use of a smaller |V| for TIP (open symbols, |*V*| = 1 cm^{-1}) produces smaller values of λ_0 and a weaker temperature dependence.

The foregoing analyses indicate that it is reasonable to treat |V| and λ_0 as temperature- independent in benzene, toluene, and cumene. Upon close inspection, either λ_0 decreases slightly or |V| increases slightly with increasing temperature in benzene and toluene. A similar situation appears to exist for mesitylene below 320 K. By contrast, it is not reasonable to treat |V| and λ_0 as temperature-independent in triisopropylbenzene unless the absolute magnitude of |V| is significantly smaller than 6 cm^{-1}. If |V| is 6 cm^{-1} or greater in TIP, then λ_0 must decrease with increasing temperature or |V| must be temperature-dependent. The opposite situation appears to hold in mesitylene above 320 K; either |V| decreases or λ_0 increases sharply with increasing temperature. To determine the

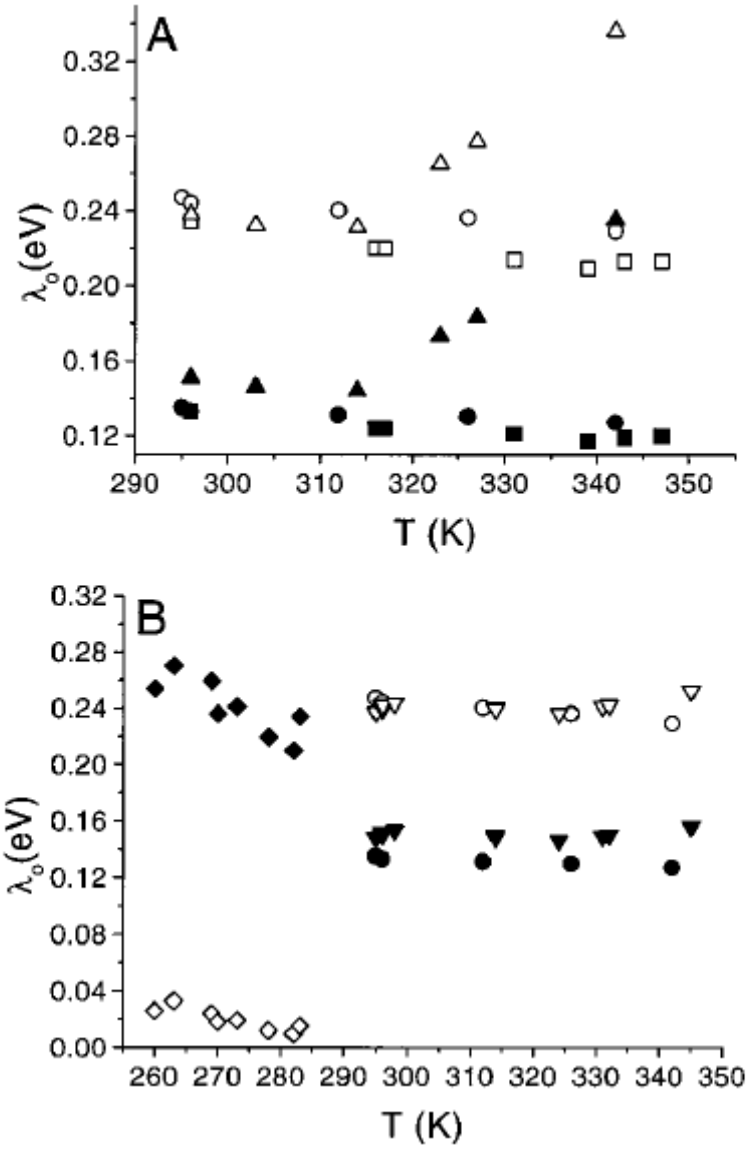

Figure 2.6 The temperature-dependent values of λ_o that are needed to reproduce the *k*for(T). Panel A shows the data for benzene (●,○) , toluene (■,□), and mesitylene (▲, △). Panel B shows the data for benzene (●,○), cumene (▼,▽), and triisopropylbenzene(♦, ◊).The filled symbols give values of λ_o for $|V|$ = 6 cm^{-1}. The open symbols give values of λ_o for $|V|$ = 10 cm^{-1} for all the solvents except TIP where it was set to $|V|$ = 1 cm^{-1}.

magnitude and possible temperature dependence of |V| requires a reasonable model for the magnitude and/or temperature dependence of λ_0 in these solvents. Continuum models are not able to predict the temperature dependence, let alone the magnitude, of in these aromatic solvents. To estimate the magnitude and temperature dependence of λ_0 a molecular- based model for the solvation energy and solvent reorganization energy was explored. The analysis and resulting estimates of |V| and λ_0 are described in the next section.

2.4 Modeling $\Delta_r G(T)$and $\lambda_0(T)$

Modeling $\Delta_r G(T)$and $\lambda_0(T)$ in the alkylbenzenes is expected to be nontrivial because of their nondipolar character. Hence one expects the dispersion and induction forces to play a significant role in the solvation and its temperature dependence.[8] In addition, the importance of quadrupole and higher order moments should, in principle, be considered. Although theoretical efforts to include such contributions are under development, their implementation remains difficult and their reliability has not been assessed.[19] The description of the solvent dependence of $\Delta_r G(T)$and $\lambda_0(T)$ used here employs a reference hard-sphere, dipolar polarizable fluid to account for the effects of solvent density variation on the solvation and hence its temperature dependence. The model accounts for both induction and dispersion forces.[8]

Matyushov[8] writes the reaction free energy $\Delta_r G$ as a sum of three components:

$$\Delta_r G = \Delta G_{\text{vacuum}} + \Delta G_{\text{dipole}} + \Delta G_{\text{dispersion}} \tag{2.8}$$

where ΔG_{vacuum} is the reaction free energy in a vacuum. The ΔG_{dipole} term contains contributions from the dipole-dipole interaction between the solute and solvent and the induction force between the solute dipole and the solvent. This term is given by[20]

$$\Delta G_{\text{dipole}} = -\frac{\Delta m}{\sigma^3}(m_e' + m_g')P(y,\rho^*,r_0) \tag{2.9}$$

where σ is the hard-sphere diameter of the solvent, ρ^* is the reduced solvent density $\rho\sigma^3$ (ρ is the solvent number density), r_0 is the distance of closest approach between the solute and solvent in reduced units ($r_0 \equiv 0.5 + R_0/\sigma$) where R_0 is the effective radius of the solute molecule - approximated as a sphere), and y is the solvent's zero frequency dipolar density ($y=(4\pi/9kT)\sigma m_s^2+(4\pi/3)\rho\sigma_s$) arising from solvent permanent dipole moments m_s and solvent molecule polarizability α_s. The difference in dipole moment between the solute CT state, m_e , and LE state, m_g is given by Δm. The solute dipole moments are renormalized as a consequence of the solute polarizability. The slanted prime indicates a renormalized magnitude induced by the solvent's zero frequency dipolar density, *y*:

$$m' = \frac{m}{\left[1 - \frac{2\alpha_0 P(y,\rho^*,r_0)}{\sigma^3}\right]} \tag{2.10}$$

where α_0 is the solute polarizability. The functions $P(y,\rho^*,r_0)$ are Padé approximants to the dipolar response function of the fluid. Their explicit form is given in Appendix 2.A.

The third term $\Delta G_{dispersion}$ is the contribution to the free energy from the dispersion interactions between the solute and solvent. It is given by

$$\Delta G_{\text{dispersion}} = \frac{\Delta\gamma'}{\alpha_s} 96\eta\epsilon_{LJ}^{s}\left(\frac{\sigma}{\sigma^{0s}}\right)^6 \int_{\sigma_{LJ}^{0s}}^{\infty} u_1^{0s}(r)\, g_{0s}^{(0)}(r) r^2\, dr \tag{2.11}$$

where η is the solvent packing fraction of the hard sphere solvent, $\sigma^{0s} = R_o + \sigma/2$ is the effective solvent-solute diameter, ε_{LJ}^{s} is the solvent Lennard-Jones energy and $g^{(0)}_{0s}$ is the solute-solvent hard sphere distribution function. The hard-sphere diameter σ was used for the Lennard-Jones diameter of the solvent in the Matyushov formulation. The term $u_1^{0s}(r)$ is equal to $u^{0s}(r)\theta(r-\sigma^{0s})$ where $u^{0s}(r)$ is the Lennard-Jones potential function and $\theta(x)$ is the Heaviside function. The term $\Delta\gamma'$ is the change in solute polarizability between the LE and CT states weighted by a ratio of solute and solvent ionization potentials[8]. Here it was treated as an adjustable solute parameter. These expressions may be evaluated, given the appropriate solute and solvent parameters, and compared to the experimentally determined free energy changes.

Matyushov[8] also derived an expression for λ_0, the outer sphere reorganization energy upon electron transfer, which has three sources:

$$\lambda_o = \lambda_{\text{dipole}} + \lambda_{\text{dispersion}} + \lambda_{\text{induction}} \tag{2.12}$$

The dipolar contribution λ_{dipole} is given by

$$\lambda_{\text{dipole}} = \frac{\Delta m}{\sigma^3}[(m_e' - m_g')P(y,\rho^*,r_0) - (m_e^{\infty} - m_g^{\infty})P(y_{\infty},\rho^*,r_0)] \quad (2.13)$$

The m^{∞} terms reflect solute dipole renormalization by the high frequency dipolar density that arises from the solvent polarizability. The dispersion contribution to the reorganization energy $\lambda_{dispersion}$ is given by [20]

$$\lambda_{\text{dispersion}} = \frac{8\eta}{3}\beta(\epsilon_{LJ}^{s}\Delta\gamma')^2[\int_0^{\infty} u_1^{0s}(r)^2 g_{0s}^{(0)}(r) r^2\, dr - (1 - m_{ss}(0))\int_0^{\infty} u_1^{0s}(r) u_1^{0s}(r+\phi) g_{0s}^{(0)}(r) g_{0s}^{(0)}(r+\phi) r(r+\phi)\, dr] \quad (2.14)$$

where $m_{ss}(0)=(1-\eta)^4/(1+2\eta)^2$ and the phase factor φ is given as a function of η in the

$$\lambda_{\text{induction}} = \frac{1}{\eta k_B T}\left(\frac{\Delta m'^2 y_{\infty}}{20\sigma^3}\right)^2 [4(2m_{\infty}^{+}(0) + m_{\infty}^{-}(0)) - 9] \times 9\int_{r_0}^{\infty} \frac{g_{0s}^{(0)}(r)}{r^{10}} dr \quad (2.15)$$

Appendix 2.A. The induction contribution $\lambda_{induction}$ is given by

where

$$m_{\infty}^{+}(0) = \frac{1}{3y_{\infty}}\left(1 - \frac{1}{\epsilon_{\infty}}\right) \quad (2.16a)$$

and

$$m_{\infty}^{-}(0) = \frac{1}{3y_{\infty}}(\epsilon_{\infty} - 1) \tag{2.16b}$$

As with the free-energy expressions, this sum must be evaluated for an appropriate choice of solute and solvent parameters.

Equations 2.8 – 2.11 were used to reproduce the experimental values of $\Delta_r G$ and its temperature dependence. Unknown parameters, such as the solute radius, were chosen to achieve the best global fit (in all solvents). The solid lines in Figure 2.4 display the resulting fits to the measured reaction free energies. The effective solute sphere radius was set equal to 5.5 Å. The change in the dipole moment between the LE and CT states was set to 34 D. The vacuum free energy change ΔG_{vacuum} was set to 0.568 eV. The LE state polarizability was set to 100 $Å^3$ and $\Delta\gamma$ was 2 $Å^3$ The solvent parameters used are reported in Table 2.2. The parameter values were obtained in a standard manner[21] for each of the solvents. In each case, the polarizability of the solvent was adjusted (by less than 10%) to improve the fit. The temperature-dependent density, the static dielectric constant and the high-frequency dielectric constant (estimated as n^2) were obtained from the literature.

The parameters determined by fitting $\Delta_r G(T)$ in the various solvents were used to predict the absolute magnitude and the temperature dependence of the reorganization energy $\lambda_0(T)$ in each solvent. The values of $\lambda_0(295)$ predicted by the "calibrated" Matyushov model are all less than 0.15 eV (see Table 2.4, column 5). In toluene and cumene, the two solvents with nonzero dipole moments, the estimated

Table 2.2 Solvent Parameters Used in the Matyushov Modeling

solvent	m, D[a]	σ, Å[b]	α_0, Å^3 [c]	ϵ^s_{LJ},k_B	$\eta(296)$	$d\lambda_o(T)/dT$, eV/K
benzene	0.01	5.277	10.7	544	0.518	-2.2×10^{-4}
toluene	0.31	5.680	11.8	596	0.543	-6.5×10^{-4}
cumene	0.39	6.286	15.5	662	0.560	-7.2×10^{-4}
mesitylene	0.01	6.400	15.3	862	0.593	-4.5×10^{-4}
TIP[d]	0.01	7.400	30.7	1117	0.534	-1.0×10^{-4}

[a] The dipole moments for benzene, mesitylene, and triisopropylbenzene were chosen to be very small but nonzero to facilitate computation. The dipole moments of toluene and cumene were taken from Riddick, J. A.; Bunger, W. B.; Sakano,T.K *Organic Solvents: Physical Properties and Methods of Purification*; Wiley: New York, NY, 1986. [b] The effective hard-sphere diameters and the Lennard-Jones parameters for the solvents were obtained using the method described by Ben-Amotz, D.; Willis, K. G. *J. Phys. Chem.* **1993**, *97*, 7736. [c] The solvent polarizabilities were taken from the CRC. In each case, they were slightly modified to give a good fit. [d] TIP is 1,3,5-triisopropylbenzene.

Table 2.3 Best Fit Values for |V| and λ_o Using the Experimentally Determined $\Delta_r G(T)$: Method 1

solvent	$\lvert V\rvert$, cm^{-1}	λ_o, eV
benzene	5.6	0.12
toluene	5.1	0.10
cumene	5.0	0.12
mesitylene	3.1	0.050
TIP[a]	1.2	0.023

[a] TIP is 1,3,5-triisopropylbenzene.

Table 2.4 Best Fit |V| and $\lambda_o(295)$ Using the Matyushov Model for $\Delta_r G(T)$

	method 2[a]		method 3[b]	
solvent	$\lvert V\rvert$, cm^{-1}	$\lambda_o(295)$, eV	$\lvert V\rvert$, cm^{-1}	$\lambda_o(295)$, eV
benzene	5.7	0.124	5.1	0.069
toluene	8.8	0.213	5.7	0.132
cumene	6.6	0.181	4.8	0.129
mesitylene	5.6	0.143	4.2	0.094
TIP[c]	0.7	0.002	1.2	0.027

[a] In method 2, $d\lambda_o(T)/dT$ is taken from the Matyushov model. [b] In Method 3, $\lambda_o(T)$ is taken from the Matyushov model. [c] TIP is 1,3,5-triisopropylbenzene.

λ_0(295) are moderately larger than in benzene and mesitylene. The λ_{dipole} term, eq 2.12, is the source of the larger reorganization energy in toluene and cumene (see Appendix 2.B). Before proceeding to the analysis of the kinetic data, it is important to point out that the parameter set used to fit $\Delta_r G(T)$ is not unique. For example, it is possible to decrease the size of the dipole moment change (Δm) and increase the solute polarizability α_0 and still obtain similar quality fits to the data.

2.5 Determination of |V| and λ_0

Values of |V| and λ_0 were extracted from the temperature dependent rate constant data using three different procedures. First, the rate data was fit using the experimental $\Delta_r G(T)$ and treating λ_0 and |V| as temperature independent, but adjustable, parameters. The results of this "*T*- independent" analysis (method 1) are presented in Table 2.3. This procedure is appropriate for the solvents that exhibit a weak temperature dependence of λ_0 when a temperature-independent |V| is assumed; i.e., benzene, toluene, and cumene. This condition is also satisfied in mesitylene at low temperatures, and the data in mesitylene at temperatures below 320 K were analyzed in this manner. Use of this method for the triisopropylbenzene data is reasonable only if |V| is considerably less than 6 cm^{-1}. Given the results of the analysis, an assumption for |V| of 1 cm^{-1} more closely represents the experimental findings (vide infra*)*. In each case the data in Figure 2.3 was well reproduced by this analysis.

According to Table 2.3, the best fit parameter values are consistent with an increase in the electronic coupling when the solvent's aromatic ring is able to position between the donor and acceptor π-functions. The benzene and monosubstituted benzene solvents have similar electronic couplings. In contrast, the electronic coupling in mesitylene, which has three bulky methyl groups equally spaced around the periphery of the ring, is ~40% smaller and the coupling in TIP, which has the greatest steric impediment to entry into the cleft, is 4-5 times smaller than that in benzene. The small |V| is consistent with the assumption of a nearly temperature independent λ_0 (Figure 2.6, vide supra). The best fit values of the reorganization energy provide additional insight into the solvent-solute interaction. The reorganization energy in benzene and the monoalkylated benzenes are similar, whereas the reorganization energy in TIP is smaller. The kinetic model does not account for the presence of the cleft in **2**. None the less, the extracted reorganization energies are strongly influenced by the solvent size. From a molecular perspective, reduced entry of the bulky solvents into the solute cleft would be expected to decrease their ability to stabilize the charge-transfer state and to produce smaller values of λ_0.

In a second approach, the electronic coupling was determined by fitting the rate data to eq 2.6 using the $\Delta_r G(T)$ and $d\lambda_0/dT$ (Table 2.2) values predicted by the "calibrated" Matyushov model: method 2. In this method, |V| and $\lambda_0(295)$ were the adjustable parameters. The best fit values are reported in Table 2.4 (columns 2 and 3) and the lines displayed in Figure 2.3 represent the result of this fitting procedure. This approach does an excellent job of reproducing both the forward and back electron-transfer data in all five solvents. In contrast to method 1, the electronic

coupling obtained for the monosubstituted benzenes is larger than benzene. The estimated coupling in mesitylene is comparable to the values found for benzene and the monoalkylated benzenes and the coupling in TIP is more than a factor of 5 smaller than the coupling found in benzene. The room temperature reorganization energies $\lambda_0(295)$ obtained in this analysis are between 0.22 and 0.12 eV in all solvents except TIP, for which the reorganization energy was found to be < 0.01 eV. The Matyushov treatment predicts that λ_0 should be largest in the slightly dipolar solvents cumene and toluene (vide infra). A dissection of the reorganization energy (see Appendix 2.B) reveals that the dipolar contribution is the source of the larger values in these two solvents. The extracted value of λ_0 in TIP is extraordinarily small, but is required to reproduce the observed increase of both the forward and reverse electron-transfer rate constants with increasing temperature.

In a final approach, the electronic coupling was determined by fitting the rate data to eq 2.6 using the $\Delta_r G(T)$ and λ_0 values predicted by the "calibrated" Matyushov model, method 3. In this method, |V| was the only adjustable parameter. This approach provides a stringent test of the Matyushov model's ability to predict the solvent reorganization energy in aromatic solvents. The best fit values of |V| are reported in Table 2.4 (column 4) along with the Matyushov model's predictions of $\lambda_0(295)$ (column 5). With the exception of TIP, the |V| generated by method 3 is as much as 40% smaller than that produced by method 2. Likewise, the $\lambda_0(295)$ value from method 3 is ~0.06 eV smaller than that from method 2. For TIP, both |V| and λ_0 produced by method 3 are larger. However, as seen in Figure 2.7, method 3 accurately reproduces the kinetic data in toluene, cumene, and mesitylene but fails to reproduce the proper

slope of the Arrhenius plots in benzene and TIP. The origin of this failure can be understood by analyzing the temperature dependence of eq 2.6 for the n = 0 term.[22] Figure 2.8 displays the dependence of the slope of k_{for} on the value of $\lambda_0(295)$. For TIP, the observed negative slope (●-●) is reproduced only by values of $\lambda_0(295)$ less than 0.01 eV,[23] whereas the Matyushov value of 0.023 eV produces a weak positive slope, as seen in Figure 2.7. The positive slope of the benzene data (○-○) is reproduced by $\lambda_0(295)$ values greater than 0.1 eV, whereas the Matyushov prediction of 0.048 eV results in a negative slope. Plots analogous to Figure 2.8 for toluene, cumene, and mesitylene predict positive Arrhenius slopes for $\lambda_0(295)$ greater than 0.08 eV. As a result, the fits to the kinetic data and the extracted values of |V| are only moderately affected by the value of $\lambda_0(295)$ in the latter three solvents.

2.6 Discussion and Conclusion

The fluorescence decay of **2** in nonpolar and weakly polar solvents is biexponential. The fast component of the decay involves depopulation of the LE state primarily through establishment of an LE ↔ CT excited-state equilibrium. The slow component arises from irreversible depopulation of the equilibrium mixture to lower energy states.[24] Analysis of the biexponential decay law, in conjunction with the intrinsic decay rate constant for the LE state in donor only analogues, enabled reliable determination of three important quantities: the forward electron-transfer rate k_{for} (LE to CT), the backward electrontransfer rate k_{back} (CT to LE), and the charge separation free energy $\Delta_r G$ The data in Figure 2.4 show that the reaction free energy $\Delta_r G(T)$ becomes increasingly endoergic with increasing temperature and with increasing alkyl

substitution of the solvents' aromatic core. The destabilization of the charge transfer state with temperature may be understood in terms of decreasing solvent density. A molecular model for the solvent is able to mimic the observed temperature dependence in this series of related solvents.

Among the set of solvents investigated, only toluene and cumene possess permanent dipole moments. The latter are small (< 0.35 D) and, in fact, benzene appears to be more effective at stabilizing the CT state. Benzene's axial quadrupole moment is slightly larger than toluene's[13a] and, at least from one edge, the unsubstituted benzene ring can get closer to the solute CT state. Although quadrupole contributions to solvation could be significant, the molecular model used here does not include them. The model incorporates the steric/size factor through the solvent's effective hard-sphere diameter, as indicated in Table 2.2. Although the molecular polarizability is larger in the more highly alkylated solvents, their size is also larger, and the $\rho\alpha$ contribution to the dipolar density remains relatively constant in these solvents. It appears that the differences in the solvation can be attributed to the smaller effective diameter of the less alkylated solvents and changes in the packing fraction η (see Table 2.2 and Appendix 2.B).

The same model and parameters that adequately reproduced in the different solvents was used to predict the magnitude and temperature dependence of the outer-sphere reorganization energy. The parametrized Matyushov model prediction of the $\lambda_0(295)$ values are all less than 0.15 eV (Table 2.4). For the three nondipolar solvents, increased solvent size (sphere diameter), molecular polarizability, and Lennard-Jones energy reduce the reorganization energy from 0.069 eV in benzene to 0.039 eV in

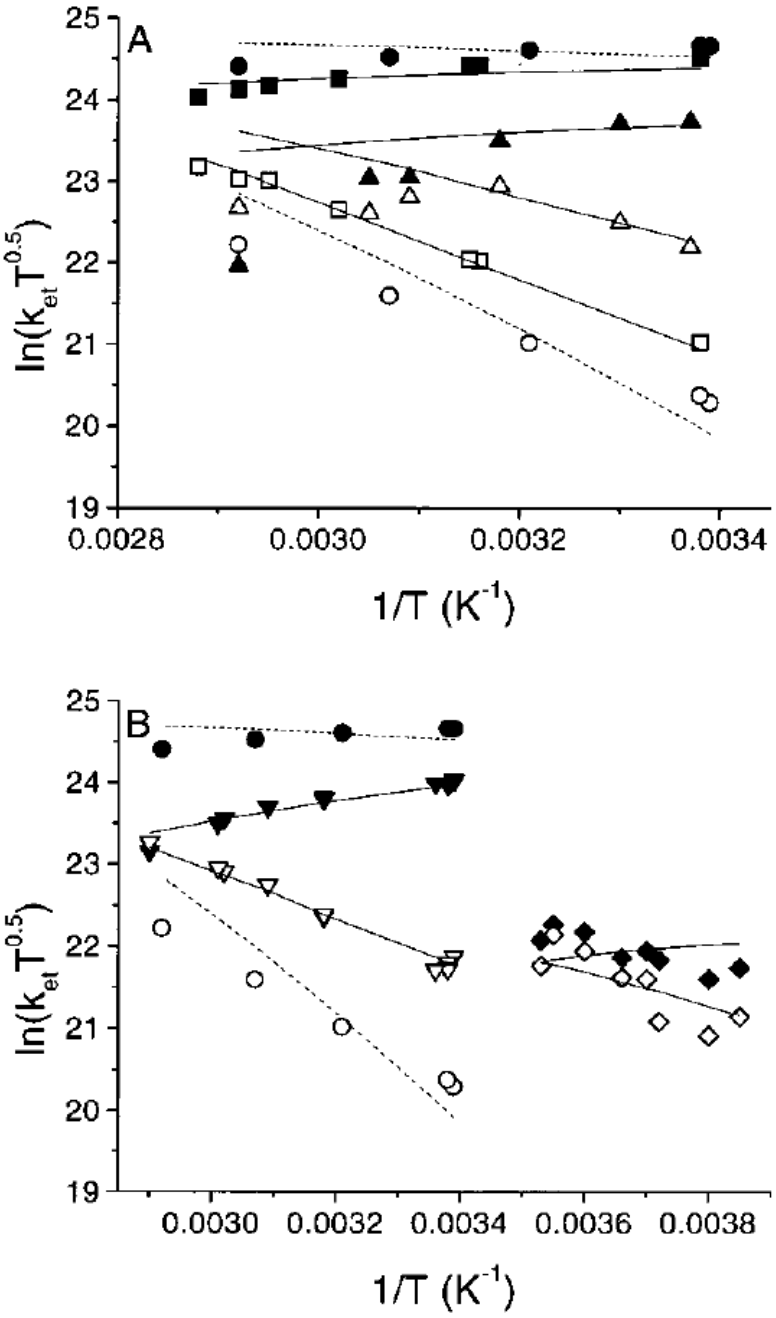

Figure 2.7 The temperature dependence of the forward (filled symbols) and backward (open symbol) electron-transfer rate constants is shown. Panel A shows the data for benzene (●,○), toluene (■,□), and mesitylene (▲,△). Panel B shows the data for benzene (●,○), cumene (▼,▽), and triisopropylbenzene (♦,◊). The lines are fits to the data using the Matyushov model for $\Delta_r G(T)$ and $\lambda_0(T)$. The dashed curves show the fits for benzene and the solid curves are for the other solvents.

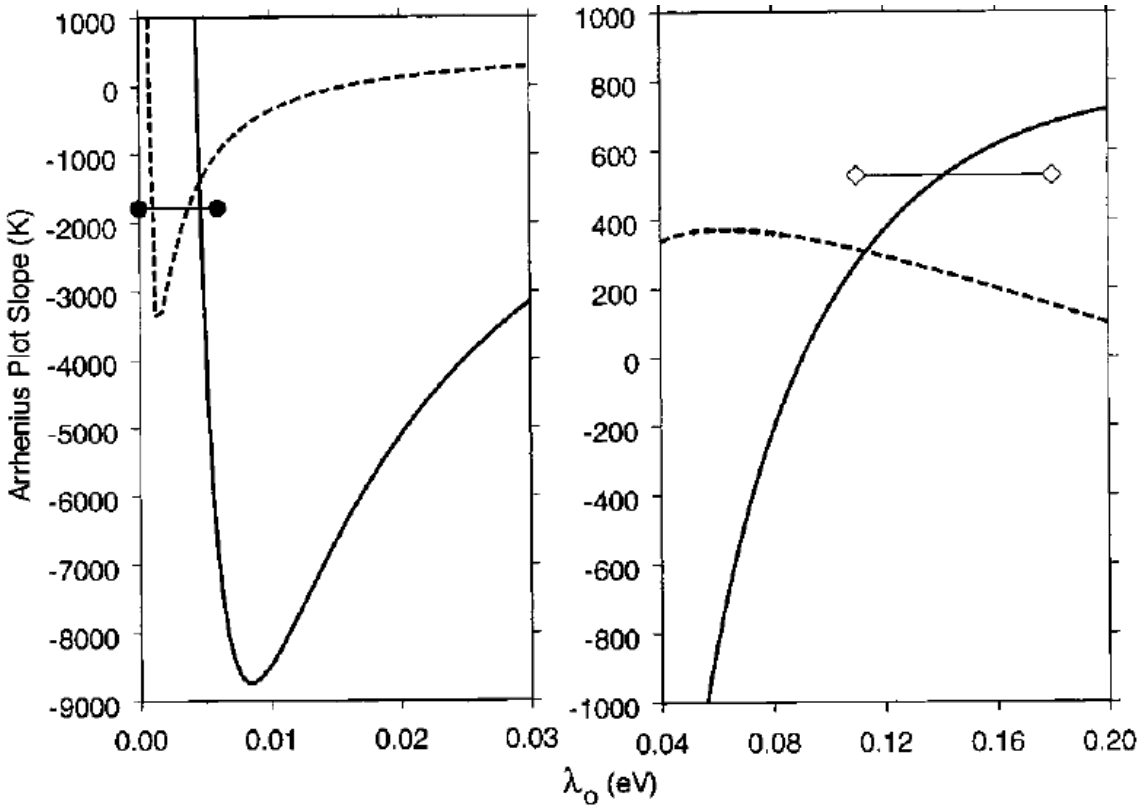

Figure 2.8 The calculated slope of $\ln(k_{for}(T)\sqrt{T})$ versus 1/T is plotted as a function of λ_0 for benzene and TIP. The solid curve is for benzene, and the dashed curve is for TIP. The left panel shows the result for 0-0.03 eV. The horizontal line with circles indicates the experimental slope for TIP. The right panel shows the result for 0.04-0.2 eV. The horizontal line with diamonds indicates the experimental slope for benzene.[27]

mesitylene and to 0.027 eV in TIP. For the nondipolar solvents, $\lambda_{dipoole}$ makes no contribution to the overall reorganization energy. However, the presence of a small dipole moment in toluene and cumene increases the overall reorganization energy 2-fold in comparison to, the otherwise similar solvent, benzene. As the dipole moment of cumene is 25% larger than that of toluene, one expects the predicted $\lambda_0(295)$ value to be greater for cumene. However, the increased size of cumene reduces the induction contribution $\lambda_{induction}$ which offsets the increased dipolar contribution $\lambda_{dipoole}$ (Appendix 2.B). As a result, the predicted reorganization energies $\lambda_0(295)$ in these two solvents are quite similar.

The molecular model predicts a weak decrease of λ_0 with increasing temperature (Table 2.2) which is corroborated by optical studies of CT emission and absorption bands in benzene[25] and other weakly polar solvents.[26] The "parametrized" Matyushov model predicts $d\lambda_0/dT$ values (Table 2.2) of about -7×10^{-4} eV/K in the dipolar solvents toluene and cumene and of -1×10^{-4} eV/K in TIP. From a practical standpoint, the parametrized Matyushov model does a reasonable job considering that it does not account for the detailed shape of the molecule. It predicts λ_0 values that are remarkably close to those required by the observed k_{ET} temperature dependence (Figure 2.8) and from a best fit to the data.

With the parametrization of a reasonable model for the temperature dependence of the reaction free energy and the outer-sphere reorganization energy, it was possible to fit the temperature-dependent electron-transfer rate constants to the semiclassical model (eq 2.6) and determine |V|. The results from the three analyses of the kinetic data clearly demonstrate that |V| is smaller in an aromatic solvent that is

too bulky to effect simultaneous overlap with the π-functions of the donor and acceptor groups. The analyses for the benzene, toluene, and cumene solvents give electronic couplings that are similar (~6 cm^{-1}). For 1,3,5-triisopropylbenzene, |V| is at least five times smaller than in benzene. The possibility that a smaller value of |V| is obtained as a result of the parametric dependence on the value of λ_0 in eq 2.6 has been evaluated. Figure 2.5 demonstrates that even if an identical value of λ_0 is assumed for this series of solvents, the calculated electronic coupling is at least 3-fold smaller for TIP than for benzene. These experiments emphasize once again the difficulty in interpreting electron-transfer rate constants determined at a single temperature. Without independent characterization of λ_0 and $\Delta_r G$ a single rate measurement can be interpreted to support any number of conclusions.

The variation of |V| with solvent may be rationalized in terms of the effect of the alkyl group steric bulk on the solvent's tendency to enter the cleft of **2** and on the resulting interactions with the D and A groups. For benzene and monosubstituted benzenes, the aromatic core can enter the cleft of **2** with minimal conformational restrictions. The comparable couplings determined for benzene, toluene and cumene suggest similar geometries and probabilities of solvent insertion into the cleft of **2** for all three solvents. For 1,3,5-triisopropylbenzene, the bulky isopropyl groups inhibit entry of the aromatic core into the cleft of **2**, causing a decrease in the electronic coupling by increasing the solvent-to-donor and solvent-to-acceptor distance. It is possible for an isopropyl group on TIP to insert into the cleft, thus providing a solvent-mediated path for D-A coupling, albeit a less effective one. Mesitylene affords an intermediate value of the coupling. The methyl groups are slightly wider than the

aromatic ring. Their presence may decrease the overlap of the ring orbitals with the donor and acceptor groups when mesitylene is located in the cleft. Alternatively, they may limit the available conformations that lead to significant electronic coupling or decrease the time average probability of finding solvent in the cleft. Further studies are required to distinguish these possibilities. The key may lie with the unusual kinetic behavior at higher temperatures in mesitylene.

We have shown that a prerequisite for effective aromatic solvent mediation of electronic coupling is placement of the aromatic core directly between the donor and acceptor groups. One way to hinder a solvent's access into the cleft is to increase its steric bulk. The results of this investigation demonstrate that preventing solvent entry into the cleft significantly reduces the efficacy of solvent-mediated coupling in electron-transfer reactions.

2.7 Appendix 2.A

The dipolar solvent response contains contributions from both solute-solvent and solvent- solvent interactions. Matyushov has shown that

$$P(y,\rho^*,r_o) = \frac{yI_{0s}^{(2)}}{1 + yI_{0s}^{(3)}/I_{0s}^{(2)}}$$

where $I^{(2)}$ and $I^{(3)}$ are the two and three particle solute-solvent integrals approximated by

$$I_{0s}^{(2)} = \frac{1}{r_o^3} + \frac{d(\rho^*)}{r_o^4} + \frac{e(\rho^*)}{r_o^5} + \frac{f(\rho^*)}{r_o^6}$$

$$I_{0s}^{(3)} = \frac{a(\rho^*)}{r_o^3} + \frac{b(\rho^*)}{r_o^4} + \frac{c(\rho^*)}{r_o^5}$$

$$I_{0s}^{(4)} = \frac{1}{r_o^9} + \frac{a(\rho^*)}{r_o^{10}} + \frac{b(\rho^*)}{r_o^{11}} + \frac{c(\rho^*)}{r_o^{12}}$$

The coefficients $a(\rho^*)$, $b(\rho^*)$, $c(\rho^*)$, etc. in the density expansion have been fitted to the calculated dependencies of the solute-solvent integrals and are provided in ref 8a. The explicit form of these integrals is given in ref 8c.

The integrals found in eqs 2.11, 2.14, and 2.15 were evaluated using the Padé form for the integrals. In our calculations,

$$\int_{\sigma_{LJ}^{0s}}^{\infty} u_1^{0s}(r) g_{0s}^{(0)}(r) r^2 \, dr = \left[\frac{I_{0s}^{(4)}}{9} - \frac{I_{0s}^{(2)}}{3}\right]$$

$$9\int_{r_0}^{\infty} \frac{g_{0s}^{(0)}(r)}{r^{10}} dr = I_{0s}^{(4)}$$

$$\left[\int_0^{\infty} u_1^{0s}(r)^2 g_{0s}^{(0)}(r) r^2 \, dr - (1 - m_{ss}(0)) \int_0^{\infty} u_1^{0s}(r) u_1^{0s}(r+\phi) g_{0s}^{(0)}(r) g_{0s}^{(0)}(r+\phi) r(r+\phi) \, dr\right] = I_{0s}^{(4)}$$

The latter integral ignores the contribution from three-body interactions. An effect which becomes increasingly important as the polarity of the solvent increases.

Table 2.5

T, K	ΔG_{dipole}, eV	$\Delta G_{dispersion}$, eV	ΔG_{total}, eV	λ_{dipole}, eV	$\lambda_{dispersion}$, eV	$\lambda_{induction}$, eV	λ_{total}, eV
			benzene				
296	−0.667	−0.018	−0.116	0	0	0.069	0.069
312	−0.648	−0.017	−0.096	0	0	0.065	0.065
326	−0.632	−0.017	−0.080	0	0	0.062	0.062
342	−0.613	−0.016	−0.061	0	0	0.058	0.058
			toluene				
296	−0.631	−0.025	−0.087	0.038	0	0.094	0.132
316	−0.608	−0.024	−0.063	0.034	0	0.083	0.118
331	−0.591	−0.024	−0.046	0.032	0	0.076	0.108
339	−0.582	−0.023	−0.037	0.031	0	0.072	0.104
347	−0.573	−0.023	−0.028	0.030	0	0.069	0.099
			mesitylene				
297	−0.552	−0.050	−0.033	0	0.001	0.092	0.093
303	−0.547	−0.049	−0.027	0	0.001	0.089	0.090
314	−0.537	−0.048	−0.016	0	0.001	0.084	0.085
324	−0.528	−0.048	−0.007	0	0.001	0.080	0.081
342	−0.512	−0.046	0.011	0	0.001	0.073	0.074
			cumene				
296	−0.591	−0.032	−0.054	0.042	0.001	0.086	0.129
314	−0.573	−0.031	−0.036	0.039	0.001	0.076	0.115
324	−0.563	−0.031	−0.025	0.037	0.001	0.070	0.108
331	−0.556	−0.031	−0.018	0.036	0.001	0.067	0.103
345	−0.543	−0.031	−0.005	0.033	0	0.060	0.094
			TIP				
260	−0.540	−0.047	−0.018	0	0.001	0.029	0.030
263	−0.538	−0.046	−0.016	0	0.001	0.029	0.030
278	−0.527	−0.046	−0.003	0	0.001	0.027	0.028
282	−0.524	−0.045	0	0	0.001	0.027	0.028

2.8 Appendix 2.B

Table 2.5 shows the different contributions to $\Delta_r G$ and λ from the dipolar, induction and dispersion interactions, according to the Matyushov model.

2.9 References

(1) Onuchic, J. N.; Beratan, D. N. *J. Chem. Phys*. **1990**, *92*, 722.

(2) (a) Kumar, K.; Lin, Z.; Waldeck, D. H.; Zimmt, M. B. *J. Am. Chem. Soc.* **1996**, *118*, 243. (b) Han, H.; Zimmt, M. B. *J. Am. Chem. Soc.* **1998**, *120*, 8001.

(3) Kumar, K.; Kurnikov, I. V.; Beratan, D. N.; Waldeck, D. H.; Zimmt, M. B. *J. Phys. Chem. A* **1998**, *102*, 5529.

(4) (a) Oevering, H.; Paddon-Row, M. N.; Heppener, M.; Oliver, A. M.; Cotsaris, E.; Verhoeven, J. W.; Hush, N. S. *J. Am. Chem. Soc.* **1987**, *109*, 3258. (b) Oliver, A. M.; Craig, D. C.; PaddonRow, M. N.; Kroon, J.; Verhoeven, J. W. *Chem. Phys. Lett.* **1988**, *150*, 366. (c) Warman, J. M.; Smit, K. J.; de Haas, M. P.; Jonker, S. A.; Paddon-Row, M. N.; Oliver, A. M.; Kroon, J.; Oevering, H.; Verhoeven, J. W. *J. Phys. Chem.* **1991**, *95*, 1979. (d) Lawson, J. M.; Paddon-Row, M. N.; Schuddeboom, W.; Warman, J. M.; Clayton, A. H. A.; Ghiggino, K. P. *J. Phys. Chem.* **1993**, *97*, 13099. (e) Roest, M. R.; Verhoeven, J. W.; Schuddeboom, W.; Warman, J. M.; Lawson, J. M.; Paddon-Row, M. N. *J. Am. Chem. Soc.* **1996**, *118*, 1762. (f) Jolliffe, K. A.; Bell, T. D. M.; Ghiggino, K. P.; Langford, S. J.; Paddon-Row, M. N. *Angew. Chem., Intl. Ed. Engl.* **1998**, *37*, 916.

(5) Gould, I.; Farid, S. *J. Am. Chem. Soc.* **1994**, *116*, 8176.

(6) Miller, J. R.; Beitz, J. V. *J. Chem. Phys*. **1981**, *74*, 6746.

(7) Cave, R. J.; Newton, M. D.; Kumar, K.; Zimmt, M. B. *J. Phys. Chem*. **1995**, *99*, 17501.

(8) (a) Matyushov, D. V. *Chem. Phys.* **1996**, *211*, 47. **(**b) Matyushov, D. V.; Schmid, R. *Mol. Phys*. **1995**, *84*, 533. (c) Matyushov, D. V.; Schmid, R. *J. Chem. Phys***. 1995**, *103*, 2034.

(9) Kumar, K.; Tepper, R. J.; Zeng, Y.; Zimmt, M. B. *J. Org. Chem.* **1995**, *60*, 4051.

(10) (a) Zeglinski, D. M.; Waldeck, D. H. *J. Phys. Chem.* **1988**, *92*, 692. (b) O'Connor, D. V.; Phillips, D. *Time Correlated Single Photon Counting*; Academic Press: New York, 1984.

(11) (a) Heitele, H.; Finckh, P.; Weeren, S.; Pöllinger, F.; Michel-Beyerle, M. E. *J. Phys. Chem.* **1989**, *93*, 5173. (b) Kroon, J.; Oevering, H.; Verhoeven, J. W.; Warman, J. M.; Oliver, A. M.; Paddon-Row, M. N. *J. Phys. Chem.* **1993**, *97*, 5065. (c) Asahi, T.; Ohkohchi, M.; Matsusaka, R.; Mataga, N.; Zhang, R. P.; Osuka, A.; Maruyama, K. *J. Am. Chem. Soc.* **1993**, *115*, 5665.

(12) (a) Marcus, R. A. *Annu. Rev. Phys. Chem.* **1964**, 15, 155. (b) Marcus, R. A. *J. Chem. Phys*. **1965**, *43*, 679.

(13) (a) Reynolds, L.; Gardecki, J. A.; Frankland, S. J. V.; Horng, M. L.; Maroncelli,

M. *J. Phys.Chem*. **1996**, *100*, 10337. (b) Gardecki, J.; Horng, M. L.; Papazyan, A.; Maroncelli, M. *J. Mol. Liq.* **1995**, *65*, 49.

(14) Jortner, J. *J. Chem. Phys*. **1976**, *64*, 4860.

(15) (a) Meyer, T. J. *Prog. Inorg. Chem.* **1983**, *30*, 389. (b) Miller, J. R.; Beitz, J. V.; Huddleston, R. K. *J. Am. Chem. Soc.* **1984**, *106*, 5057.

(16) Barbara, P. F.; Meyer, T. J.; Ratner, M. A. *J. Phys. Chem.* **1996**, *100*, 13148.

(17) Shephard, M. H.; Paddon-Row, M. N. *J. Phys. Chem. A* **1999**, *103*, 3347.

(18) (a) Hupp, J. T.; Neyhard, G. A.; Meyer, T. J. *J. Phys. Chem.* **1992**, *96*, 10820. (b) Dong, Y.; Hupp, J. T. *Inorg. Chem*. **1992**, *31*, 3322. (c) Dong, Y.; Hupp, J. T. *J. Am. Chem. Soc.* **1993**, *115*, 6428.

(19) (a) Chitanvis, S. M. *J. Chem. Phys.* **1996**, *104*, 9065. (b) Koga, K.; Tanaka, H.; Zeng, X. C. *J. Phys. Chem.* **1996**, *100*, 16711. (c) Bliznyuk, A. A.; Gready, J. E. *J. Phys. Chem.* **1995**, *99*, 14506. (d) Kim, H. J. *J. Chem. Phys.* **1996**, *105*, 6818. (e) Perng, B.-C.; Newton, M. D.; Raineri, F. O.; Friedman, H. L. *J. Chem. Phys*. **1996**, *104*, 713. (f) Perng, B.-C.; Newton, M. D.; Raineri, F. O.; Friedman, H. L. *J. Chem. Phys*. **1996**, *104*, 7177.

(20) Equations 2.9 and 2.14 given here are a correction of the originally published equations (ref 8). The authors thank Dmitry Matyushov for pointing out the errors.

(21) Ben-Amotz, D.; Herschbach, D. R. *J. Phys. Chem*. **1990**, *94*, 1038.

(22) In these systems, the $n = 0$ terms contribute greater than 95% of the rate calculated using eq 2.6.

(23) The λ_0 value less than 0.003 eV also produces the experimental slope at the indicated temperature; however, use of this λ_0 leads to a 5 order of magnitude reduction in the rate constant over the experimental temperature range, in contrast to the small change that is observed.

(24) In benzene, greater than 20% of the CT state of **2** decays by intersystem crossing to form the anthracene triplet state. Professor J. Goodman (University of Rochester), unpublished results.

(25) Vath, P. A.; Zimmt, M. B. Unpublished results.

(26) (a) Tepper, R. J.; Zimmt, M. B. *Chem. Phys. Lett.* **1995**, *241*, 566. (b) Corte´s, J.; Heitele, H.; Jortner, J. *J. Phys. Chem.* **1994**, *98*, 2527.

(27) The calculation of these curves requires values of $\Delta_r G(T)$, $d\Delta_r G(T)/dT$ and $d\lambda_0(T)/dT$. The $\Delta_r G(T)$ and $d\Delta_r G(T)/dT$ were obtained from the experimental data. The

$d\lambda_0(T)/dT$ was evaluated by the Matyushov model.

$$\text{slope} = \left[-\frac{(\Delta G + \lambda)^2}{4\lambda k_B}\right] + \frac{(\Delta G + \lambda)T}{2\lambda k_B}\left(\frac{\partial(\Delta G)}{\partial T}\right) + \frac{T}{k_B}\left[\frac{2\lambda k_B T + 2\lambda(\Delta G + \lambda) - (\Delta G + \lambda)^2}{4\lambda^2}\right]\left(\frac{\partial \lambda}{\partial T}\right)$$

Chapter 3 Electron Transfer in Aromatic Solvents: The Importance of Quadrupolar Interactions

Molecular solvation calculations are performed on a donor-bridge-acceptor (DBA) molecule in polar and nonpolar environments. A strictly dipolar treatment of solvation reproduces experimental values of the reaction free energy, $\Delta_r G$, determined in nondipolar and weakly dipolar aromatic solvents but does not simultaneously predict accurate values of $\Delta_r G$ in highly dipolar solvents. By contrast, a solvation model that includes contributions from solvent dipole and quadrupole moments (*J. Chem. Phys.* **1999**, 111, 3630[1]) reproduces $\Delta_r G$ values over a large polarity range. The reliability of the predicted $\Delta_r G$ and solvent reorganization energies, λ_0 are assessed through fitting experimental rate data. The fits display good agreement with the experimental data and the donor-acceptor electronic couplings derived via these analyses agree with prior determinations. The availability of a model that generates reasonable predictions of $\Delta_r G$ and λ_0 allows a first exploration of the temperature dependence of solvent mediated electronic coupling[2]

[2] This chapter was previously published as: Read, I.; Napper, A.; Zimmt, M. B.; Waldeck, D. H.; *J. Phys. Chem. A.;* **2000**; 104(4 1); 93 85-9394.

3.1 Introduction

Electron transfer between two chemical species or subunits represents a fundamental theme in many chemical transformations.[2,3,4] Although the understanding of electron transfer reactions has evolved considerably in the past few decades, the ability to quantify solvent effects on electron transfer rates with simple analytical models has remained elusive. Continuum models are the most widely used approaches to calculation of solvation and solvent reorganization energies.[5] This work combines recently obtained[5b,6a] electron transfer rate data over a range of solvent polarity with new data in 1,2,4-trimethylbenzene to evaluate two recently proposed molecular models for solvation and solvent reorganization energies in electron-transfer reactions.[1,7] The results demonstrate the importance of including quadrupolar interactions for the interpretation of rate data in nondipolar and weakly dipolar aromatic solvents.

In the past two decades, much of the progress toward understanding electron transfer reactions has been made in characterizing the electronic coupling between the electron donor (D) and acceptor (A) groups, and its dependence on the structural and chemical features of the system under study.[3] Donor-bridge-acceptor (DBA) systems figure prominently in these advances because of their ability to control the D/A geometry at which transfer occurs. The electron transfer rate constant's dependence on bridge length, bonding topology, state symmetry, and solvent environment have been characterized.[3,4] In systems where the D and A groups are widely separated, the (nonadiabatic) transfer is viewed as an electron tunneling event, mediated by the orbitals of the intervening atoms (or molecules). A perturbation treatment of this

process, known as "superexchange",[8] successfully describes the D/A electronic interactions, whether they occur through space,[9] through covalent bridges,[4] or through solvent molecules.[6]

Recent studies from our collaboration[5b,6a,10] focus on understanding electron transfer in highly curved DBA molecules. In these molecules, solvent influences the transfer dynamics through solvation and by mediating the superexchange interaction between the D and A groups. Given tractable theories of solvation and solvent-mediated superexchange, an accurate separation of these two effects is a particular challenge.

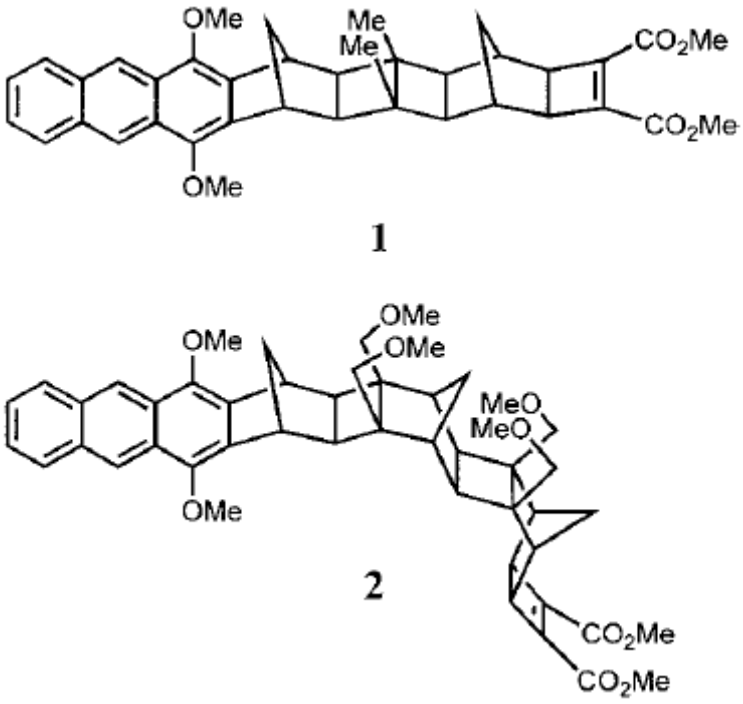

Figure 3.1 Molecular structure of the DBA molecules used in this work.

This study explores the ability of two recent molecular treatments of solvation[1,7] to reproduce the solvent's influence on the thermodynamics of electron transfer and to allow precise determination of the electronic coupling as a function of solvent and temperature. The DBA structures used in these investigations are shown in Figure 3.1. Each molecule consists of (1) a dimethoxyanthracene unit that acts as the electron donor upon promotion to its lowest singlet excited state, (2) a cyclobutene dicarboxylate derivative that acts as the electron acceptor, and (3) a rigid, connecting bridge. The dominant source of D/A coupling in **1** is superexchange mediated by the linear bridge.[5b,10] Thus, the solvent's primary influence on the transfer dynamics in **1** is by way of solvation. The curved bridge in **2** forms a cleft between the donor and acceptor units. The cleft is sufficiently large to accommodate a solvent molecule. The magnitude and solvent dependence of the electron-transfer rate constants in **2** demonstrate that solvents, and in particular aromatic solvents, effectively mediate the required D/A interactions.

The rate constants obtained from these studies are interpreted through the semiclassical expression for the rate constant,[11]

$$k_{ET} = \frac{2\pi|V|^2}{\hbar\sqrt{4\lambda_o \pi k_B T}} \sum_{n=0}^{\infty} e^{-S}\left(\frac{S^n}{n!}\right) \exp\left[\frac{-(\Delta_r G + \lambda_o + nh\nu)^2}{4\lambda_o k_B T}\right] \quad (3.1)$$

where $\Delta_r G$ is the reaction free-energy, λ_0 is the outer-sphere (solvent) reorganization energy, ν is the frequency of the effective vibrational mode, and S is the Huang-Rhys factor given as the ratio of the inner-sphere reorganization energy, λ_i to $h\nu$ This treatment assumes that the molecule's vibrational modes can be represented using a

single effective high-frequency mode. The low- frequency solute and solvent vibrational modes are treated classically. The electronic coupling |V| is typically estimated or calculated. A major focus of this and our previous studies is to extract the coupling magnitude from experimental rate data.

Experimental determination of each parameter ($\Delta_r G$, ν, λ_i, λ_0, |V|) in eq 3.1 is desirable, although never achieved. Typically, the effective mode frequency ν and λ_i values are determined through fitting of experimental data (such as charge-transfer spectra[12]) or are calculated quantum chemically. The value of $\Delta_r G$ is often estimated through a combination of experimental redox data and dielectric continuum corrections to the solvation energy. The outer sphere reorganization energy λ_0 is usually calculated from continuum solvation theory, or in some cases may be extracted from charge-transfer spectra. A major problem with the dielectric continuum model is its failure to reproduce solvation and reorganization energies in nondipolar solvents[13] and its prediction of unreasonable temperature dependencies in highly dipolar solvents.[7] To date, molecular based models which are applicable in nondipolar or weakly dipolar solvents are unable to predict physically meaningful results in polar environments.[14] A need exists for a model capable of computing free energies and reorganization energies across a large polarity range. Once appropriate values of the four solvation and reorganization parameters are generated, the electronic coupling |V| can be extracted from experimental rate data. The absolute magnitude of the calculated electronic coupling is a strong function of the parameter set used. Nonetheless, comparisons between appropriately chosen systems are robust (see ref 10 for a detailed discussion of this issue).

The reaction free energy, $\Delta_r G$, for charge separation within **2** in aromatic solvents was previously evaluated directly from the rate constants of charge separation ($S_1 \rightarrow$ CT) and recombination (CT $\rightarrow S_1$) that interconvert the anthracene excited state (S_1) and the charge transfer state (CT).[6a] That investigation also demonstrated a very weak temperature dependence of the outer-sphere reorganization energy, λ_0 .[15] In conjunction with λ_i and ν values from CT spectra and calculations,[16] it was possible to extract the electronic couplings for **2** in each solvent without the need for calculation of $\Delta_r G$ and λ_0. The experimental $\Delta_r G$ and λ_0 were compared to the predictions of a molecular based solvation model that accounted for solvent molecule dipole moment and polarizability.[6a,14] This model was able to reproduce the experimentally measured $\Delta_r G$ values and predicted a reasonable temperature dependence for λ_0 in a variety of alkyl substituted benzene solvents.

This work presents the application of recently developed molecular based solvation models[1,7] to the thermodynamic and rate data from **2** for a wide range of solvents and as a function of temperature. The more recently developed molecular model accounts for solvent dipole and quadrupole interactions with the solute and incorporates second-order contributions to the solvation chemical potential.[1,7] This model should provide a more realistic description of $\Delta_r G$ and λ_0 as a function of solvent and temperature. This work has two goals. First, it assesses the ability of the solvation models to mimic experimentally measured reaction free energies in nondipolar and weakly dipolar solvents and predict those in highly dipolar solvents. Second, it uses the calculated reorganization energies and reaction free energies to extract the solvent dependence of the electronic coupling $|V|$. The ultimate objective is

to generate a thorough understanding of solvent's roles in determining the barrier, which impedes, and the coupling, which promotes, electron transfer.

3.2 Background

3.2.1. Continuum Prediction of $\Delta_r G$ and λ_0.

A crude, but often useful, treatment of the electron-transfer energetics models the solvent as a dielectric continuum. In this treatment, the donor- acceptor moieties are typically represented as individual spheres immersed in the continuum and separated by a distance, R_{CC}. $\Delta_r G$ is calculated using the Rehm-Weller equation,[17]

$$\Delta_r G = \Delta_{vac} G + \frac{e^2}{4\pi\epsilon_o}\left(\frac{1}{2r_d} + \frac{1}{2r_a} - \frac{1}{R_{cc}}\right)\left(\frac{1}{\epsilon} - 1\right) \tag{3.2}$$

where $\Delta_{vac}G$ is the free energy of the electron transfer in a vacuum, e is the charge on the electron, and ε is the solvent's static dielectric constant. r_d and r_a are the spherical radii of the donor and acceptor. Results from these calculations are used to provide a reference point for the molecular model's predictions. The solvent reorganization energy may also be calculated using continuum theory, by the relation

$$\lambda_o = \frac{e^2}{4\pi\epsilon_o}\left(\frac{1}{2r_d} + \frac{1}{2r_a} - \frac{1}{R_{cc}}\right)\left(\frac{1}{\epsilon_\infty} - \frac{1}{\epsilon}\right) \tag{3.3}$$

where ε_∞ is the high-frequency dielectric constant, taken to be the square of the solvent's refractive index.

3.2.2. Molecular Model for $\Delta_r G$.

In earlier work, a dipolar, polarizable hard sphere model for the solvent was used to compute both $\Delta_r G(T)$ and $\lambda_0(T)$ for **2** in weakly dipolar aromatic solvents.[6a,14] The model treated the solute as a polarizable sphere with different permanent dipole moments for the locally excited and charge transfer states. The model was developed particularly for application to weakly dipolar systems and is expected to fail in highly dipolar solvents since solute-solventsolvent correlations are neglected. The present investigation uses a more sophisticated treatment of the solute-solvent interactions and compares two separate approaches to the modeling. First, the $\Delta_r G$ values are computed using a revised dipolar, polarizable model.[7] This treatment includes higher order contributions to the solvation energy, thus providing a more accurate description of solvation in highly dipolar solvents. Second, a solvation model that also explicitly incorporates quadrupolar interactions is used to compute the solvation energies.[1] In both cases, the gas phase solvent dipole moments are renormalized to account for inductive dipolar and quadrupolar (when relevant) interactions with the surrounding solvent. This renormalization procedure is outlined by Gray and Gubbins.[18]

Matyushov calculates $\Delta_r G$ as the sum of four contributions,

$$\Delta_r G = \Delta_{vac} G + \Delta_{dq,i} G^{(1)} + \Delta_{disp} G + \Delta_i G^{(2)} \tag{3.4}$$

where $\Delta_{vac} G$ is the free energy of the process in a vacuum, $\Delta_{dq,i} G^{(1)}$ is the contribution from first- order dipole, quadrupole, and induction interactions, $\Delta_{disp} G$ is the contribution from dispersion interactions and $\Delta_i G^{(2)}$ is the contribution from second-order induction

interactions. The $\Delta_{dq,i}G^{(1)}$ term includes dipole-dipole and dipole-quadrupole interactions between the solute dipole and the solvent electric moments and includes the induction interactions that arise from the polarizability of both the solute and solvent. It is calculated through the relationship

$$\Delta_{dq,i}G^{(1)} = -\frac{(m_e^{\,2} - m_g^{\,2})}{R_{eff}^{\,3}} f(y_d, y_q)\, \Psi^P(y_d, y_q) \tag{3.5}$$

where m_e is the solute dipole moment of the charge transfer state, and m_g is the reactant state dipole moment. The function $f(y_d, y_q)$ renormalizes the solute dipole moment to account for its size and polarizability. It is given by

$$f(y_d, y_q) = \left[1 - \frac{2\alpha_0}{R_{eff}^{\,3}} \Psi^P(y_d, y_q)\right]^{-1} \tag{3.6}$$

Here α_0 is the solute polarizability and $\Psi^P(y_d, y_q)$ is referred to as the "polarity response function". R_{eff} represents the effective radius of a spherical dipolar solute. It accounts for the local packing of solvent molecules against the solute sphere and is determined through the solute-solvent hard sphere pair distribution function, $g^{(0)}(r)$, namely

$$\frac{1}{R_{eff}^{\,3}} = 3\int_0^\infty \frac{dr}{r^4} g_{0s}^{(0)}(r) \tag{3.7}$$

Matyushov evaluated the integral numerically and fit it to the following polynomial form; i.e.

$$\frac{1}{R_{\text{eff}}^{\,3}} = \frac{I_{0s}^{(2)}}{\sigma^3} \tag{3.8}$$

The form of the $I_{0s}^{(2)}$ is given explicitly in the Appendix. The polarity response function, $\Psi^{P}(y_d, y_q)$, is written in terms of the reduced dipolar density, y_d , the quadrupolar density, y_q, and the solute-solvent perturbation integrals. The densities are computed using the relations

$$y_{\text{d}} = \frac{4\pi}{9}\frac{\rho}{kT}m'^2 + \frac{4\pi}{3}\rho\alpha \tag{3.9a}$$

$$y_{\text{q}} = \frac{2\pi}{5}\frac{\rho}{\sigma^2 kT}Q^2 \tag{3.9b}$$

where Q is the average quadrupole moment (Table 3.2), m' is the renormalized solvent dipole moment,[1,7] ρ is the solvent number density, α is the solvent polarizability, and σ is the solvent hard sphere diameter. Matyushov[1,7] has shown that the perturbation integrals are well represented by a polynomial interpolation and writes $\Psi^{P}(y_d, y_q)$ as

$$\Psi^{\text{P}}(y_{\text{d}}, y_{\text{q}}) = \frac{\dfrac{y_{\text{d}}I_{0s}^{(2)} + y_{\text{q}}I_{6}^{(2)}}{I_{0s}^{(2)}}}{1 + \dfrac{y_{\text{d}}^{\,2}\kappa_{\text{d}}I_{0s}^{(3)} + y_{\text{d}}y_{\text{q}}\kappa_{\text{dq}}I_{\text{DDQ}}^{(3)} + y_{\text{q}}^{\,2}\kappa_{\text{q}}I_{\text{DQQ}}^{(3)}}{y_{\text{d}}I_{0s}^{(2)} + y_{\text{q}}I_{6}^{(2)}}} \tag{3.10}$$

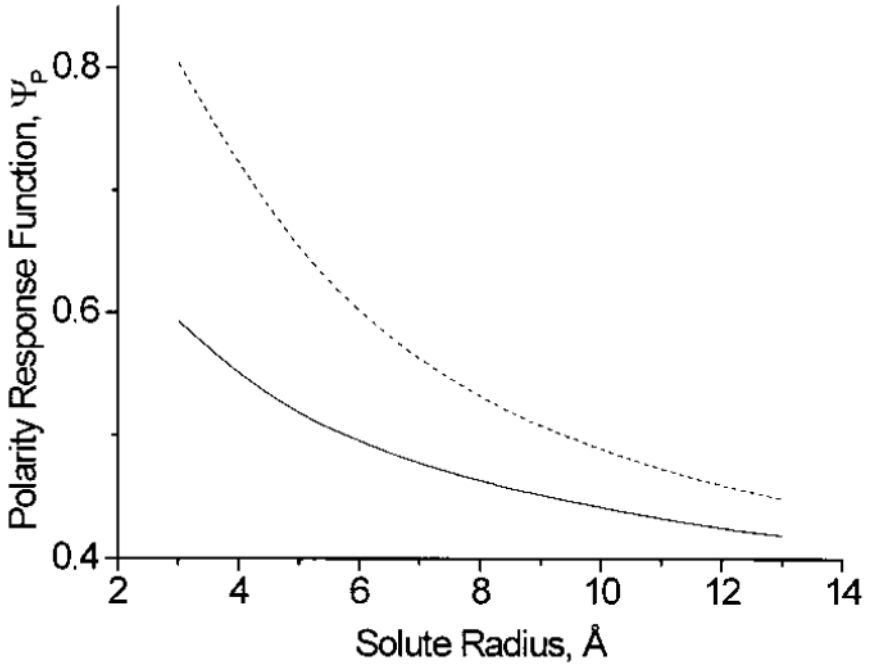

Figure 3.2 Behavior of the polarity response function for the dipole (solid line, <Q> = 0 D Å) and dipole-quadrupole (dashed line, <Q> = 3 D Å) models are shown as a function of the solute radius.

The explicit form of the polynomial interpolation for the two-and three-particle perturbation integrals ($I^{(2)}$, $I^{(3)}$) are written in the Appendix.[19] The κ_i parameters correct for saturation of the solvent response that arises from three particle (solute-solvent- solvent) correlations.[1] These factors depend on the ratio of solute-solvent diameters, $d = 2R_0/\sigma$ through the relations,

$$\kappa_d = 1 + \left[\frac{d}{(d+1)}\right]^2 \qquad \kappa_q = 2 + \frac{1}{(d^5+2)}$$

$$\kappa_{dq} = 2 - \frac{d^5}{(d^5+2)}$$

Figure 3.2 shows the dependence of the response function (eq 3.10) on the effective solute radius, R_0, for the dipole model (Q = 0, solid line) and the dipole-

quadrupole model (Q = 3.0 DÅ, dashed line). These calculations were performed using constant values for the solvent hard sphere diameter (5 Å), solvent polarizability (10 $Å^3$), and dipole moment (2 D). The solute polarizability and dipole moment were chosen to be 70 $Å^3$ and 34 D, respectively. In both models, the magnitude of the calculated response function decreases with increasing solute radius. According to eq 3.5, the predicted free energies become more negative as the size of the solute decreases. Figure 3.2 also shows that inclusion of quadrupolar interactions increases the magnitude of the polarity response function. This behavior indicates that quadrupolar interactions are stabilizing, and that their inclusion will require a larger solute radius, relative to the dipolar model, to reproduce a given value of the reaction free energy, $\Delta_r G$

Second-order induction interactions of the solute dipole with the solvent molecules are accounted for by the $\Delta_i G^{(2)}$ term. These interactions arise from correlations of polarization fluctuations generated by the solvent's induced dipoles.[7] Matyushov relates these interactions to the solvent polarizability and the high-frequency dielectric constant, ε_∞ , and writes,

$$\Delta_i G^{(2)} = -(m_e{}^4 - m_g{}^4) f(y_e) \frac{1}{200\pi\rho kT} \frac{(\epsilon_\infty - 1)^2}{(\epsilon_\infty + 2)^2} \times [9 + 8(\epsilon_\infty - 1)^2] I_{0s}^{(4)} \tag{3.11}$$

where the quantity $y_e = (4\pi/3)\rho\alpha$ is the reduced polarizability density of the solvent. The function $f(y_e)$ renormalizes the solute dipole by the polarizability response of the solvent. Its value is calculated using

$$f(y_e) = \left[1 - \frac{2\alpha_0}{R_{eff}^3}\Psi^P(y_e)\right]^{-1} \tag{3.12}$$

The polarizability response function, $\Psi^P(y_e)$ is given by

$$\Psi^P(y_e) = \frac{y_e}{1 + \kappa_d y_e I_{0s}^{(3)}/I_{0s}^{(2)}} \tag{3.13}$$

Note that eq 3.13 is derived directly from the polarity response function (eq 3.10). When the solvent has no permanent dipole or quadrupole moment, the polarizability response function of the fluid is given by this term.

The dispersion contribution, $\Delta_{disp}G$ has a relatively small effect on the overall free energy (see Table 3.7). Its value can be calculated from the solvent-solvent Lennard-Jones energy, ε_{LJ} and the solvent hard sphere diameter σ. These parameters were obtained through the additivity method described by Ben-Amotz[20]. $\Delta_{disp}G$ is given by

$$\Delta_{disp}G = -\frac{\Delta\gamma'}{\alpha_s} 8\eta\epsilon_{LJ}\left(\frac{\sigma}{R_{eff}}\right)^3 \tag{3.14}$$

where η is the reduced packing density, defined as $(\pi/6)\rho\sigma^3$ and α_S is the solvent polarizability. The parameter $\Delta\gamma'$ is determined by

$$\Delta\gamma' = \Delta\alpha_o \frac{2I_o}{I_o + I_s} \tag{3.15}$$

where $\Delta\alpha_0$ is the change in polarizability between the locally excited state and the charge transfer state of the solute, I_0 is the ionization potential of the solute and I_s is the ionization potential of the solvent $\Delta\gamma'$ is one of three adjustable parameters determined by a simultaneous fit of the experimental Δ_rG values measured as a

function of temperature in all of the alkylated benzene solvents (The best fit values are reported in Table 3.1). Values for the individual contributions to $\Delta_r G$ are listed in Table 3.7.

3.2.3. Molecular Model for the Reorganization Energy, λ_0.

The same polarizable hard-sphere model[1] is used to compute the reorganization energy λ_0. The reorganization energy is written as a sum of three components $\lambda_0 = \lambda_p + \lambda_{ind} + \lambda_{disp}$ where λ_p accounts for solvent reorganization arising from the solvent dipole and quadrupole moments, λ_{ind} is the contribution from induction forces and λ_{disp} accounts for the dispersion interactions. An expression for λ_p was derived using the linear response approximation for the chemical potential,[14] so that

$$\lambda_p = \frac{(m_e - m_g)^2}{R_{eff}^3}[f(y_d, y_q)\,\Psi^P(y_d, y_q) - f(y_e)\,\Psi^P(y_e)] \tag{3.16}$$

where $\Psi^P(y_d, y_q)$ is given by eq 3.10 and $\Psi^P(y_e)$ is given by eq 3.13. This contribution accounts for the reequilibration of the solvent's nuclear modes to the newly formed electronic configuration of the charge transfer state. Although the induction forces make a relatively small contribution to the overall reorganization energy in highly polar solvents, in weakly polar systems the dipolar contributions are small and induction interactions are significant. According to ref 7, the induction term can be calculated through,

$$\lambda_{ind} = \frac{(m_e^2 - m_g^2)^2 f(y_e)^2}{kT400\eta\sigma^6}\frac{(\epsilon_\infty - 1)^2}{(\epsilon_\infty + 2)^2}\left[3 + \frac{8}{3}(\epsilon_\infty - 1)^2\right]I_{0s}^{(4)} \tag{3.17}$$

The polynomial form of the two-particle perturbation integral $I_{0s}^{(4)}$ is given in the Appendix. The contribution from the dispersion forces is expected to be small in both dipolar and nondipolar solvents and in most cases these energies can be neglected. However, they can become significant if the solvent diameter and density is large. Matyushov defines λ_{disp} as a second- order perturbation over the solute-solvent dispersion potential so that

$$\lambda_{\text{disp}} = \frac{\Delta\gamma'^2}{\alpha_s^2}\frac{8\eta}{3}\beta\epsilon_{\text{LJ}}{}^2 J_1(\rho^*, r_{0s}) \tag{3.18}$$

The polynomial form of the integral J_1 is given in the Appendix along with the calculated values of λ_0, λ_p, λ_{disp}, λ_{ind} predicted by the two treatments.[22]

Table 3.1 Best Fit Parameters Used in $\Delta_r G$ Calibrations.

	model		
	dipole	dipole−quadrupole	lit.[a]
solute radius (Å)	6.19	7.25	
$\Delta_{vac}G$ (eV)	0.326	0.340	
$\Delta\gamma'$ (Å^3)	−9.5	1.7	
	Solvent Polarizability (Å^3)		
benzene	10.3	9.5	10.0
toluene	11.8	10.9	11.8
cumene	15.5	16.3	16.0
mesitylene	15.2	14.8	15.5
TMB[b]	14.6	15.5	
TIP[c]	26.9	31.7	31.8[d]

[a] Literature values obtained from *CRC Handbook*, 78th ed.; CRC Press: Boca Raton, FL, 1998. [b] TMB is 1,2,4-trimethylbenzene. [c] TIP is 1,3,5-triisopropylbenzene. [d] Literature value could not be found. Value listed is for 1,3,5-tri-*tert*-butylbenzene.

3.3 Results and Discussion

3.3.1. Calculation of $\Delta_r G$.

Simulation of the $\Delta_r G$ values using the molecular model requires determination of three parameters: $\Delta_{vac} G$ the solute radius R_0 and $\Delta\gamma'$. The $\Delta_r G$ values for **2** in every solvent (benzene, toluene, cumene, mesitylene, 1,2,4-trimethylbenzene (TMB), and triisopropylbenzene (TIP)) and temperature were fit, simultaneously, to eq 3.4 using Microsoft Excel 97 on a Pentium based PC. The solvent dipole and quadrupole moments were calculated at the RHF/6-31G**// RHF/6-31G** level of theory using Gaussian 98[23] on a Silicon Graphics Power Indigo workstation (Tables 3.2 and 3.3). The effective quadrupole moment <Q> reported in Table 3.3 was used in the calculations. This effective quadrupole gives exact results for axially symmetric quadrupole tensors and is correct through second order for nonaxially symmetric quadrupole tensors. With the exception of benzonitrile, the quadrupole tensors of the investigated solvents are axially symmetric, or nearly so. The dipole moment of the anthracene excited state was set to 0 D and the dipole moment of the charge separated state was calculated to be 34D.[24] In previous work, the solute polarizability was estimated as 100 $Å^3$, but recent calculations (RHF/6-31+G(d)) suggest that this value is too high and a solute ground-state polarizability of 70 $Å^3$ was used. After initial values of the three parameters were determined, the literature value of the solvent's polarizability was adjusted (<10%) to improve the fits (see Table 3.1). The solvent parameters used in the calculations are given in Tables 3.1-3.3.

Table 3.2 Solvent Parameters Used in Matyushov Modeling[a]

solvent	m^b (D)	σ^c (Å)	$\epsilon_{LJ}{}^d$ (K)	η^e
benzene	0	5.28	544	0.520
toluene	0.29	5.68	603	0.543
cumene	0.25	6.29	679	0.561
mesitylene	0.07	6.40	720	0.593
TMB	0.30	6.31	720	0.579
TIP	0.08	7.40	949	0.552
acetonitrile	4.06	4.14	405	0.425
benzonitrile	4.2	5.68	698	0.562

[a] TMB is 1,2,4-trimethylbenzene. TIP is 1,3,5-triisopropylbenzene. [b] The vacuum dipole moment. [c] The hard sphere solvent diameter. [d] The Lennard-Jones energy parameter. [e] The packing fraction at 295 K.

Table 3.3 Diagonal Quadrupole Moment Tensor Components Used To Compute <*Q*> [a]

solvent	Q_{xx} (D Å)	Q_{yy} (D Å)	Q_{zz} (D Å)	$\langle Q \rangle$ (D Å)
benzene	4.146	4.146	−8.288	8.288
toluene	4.122	4.122	−7.893	7.896
cumene	3.624	4.206	−7.830	7.836
mesitylene	3.954	3.519	−7.464	7.467
TIP	2.848	4.835	−7.683	7.770
TMB	4.209	3.088	−7.299	7.326
acetonitrile	−3.369	1.685	1.685	3.369
benzonitrile	−12.61	13.82	−1.214	15.39

[a] TMB is 1,2,4-trimethylbenzene. TIP is 1,3,5-triisopropylbenzene. $\langle Q \rangle = |\sqrt{{}^2/_3 \Sigma Q_{ii}{}^2}|$.

Figure 3.3 presents the fits of the two models to the experimental $\Delta_r G$ data, and Table 3.1 presents the parameter set for each fit. It is clear from the plots that both models can reproduce the data in nondipolar solvents but they predict very different $\Delta_r G$ values in highly dipolar solvents. In the nitrile solvents the $S_1 \leftrightarrow$ CT equilibrium was not measurable. As a result a comparison of calculated and experimental $\Delta_r G$ values is not possible. The best fit value of the solute radius in the dipole-quadrupole model, 7.25 Å, is considerably larger than in the dipole analysis, 6.19 Å. This difference is consistent with the larger polarity response function and increased stabilization energy predicted by the model that includes solvent quadrupoles (Figure 3.2). AM1 calculations of **2** indicate that a sphere of ~7.0 Å is required to fully encapsulate the solute. This result is consistent with the best fit solute radius found using the dipole-quadrupole model. The best fit $\Delta\gamma'$ was found to be ~-9.5 $Å^3$ for the dipole model and 1.7 $Å^3$ for the dipole-quadrupole model. In both cases, the small size of $\Delta\gamma'$ suggests similar polarizabilities for the LE and CT states. In the dipole-quadrupole model the dispersion makes a neglible contribution to the reaction free energy. In the dipole model the dispersion term plays a significant role in determining the proper ordering of $\Delta_r G$ with solvent. Quantum chemical calculations of $\Delta_{vac} G$ were performed using the vacuum ionization potentials and electron affinities of the donor-acceptor pair. The results predict that $\Delta_{vac} G$ is ~ 1.1 ± 1.0 eV. Table 3.1 shows that the best fit value for each model lies within the uncertainty limit of the calculation. Since the values of $\Delta_{vac} G$ for each model are similar, their absolute magnitude is not expected to effect the overall results. Among the three fit parameters, variation of the solute hard sphere radius, R_0,

between the values determined in the two models, exerts the greatest impact on the fitting results.

Figure 3.3 shows that both molecular approaches accurately reproduce the observed free energies in nondipolar and weakly dipolar solvents. Because of model specific differences in the best fit solute parameters, the predicted $\Delta_r G$ values are strikingly different in the nitrile solvents. The dipolar model predicts a free energy of -1.47 eV in acetonitrile and - 1.57 eV in benzonitrile at 300 K, whereas the dipole-quadrupole model predicts a $\Delta_r G$ of -0.71 eV in acetonitrile and -0.88 eV in benzonitrile. It is evident that use of the dipole-quadrupole model leads to significantly smaller estimates of the reaction exoergocity in polar solvents. The experimental redox potentials in acetonitrile place the energy of the infinitely separated D^+ and A^- ions -0.51 eV below the energy of the anthracene excited state.[16] Use of continuum models for Coulomb attraction and solvation corrections (eq 3.2) suggest the $\Delta_r G$ values are -0.56 eV in acetonitrile and -0.53 eV in benzonitrile (Table 3.4). These comparisons indicate that the dipole model predicts unrealistically negative $\Delta_r G$ values in both of the nitrile solvents. The inclusion of quadrupole moments when fitting the data in the nondipolar and weakly dipolar aromatic solvents provides more realistic solute parameters and generates more reasonable $\Delta_r G$ values across a wider range of polarity. The dipole-quadrupole model's prediction of a more negative $\Delta_r G$ in benzonitrile than in acetonitrile arises from the difference in their quadrupole moments and warrants comment. The model[1] assumes that the dipole moment vector and the principal axis of the quadrupole tensor are collinear, which is incorrect for benzonitrile. Since the quadrupole tensor of benzonitrile is nonaxial, corrections

beyond second order may be important.[25] As a result the sum of the two solvation contributions may be less effective than that predicted by the model.

Table 3.4 Experimental and Calculated $\Delta_r G$(eV) at 295 K [a]

		model		
	expt	dipole	dipole−quadrupole	continuum
benzene	−0.109	−0.112	−0.115	−0.072
toluene	−0.089	−0.086	−0.083	−0.094
cumene	−0.058	−0.054	−0.051	−0.094
mesitylene	−0.039	−0.033	−0.032	−0.070
TMB	−0.064	−0.062	−0.057	−0.060
TIP[b]	−0.013	−0.020	−0.018	−0.070
acetonitrile		−1.467	−0.713	−0.560
benzonitrile		−1.570	−0.882	−0.530

[a] TMB is 1,2,4-trimethylbenzene. TIP is 1,3,5-triisopropylbenzene.
[b] Results tabulated at 282 K.

For the dipole model, the dipolar density, y_d, is the primary solvent parameter controlling the magnitude of the polarity response function. It accounts for interactions involving the solvent permanent dipole and the solvent polarizability (eq 3.9a). Many of the aromatic solvents employed in this investigation possess small (or zero) permanent dipole moments; thus the stabilization energy from induction forces dominates $\Delta_r G$. Since these interactions are small, the experimental free energies and their temperature dependencies are reproduced by decreasing the solute radius, which enhances the solvent's polarity response function, $\Psi^P(y_d, 0)$. Although the required, best fit solute radius is clearly too small, one obtains a reasonable fit to the data in a similar set of solvents, such as the alkylbenzenes. However, in those

solvents where the polarity response function is dominated by permanent dipole moments, as in acetonitrile and benzonitrile, the small cavity radius predicts unrealistically large solvation energies. The small differences between the predicted $\Delta_r G$ values in acetonitrile and benzonitrile result from their different polarizabilities.

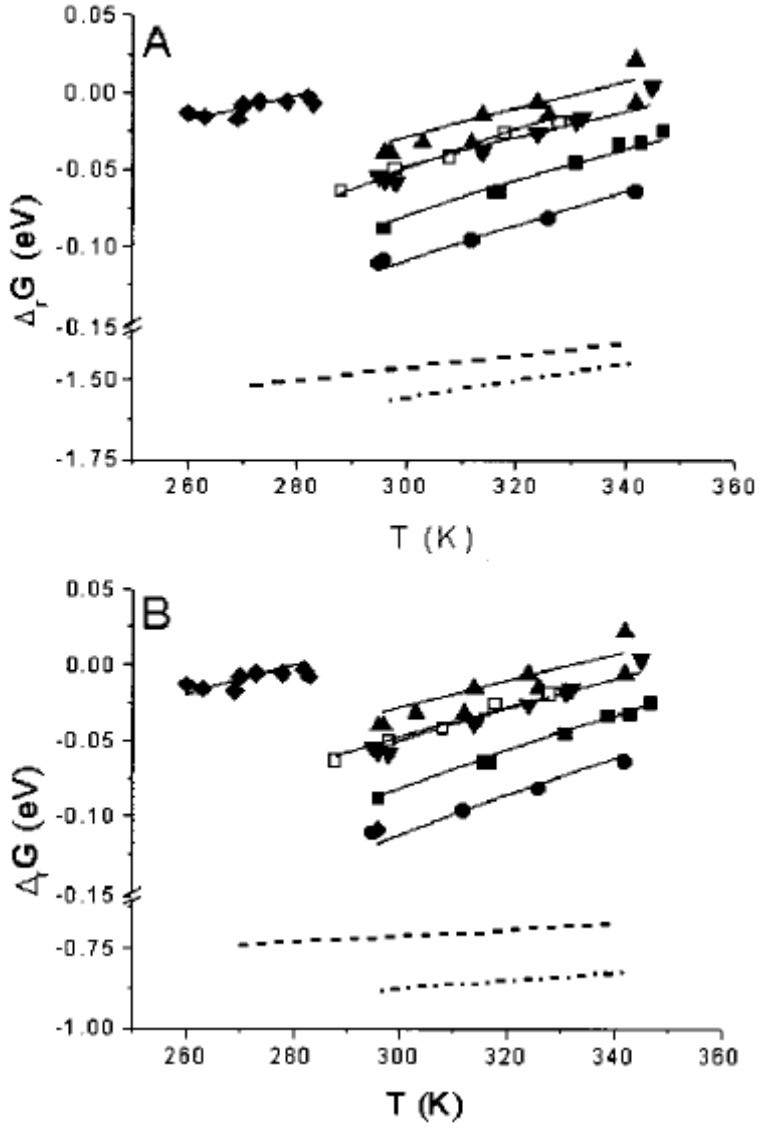

Figure 3.3 The lines show the temperature-dependent free energies calculated using the dipole model in panel A and the dipole-quadrupole model in Panel B. The solid lines show the predicted free energies in alkylbenzenes, the dashed line shows the predicted free energy in acetonitrile and the dashed-dotted line shows the predicted free energy in benzonitrile. Experimental data is shown for benzene (●), toluene (■), cumene(▼), mesitylene (▲), TMB (□) and TIP (♦). Note that the y-axis is broken in both plots.

Inclusion of quadrupole solvation provides a more realistic description of the intermolecular forces experienced by the solute in aromatic solvents. The best fit solute radius is larger than that found with the dipole model and is in reasonable agreement with the molecule's van der Waals radius. The $\Delta_r G$ values calculated using the dipole-quadrupole model are shown in Figure 3.3B. (The dipole-quadrupole polarity response function (eq 3.10) includes both y_d and y_q.) For the nondipolar and weakly dipolar aromatic solvents, y_q and y_d are comparable, so that one observes a large increase in the stabilization energy for the quadrupole model compared to the dipole model. This produces a 1.1 Å increase in the best fit solute radius compared to the dipole only model. As a result, the $\Delta_r G$ values in the nitrile solvents are markedly different from those calculated when the quadrupole terms are not included (see Table 3.4). This change reflects the decreased solvation provided by the dipole density for larger R_0 values. Because the quadrupolar density makes only a small contribution to the polarity response function in acetonitrile, the $\Delta_r G$ value is largely determined by dipole interactions.

The results show that the dipole-quadrupole model can predict reasonable $\Delta_r G$ values across a wide range of polarity. For comparison, calculations of $\Delta_r G$ using continuum theory are presented in Table 3.4. The results show that these solvents can be divided into three groups: nondipolar (benzene, mesitylene, TIP), weakly dipolar (toluene, cumene), and highly dipolar (acetonitrile, benzonitrile). In each group, the continuum estimates are identical: -0.07 (nondipolar), -0.094 (weakly dipolar), and ~ -0.54 (highly dipolar). As expected, these results do not agree with experiment. The value of $\Delta_r G$ in the alkylated benzene solvents are determined primarily by the size of

the solvent molecules (an observation consistent with the solvents ability to pack against the solute). For the nitrile solvents, exact experimental data is not available, but because the quadrupole moment of acetonitrile is significantly smaller than benzonitrile, one expects different $\Delta_r G$ values in these two solvents. In addition, the continuum model overestimates the stabilization energy of the weakly dipolar solvents toluene and cumene. These findings confirm the inability of the continuum model to reproduce the experimentally determined $\Delta_r G$ values.

3.3.2. Calculation of the Reorganization Energy.

Table 3.7 presents the calculated λ_0 values from both models and list the individual contributions to the reorganization energy as a function of temperature. Although the calculated λ_0 are physically reasonable, it is difficult to assess their accuracy as very little experimental data is available for λ_0, In the nondipolar and weakly dipolar solvents, the dipole only model predicts λ_{ind} to be the dominant contributor to the overall reorganization energy. In contrast, when the quadrupole moments are included, λ_p is the dominant term in every solvent. This result can be understood in terms of the dipole and quadrupole densities. In the dipole model, dipolar and polarization interactions contribute to the polarity response function of the fluid. For a nondipolar solvent, $\Psi^P(y_d, 0)$ and $f(y_d, 0)$ reduce to $\Psi^P(y_e)$ and $f(y_e)$, respectively. The two terms in eq 3.16 cancel and λ_p is zero. If the solvent molecule possesses a dipole moment, the dipolar density increases to a value greater than the polarizability density, y_e, In highly polar solvent, e.g., nitriles, the dipole contribution

dominates. In the dipole-quadrupole model, λ_p contains an additional contribution from the quadrupole density, y_q. Because the quadrupole density exceeds the polarizability density in every solvent, λ_p always makes the dominant contribution to the overall reorganization energy. The best fit solute radius is larger when quadrupole moments are included in the data fitting; thus contributions from induction forces are reduced compared to those in the dipole model. Both the dipole and dipole-quadrupole models suggest that λ_0 decreases with increasing temperature in all solvents. This prediction agrees with experimental results.[7,26] By contrast, the continuum model predicts that λ_0 increases with temperature in highly dipolar solvents.

Dispersion interactions make negligible contributions to λ_0 in highly dipolar solvents but increase in importance as the polarity of the solvent decreases. According to eq 3.18, λ_{disp} depends quadratically on the Lennard-Jones energy ε_{LJ} (the magnitude of which is correlated to the size and number of substituents on the aromatic ring[20]) and the reduced packing density, η. The dipole model predicts significant λ_{disp} values in the nondipolar aromatic systems because of the increased contribution from the perturbation integral, J_1. This contribution is less significant for larger values of R_0. As a result, the dipole-quadrupole model predicts negligible values for λ_{disp} in every solvent.

3.3.3. Fitting the Rate Constants.

With values for λ_i, ν, λ_0, and $\Delta_r G$ it is possible to fit the experimentally determined electron-transfer rate data to the semiclassical rate equation and to determine the electronic coupling, |V|. As discussed elsewhere for **2**,[10] λ_i was taken to

be 0.39 eV and ν was taken to be 1410 cm^{-1}. The rate constants were fit using the results from both the dipole and the dipole- quadrupole model. As found previously,[6a] attempts to reproduce the observed rate constants using the λ_0 predicted by the models and a constant |V| were not entirely successful. The solid lines in Figure 3.4 show the predicted temperature dependence of the electron-transfer rate constants in the nitrile solvents. These curves were obtained using the $\Delta_r G$ and λ_0 derived from the dipole-quadrupole model and a temperature independent value of |V|. Clearly, the fits are poor. The dashed lines represent fits in which |V| and λ_0(295 K) are treated as adjustable parameters. The temperature dependence of the reorganization energy was predicted by the dipole- quadrupole model. These fits are excellent and predict electronic couplings of 27 cm^{-1} in acetonitrile and 93 cm^{-1} in benzonitrile. These values agree well with those found from an earlier continuum treatment,[5b] but are 4-5-fold larger than values predicted using an alternate ion pair solvation model.[10]

Two different approaches were taken to fit the data in the alkylated aromatic solvents. In the first approach, the $\Delta_r G$ and $d\lambda_0/dT$ were taken from the model. Both |V| (assumed temperature independent) and λ_0(295 K) were allowed to vary in each solvent. The fits to the rate constant data for the alkylated benzene solvents are shown as a function of temperature in Figure 3.5 for the dipole model (panel A) and the dipole- quadrupole model (panel B). In every case, the sum of eq 3.1 was evaluated through the sixth term. The best fit parameters obtained from each method are summarized in Table 3.5. In the second approach, it was assumed that the $\Delta_r G$ and λ_0 values predicted by the dipole-quadrupole model are accurate and the electronic

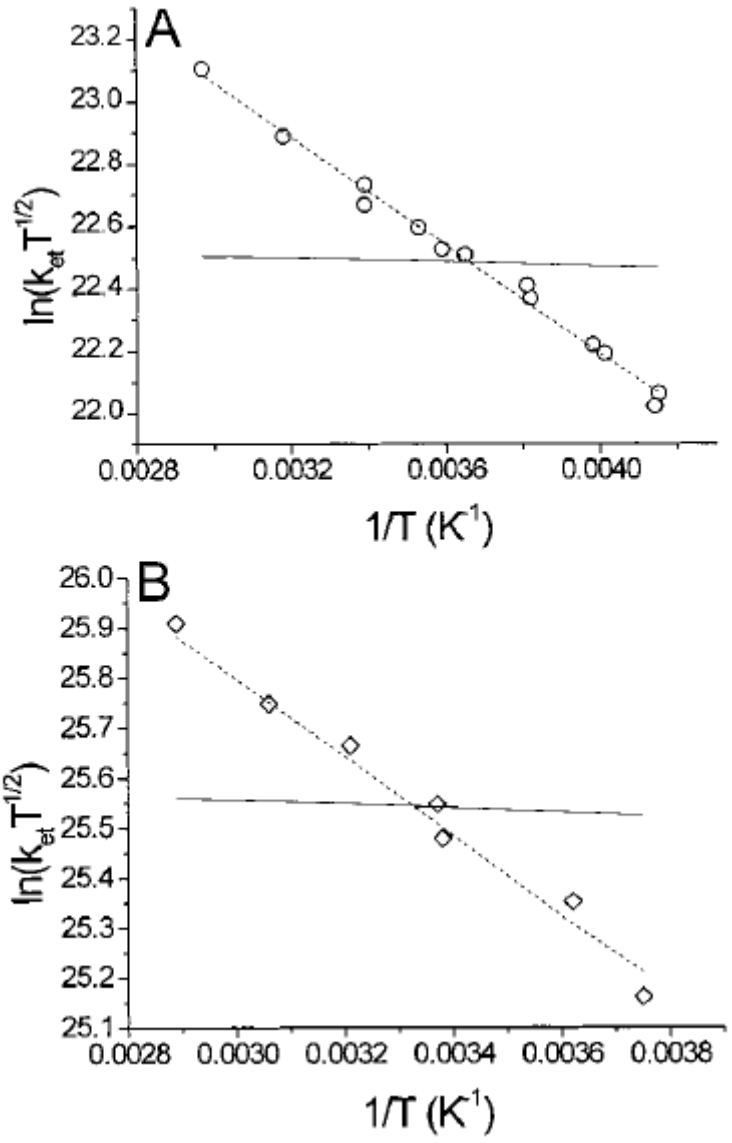

Figure 3.4 Experimental rate data is shown for acetonitrile (O, Panel A) and benzonitrile (◊, Panel B). The solid lines represent fits using the free energy and reorganization energy calculated using the dipole-quadrupole model. The dashed lines represent the calculated rate constants when the free energies and the temperature dependence of λ_0 was calculated using the dipole-quadrupole model but λ_0(295 K) was varied.

coupling was treated as both solvent and temperature dependent. The results of this analysis are shown in Figure 3.6.

In the first approach, fitting the rate constant data (Figures 3.4 and 3.5) provides values for the electronic coupling and the room temperature reorganization energy as a function of solvent (see Table 3.5). The electronic coupling decreases monotonically as the alkyl substitution on the phenyl ring increases for both models. As discussed elsewhere,[6a] this trend results from increased steric bulk of the solvent molecules inhibiting access of the aromatic core to the molecular cleft between the donor and acceptor groups. This results in decreased through solvent coupling. The magnitudes of the coupling elements are slightly different from those reported earlier. In cumene and mesitylene, a decreased quality of the fitted curves is observed. There are several possible explanations for the effect. First, the temperature dependence of λ_0 calculated by the molecular models may be too steep. The fits to the data using a constant λ_0 are significantly better than those shown here. However, this explanation cannot explain the particularly steep decrease of the rate constant in mesitylene with increasing temperature. Second, both models predict a quasi-linear temperature dependence for λ_0 which may not be accurate in these solvent systems. If the equilibrium between solvent bound and solvent unbound "clefts" changes significantly through this temperature range, nonlinear changes in λ_0 and |V| with temperature would be expected. We are currently exploring the origin of these steep drops in rate with temperature in the bulkier aromatic solvents.

Table 3.5 Regression Estimates of the Electronic Couplings and Reorganization Energies Obtained Using the Matyushov Solvation Model [a]

	model			
	dipole		dipole−quadrupole	
solvent	$\|V\|$ (cm^{-1})	$\lambda_o(295)$ (eV)	$\|V\|$ (cm^{-1})	$\lambda_o(295)$ (eV)
benzene	9.47	0.239	10.1	0.258
toluene	8.84	0.220	8.93	0.217
cumene	6.70	0.180	6.33	0.167
mesitylene	6.12	0.152	5.91	0.144
TMB	7.99	0.189	6.98	0.162
TIP	1.03	0.001	1.09	0.009
acetonitrile	31.6	2.51	27.7	1.49
benzonitrile	116.7	2.60	92.7	1.67

[a] TMB is 1,2,4-trimethylbenzene. TIP is 1,3,5-triisopropylbenzene.

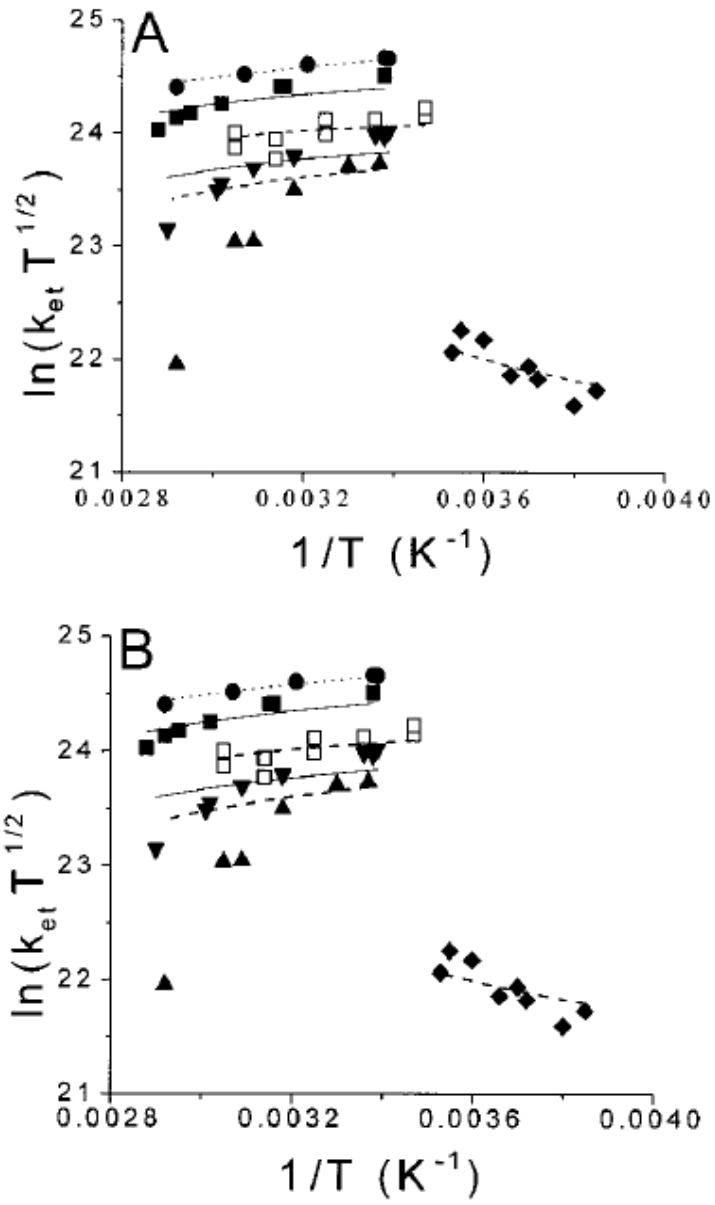

Figure 3.5 Experimental rate data (k_{et}) are shown for benzene (•), toluene (■), cumene(▼), mesitylene(▲), TMB (□), and TIP (♦). Panel A shows the fits using the free energy and temperature dependence of the outer sphere reorganization energy predicted by the dipole model. Panel B shows the fits using the energies predicted by the dipole- quadrupole model. The dotted curve shows the fit for the benzene data, the solid curve shows the fits for the singly substituted benzenes (toluene and cumene), and the dashed curves show the fits for the triply substituted benzenes (mesitylene, 1,2,4-trimethylbenzene, TIP). In each case, the electronic coupling and reorganization energy at 295 K were fitting parameters.

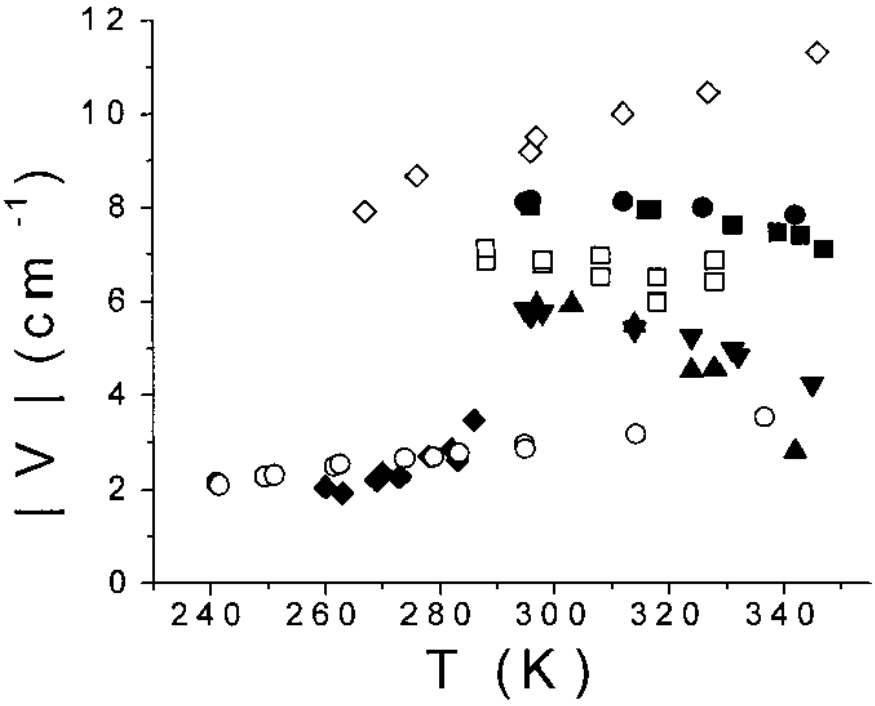

Figure 3.6 Temperature-dependent electronic couplings are shown. These values are calculated from eq 3.1 using the absolute $\Delta_r G$ and λ_0 values from the dipole-quadrupole model. Data are shown for benzene (•), toluene (■), cumene(▼), mesitylene(▲), TMB (□), and TIP (♦), acetonitrile (O), and benzonitrile (◊).

The second approach to fitting the rate data hypothesizes that the electronic coupling is temperature dependent. In this approach, the values of $\Delta_r G$ and λ_0 predicted by the dipole- quadrupole model (see Table 3.7) were used, and the value of |V| at each temperature was derived from the experimental rate constants. Figure 3.6 shows a plot of the electronic couplings as a function of temperature. It is clear from the plot that solvents in which an aromatic core can access the cleft display the largest electronic couplings. In the nondipolar and weakly dipolar aromatic solvents (other than TIP), the coupling displays a systematic but small decrease as the temperature increases (resulting in a predicted decrease of rate by 10-60% over a 40 to 50 K temperature range). To speculate, this behavior could indicate a shift in the distribution of solvent-

bound and solvent-unbound DBA "clefts" in solution. With increasing temperature, the population of unbound "clefts" increases and the ensemble averaged value of the electronic coupling decreases because the solvent-unbound structure lacks the through solvent coupling pathway. This trend is correlated to solvent size and is most apparent in cumene and mesitylene. The triisopropyl solvent exhibits the opposite behavior; i.e., the coupling increases as the temperature increases. Previously, it was demonstrated that this solvent experiences a large energy barrier to placement of its aromatic core within the cleft, between the D and A groups. Higher temperatures may increase the probability of placing the solvent's aromatic core between the D and A groups. In the polar solvents, the coupling increases with temperature also, enhancing the rate constant by 1.5-3-fold. While this approach to fitting the rate data provides stimulating conjecture into the temperature dependence of the electronic coupling, the observed changes may result from systematic errors in the determination of $\Delta_r G$ and/or λ_0. More experimental work is necessary before a reliable conclusion can be reached.

3.4 Conclusions

Measurement of $\Delta_r G$ and rate constants for electron transfer in highly dipolar, weakly dipolar and nondipolar solvents were used to evaluate two molecular models of solvation. The analysis shows that quadrupolar interactions must be included when computing solvation energies in nondipolar and weakly dipolar aromatic solvents. The quadrupole model was shown to accurately reproduce experimental free energy data and to make reasonable predictions of these energies in the polar solvents acetonitrile

and benzonitrile. The analysis shows that λ_{disp} is inconsequential and may be ignored. In addition, the quadrupole model was able to produce physically reasonable values of λ_0. Two separate approaches were used to fit the experimental rate constants. First, the calculated temperature dependence of λ_0 was used, and the electronic coupling and λ_0 at 295 K were treated as adjustable parameters. The electronic couplings obtained from these fits are in good agreement with those values found previously. The extent of the solvent mediated superexchange mechanism was found to decrease significantly with an increase in the number and size of alkyl groups attached to the benzene core. In the second approach, the calculated $\Delta_r G$ and $\lambda_0$values were used to determine the electronic coupling at each temperature. The results show a steep decrease with increasing temperature of the D/A coupling in mesitylene and a less dramatic change in the other solvents that readily fit between the D and A groups. Molecular association could be the source of the decreased coupling at higher temperatures but further experimental work is necessary to determine this conclusively.

The Matyushov dipole-quadrupole solvation model is able to accurately reproduce and, in some cases predict, free energies in solvents ranging from nondipolar to highly dipolar. The model requires the vacuum free energy difference, $\Delta_{vac} G$ the difference in polarizability between the solute neutral and CT states, $\Delta\gamma$ and an effective solute radius, R_{eff}. Calculations of these parameters may pose a significant problem, especially for large solutes. In addition, the use of the point dipole approximation for the charge redistribution in longer distance charge-transfer systems may be a limitation.[27] To conclude, the dipole-quadrupole model reproduces experimental

rate data and provides insight into the solvent and temperature dependence of donor-acceptor electronic couplings.

3.5 Acknowledgment.

This work was supported in part by the National Science Foundation (Grants CHE970835 1 (M.B.Z.) and CHE-941693 (D.H.W.)) We acknowledge numerous discussions with Dr. Dmitry Matyushov (University of Utah) and Prof. K. D. Jordan (University of Pittsburgh).

3.6 Appendix: Polynomial Forms of the Perturbation Integrals

$$I_{0s}^{(2)} = \frac{1}{r_0^3} + \frac{a(\rho^*)}{r_0^4} + \frac{b(\rho^*)}{r_0^5} + \frac{c(\rho^*)}{r_0^6}$$

$$I_{6}^{(2)} = \frac{a(\rho^*)}{r_0^5} + \frac{b(\rho^*)}{r_0^6} + \frac{c(\rho^*)}{r_0^7} + \frac{d(\rho^*)}{r_0^8}$$

$$I_{0s}^{(3)} = \frac{a(\rho^*)}{r_0^3} + \frac{b(\rho^*)}{r_0^4} + \frac{c(\rho^*)}{r_0^6}$$

$$I_{0s}^{(4)} = \frac{1}{r_0^9} + \frac{a(\rho^*)}{r_0^{10}} + \frac{b(\rho^*)}{r_0^{11}} + \frac{c(\rho^*)}{r_0^{12}}$$

$$I_{DQQ}^{(3)} = \frac{a(\rho^*)}{r_0^6} + \frac{b(\rho^*)}{r_0^7} + \frac{c(\rho^*)}{r_0^8} + \frac{d(\rho^*)}{r_0^9}$$

$$I_{DDQ}^{(3)} = \frac{a(\rho^*)}{r_0^5} + \frac{b(\rho^*)}{r_0^6} + \frac{c(\rho^*)}{r_0^7} + \frac{d(\rho^*)}{r_0^8}$$

$$J_1 = \frac{a(\rho^*)}{r_0^9} + \frac{b(\rho^*)}{r_0^{10}} + \frac{c(\rho^*)}{r_0^{11}}$$

In each case, r_0 is the reduced solute-solvent distance of closest approach, $r_0 = R_0/\sigma + 0.5$, and the functions $a(\rho^*)$, $b(\rho^*)$, etc. are fit to third-order polynomials over the reduced density, $\rho^* \equiv \rho\sigma^3$ such that

$$a(\rho^*) = a_0 + a_1\rho^* + a_2\rho^{*2} + a_3\rho^{*3}$$

These coefficients are listed in Table 3.6.

Table 3.6 Values of the Coefficients for the Polynomial Forms

	$I_{0s}^{(2)}$			$I_{0s}^{(3)}$			$I_{6}^{(2)}$				$I_{0s}^{(4)}$		
i	a_i	b_i	c_i	a_i	b_i	c_i	a_i	b_i	c_i	d_i	a_i	b_i	c_i
0	0.000	0.000	0.000	1.000	−0.563	0.031	1.000	0.000	0.000	0.000	0.000	0.000	0.000
1	1.935	−1.675	0.439	0.602	0.255	−0.256	0.586	1.062	−0.970	0.241	3.212	−2.580	0.608
2	−0.972	2.183	−1.051	−0.381	0.848	−0.263	−1.390	4.608	−4.134	1.194	2.862	−4.349	1.564
3	0.398	−0.831	0.465	−0.061	−0.107	0.098	0.776	−2.964	3.798	−1.393	−0.695	3.066	−1.447

	$I_{DQQ}^{(3)}$				$I_{DDQ}^{(3)}$				J_1		
i	a_i	b_i	c_i	d_i	a_i	b_i	c_i	d_i	a_i	b_i	c_i
0	0.208	0.000	−0.078	0.008	0.800	−0.500	0.000	0.031	0.774	0.021	1.140
1	0.936	−1.629	10.350	−6.712	0.365	1.652	−1.510	0.044	0.412	0.445	0.739
2	0.330	0.509	−20.530	13.990	−0.656	4.779	−7.378	3.770	0.885	0.372	0.751
3	−0.216	1.005	10.300	−7.512	0.179	−2.297	5.087	−2.928	0.565	0.361	0.410

Table 3.7 Individual Contributions to $\Delta_r G$ and λ_0 (All Values in eV) [a]

Dipole Model Values for ΔG and λ ($\Delta_{vac}G = 0.326$)								Dipole−Quadrupole Model Values for ΔG and λ ($\Delta_{vac}G = 0.340$)							
T (K)	$\Delta_{dq,i}G^{(1)}$	$\Delta_i G^{(2)}$	$\Delta_{disp}G$	$\Delta_r G$	λ_p	λ_{ind}	λ_{disp}	λ_o	T (K)	$\Delta_{dq,i}G^{(1)}$	$\Delta_i G^{(2)}$	$\Delta_{disp}G$	$\Delta_r G$	λ_p	λ_{ind}	λ_{disp}	λ_o
Benzene																	
296	−0.407	−0.095	0.064	−0.112	0.000	0.095	0.003	0.099	296	−0.415	−0.031	−0.008	−0.115	0.163	0.031	0.000	0.194
312	−0.397	−0.086	0.062	−0.095	0.000	0.086	0.003	0.089	312	−0.399	−0.028	−0.008	−0.096	0.153	0.028	0.000	0.181
326	−0.388	−0.079	0.061	−0.081	0.000	0.079	0.003	0.082	326	−0.386	−0.026	−0.008	−0.080	0.144	0.026	0.000	0.170
342	−0.378	−0.072	0.059	−0.065	0.000	0.072	0.002	0.074	342	−0.371	−0.024	−0.008	−0.063	0.136	0.024	0.000	0.159
Toluene																	
296	−0.404	−0.097	0.089	−0.086	0.021	0.097	0.005	0.123	296	−0.379	−0.033	−0.012	−0.083	0.139	0.033	0.000	0.171
316	−0.391	−0.084	0.086	−0.063	0.019	0.084	0.005	0.108	316	−0.361	−0.028	−0.011	−0.061	0.127	0.028	0.000	0.156
331	−0.382	−0.076	0.084	−0.048	0.018	0.076	0.004	0.098	331	−0.348	−0.026	−0.011	−0.045	0.120	0.026	0.000	0.145
339	−0.377	−0.072	0.083	−0.040	0.017	0.072	0.004	0.093	339	−0.342	−0.024	−0.011	−0.037	0.116	0.024	0.000	0.140
347	−0.372	−0.068	0.082	−0.032	0.016	0.068	0.004	0.089	347	−0.335	−0.023	−0.011	−0.030	0.112	0.023	0.000	0.135
Cumene																	
296	−0.372	−0.097	0.088	−0.054	0.011	0.097	0.008	0.115	296	−0.347	−0.034	−0.010	−0.051	0.094	0.034	0.000	0.128
314	−0.362	−0.084	0.086	−0.035	0.010	0.084	0.007	0.101	314	−0.334	−0.030	−0.010	−0.034	0.087	0.030	0.000	0.117
324	−0.357	−0.078	0.084	−0.025	0.009	0.078	0.007	0.094	324	−0.328	−0.028	−0.010	−0.025	0.083	0.028	0.000	0.111
331	−0.354	−0.074	0.084	−0.018	0.009	0.074	0.006	0.090	331	−0.323	−0.026	−0.010	−0.019	0.081	0.026	0.000	0.107
345	−0.347	−0.067	0.082	−0.006	0.008	0.067	0.006	0.081	345	−0.314	−0.024	−0.010	−0.008	0.076	0.024	0.000	0.100
TMB																	
288	−0.382	−0.111	0.105	−0.062	0.026	0.111	0.011	0.148	288	−0.346	−0.039	−0.012	−0.057	0.094	0.039	0.000	0.134
298	−0.376	−0.104	0.103	−0.051	0.025	0.104	0.011	0.139	298	−0.339	−0.037	−0.012	−0.048	0.091	0.037	0.000	0.128
308	−0.370	−0.097	0.102	−0.040	0.023	0.097	0.010	0.131	308	−0.333	−0.034	−0.012	−0.040	0.088	0.034	0.000	0.123
318	−0.364	−0.091	0.100	−0.029	0.022	0.091	0.009	0.123	318	−0.328	−0.032	−0.012	−0.032	0.086	0.032	0.000	0.118
328	−0.359	−0.086	0.099	−0.020	0.021	0.086	0.009	0.116	328	−0.322	−0.030	−0.012	−0.024	0.083	0.030	0.000	0.113
Mesitylene																	
297	−0.365	−0.101	0.107	−0.033	0.001	0.101	0.011	0.114	297	−0.322	−0.036	−0.014	−0.032	0.081	0.036	0.000	0.117
303	−0.361	−0.097	0.106	−0.027	0.001	0.097	0.011	0.109	303	−0.318	−0.034	−0.013	−0.026	0.079	0.034	0.000	0.114
314	−0.356	−0.091	0.104	−0.016	0.001	0.091	0.010	0.102	314	−0.310	−0.032	−0.013	−0.016	0.075	0.032	0.000	0.107
324	−0.350	−0.085	0.103	−0.007	0.001	0.085	0.010	0.096	324	−0.304	−0.030	−0.013	−0.007	0.072	0.030	0.000	0.102
342	−0.341	−0.076	0.100	0.009	0.001	0.076	0.009	0.085	342	−0.293	−0.027	−0.013	0.008	0.067	0.027	0.000	0.094
TIP																	
260	−0.326	−0.117	0.097	−0.020	0.001	0.117	0.015	0.133	260	−0.303	−0.044	−0.010	−0.018	0.048	0.044	0.000	0.092
263	−0.325	−0.115	0.097	−0.017	0.001	0.115	0.014	0.130	263	−0.301	−0.044	−0.010	−0.016	0.047	0.044	0.000	0.091
278	−0.319	−0.104	0.095	−0.002	0.001	0.104	0.013	0.118	278	−0.294	−0.039	−0.010	−0.003	0.044	0.039	0.000	0.083
282	−0.317	−0.101	0.094	0.002	0.001	0.101	0.013	0.115	282	−0.292	−0.038	−0.010	0.000	0.043	0.038	0.000	0.081
Acetonitrile																	
250	−1.906	−0.038	0.051	−1.567	1.544	0.038	0.002	1.583	250	−1.083	−0.012	−0.006	−0.761	0.848	0.012	0.000	0.859
270	−1.868	−0.033	0.049	−1.526	1.517	0.033	0.001	1.552	270	−1.065	−0.010	−0.006	−0.741	0.837	0.010	0.000	0.847
300	−1.813	−0.027	0.046	−1.467	1.478	0.027	0.001	1.506	300	−1.039	−0.008	−0.006	−0.713	0.821	0.008	0.000	0.829
320	−1.776	−0.023	0.045	−1.429	1.452	0.023	0.001	1.477	320	−1.021	−0.007	−0.005	−0.694	0.810	0.007	0.000	0.817
340	−1.740	−0.020	0.043	−1.391	1.427	0.020	0.001	1.448	340	−1.004	−0.006	−0.005	−0.676	0.799	0.006	0.000	0.806
Benzonitrile																	
296	−1.864	−0.121	0.089	−1.570	1.444	0.121	0.007	1.572	296	−1.170	−0.041	−0.011	−0.882	0.892	0.041	0.000	0.933
312	−1.832	−0.109	0.088	−1.527	1.419	0.109	0.006	1.534	312	−1.154	−0.037	−0.011	−0.862	0.881	0.037	0.000	0.917
324	−1.807	−0.101	0.086	−1.496	1.400	0.101	0.006	1.507	324	−1.143	−0.034	−0.011	−0.847	0.872	0.034	0.000	0.906
342	−1.770	−0.090	0.084	−1.450	1.371	0.090	0.005	1.467	342	−1.125	−0.030	−0.010	−0.826	0.860	0.030	0.000	0.890

[a] TMB is 1,2,4-trimethylbenzene; TIP is 1,3,5-triisopropylbenzene.

3.7 References.

(1) Matyushov, D. V.; Voth, G. A. *J. Chem. Phys.* **1999**, 111, 3630. The formulation used in this manuscript includes solvent polarizability. We thank Dr. D. Matyushov for providing access to this form of the model.

(2) (a) Electron Transfer - From Isolated Molecules to Biomolecules. *Adv. Chem. Phys.*, Jortner, J., Bixon, M., Eds., (Wiley: NY **1999**) (b) Barbara, P. F.; Meyer, T. J.; Ratner, M. A. *J. Phys. Chem.* **1996**, 100, 13148. (c) Newton, M. D. *Chem. Rev.* **1991**, 91, 767. (d) Closs, G. L.; Miller, J. R. *Science* **1988**, 240, 440. (e) Marcus, R. A.; Sutin, N. *Biochimica et Biophysica Acta* **1985**, 811, 265.

(3) (a) Newton, M. D. *Adv. Chem. Phys.* **1999**, 106, 303. (b) Gray, H. B.; Winkler, J. R. *Annu. Rev. Biochem.* **1996**, 65, 537. (c) Closs, G. L.; Calcaterra, L. T.; Green, N. J.; Penfield, K. W.; Miller, J. R. *J. Phys. Chem.* **1986**, 90, 3673; (d) Jordan, K. D.; Paddon-Row, M. N. *Chem. Rev.* **1992**, 92, 395.

(4) (a) Nitzan, A.; Mujica, V.; Davis, W. B.; Wasielewski, M. R.; Ratner, M. A. *J. Phys. Chem.* **1997**, 101, 6158. (b) Häberle, T.; Hirsch, J.; Pöllinger, F.; Heitele, H.; Michel-Beyerle, M. E.; Anders, C.; Döhling, A.; Krieger, C.; Rückemann, A.; Staab, H. A. *J. Phys. Chem.* **1996**, 100, 18269. (c) Heitele, H.; Pöllinger, F.; Häberle, T.; Michel-Beyerle, M. E.; Staab, H. A. *J. Phys. Chem.* **1994**, 98, 7402. (d) Liu, J.; Schmidt, J. A.; Bolton, J. R. *J. Phys. Chem.* **1991**, 95, 6924. (e) Ratner, M. A. *J. Phys. Chem.* **1990**, 94, 4877. (e) Larsson, S. *Chem. Phys. Lett.* **1982**, 90, 136. (f) Helms, A.; Heiler, D.; McLendon, G. *J. Am. Chem. Soc.* **1991**, 113, 4325.

(5) (a) Liang, N.; Miller, J. R.; Closs, G. L. *J. Am. Chem. Soc.* **1989**, 111, 8740. (b) Kumar, K.; Lin, Z.; Waldeck, D. H.; Zimmt, M. B. *J. Am. Chem. Soc.* **1996**, 118, 243. (c) Kroon, J.; Oevering, H.; Verhoeven, J. W.; Warman, J. M.; Oliver, A. M.; Paddon-Row: M. N. *J. Phys. Chem.* **1993**, 97, 5065. (d) Wasielewski, M. R.; Gaines, G. L. III,; O'Neill, M. P.; Svec, W. A.; Niemczyk, M. P.; Prodi, L.; Gosztola, D. in 'Dynamics and Mechanisms of Photoinduced Electron Transfer and Related Phenomena,' Mataga, N., Okada, T., Masuhara, H., Eds., Elsevier, **1992**; p 87.

(6) (a) Read, I.; Napper, A.; Kaplan, R.; Zimmt, M. B.; Waldeck, D. H. *J. Am. Chem. Soc.* **1999**, 121, 10976. (b) Han, H.; Zimmt, M. B. *J. Am. Chem. Soc.* **1998**, 120, 8001. (c) Roest, M. R.; Verhoeven, J. W.; Schuddeboom, W.; Warman, J. M.; Lawson, J. M.; Paddon-Row, M. N. *J. Am. Chem. Soc.* **1996**, 118, 1762.

(7) Vath, P.; Zimmt, M. B.; Matyushov, D. V.; Voth, G. A. *J. Phys. Chem. B* **1999**, 103, 9130.

(8) McConnell, H. M. *J. Chem. Phys.* **1961,** 35, 508.

(9) Gosztola, D.; Wang, B.; Wasielewski, M. R. *J. Photochem. Photobio. A.* **1996**, 102, 71.

(10) Kumar, K.; Kurnikov. I. V.; Beratan, D. N.; Waldeck, D. H.; Zimmt, M. B. *J. Phys. Chem. A.* **1998**, 102, 5529.

(11) Jortner, J. *J. Chem. Phys.* **1976**, 64, 4860.

(12) (a) Marcus, R. A. *J. Phys. Chem.* **1989**, 93, 3078. (b) Lilichenko. M.; Tittelbach-Helmrich, D.; Verhoeven, J. W.; Gould I. R.; Myers, A. B. *J. Chem. Phys.* **1998**, 109, 10958. (c) Gould, I. R.; Noukakis, D.; Goodman, J. L.; Young, R. H.; Farid, S. *J. Am. Chem. Soc.* **1993**, 115, 3830.

(13) Reynolds, L.; Frankland, S. J. V.; Horng, M. L.; Maroncelli, M. *J. Phys. Chem.* **1996**, 100, 10337.

(14) Matyushov, D. V. *Chem. Phys.* **1996**, 211, 47.

(15) Given the experimental rate constants, free energies, and the previous predictions of λ_i and ν it was possible to compute the temperature dependence of λ_o at three values of the electronic coupling (ref 6a). The results gave nearly constant values of λ_o in every solvent but mesitylene. The origin of this temperature dependence in mesitylene is under investigation.

(16) Zeng, Y.; Zimmt, M. B. *J. Phys. Chem.* **1992**, 96, 8395.

(17) Rehm, D.; Weller, A. Z. *Phys. Chem. (Munich)* **1970**, 69, 183.

(18) Gubbins, K. E.; Joslin, C. G.; Gray, C. G. *Mol. Phys.* **1985**, 54, 1117.

(19) (a) Matyushov, D. V.; Schmid, R. *J. Chem. Phys.* **1996**, 105, 4729. This reference reports an erroneous value for the c3 coefficient in the *I* 0*s*(2) polynomial form. Its value should be + 0.0983. See b) Matyushov. D. V.; Ladanyi, B. M. *J. Chem. Phys.* **1999**, 110, 994.

(20) Ben-Amotz, D.; Willis, K. G. *J. Phys. Chem.* **1993**, 97, 7736.

(21) Matyushov, personal communication.

(22) The values for the integral *J*1 were provided by Dr Matyushov and fit to the polynomial form in the Appendix.

(23) Frisch, M. J.; Trucks, G. W.; Schlegel, H. B.; Scuseria, G. E.; Robb, M. A.; Cheeseman, J. R.; Zakrzewski, V. G.; Montgomery, J. A., Jr.; Stratmann, R. E.; Burant, J. C.; Dapprich, S.; Millam, J. M.; Daniels, A. D.; Kudin, K. N.; Strain, M. C.; Farkas, O.; Tomasi, J.; Barone, V.; Cossi, M.; Cammi, R.; Mennucci, B.; Pomelli, C.; Adamo, C.; Clifford, S.; Ochterski, J.; Petersson, G. A.; Ayala, P. Y.; Cui, Q.; Morokuma, K.; Malick, D. K.; Rabuck, A. D.; Raghavachari, K.; Foresman, J. B.; Cioslowski, J.; Ortiz, J. V.; Stefanov, B. B.; Liu, G.; Liashenko, A.; Piskorz, P.; Komaromi, I.; Gomperts, R.; Martin, R. L.; Fox, D. J.; Keith, T.; AlLaham, M. A.; Peng, C. Y.; Nanayakkara, A.; Gonzalez, C.; Challacombe, M.; Gill, P. M. W.;Johnson, B.

G.; Chen, W.; Wong, M. W.; Andres, J. L.; Head-Gordon, M.; Replogle, E. S.; Pople, J. A. Gaussian 98, revision A.4; Gaussian, Inc.: Pittsburgh, PA, 1998.

(24) The dipole moment of the charge transfer state was calculated assuming a point charge separation of 7.1 Å.

(25) Gubbins, K. E.; Gray, C. G.; Machado, J. R. S. *Mol. Phys.* **1981**, 42, 817.

(26) (a) Vath, P.; Zimmt, M. B. *J. Phys. Chem. A* **2000**, 104, 2626. (b) Cortés, J.; Heitele, H.; Jortner, J. *J. Phys. Chem.* **1994**, 98, 2527.

(27) Zimmt, M. B. Unpublished results.

Chapter 4 An Unequivocal Demonstration of the Importance of Nonbonded Contacts in the Electronic Coupling between Electron Donor and Acceptor Units of Donor-Bridge-Acceptor Molecules

Because of their ubiquity, electron transfer (ET) reactions have received considerable attention over the past few decades. The current view of a superexchange mechanism to treat the electronic interaction for electron-transfer processes in the nonadiabatic limit has been quite successful. Although it is widely believed that covalent linkages between donor and acceptor units provide the dominant pathway for this mechanism,[1] recent work suggests that other pathways involving hydrogen-bonded linkages[2,3] and non-bonded interactions[4,5] can be important. This work assesses the importance of nonbonded contacts by comparing three different unimolecular ET systems that differ by the juxtaposition of a pendant group between the electron donor and acceptor units. This design provides an avenue to quantify the importance of an aromatic moiety's placement on the electron-transfer rate. The work presents unequivocal evidence that electronic coupling through nonbonded moieties can compete effectively with covalent linkages, when the mediating moiety lies between the electron donor and acceptor groups.[††]

This study utilizes a U-shaped donor-bridge-acceptor (DBA) dyad in which a pendant moiety (P) is placed between the electron donor and acceptor units by a covalent linkage to the bridge (see the cartoon in Chart 4.1). Through systematic change of the pendant molecular unit it is possible to demonstrate its importance to the

[††] This chapter was previously published as: Napper, A. M.; Read, I.; Waldeck, D. H.; Head, N. J.; Oliver, A. M.; Paddon-Row, M. N.; *J. Am. Chem. Soc.;* **2000**; 122(21); 5220-5221

ET and the role of its placement on the efficiency of ET. This approach has several advantages over earlier approaches. First, the moiety that mediates the superexchange interaction (solvent molecule in earlier studies[4,5]) is clearly located between the donor and acceptor groups. Second, the nature of P can be changed, and a homologous series of DBA molecules can be studied in a single solvent, thereby minimizing any differences in the reaction free energy and outer sphere reorganization energy that may result from solvation changes. These systems also promise an ability to change the geometry of the mediating unit and to investigate how its nuclear dynamics impact the ET.

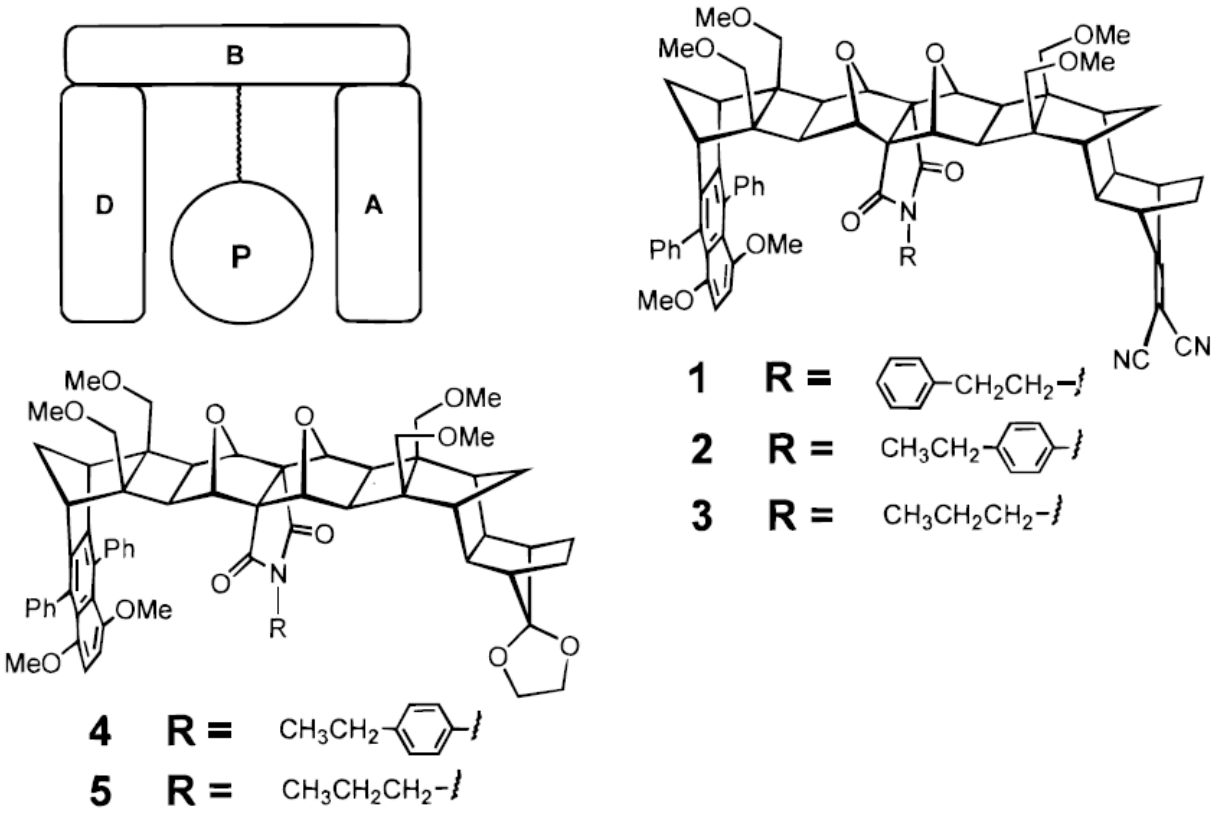

Chart 4.1 Chemical structures of the molecules studied in this paper.

The ET rates of **1**-**3** in Chart 4.1 were studied in three different solvents (acetonitrile, dichloromethane, and tetrahydrofuran) as a function of temperature. The general synthetic strategy for these molecules and the specific synthesis of **3** has been reported elsewhere.[6] The molecules in Chart 4.1 have the same electron donor unit, 1,4-dimethoxy-5,8-diphenylnaphthalene. Molecules **1**, **2**, and **3** have a 1,1-dicyanovinyl (DCV) acceptor unit, and ET occurs when the naphthalene moiety is electronically excited by 300 nm light. These donor and acceptor units have been used for intramolecular ET studies in the past.[1c] Molecules **4** and **5** have a 1,3-dioxolane unit in place of the DCV acceptor. These molecules do not undergo ET and are used as experimental controls. A comparison of the ET rate constant for **1**, **2**, and **3** provides information on the effectiveness of an aromatic ring for mediating the electronic coupling in the ET, as compared to that of an alkyl unit, and addresses the importance of its placement. The ET rate constant was determined by subtracting the excited-state relaxation rate of the control molecules (**4** and **5**) from that of the ET molecules (**1**, **2**, and **3**).

The ET rate constants as a function of temperature are shown in Figure 4.1 for compounds **1**, **2**, and **3**. In each solvent studied the ET rate for **2** is significantly faster than that found for the other compounds. The larger ET rate constant for **2** compared to **3** demonstrates the benefit of placing an aromatic unit between the electron donor and acceptor rather than an alkyl unit. The larger ET rate constant for **2** compared to that for **1** demonstrates the importance of the aromatic unit's placement between the donor and acceptor groups. Molecular modeling calculations of the molecular geometries of **1** and **2** show that the phenyl ring in compound **2** is in the

"line-of-sight" between the donor and acceptor groups (see Figure 4.2), whereas the phenyl ring in compound **1** is shifted down from the line-of-sight position.[7] The very similar rates for **3** and **1** corroborate this conclusion. In short, the propyl **3** and 2-phenylethyl **1** pendant units are similar with respect to their influence on the ET, but the p-ethylphenyl unit in **2** is markedly different. These comparisons imply enhanced tunneling when the phenyl ring is in line-of-sight.

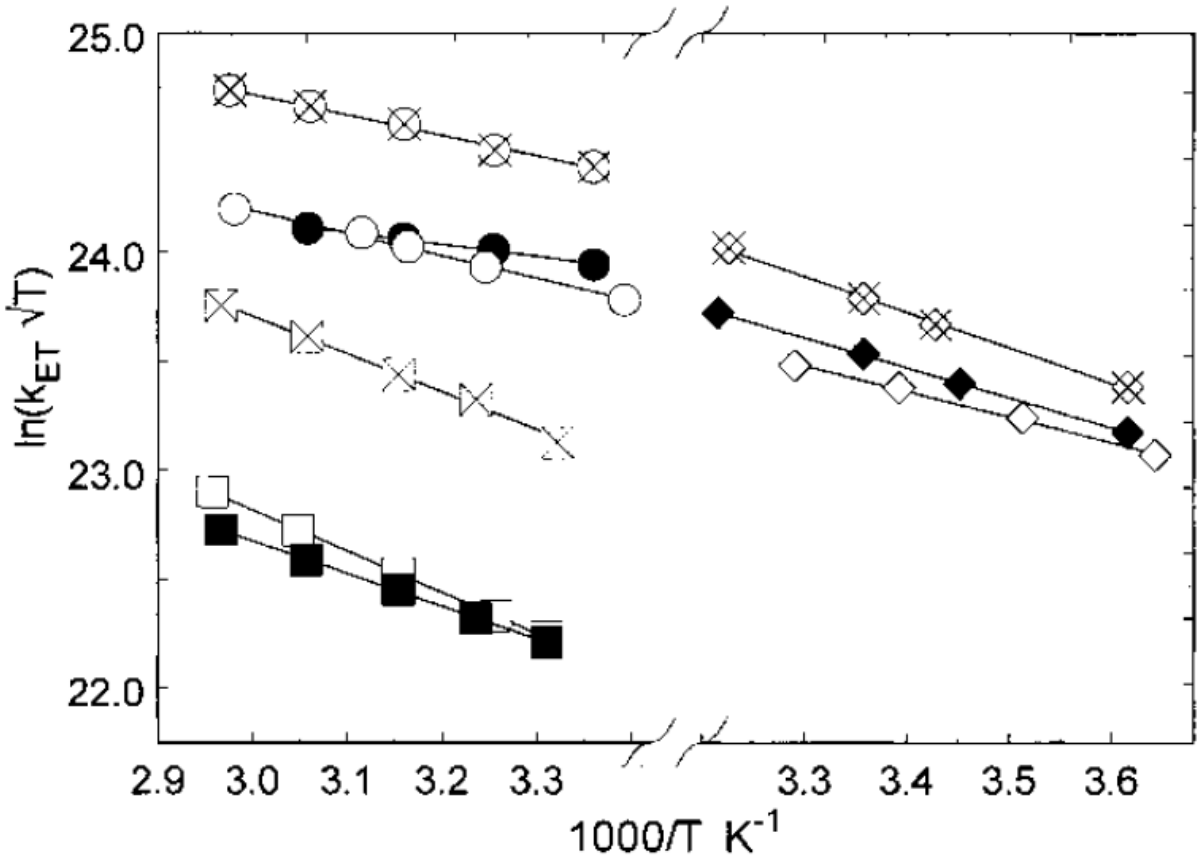

Figure 4.1 These plots show the temperature dependence of the ET rate constant $_{k\mathrm{ET}}$ in three solvents: acetonitrile (squares), dichloromethane (diamonds), and tetrahydrofuran (circles). The filled symbols represent the data for 1, the open symbols with an x represent the data for 2, and the open symbols represent the data for 3. The lines are linear regression fits to the data.

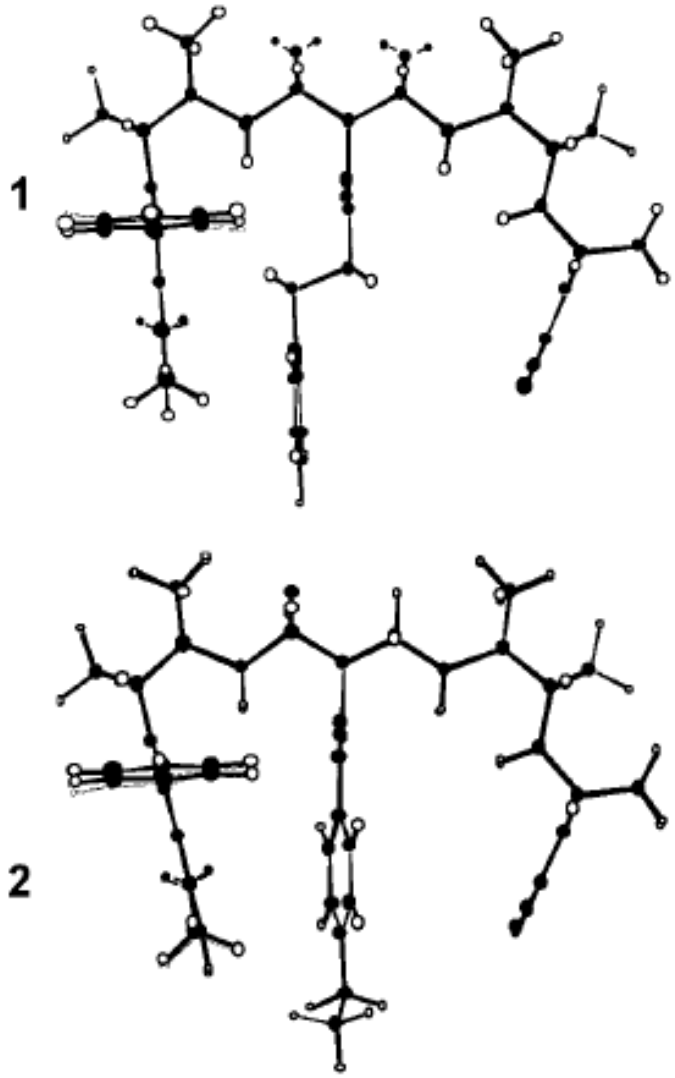

Figure 4.2 This figure shows ball-and-stick renderings of MM2 optimized structures of the DBA molecules 1 and 2. The phenyl ring of the pendant group in 2 is on the line-of-sight between the donor and acceptor units.

In each solvent system, the ET rate displays a temperature dependence. A fit of the data provides activation energies between 2 and 4 kcal/mol. The similarity of the activation suggests that the Franck-Condon terms (the reaction free energy $\Delta_r G$ and the reorganization energies λ) are similar for the three compounds. The ET activation energies for **1**-**3** display a solvent dependence, decreasing by a factor of ~2, upon changing the solvent from acetonitrile to tetrahydrofuran. If the Franck-Condon factors are not changing for the compounds in a single solvent, the difference in the rate constants reflects a change in the electronic coupling |V|. This logic is supported by the very similar rates that are observed for **1** and **3** in each of the different solvents. From an analysis of the temperature dependence in each solvent and assuming that the reorganization energy in a given solvent is the same for each of the molecules **1**-**3**, it is possible to extract reliable relative electronic couplings. Table 4.1 presents the relative electronic couplings in acetonitrile. The results reveal that the coupling in **2** is 2.5 times larger than in **3** and 30% larger than in **1**. Similar differences in the electronic couplings are found in tetrahydrofuran and CH_2Cl_2.

Comparison of these rate constants with those from earlier studies supports the conclusion that ET in **1**-**3** is occurring through the pendant group and not through the covalent bonds of the bridge (see Table 4.1). In all three dyads, **1**-**3**, the bridge is 12 bonds long and has two cisoid kinks. The rate constants for **1**-**3** are all larger than that for the all-trans 12-bond DMN-DCV (see **6** of Chart 4.2) for the same solvents.[1a] This comparison becomes more significant when one realizes that ET through an all-trans bridge is much faster than that through a bridge having two cisoid

kinks.[8] For example, the ET rate constant for the all-trans **7** is up to 14 times larger than that for **8**, which

Table 4.1 Comparison of Rate Constants k_{ET} and Relative Electronic Couplings |*V*rel| in Acetonitrile Solvent at 300 K.

compd	1	2	3	6	7	8
k_{ET} (ns^{-1})	0.25	0.64	0.245	0.16	30.	2.2
$\|V_{rel}\|^a$	1.9	2.4	1			

[a] The electronic couplings are compared to the value for **3**

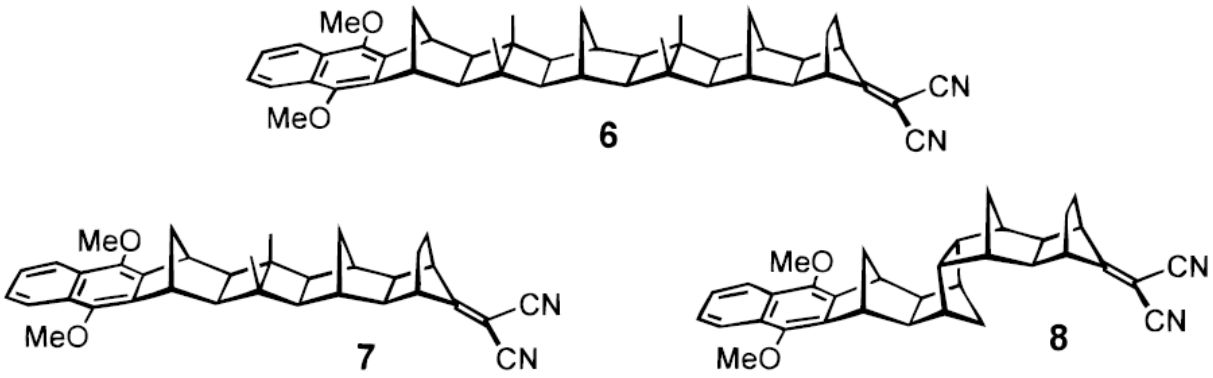

Chart 4.2 Chemical Structures of Linear Bridged Donor-Bridge-Acceptor Molecules Previously Studied.[1a]

has two cisoid links.[8] These considerations suggest that the propyl chain in **3** mediates ET more efficiently than does its 12-bond, double-kinked, covalent bridge! A caveat to these comparisons is that the $\Delta_r G$ and λ could be changing, because of the smaller donor-acceptor separation in **1**-**3** (9.0 - 9.9 Å), compared to that in **6** (~14 Å). Initial investigations indicate that the free energies in these systems are similar,[9] however more studies are required to better quantify these considerations.

A comparison of ET rates in the different DBA molecules **1**, **2**, and **3** demonstrates the importance of the molecular functionality that lies between the donor and acceptor units, even though it does not covalently link them. By changing the pendant unit that lies between the electron donor and acceptor, it has been possible to explore how its nature and its placement impact the ET rate. A more quantitative study of these systems and their electronic coupling is underway. Nonbonded contacts are ubiquitous in chemical and biological systems, and it will be interesting to investigate a wider range of systems. In particular, we are currently synthesizing variants of **2**, in which the ethyl substituent of the phenyl ring is replaced by groups having different electronegativities, to delineate how the donor-acceptor electronic coupling depends on the electronic properties of the pendant aromatic group.

4.1 References.

(1) (a) Oevering, H.; Paddon-Row, M. N.; Heppener, H.; Oliver, A. M.; Cotsaris, E.; Verhoeven, J. W.; Hush, N. S. *J. Am. Chem. Soc.* **1987**, 109, 3258. (b) Closs, G. L.; Miller, J. R. *Science* **1988**, 240, 440-447. (c) Paddon-Row, M. N. *Acc. Chem. Res.* **1994**, 27, 18.

(2) (a) Berman, A.; Izraeli, E. S.; Levanon, H.; Wang B.; Sessler, J. L. *J. Am. Chem. Soc.* **1995**, 117, 8252. (b) Roberts, J. A.; Kirby, J. P.; Nocera, D. G. *J. Am. Chem. Soc.* **1995**, 117, 8051. (c) de Rege, P. J. F.; Williams, S. A.; Therien, M. J. *Science* **1995**, 269, 1409. (d) LeCours, S. M.; Philips, C. M.; DePaula, J. C.; Therien, M. J.; *J. Am. Chem. Soc.* **1997**, 119, 12578. (e) Turro, C.; Chang, C. K.; Leroi, G. E.; Cukier, R. I.; Nocera, D. G. *J. Am. Chem. Soc.* **1992**, 114, 4013. (f) Arimura, T.; Brown, C. T.; Springs, S. L.; Sessler, J. L. *Chem. Commun.* **1996**, 2293.

(3) (a) Beratan, D. N.; Onuchic, J. N. Protein Electron Transfer; Bendall, D. S., Ed.; BIOS Scientific Publishers Ltd.: Oxford, **1996**; p 23. (b) Nocek, J. M.; Zhou, J. S.; De Forest, S.; Priyadarshy, S.; Beratan, D. N.; Onuchic, J. N.; Hoffman, B. M. *Chem. Rev.* **1996**, 96, 2459.

(4) (a) Kumar, K.; Lin, Z.; Waldeck, D. H.; Zimmt, M. B. *J. Am. Chem. Soc.* **1996**, 118, 243. (b) Gu, Y.; Kumar, K.; Lin, Z.; Read, I.; Zimmt, M. B.; Waldeck, D. H. *J. Photochem. Photobiol. A* **1997**, 105, 189. (c) Kumar, K.; Kurnikov, I.; Beratan, D.; Waldeck, D. H.; Zimmt, M. B.; *J. Phys. Chem. B* **1998**, 102, 5394. (d) Read, I.; Napper, A.; Kaplan, R.; Zimmt, M. B.; Waldeck, D. H. *J. Am. Chem. Soc.* **1999**, 121, 10976.

(5) (a) Oliver, A. M.; Craig, D. C.; Paddon-Row, M. N.; Kroon, J.; Verhoeven, J. W. *Chem. Phys. Lett.* **1988**, 150, 366. (b) Lawson, J. M.; Paddon-Row: M. N.; Schuddeboom, W.; Warman, J. M.; Clayton, A. H.; Ghiggino, K. P. *J. Phys. Chem.* **1993**, 97, 13099. (c) Roest, M. R.; Lawson, J. M.; Paddon-Row, M. N.; Verhoeven, J. W. *Chem. Phys. Lett.* **1994**, 230, 536. (d) Roest, M. R.; Verhoeven, J. W.; Schuddeboom, W.; Warman, J. M.; Lawson, J. M.; PaddonRow, M. N. *J. Am. Chem. Soc.* **1996**, 118, 1762. (e) Verhoeven, J. W.; Koeberg, M.; Roest, M. R.; Paddon-Row, M. N.; Lawson, J. M. In Biological Electron-Transfer Chains: Genetics, Composition and Mode of Operation; Canters, G. W., Vijgenboom, E., Eds.; Kluwer: Dordrecht, **1998**; pp 5 1-61. (f) Jolliffe, K. A.; Bell, T. D. M.; Ghiggino, K. P.; Langford, S. J.; Paddon-Row, M. N. *Angew. Chem., Int. Ed.* **1998**, 37, 916.

(6) Head, N. J.; Oliver, A. M.; Look, K.; Lokan, N. R.; Jones, G. A.; Paddon-Row, M. N. *Angew. Chem., Int. Ed.* **1999**, 38, 3219.

(7) The images in Figure 4.2 were calculated at the MM2 level. More sophisticated geometry calculations are underway. Preliminary calculations on **2** at the HF 3-21G level indicate that the phenyl ring is located on a line of sight between the donor and acceptor, but it is twisted (~70°) from the plane of the imide ring.

(8) Oliver, A. M.; Craig, D. C.; Paddon-Row: M. N.; Kroon, J.; Verhoeven, J. W. *Chem. Phys. Lett.* **1988**, 150, 366.

(9) The oxidation potential of the dimethoxynaphthalene in **6** is 0.1 eV smaller than dimethoxydiphenylnaphthalene group in **1** to **3**, and the ground to locally excited-state energy of **6** is 0.2 eV larger than in **1** to **3**, implying about 0.3 eV more driving force for the reaction. However, the Coulomb stabilization of the charge transfer state in **6** is about 0.2 eV smaller than in **1** to **3**. This suggests that the reaction free energies will be close to one another, within 0.1 to 0.2 eV.

Chapter 5 Solvent Mediated Superexchange in a C-Clamp Shaped Donor-Bridge-Acceptor Molecule: The Correlation between Solvent Electron Affinity and Electronic Coupling

5.1 Introduction

Electron-transfer reactions remain of fundamental and practical importance. The understanding of how energetic factors, such as reorganization energy and reaction free energy, impact reaction rates is well established; however, our ability to model or calculate these properties remains limited.[1,2] For electron transfer reactions in the nonadiabatic limit, the transfer process is well described by an electron tunneling mechanism. In this scenario, rearrangement of the surrounding medium, consisting of both intramolecular (innersphere) and intermolecular (outersphere) nuclear motions, allows exploration of those parts of phase space where the initial and final electronic states are in resonance. Electron transfer occurs in this crossing region, although the system may pass through it many times before the transfer event.[3] The electronic coupling matrix element |V| is a measure of the interaction energy between the initial and final electronic states in the crossing region and is directly related to the electron-transfer rate constant.[4] This study explores how the electronic coupling, or electron tunneling, between an electron donor and electron acceptor depends on the electronic structure of an intervening molecule. A correlation between the electronic coupling and the electron affinity of the intervening molecule is identified.[‡‡]

[‡‡] This chapter was previously published as: Napper, A. M.; Read, I.; Kaplan, R.; Zimmt, M. B.; Waldeck, D. H.; *J. Phys. Chem. A.;* **2002**; 106(21); 5288-5296.

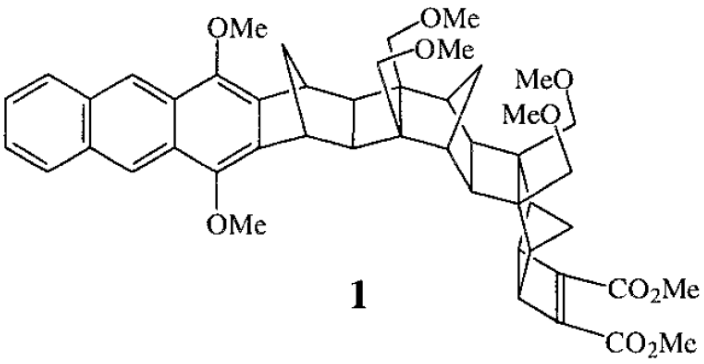

1

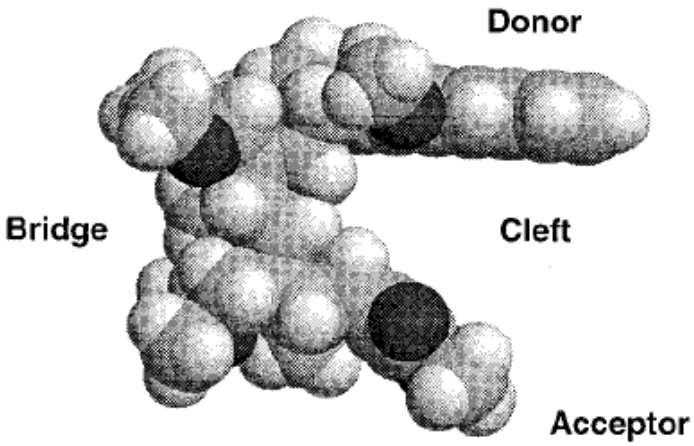

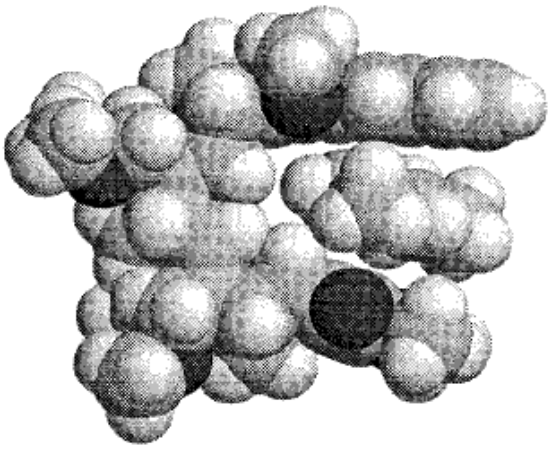

Chart 5.1 Line Structure and Space-filling Representations of 1. In the bottom part, a space- filling model with 1,2,4-trimethylbenzene in the cleft of 1 is shown.

This study uses molecule **1** which contains an electron donor (D) and electron acceptor (A) that are joined together by a "rigid" saturated bridge (a DBA molecule).[5] Chart 5.1 provides a space filling, CPK rendering of **1** that illustrates the vacant "cleft" which lies directly between the donor and acceptor groups. For a molecule of this topology, electron tunneling through the cleft occurs in addition to tunneling mediated by the covalent linkages of the bridge. Previous work[2,6] has shown that the presence of a solvent molecule within the cleft enhances the rate of tunneling as compared to that through the bridge. The simultaneous interaction of the solvent, e.g., 1,2,4-trimethylbenzene (Chart 5.1), with the donor and acceptor groups is believed to cause the enhancement. An earlier study found that increasing the size of alkyl substituents on aromatic solvents reduces the electronic coupling magnitude because bulky alkyl groups, such as isopropyl, impede access of the solvents' aromatic core to the cleft of **1**. In contrast, the current work explores how the electronic coupling depends on the *electronic* characteristics of the substituted benzene, rather than on its steric bulk.

In the nonadiabatic limit, Fermi's Golden Rule can be used to calculate the electron- transfer rate constant, k_{et}

$$k_{et} = \frac{2\pi}{\hbar}|V|^2 \mathrm{FCWDS} \tag{5.1}$$

$|V|$ is the donor/acceptor electronic coupling, and FCWDS is the Franck-Condon weighted density of states, which accounts for the nuclear rearrangement that must precede the electron tunneling event. Among solvents that provide similar FCWDS factors, the donor-acceptor electronic coupling will determine the relative magnitudes of the transfer rate constants. Molecules that lie between the donor and acceptor can

enhance the electronic coupling through interaction of their molecular orbitals with those of the donor and acceptor. When the electronic coupling is weak enough, it can be calculated using a perturbation theory approach, known as superexchange.[7] The superexchange mechanism predicts a dependence of the electronic coupling on the energy of electronic states that mediate the electron's (or a hole's) movement from donor to acceptor. Previous studies have suggested that electron mediated superexchange is more important than hole mediated superexchange for the transfer of an electron from the locally excited state of **1**.[8] For a single site between the donor and acceptor (see Figure 5.2), the superexchange expression for an electron-mediated process is given by

$$|V| = \frac{H_{\mathrm{D^*S}} H_{\mathrm{SA}}}{E_{\mathrm{D^+S^-A}} - E_{\mathrm{D^*SA}}} \tag{5.2}$$

where H_{D^*S} and H_{SA} are the donor/solvent and solvent/acceptor exchange integrals, respectively. E_{D^*SA} and E_{D+S-A} represent the energies of the transition state and the vertically displaced superexchange state (D^+S^-A). By using solvents with differing vertical electron affinities (EA_v), it should be possible to manipulate the size of the denominator in eq 5.2 and tune $|V|$. In particular, solvents that are more favorable toward electron attachment (more positive values of EA_v) are predicted to stabilize the superexchange state D^+S^-A and enhance the total electronic coupling, $|V|$.

Previous studies of solvent mediated superexchange with **1** identified a significantly larger value of the electronic coupling for benzonitrile in the cleft than for benzene or alkylbenzenes. The current study explores how the solvent molecule's electronic character affects the size of the superexchange coupling. The earlier data in

benzonitrile and alkylbenzene solvents showed that methyl substitution of the aromatic ring reduced the electronic coupling slightly. By contrast, those studies showed that multiple isopropyl groups on a benzene kept its aromatic core out of the cleft of **1**. The current study compares the coupling provided by methyl- substituted aromatic solvents with correspondingly substituted chloro aromatic solvents (see Chart 5.2). The similar size of methyl and chloro groups should produce similar steric effects, thus allowing the electronic effects to be identified (the new feature of this study). Two pairs of solvents (pair 1: *meta*-chlorotoluene/*meta*-dichlorobenzene; pair 2: 2,5-dichlorotoluene/ 1,2,4-trimethylbenzene) are investigated. The solvents in each pair have significantly different electron affinity, but have similar sizes, shapes, and electrostatic properties (see Table 5.2) and should give rise to similar FCWDS terms. The *meta*-chlorotoluene/*meta*-dichlorobenzene pair was chosen because it is moderately polar, and the 2,5-dichlorotoluene/1,2,4-trimethylbenzene pair was chosen because it is weakly polar and should allow an accurate determination of the reaction free energies. To the extent that the FCWDS factors are the same for each solvent pair, a direct comparison of the electron transfer rate constants can be ascribed directly to variation of the coupling magnitude,[9] and the correlation between $|V|$ and solvent electron affinity may then be analyzed.

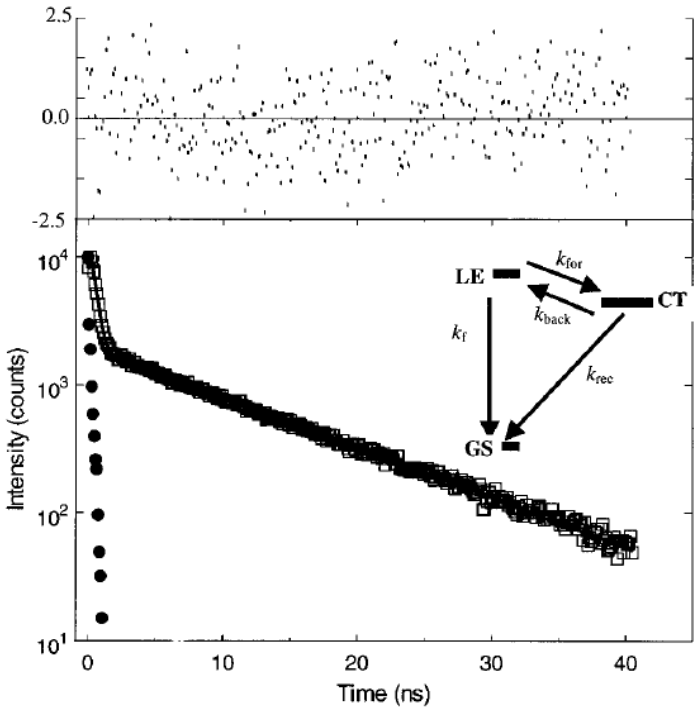

Figure 5.1 A fluorescence decay profile is shown for 1 in 2,5-dichlorotoluene at 338 K. The best fit parameters are 311 ps (90%), 11.15 ns (10%) and a χ^2 of 1.14. The top graph plots the residuals for the best-fit decay law (thick line through data points). For clarity, only every tenth data point is plotted here. The inset shows the level kinetics used to interpret these data.

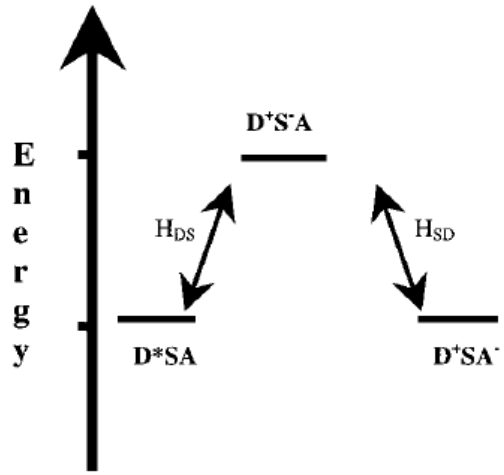

Figure 5.2 This diagram illustrates the energy level scheme that is used in the superexchange model to calculate | *V*|.

This work proceeds by measuring the electron-transfer rates as a function of temperature in each of the solvents. Extracting the electronic coupling from the data requires an accurate modeling of the FCWDS in each solvent as a function of temperature. Use of different FCWDS models yields different estimates of the coupling, but *relative* coupling magnitudes in different solvents are robust to changes in the FCWDS model [these affects have been discussed elsewhere[10]]. The results are analyzed using two different models for the FCWDS: a dielectric continuum treatment and a molecular based treatment. The molecular treatment is the same as that used previously to describe the temperature-dependent electron-transfer rate constant and reaction free energy in a series of alkyl-substituted benzenes.[6] This study extends the application of this model to the more polar chlorobenzene solvents and benzonitrile, identifying its limitations for characterizing the reaction free energy, solvent reorganization energy and their temperature dependencies. A dielectric continuum treatment is also used to model the FCWDS. This model is expected to provide reasonable estimates in the polar solvents and act as a point of reference for the molecular treatment. Combining these models for $\Delta_r G$ with previous results for the internal reorganization energy parameters, allows the solvent dependent reorganization energy $\lambda_o(T)$ and the electronic coupling magnitude $|V|$ to be determined from the temperature dependence of the rate constant. The correlation of $|V|$ with the solvent's electronic character could then be analyzed.

Table 5.1 Reaction Free Energies $\Delta_r G$, Reorganization Energies λ_o, and FCWDS Are Given at T = 295 K for the Electron Transfer Reaction Using Different Models[a]

	continuum[b]			molecular			from $k(T)$ data	
solvent[c]	$\Delta_r G$, eV	λ_o, eV	FCWDS, eV^{-1}	$\Delta_r G$, eV	λ_o, eV	FCWDS, eV^{-1}	$\Delta_r G$, eV	λ_o, eV
mesitylene	−0.19	0.0038	50	−0.044	0.06	6.7	−0.039	0.03
toluene	−0.20	0.016	30	−0.090	0.09	6.8	−0.089	0.09
benzene	−0.19	0.0045	47	−0.11	0.10	6.3	−0.11	0.10
TMB	−0.20	0.013	31	−0.054	0.07	3.7	−0.057	0.09
DCT	−0.26	0.053	15	−0.10	0.15	0.053	−0.10	0.15
DCB	−0.35	0.14	13	−0.28	0.32	0.25		0.60 ± 0.08
MCT	−0.35	0.14	13	−0.31	0.36	2.8		0.39± 0.03
CB	−0.32	0.14	13	−0.32	0.33	1.5		0.47± 0.04
benzonitrile	−0.47	0.28	12	−0.52	0.52	0.084		1.06± 0.05

[a] The error estimates in the polar solvents represent the effect of different models for the reaction free energy's temperature dependence. See text for details.[b] The solute parameters used in both calculations are 8.51 Å for the cavity radius, 34 D for the CT state dipole moment, and 0.08 eV for the gas-phase driving force. Relevant solvent parameters are reported in Table 5.2. [c] Solvent abbreviations correspond to the structures in Chart 5.2.

5.2 Background

The single-mode semiclassical expression for the FCWDS models interactions with the solvent classically and treats solute vibrations using a single effective high-frequency, quantum mechanical, mode.[1b,11] The rate constant expression is

$$k_{et} = \frac{4\pi^2}{h}|V|^2 \frac{1}{\sqrt{4\lambda_o \pi k_B T}} \sum_{n=0}^{\infty} \exp(-S)\left(\frac{S^n}{n!}\right) \times \exp\left[-\frac{(\Delta_r G + \lambda_o + nh\nu)^2}{4\lambda_o k_B T}\right] \quad (5.3)$$

This equation has five parameters: $\Delta_r G$ (the change in reaction Gibbs free energy), λ_o (low frequency-primarily solvent reorganization energy), λ_i (high frequency-primarily solute reorganization energy), ν (the effective frequency of the quantum mechanical mode), and $|V|$ (donor/acceptor electronic coupling). S (the Huang-Rhys factor) is defined as

$$S = \frac{\lambda_i}{h\nu} \tag{5.4}$$

Of these five parameters, λ_i and ν can be estimated from analysis of charge-transfer absorption and emission spectra.[10,11] Typically, $\Delta_r G$ and λ_o are estimated using a theoretical model. In this study, $\Delta_r G$ was determined experimentally in the weakly dipolar solvents, where its magnitude was within 0.1 eV of zero, and was modeled in the more polar solvents of the series. The molecular model employed (vide infra) provides $\Delta_r G$ values that are in reasonable agreement with the experimental values from the weakly polar solvents and with predictions of a dielectric continuum model for the highly polar solvents. Once reliable values of $\Delta_r G$, λ_i and ν have been obtained, the electronic coupling matrix element $|V|$ and the solvent reorganization energy $\lambda_o(T)$ can be extracted from analysis of the temperature-dependent rate constant by way of eq 5.3.

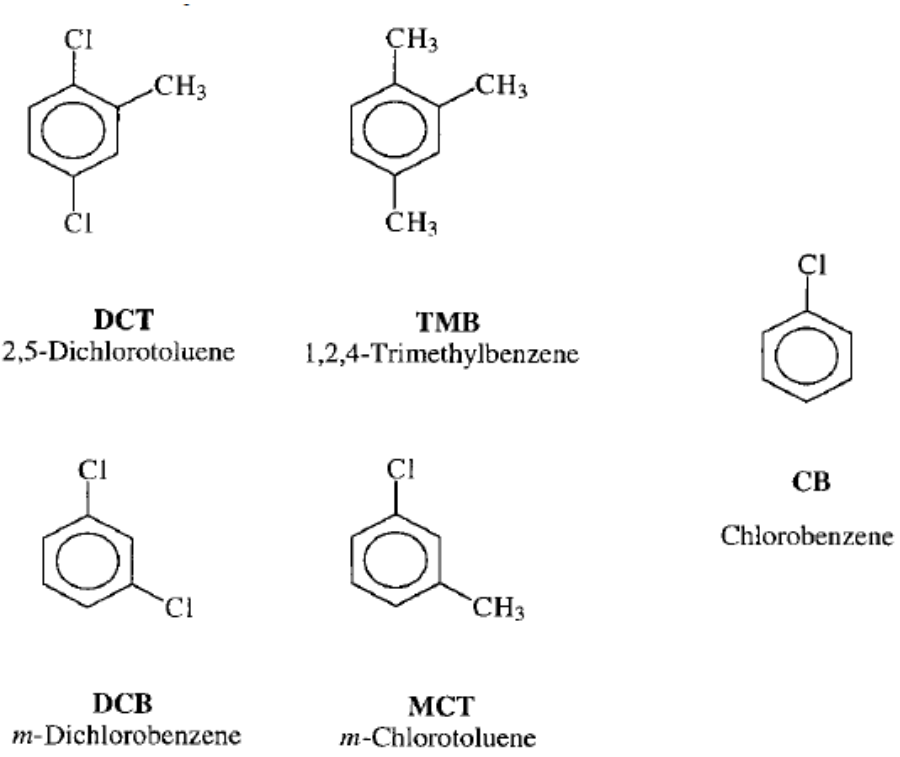

[a] Their abbreviations are included for easy reference.

Chart 5.2 Molecular Structures for the Five Solvents in This Study[a]

5.2.1 Continuum Approaches to $\Delta_r G$ and λ_o.

The simplest means of estimating $\Delta_r G$ and λ_o is to use a dielectric continuum model for the solute-solvent interaction. Such treatments have been used successfully to describe the solvent reorganization energy and reaction free energy for electron transfer in polar solvents. The continuum model used here treats the charge-separated state as a point dipole μ embedded in a spherical cavity that is immersed in a dielectric continuum. This description of the solute shape and electrostatic character is the same as that used in the molecular model and allows a direct comparison between the two treatments. The continuum reorganization energy λ_o is given by

$$\lambda_{o,cont} = \frac{\mu^2}{a_0^3}\left(\frac{\epsilon - 1}{2\epsilon + 1} - \frac{n^2 - 1}{2n^2 + 1}\right) \tag{5.5}$$

where a_0 is the effective cavity radius, ε is the static dielectric constant of the solvent, and *n* is the refractive index of the solvent. In this same approximation the reaction Gibbs free energy can be written as

$$\Delta_r G = \Delta_{vac} G - \left[\frac{\mu^2}{a_0^3}\right]\left(\frac{\epsilon - 1}{2\epsilon + 1}\right) \tag{5.6}$$

where $\Delta_{vac}G$ is the reaction Gibbs free energy in the absence of solvation. Although this continuum treatment of the solute-solvent interaction is useful in some situations, recent results[2] have shown that a molecular approach provides more accurate values of $\Delta_r G$ and λ_o for weakly dipolar solvents and especially for aromatic solvents where quadrupole interactions are important. A number of workers have constructed more elaborate models for the solvent cavity[10,12] and the medium's dielectric response.[13] As a point of reference, the spherical cavity dielectric continuum model is used to predict values for λ_o (outer sphere reorganization energy), $\Delta_r G$ and the FCWDS for the solvents studied here, see Table 5.1.

5.2.2 Molecular Approach to $\Delta_r G$ and λ_o.

Previous work showed[6] that a molecular description of solute-solvent interactions was important for accurately characterizing the reorganization energy, the reaction free energy, and their temperature dependencies in aromatic solvents. Matyushov[14] has developed a model that treats the solute and solvent molecules as polarizable

spheres, with imbedded point dipole moments, and, in the case of solvent, an imbedded point quadrupole moment. The solute dipole moment magnitude μ is given by ΔqR_{DA}, in which Δq is the charge transferred from the donor to the acceptor and R_{DA} is the charge separation distance. This model was successfully used to simulate the solvent and temperature dependencies of the reaction free energy for **1** in a series of six alkylbenzene solvents using only four parameters to represent the solute.[2] The molecular model treats the reaction free energy as a sum of four components

$$\Delta_r G = \Delta_{vac} G + \Delta_{dq,i} G^{(1)} + \Delta_{disp} G + \Delta_i G^{(2)} \tag{5.7}$$

in which $\Delta_{vac}G$ corresponds to the reaction free energy in a vacuum and the other three terms account for solvation effects. This earlier study showed that the electrostatic and induction terms ($\Delta_{dq,i}G^{(1)}$ and $\Delta_i G^{(2)}$) make the dominant contributions to the solvation free energy and that the dispersion term $\Delta_{disp}G$ plays a minor part and may be ignored. The reorganization energy was expressed as a sum of three terms

$$\lambda_o = \lambda_p + \lambda_{ind} + \lambda_{disp} \tag{5.8}$$

in which λ_p accounts for solvent reorganization arising from electrostatic interactions, λ_{ind} is the contribution from induction forces, and λ_{disp} accounts for dispersion

interactions. A more detailed description of this model and its application to **1** may be found elsewhere.[2]

5.2.3 Internal Reorganization Parameters.

The internal reorganization energy λ_i and the effective frequency ν significantly influence the quantitative data analysis, but do not have a significant solvent dependence. Although the absolute value of the electronic couplings that are extracted from the measured electron-transfer rates depend on the values used for the internal reorganization parameters, the relative coupling magnitudes for **1** in different solvents do not depend on the values used for the internal reorganization parameters. The correlation between parameters in this system is discussed at length elsewhere.[10] The value used for λ_i is 0.39 eV and that used for ν is 1412 cm^{-1}. These are the same values that were used in previous studies[2,6] and were obtained through a combination of quantum chemical calculations and the analysis of charge-transfer spectra.

5.2.4 Kinetic Analysis.

Photoexcitation of the anthracene donor moiety creates a locally excited state that is slightly higher in energy than the charge separated state. Figure 5.1 shows the level kinetics scheme that is used to describe the decay of the locally excited (LE) state prepared by the light pulse. In highly dipolar solvents where k_{back} is small, the fluorescence decay of the locally excited state is single exponential with a decay constant that is the sum of the forward electron- transfer rate constant k_{for} and the intrinsic fluorescence decay rate constant of the chromophore. By measuring the deactivation of the locally excited state (k_f) in an analogue of **1** that has no electron

acceptor, it is possible to extract the electron transfer rate constant. This procedure can be used to assess any contributions from the external heavy atom effect or exciplex formation with chlorinated aromatic solvents and quantitatively account for them. The fluorescence decay rate of the donor only compound does not change in any significant way with the chlorine content of the solvent (see the Supporting Information and ref 8). To reiterate, the analysis assumes that the difference in fluorescence decay between the locally excited state of **1** and a donor only control compound in the same solvent arises from the electron transfer deactivation channel in **1**.

In weakly dipolar solvents the fluorescence decay law becomes double exponential because k_{back} is no longer small. In this case the analysis must account for the excited-state equilibrium and provides the three rate constants: k_{for}, k_{back}, and k_{rec} [see footnote 15 for details of this analysis]. The Gibbs free energy of the forward reaction is obtained from the ratio of the forward and back rate constants via

$$\Delta_r G = -RT \ln(k_{for}/k_{back}) \tag{5.9}$$

It is empirically found that $\Delta_r G$ values ≥ -0.1 eV can be reliably determined. More negative values have a small amplitude of the second decay component, which causes large uncertainty in the determination of k_{back} and of $\Delta_r G$.

5.3 Experimental Section

Solutions of **1** were prepared with an optical density of ca. 0.05 at the laser excitation wavelength, 375 nm. The preparation of **1** was reported elsewhere.[16] Chlorobenzene (99.9+%, HPLC grade), *m*-chlorotoluene (98%), *m*-dichlorobenzene (9 8%), 1 ,2,4-trimethylbenzene (98%), and 2,5-dichlorotoluene (98%) were purchased from Aldrich. The chlorinated solvents were dried over $CaCl_2$ for 2 days, filtered, and then fractionally distilled using a vigreux column. The purified fractions were used immediately in all the experiments. 1,2,4-trimethylbenzene was dried with anhydrous magnesium sulfate, filtered, and then refluxed over sodium for 2 days. The solution was then fractionally distilled using a vigreux column, and the purified fraction was immediately used to prepare the sample. Each solution was freeze-pump-thawed a minimum of three times. The samples were back-filled with Ar to reduce evaporation at the higher experimental temperatures.

Excitation of the sample was performed at 375 nm by the frequency-doubled cavity- dumped output of a Coherent CR-599-01 dye laser using LDS750 (Exciton) dye, which was pumped by a modelocked Coherent Antares Nd:YAG. The dye laser pulse train had a repetition rate of ca. 300 kHz. Pulse energies were kept below 1 nJ, and the count rates were kept below 3 kHz. All fluorescence measurements were made at the magic angle. Other specifics of the apparatus have been reported elsewhere.[17] The temperature cell was fabricated out of aluminum and was controlled by a NESLAB RTE-110 chiller. Temperatures were measured using a Type- K thermocouple (Fisher-Scientific), accurate to within 0.1 °C.

The fluorescence decays were fit to a sum of two exponentials using the Marquardt-Levenberg nonlinear least squares algorithm. Instrument response functions were measured using a sample of colloidal $BaSO_4$ in glycerol. Figure 5.1 shows a fluorescence decay from **1** in 2,5-dichlorotoluene at 338 K, the best fit to a sum of two-exponential and the fitting residuals.

Fitting to the semiclassical equation (eq 5.3) was performed using Microsoft Excel 2000. The FCWDS sum rapidly converges for the solvents in this study, and was not evaluated past the sixth term.

5.4 Results and Discussion

Fluorescence decay profiles of **1** and its donor only analogue were measured in the five aromatic solvents shown in Chart 5.2. The rate data is provided in the Supplemental Information. The lifetimes obtained for the donor only compound in each solvent do not differ greatly and do not display a significant temperature dependence. The donor only compound's fluorescence lifetimes were not significantly different from lifetimes measured in previous studies,[18] muting possible concerns about the chlorinated aromatic solvents affecting the intrinsic photophysics of the dimethoxyanthracene moiety. The fluorescence decays from **1** in the different solvents were analyzed using the kinetic scheme in Figure 5.1. The decay profiles in 1,2,4-trimethylbenzene and 2,5-dichlorotoluene, the pair of solvents with the smallest dipole moments, had a significant long time constant component, which allowed an accurate determination of k_{back} and $\Delta_r G$. Although a second decay component could be identified in the more polar chlorinated solvents, a single exponential dominated

the decay profiles, making it too difficult to reliably determine k_{back} and, hence, $\Delta_r G$. The amplitude of the long lifetime component correlated with the size of the solvent dipole moment, in accordance with its critical role in determining the solvation of the charge separated state. The present analysis is limited to the behavior of the forward rate constants, because they could be reliably determined for all of the solvents.

The charge separation rate constant for **1** in 2,5-dichlorotoluene is larger than that in 1,2,4-trimethylbenzene at all temperatures investigated (see Figure 5.4). The rate constant ratio varied from 1.5 at 295 K to 2.2 at 328 K. Determination of the relative electronic coupling magnitudes in these two solvents requires estimation of the FCWDS. Before proceeding with quantitative modeling of the reaction free energy $\Delta_r G(T)$ and the outer sphere reorganization energy $\lambda_o(T)$ by way of a molecular solvation model, it is useful to consider the predictions of a simple dielectric continuum model. The dielectric continuum treatment was used to predict the FCWDS terms at 295 K for each of the solvent pairs, 1,2,4-trimethylbenzene / 2,5-dichlorotoluene and *m*-dichlorobenzene/*m*-chlorotoluene, see Table 5.1.[19] The continuum model estimate of the FCWDS factor in 2,5-dichlorotoluene is half of its value in 1,2,4-trimethylbenzene. Accordingly, the ratio of the square of the electronic coupling magnitudes is 3, via eq 5.3. This indicates that the electronic coupling for **1** in 2,5-dichlorotoluene is 75% larger than that in 1,2,4-trimethylbenzene. It is important to realize that the continuum model prediction for the FCWDS in this weakly polar pair of solvents may not be reliable; e.g., quadrupole contributions to the solvation could be quite different for the two solvents. For the *m*-dichlorobenzene/*m*-chlorotoluene pair, the charge separation rate constant of **1** in *m*-dichlorobenzene is larger than that of

m-chlorotoluene at all temperatures (see Figure 5.4). At 295K the *m*-dichlorobenzene rate constant is 1.3 times larger. The continuum model predicts that the FCWDS for **1** in *m*-dichlorobenzene is the same as in *m*-chlorotoluene, so that the ratio of the squares of the electronic coupling terms is 1.3. This ratio gives an electronic coupling for **1** in *m*-dichlorobenzene that is about 15% larger than that in *m*-chlorotoluene. This analysis suggests that the difference in the electron transfer rate constants between the structurally similar solvents can be attributed, at least in part, to differences in the $|V|$. In addition, the continuum treatment provides a reference point for the molecular model described below.

5.4.1 Molecular Model.

Quantitative modeling of the reaction free energy and the reorganization energy was performed with a molecular model that accounts for solvent dipole, polarizability and quadrupole interactions.[2,14] The solvent molecule parameters needed for the model are reported in Table 5.2. An earlier study demonstrated that this model accurately reproduces the magnitudes and temperature dependence of the reaction free energy in a homologous series of alkylbenzenes. The model has four parameters for the solute. For **1** in the alkylbenzene solvents, these parameters were a cavity radius of 7.25 Å, a charge separated state dipole moment of 34 D, a solute molecular polarizability of 70 $Å^3$ and a vacuum reaction free energy, $\Delta_{vac}G$, of 0.34 eV.[2] Use of these parameters to calculate Δ_rG in 2,5-dichlorotoluene generates a value that is 0.15 eV too exoergic. One can adjust the four solute parameters in an effort to improve the agreement between the experimental and calculated Δ_rG values. However, it was not

possible to produce an accurate fit of the free energy data in all the solvents as a function of temperature. It was possible to fit $\Delta_r G$ at 295 K from 2,5-dichlorotoluene and from all of the alkylbenzene solvents. The parameters needed to accurately describe the data at 295 K were a cavity radius of 8.51 Å, a dipole moment of 34 D, a solute polarizability of 100 $Å^3$, and a $\Delta_{vac} G$ of 0.08 eV. The calculated solvent dependence of the free energy data is most sensitive to the cavity radius. The larger radius used for the fit at 295 K reduces the size of the electrostatic solvation and predicts a temperature dependence for the free energy that is much smaller than the experimentally observed dependence (e.g., the model predicts a free energy change for **1** in 2,5-dichlorotoluene of 0.025 eV from 295 to 347 K, whereas the observed change is 0.049 eV).

Figure 5.3 shows the reaction free energies for the solvents reported here as a function of temperature. It was found empirically that the average temperature dependence of the reaction free energy in the alkylbenzene and dichlorotoluene solvents is about 1 meV/K. The solid lines in the figure show a linear fit to the reaction free energy's temperature dependence. The observed temperature dependencies are 0.83 meV/K for 2,5-dichlorotoluene, 1.1 meV/K for 1 2,4-trimethylbenzene, 0.96 meV/K for benzene, 1.2 meV/K for toluene, and 1.3 meV/K for mesitylene. The quality of the fit is evident in Figure 5.3A, which expands the free energy scale about the experimental values found in the weakly dipolar solvents. The average of these slopes is 1.1 meV/K Because the reaction free energy is not available in the more polar solvents and a physical model is not available to guide the change

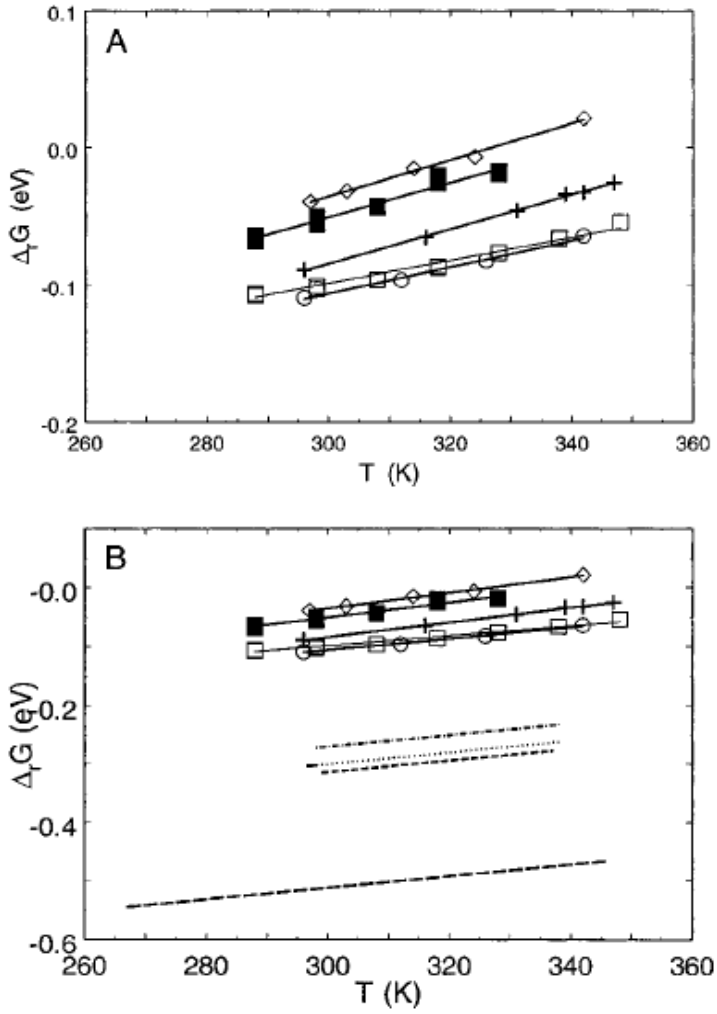

Figure 5.3 The experimental $\Delta_r G$ data for 2,5-dichlorotoluene (open squares), 1,2,4-trimethylbenzene (filled squares), toluene (+), benzene (open circle), and mesitylene (open diamonds) are shown here. Panel A shows an expanded view of the data for which experimental $\Delta_r G$ data are available. The best fit predictions from the molecular model are shown as solid lines for each data set (see text for details). Panel B shows the predicted free energies for all the solvents. The long dashed curve is the prediction for benzonitrile, the short dashed curve is the prediction for chlorobenzene, the dotted curve is the prediction for *m*-chlorotoluene, and the dashed-dotted curve is the prediction for *m*-dichlorobenzene.

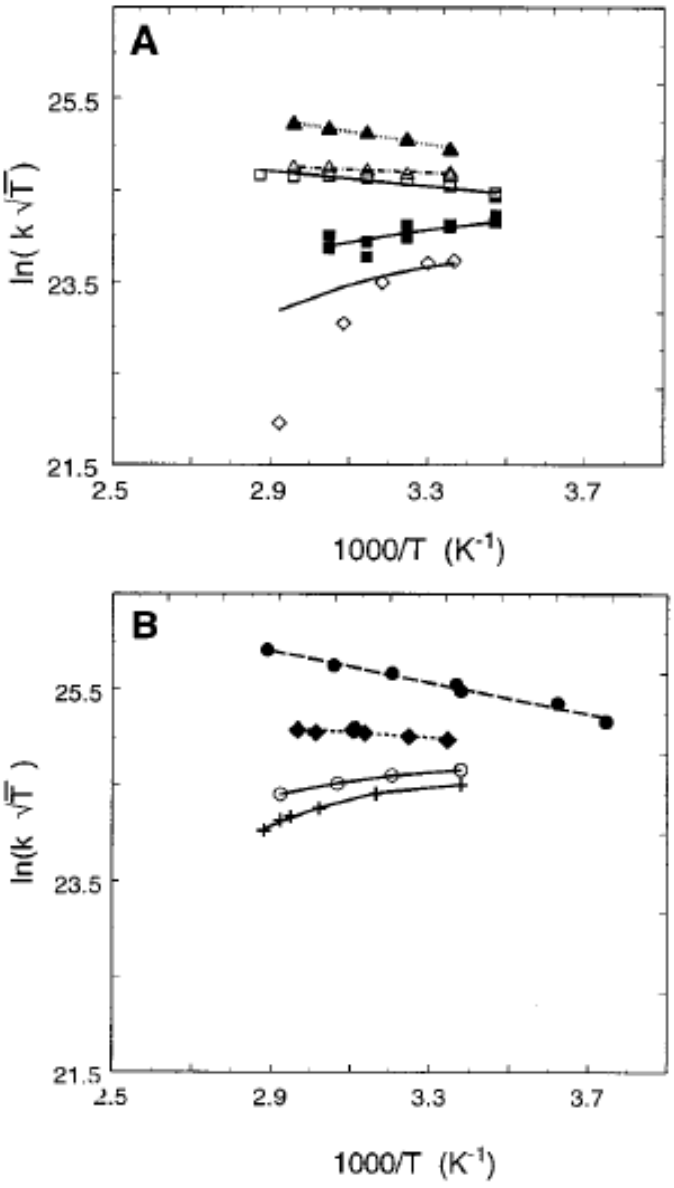

Figure 5.4 The temperature-dependent rate data are fit to the semiclassical expression in each of the solvents. The data are plotted in two panels for clarity, however the axis scales are identical. Part A plots the data for *m*-dichlorobenzene (filled triangles), *m*-chlorotoluene (open triangles), 2,5-dichlorotoluene (open squares), 1,2,4-trimethylbenzene (filled squares), and mesitylene (open diamonds). Part B plots the data for benzonitrile (filled circles), chlorobenzene (filled diamonds), benzene (open circles), and toluene (+). The lines represent best fit curves using the semiclassical equation (see Figure 5.3 for convention on line type).

in temperature dependence through the different solvent systems studied here, an empirical value of 1 meV/K was used in these solvents (vide infra).

Figure 5.3B shows the data of Figure 5.3A along with the reaction free energies that are predicted using the molecular solvation model and the new parameter set for **1** in chlorobenzene, *m*-chlorotoluene, *m*-dichlorobenzene, and benzonitrile. $\Delta_r G$ in these solvents is too negative to be determined experimentally from the fluorescence decays. The molecular model predictions of the free energies at 295 K can be compared with the continuum model predictions (see Table 5.1). For the more polar solvents, i.e., for solvents with $\varepsilon_S \geq 5$, the largest deviation between the two sets of predicted values occurs for *m*-dichlorobenzene and represents a 20% difference, 0.07 eV in magnitude. The continuum model and molecular model predictions deviate much more significantly in the nondipolar and weakly dipolar solvents, where the dielectric continuum treatment is expected to fail. The dielectric continuum model performs reasonably well for **1** in more polar solvents, as discussed previously for the electron transfer of **1** in acetonitrile and benzonitrile.[10] This agreement between the continuum model and the molecular model in the polar solvents and between the experimental measurements and the molecular model in the weakly dipolar solvents supports the reliability of the molecular model's $\Delta_r G$ prediction at 295 K.

The electronic coupling magnitude can be determined from the rate data and eq 5.3 provided accurate values of the solvent reorganization energy and its temperature dependence are available. The failure of the molecular model, with the new parameter set, to reproduce the temperature dependence of $\Delta_r G$ in this set of solvents requires use of an alternate method (vide infra) to evaluate λ_S and its

temperature dependence. The results of the analysis are sensitive to the value used for the temperature derivative of $\Delta_r G$. To estimate the uncertainty in the derived values of the reorganization energy and the electronic coupling, three different values of $d(\Delta_r G)/dT$ were used for solvents in which this quantity was not directly measured; benzonitrile, 1,3-dichlorobenzene, chlorobenzene, and 3-chlorotoluene. Because the temperature dependencies of the reaction free energy in the nonpolar and weakly polar solvents are clustered near 1 meV/K, this value was used as the best estimate. This is the value used for preparation of the plots shown in Figures 5.3 through 5.6. To estimate the error in this value for the reaction free energy's temperature dependence, an upper bound was obtained by using a slope of 2 meV/K and a lower bound was obtained by using the predicted slope from the continuum model.[20] Independent fits to the data were performed with these estimates and used to determine the upper and lower bounds on the solvent reorganization energy and the electronic coupling (see Tables 5.1 and 5.3).[21]

Table 5.2 This Data Provides Physical Parameters of the Solvents Used in This Study

solvent	n_D[a]	ϵ[a]	IP, eV[b]	EA_v, eV[c]	μ, D[d]	$\langle Q \rangle$, D Å[d]	α, Å^3[e]	σ, Å	ϵ_{LJ}, K	η
mesitylene	1.50	2.27	8.4	−1.03	0.07	7.4	17.0	6.26	870	0.556
toluene	1.49	2.38	8.8	−1.11	0.29	7.8	12.4	5.66	704	0.538
benzene	1.50	2.28	9.2	−1.12	0.00	8.2	10	5.27	614	0.518
TMB	1.50	2.38	8.4−8.6	−1.07	0.30	7.3	17.0	6.26	865	0.562
DCT	1.55	3.01	8.8	−0.31	0.57	14	17.0	6.36	972	0.630
DCB	1.55	5.02	9.1	−0.31	2.03	10	13.2	5.97	882	0.587
MCT	1.52	5.55	8.7	−0.75	2.34	7.8	13.2	6.01	838	0.579
CB	1.52	5.62	9.1	−0.75	2.15	8.4	11.5	5.62	748	0.552
benzonitrile	1.53	25.9	9.7	0.24	4.85	15.2	12.5	5.69	741	0.565

[§]See Chart 5.2 for solvent abbreviations. [a] Data were obtained from Landolt-Bornstein. The value for DCT was estimated using the Debye formula and the vacuum dipole moment. [b] NIST Webbook at webbook.nist.gov. [c] Electron Affinities were obtained from ref 22. [d] The dipole moment and quadrupole moments were calculated at the RHF/6-31G**//RHF/6-31G** level using Gaussian 98. [e] Polarizabilities were obtained from the literature *(CRC Handbook*, 78th ed.; CRC Press: Boca Raton, FL, 1998), but optimized, by <10%, for a best fit of the $\Delta_r G$(295 K) data. [f] The hard sphere diameter, α and the Lennard-Jones energy parameter ε_{LJ} were obtained from the literature.[28g] The reduced packing density, $\eta = \pi\rho\sigma^3/6$, was determined using literature values of the density (CRC Handbook (vide supra)).

Given the difficulty in using the molecular model to quantitatively reproduce the temperature dependence of the reaction free energies, the model was not employed to make predictions of the solvent reorganization energies, for which no direct experimental data is available. Nonetheless, it was possible to evaluate the temperature-dependent reorganization energy and the electronic coupling from the rate data using eq 5.3 and the available information. The temperature-dependent reorganization energy was determined from the temperature dependence of the rate data through the slope of the plot in Figure 5.4. The derivative, $(\partial \ln(k_{et}\sqrt{T})/\partial(1/T))$, was evaluated analytically from eq 5.3 and was fit to the temperature- dependent slope to determine the solvent reorganization energy at each temperature (vide infra). Figure 5.5 shows the temperature dependent solvent reorganization energies obtained from this analysis, and Table 5.1 presents values for the reorganization energies at 295 K. A comparison of the 295 K reorganization energies with those predicted by the continuum model and the molecular model can be made from Table 5.1. In the nondipolar solvents the molecular model and the experimentally derived reorganization energies are in good agreement, whereas the continuum model predicts a reorganization energy that is much too small. The latter result is expected since the continuum model does not account for solvent quadrupoles, which are significant contributors to solvation, in these solvents. In the polar solvents, the predictions of both models deviate strongly from the experimentally derived values. Among the chlorinated solvents, the continuum model predicts that the reorganization energies in chlorobenzene, *m*-dichlorobenzene, and *m*-chlorotoluene

(the three solvents with >2 D dipole moments) are comparable and are 3-fold larger than the reorganization energy in 2,5-dichlorotoluene (μ = 0.57 D).

Table 5.3 The Best Fit |*V*|, the Electron Affinity EA, and the Ionization Potential IP

solvent[a]	$\|V\|$, cm^{-1}	IP,[b] eV	EA_v,[c] eV
mesitylene	2.8	8.4	−1.03
toluene	4.7	8.8	−1.11
benzene	5.3	9.2	−1.12
TMB	4.6	8.4−8.6	−1.07
DCT	9.6	8.8	−0.31
DCB	22 ± 8	9.1	−0.31
MCT	7.3 ± 1	8.7	−0.75
CB	11 ± 2	9.1	−0.75
benzonitrile	55 ± 13	9.7	0.24

[a] Solvent abbreviations correspond to the structures in Chart 2. [b] The ionization potentials are taken from the NIST Webbook at webbook.nist.gov. [c] The electron affinities are taken from ref 27. The error estimates in the polar solvents represent the effect of different models for the reaction free energy's temperature dependence. See text for details.

The molecular model predictions of λ_o are two to 3-fold larger than the continuum predictions.The molecular model also predicts that λ_o values among the first three solvents (chlorobenzene,*m*-dichlorobenzene and *m*-chlorotoluene) are comparable and are roughly 2-fold larger than those for 2,5-dichlorotoluene. The experimentally derived values of λ_o are roughly 66% larger than the values obtained from the molecular model and show similar grouping by solvent, albeit with considerably more scatter. The temperature dependence of the experimental reorganization energies are weak, Figure 5.5, a finding that is consistent with the weak dependence predicted by the molecular model.[23]

Figure 5.4 presents the rate constant data for the five solvents in Chart 2 and also previously published data in benzene, toluene, mesitylene, and benzonitrile. The solid curves correspond to a best fit to these data by the semiclassical expression, eq 5.3, using the reaction free energies (vide supra) and the internal reorganization energies found previously for **1**.[10] The data were fit in a two step process that decoupled the electronic coupling parameter $|V|$, assumed to be temperature independent, from the temperature-dependent reorganization energy $\lambda_o(T)$. In the first step, the temperature-dependent slope was fit to obtain the reorganization energy, as described above. In the second step, the temperature-dependent reorganization energies were input to eq 5.3 and the $|V|$ parameter was adjusted to fit the data. The best fit curves are displayed in Figure 5.4. The best fit $|V|$ values are reported in Table 5.3.

The rate constants in Figure 5.4 are reproduced accurately by the semiclassical expression for all the solvents except mesitylene. In the latter case the rate constant displays an anomalous decline at higher temperatures. This feature of the kinetics will be discussed elsewhere.[24] The rate constants in the alkylbenzene solvents appear to lie near the peak of the Marcus curve (see λ_o in Table 5.1 and $\Delta_r G$ in Figure 5.3), whereas the rate constant in the more polar solvents clearly lie in the normal region. The electronic couplings obtained from these fits are presented in Table 5.3 with the solvent molecules' electron affinity and ionization potential. The value for the electronic coupling of 2,5-dichlorotoluene is two times larger than that for the similarly shaped 1,2,4-trimethylbenzene, and the electronic coupling for *m*-dichlorobenzene is three times larger than that of the structurally similar *m*-

chlorotoluene. These results are in qualitative agreement with the conclusions drawn from the continuum treatment; however, the magnitudes of the electronic coupling changes are larger in magnitude.

The electronic couplings reported for the alkylbenzenes and benzonitrile are smaller than the values reported previously.[6] This difference arises from the different reorganization energy values used in the different analyses and reflects the sensitivity of the electronic coupling magnitude to quantitative details of the modeling.

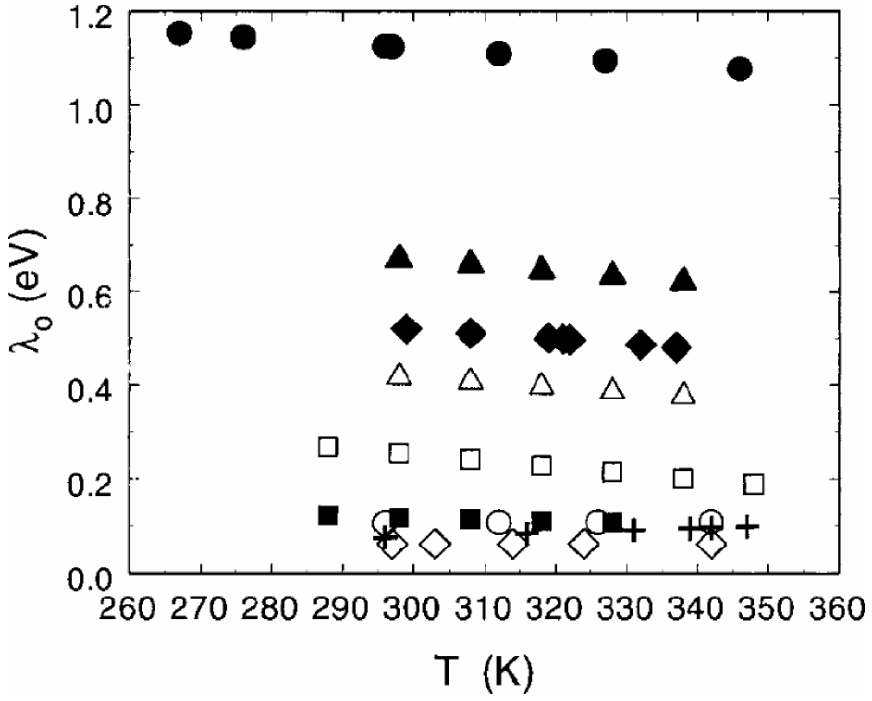

Figure 5.5 The temperature-dependent reorganization energies, predicted by the molecular- based model, are presented here for each of the solvents. The symbol convention is the same as that in Figure 5.4.

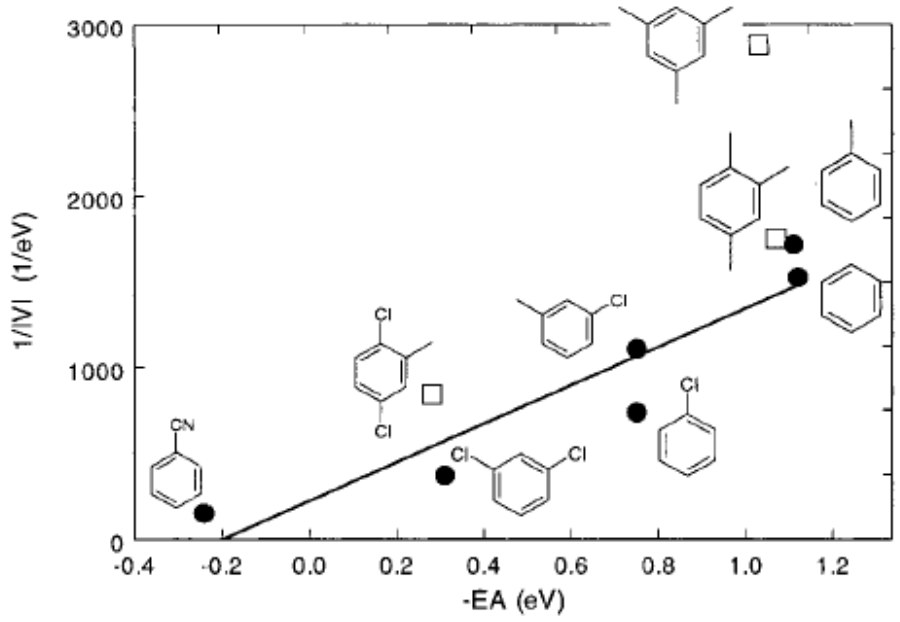

Figure 5.6 The inverse of the electronic coupling is plotted as a function of -EA for different solvents. EA values are taken from ref 26. The line represents a best fit to the monosubstituted and di-substituted benzene data (filled circles). The open squares are the trisubstituted benzene data.

A comparison of the electronic coupling values to the reported ionization potentials of the solvent molecules indicates no apparent correlation or dependence. A comparison of the electronic coupling magnitudes with the vertical electron affinities of the solvent molecules displays a correlation: see Figure 5.6. Equation 5.2 predicts that a plot of $1/|V|$ versus (E_{D+S-A-} - E_{D^*BA}) should be linear. The vertical electron affinity of the solvent molecule, which is hypothesized to be proportional to the difference in energy between the transition state and the mediating superexchange state,[25] is used as a measure of this energy gap in Figure 5.6. As expected from the superexchange treatment, the graph shows a general correlation between –EA and $1/|V|$. This correlation shows that solvents with more positive electron affinities (more readily accept an electron) have a larger $|V|$ than solvents with more

negative electron affinities (less readily accept an electron). The value of the electronic coupling is also dependent on the solvent size and this adds a degree of scatter to the plot. The plot shows that the bulkier, trisubstituted solvents (open squares) generate a smaller electronic coupling than smaller solvents (filled circles) of a comparable electron affinity. Presumably, the more highly substituted solvents are less effective at mediating electron transfer because of their reduced ability to access geometries that have good electronic wave function overlap with the donor and acceptor moieties, described by the exchange terms in eq 5.2. The reasonable correlation between –EA and 1/| *V*| indicates that electron mediated superexchange involving solvent is the dominant source of coupling in this system.

The line in Figure 5.6 represents a linear fit to the couplings in all the solvents that are not triply substituted; i.e., filled circles. The slope of this line (1123 eV-2) can be used to estimate the geometric mean of the two exchange couplings H_{D^*S} and H_{AS}; $\beta \equiv \sqrt{H_{D^*S}H_{AS}}$ = 0.030 eV or 240 cm-1. This value is 3-6 times smaller than couplings found for cyanoanthracene-alkylbenzene contact ion pairs formed by excitation of charge transfer complexes.27 Coulomb attraction between the ions presumably reduces the separation and enhances the exchange coupling in the contact ion pairs. The estimate of β for 1 with aromatic solvents is only about fifteen percent larger than the b found for solvents spanning the wider, 10 Å cleft of a related C-shaped molecule.8a The smaller cleft for 1 would be expected to support more extensive, simultaneous interactions between the donor, “cleft resident” solvent, and the acceptor and, therefore, to produce an even larger mean value of β. A difference of

the electronic symmetry in the active orbitals on the donor and acceptor may act to reduce the effective mean β for **1**, as compared to the previously studied case.[28]

5.5 Summary and Conclusions

A molecular model that describes the reaction free energy and solvent reorganization energy in alkylbenzene solvents was extended to electron-transfer studies in chlorinated benzene solvents. The previous calibration of this model for solute molecule **1** resulted in reaction free energies in the chlorinated solvents that were more negative than observed experimentally. The model was parametrized to characterize the reaction free energy at 295 K for the alkylbenzenes and dichlorotoluene. In particular, the cavity radius of the solute was increased in order to not overestimate the amount of solvation in dichlorotoluene. This procedure predicted a temperature dependence for the reaction free energy that was weaker than that observed experimentally. For the nonpolar and weakly polar solvents the temperature dependent reaction free energy was determined empirically. Although the molecular model successfully replicates the solvation provided by a homologous series of solvents; e.g., the alkylbenzenes, it fails to extrapolate well to a broader range of solvents.

To obtain an accurate modeling for the reaction free energy through the range of solvents studied here, the molecular model was fit to the experimental data in nonpolar solvents at 295 K. The reaction free energies that this model predicts in the more polar solvents are in good agreement with the values predicted by the dielectric continuum model. The temperature dependence of the reaction free energy in the

polar solvents was treated as linear. Three different values of the slope ($d\Delta_rG/dT$) were used in order to span a reasonable range of values. With the reaction free energy in hand, the temperature-dependent rate data was used to obtain the solvent reorganization energy and the electronic coupling magnitude. The analysis generated solvent reorganization energies that were larger than those predicted by the molecular model and the dielectric continuum model. The electronic couplings found for the aromatic solvents correlated with the vertical electron affinities of the solvent molecules; *more positive* electron affinities produce a *larger* electronic coupling for **1** than solvents with less positive electron affinities. This observation is consistent with a superexchange mechanism that predicts an increase in the electronic coupling when the energy separation between the electron-transfer transition state (D*SA) and the superexchange state (D^+S^-A) is reduced. This energy separation should be smaller in solvents with more positive electron affinities. The poor correlation of $1/|V|$ with solvent ionization potential indicates that the electronic coupling is dominated by electron mediated pathways rather than hole-mediated pathways. These data also show that more highly substituted aromatic solvents are less effective at mediating electron transfer in **1** than sparsely substituted solvents of similar electron affinity. This decreased efficiency is rationalized as an inability of the solvent to enter the cleft, and/or its decreased ability to access favorable orientations once inside the cleft.

5.6 References

(1) (a) Jortner, J., Bixon, M., Eds. Electron Transfer-From Isolated Molecules to Biomolecules. In *Advances in Chemical Physics*; Wiley: New York, 1999. (b) Barbara, P. F.;. Meyer, T. J; Ratner, M. A. *J. Phys. Chem.* **1996**, *100*, 13148.

(2) Read, I.; Napper, A.; Zimmt, M. B.; Waldeck, D. H. *J. Phys. Chem. A* **2000**, *104*, 9385.

(3) (a) Newton, M. D. *Chem. Rev.* **1991**, *91*, 767; (b) Jordan, K. D.; Paddon-Row, M. N. *Chem. Rev.* **1992**, *92*, 395.

(4) (a) Nitzan, A. *J. Phys. Chem. A* **2001**, ASAP. (b) Segal, D.; Nitzan, A.; Ratner, M.; Davis, W.B. *J. Phys. Chem. B* **2000**, *104*, 2790; (c) Nitzan, A.; Jortner, J.; Wilkie, J.; Burin, A. L.; Ratner, M. A. *J. Phys. Chem. B* **2000**, *104*, 5661.

(5) The word “rigid” is used to indicate that the bridge has only one (not multiple) minimum energy conformation.

(6) (a) Read, I.; Napper, A.; Kaplan, R.; Zimmt, M. B.; Waldeck, D. H. *J. Am. Chem. Soc*. **1999**, *121*, 10976; (b) Kumar, K.; Lin, Z.; Waldeck, D. H.; Zimmt, M. B. *J. Am. Chem. Soc.* **1996**, *118*, 243.

(7) (a) McConnell, H. M. *J. Chem. Phys.* **1961**, 35, 508. (b) Newton, M. D. *Chem. Rev*. **1991**, *91*, 767. (c) Ratner, M. A. *J. Phys. Chem.* **1990**, *94*, 4877.

(8) (a) Kaplan, R.; Napper, A. M.; Waldeck, D. H.; Zimmt, M. B. *J. Phys. Chem. A*. **2002**, *106*,
1917. (b) Kaplan, R. W.; Napper, A. M.; Waldeck, D. H.; Zimmt, M. B. *J. Am. Chem. Soc*. **2000**, *122*, 12039.

(9) If the FCWDS for each solvent pair is constant, then an increase in rate constant for the solvent pair may be linked to an enhanced electronic coupling, since

$$\frac{k_1}{k_2} = \frac{\frac{2\pi}{\hbar}|V_1|^2 \mathrm{FCWDS}_1}{\frac{2\pi}{\hbar}|V_2|^2 \mathrm{FCWDS}_2} = \frac{|V_1|^2}{|V_2|^2}$$

A qualitative analysis of this sort in a broad range of solvents is reported elsewhere.[8] These comparisons provide good evidence that the electronic coupling is correlated to the solvent molecule’s electron affinity, so that an electron mediated superexchange mechanism is operative for **1**’s photoinduced electron transfer.

(10) Kumar, K.; Kurnikov, I. V.; Beratan, D. N.; Waldeck, D. H.; Zimmt, M. B. *J. Phys. Chem. A* **1998**, *102*, 5529.

(11) (a) Marcus, R. A. *J. Phys. Chem.* **1989**, *93*, 3078. (b) Zeng, Y.; Zimmt, M. B. *J. Phys. Chem.* **1992**, *96*, 8395.

(12) (a) Brunschwig, B. S.; Ehrenson, S.; Sutin, N. *J. Phys. Chem.* **1986**, *90*, 3657. (b) Barzykin, A. V.; Tachiya, M. *Chem. Phys. Lett.* **1998**, *285*, 150.

(13) (a) Jeon, J.; Kim, H. J. *J. Phys. Chem. A* **2000**, *104*, 9812. (b) Zhou, Y.; Griedman, H.; Stell, G. *J. Chem. Phys.* **1989**, *91*, 4885.

(14) Matyushov, D. V.; Voth, G. A. *J. Chem. Phys.* **1999**, *111*, 3630.

(15) The fluorescence decay of **1** in 1 ,2,4-trimethylbenzene is fit to the biexponential form: $I(t) = a_+e^{-k_+t} + (1 - a_+)e^{-k-t}$. The forward electron transfer rate constant k_{for} is obtained from $k$for = $a_+(k_+ - k_-) - k_f + k_-$, and the reverse electron-transfer rate constant k_{back} is obtained from $k_{back} = [(k_+ - k_-)^2 - (2k_f + 2k_{for} - k_+ - k_-)2]/4k_{for.}$ k_f, the donor only decay rate constant, is equated to the rate constant measured for the donor only analogue in the same solvent and temperature.

(16) Details concerning the preparation of the DBA compound have been reported elsewhere. (a) Kumar, K.; Tepper, R. J.; Zeng, Y.; Zimmt, M. B. *J. Org. Chem.* **1995**, *60*, 4051. (b) Kaplan, R. Ph. D. Thesis, Brown University, Providence, RI, 2001.

(17) (a) Zeglinski, D. M.; Waldeck, D. H. *J. Phys. Chem.* **1988**, *92*, 692. (b) O'Connor, D. V.; Phillips, D. *Time Correlated Single Photon Counting*; Academic Press: New York, 1984.

(18) Kaplan, R. W.; Napper, A.; Zimmt, M. B.; Waldeck, D. H. *J. Am. Chem. Soc.* **2000**, *122*, 12039.

(19) The parameters in the continuum calculation (cavity radius, vacuum free energy difference and dipole moment change) were chosen to match the parameters in the molecular treatment. This choice allowed a direct comparison between the two models.

(20) The slopes found via the continuum model were 0.30 meV/K for 1 ,3-dichlorobenzene, 0.40 meV/K for chlorobenzene, 0.40 meV/K for chlorotoluene, and 0.12 meV/K for benzonitrile. Previous work (Vath, P.; Zimmt, M. B. *J. Phys. Chem. A* **2000**, *104*, 2626) showed that the continuum model underestimates the temperature dependence of the reaction free energy.

(21) (a) With a temperature dependence of 2 meV/K for Δ_rG, one finds λ_o = 0.44 eV and $|V|$ = 9.6 cm^{-1} in chlorobenzene, λ_o = 0.53 eV and $|V|$ = 16.6 cm^{-1} in dichlorobenzene, λ_o = 0.37 eV and $|V|$ = 6.9 cm^{-1} in *meta*-chlorotoluene, and λ_o = 1.0 eV and $|V|$ = 42 cm^{-1} in benzonitrile. (b) With the continuum model's temperature dependence for Δ_rG (see ref 20), one finds λ_o = 0.51 eV and $|V|$ = 12 cm^{-1} in chlorobenzene, λ_o = 0.68 eV and $|V|$ = 31 cm^{-1} in dichlorobenzene, λ_o = 0.42 eV, and $|V|$ = 8.1 cm^{-1} in *meta*-chlorotoluene, and λ_o = 1.1 eV and $|V|$ = 65 cm^{-1} in benzonitrile.

(22) (a) Matyushov, D. V.; Schmid, R. *J. Chem. Phys.* **1996**, *104*, 8627. (b) Ben-Amotz, D.; Willis, K. G. *J. Phys. Chem.* **1993**, *97*, 7736.

(23) The apparent, slight increase of the solvent reorganization energy with temperature (Figure 5.5) does not agree with the slight decrease observed in experiments[20] or predicted by modern solvation theory.[14] This slight difference is likely a result of the assumed temperature independence of the electronic coupling. See ref 24.

(24) Napper, A. M.; Read, I.; Waldeck, D. H.; Kaplan, R. W.; Zimmt, M. B. *J. Phys. Chem. A.;* 2002; *106*(18); 4784-4793.

(25) For the situation in which the solvent mediated pathway dominates the other contributions to the electronic coupling magnitude, the superexchange state is depicted by D^+S^-A (for a reaction "mechanism" of D*SA - D^+S^-A - D^+SA^-). Between the different solvent systems being studied, the major change in energetics of the superexchange state will arise from the energetics of S^-. The solvent dependence of the donor's ionization potential is assumed to be small. Hence, the electron affinity of the solvent gauges the change in energetics.

(26) (a) Jordan, K. D.; Michejda, J. A.; Burrow, P. D. *J. Am. Chem. Soc.* **1976**, *98*, 7189. (b) Burrow, P. D.; Modeli, A.; Jordan, K. D. *Chem. Phys. Lett.* **1986**, *132*, 441. (c) Burrow, P. D.; Howard, A. E.; Johnston, A. R.; Jordan, K. D. *J. Phys. Chem.* **1992**, *96*, 7570 and references therein.

(27) Gould, I. R.; Young, R. H.; Mueller, L. J.; Albrecht, A. C.; Farid, S. *J. Am. Chem. Soc.* **1994**, *116*, 8188.

(28) Cave, R. J.; Newton, M. D.; Kumar, K.; Zimmt, M. B. *J. Phys. Chem.* **1995**, *99*, 17501.

Chapter 6 Electron Transfer Reactions of C-shaped Molecules in Alkylated Aromatic Solvents: Evidence that the Effective Electronic Coupling Magnitude Is Temperature- Dependent

6.1 Introduction

The requirements for fast electron-transfer processes are favorable Franck-Condon factors and significant electronic coupling between the donor and acceptor groups. Electronic coupling magnitudes in electron-transfer systems vary from thousands of wavenumbers, e.g., for contact ion pairs,[1] to hundredths of wavenumbers for donor and acceptor groups separated by tens of angstroms, e.g., in proteins and glasses.[2] Different methods are used to determine coupling magnitudes from experimental data. Systems with moderate couplings (10 – 200 cm^{-1}) often exhibit charge transfer (CT) absorption and/or CT emission bands. Analysis of these bands' transition intensities provides values of the donor-acceptor electronic coupling.[1,3] For systems with smaller donor-acceptor couplings, CT transitions are usually too weak to detect and analyze. The electronic coupling magnitudes in "weakly coupled" systems may be determined through analysis of electron-transfer rate constants, once the appropriate Franck-Condon factors have been determined or estimated. Despite the indirect nature of this approach, a number of such investigations have successfully identified relationships between the electronic coupling magnitude and the underlying molecular structure and/or properties of the medium between the donor and acceptor groups.[4,§§]

[§§] This chapter was previously published as: Napper, A. M.; Read, I.; Waldeck, D. H.; Kaplan, R. W.; Zimmt, M. B.; *J. Phys. Chem. A.;* **2002**; 106(18); 4784-4793.

It has long been appreciated that the structure of the medium between the donor and acceptor groups influences the rates of electron transfer. Less widely recognized is the important role that dynamics can exert. For many electron transfer reactions, the structure of the medium through which the electron tunnels is dynamic. Theoretical investigations have indicated that intervening medium motions, including vibrations, librations, conformational changes, and diffusion of mobile components, can significantly modulate donor-acceptor electronic coupling magnitudes.[5] The size of the coupling magnitude fluctuations depends on the amplitudes of the medium motions and the details of the electronic coupling pathways. A dramatic manifestation of the influence of dynamics is "conformational gating",[6] which has been observed for protein and intramolecular electron transfer reactions. This phenomenon occurs in long-range electron transfer systems when the electron transfer rates for a subset of the thermally accessible conformations is fast relative to the transfer rates in the most populated conformations. The observed transfer rate is influenced by the kinetics of interconversion among conformations. Larger coupling magnitudes in the "fast" conformations can contribute to the "gating" effect. The variation of coupling magnitude with conformation constitutes a break down of the Condon approximation.

It is difficult to quantify the influence of structural fluctuations on coupling magnitudes in electron transfer systems with small electronic couplings because electron transfer rates, not coupling magnitudes, are the experimental observables. Extraction of the coupling magnitude from experimental rate data requires reliable evaluation of activation barriers, nuclear factors, and solvation. Generally, it is difficult to ascertain the existence and/or magnitude of coupling fluctuations from such an

analysis. In those intramolecular electron transfer systems where a structurally rigid bridge connects the donor and acceptor, structural distortions of the bridge and coupling magnitude fluctuations are likely small.[7] For intra- and intermolecular electron-transfer systems in which the structure of the intervening medium fluctuates significantly, the donor- acceptor electronic coupling may also fluctuate significantly. Hence, the electronic coupling, extracted from rate constant analysis, represents a (dynamically) averaged electronic coupling matrix element, or an "effective" coupling magnitude. As the majority of investigations are not posed to investigate these effects, little evidence for or against characterization of medium induced fluctuations of the electronic coupling is available.

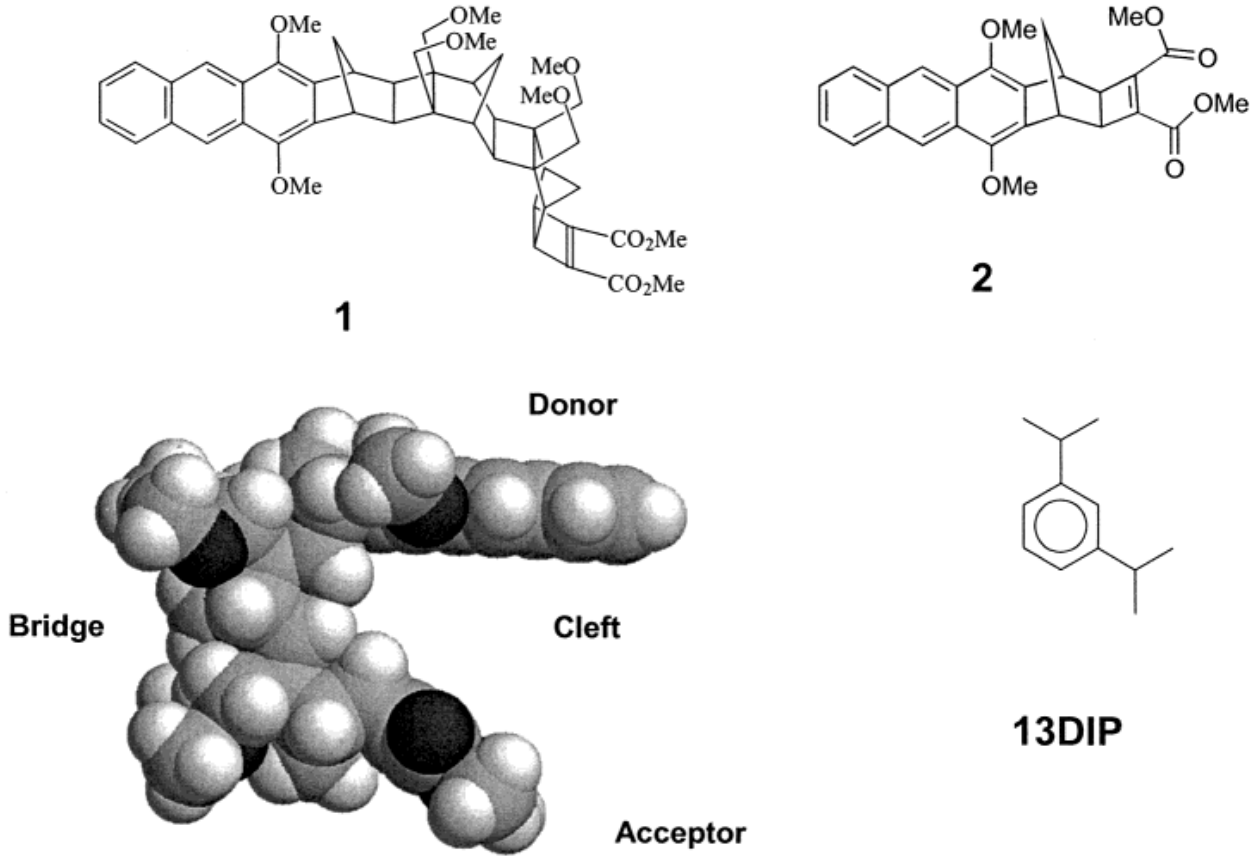

Chart 6.1 Molecular Structures of the Electron Transfer Molecules 1, 2, and the Solvent 1,3-Diisopropylbenzene.

Recent investigations of some highly curved donor-bridge-acceptor molecules indicate that their electronic coupling may derive from "pathways" constituted by solvent molecules.[8] The coupling magnitudes in these systems are influenced by the solvent molecules' electronic structure, size, shape, and the size of the solvent accessible gap between the donor and acceptor groups.[8] Calculations suggest that the magnitude and sign of the electronic coupling mediated by solvent molecules varies significantly with the latter's placement and orientation relative to the donor and acceptor. Consequently, the relatively rapid and unconstrained motions of the solvent molecules should give rise to a fluctuating electronic coupling magnitude.[5e] Additionally, environmental variables that alter the solvent dynamics and/or accessible conformations, e.g., pressure[9] or temperature, may influence the "effective" value of the electronic coupling that is determined through analysis of rate constant data. As is true for systems exhibiting conformational gating,[6] fluctuation of the donor-acceptor coupling associated with solvent motion constitutes a breakdown of the Condon approximation. Previous investigations have provided some evidence that solvent mediated electronic coupling magnitudes are temperature dependent.[10] This investigation reports data that indicate a strong temperature dependence of the solvent-mediated, donor-acceptor electronic coupling for a C- shaped molecule, **1** (Chart 6.1). The evidence of temperature-dependent coupling is particularly compelling for extensively alkylated aromatic solvents.

Compound **1** (see Chart 6.1) juxtaposes a dimethoxyanthracene donor and a cyclobutene diester acceptor on opposite sides of a 7 Å cleft that is accessible to solvent molecules. The electron transfer dynamics of **1** have been investigated in highly polar,[8b] alkylated-aromatic,[8c,10] and halo-aromatic solvents.[11] The electronic coupling magnitude determined for **1** in each solvent depends on the solvent's electronic energy levels and its three-dimensional structure.[8,10,11] The electron-transfer reactions of **1** in alkylated benzene solvents afford an unusual opportunity for in-depth investigation of the factors that control rate constants. The reaction free energy, $\Delta_r G$, is almost zero for electron transfer from the lowest energy, singlet-excited state (S_1) of the anthracene donor to the acceptor. An equilibrium between the anthracene S_1 excited state and the charge separated state influences the fluorescence dynamics and allows determination of all three electron-transfer rate constants after the $S_0 \rightarrow S_1$ excitation:[8c] the charge separation, electron-transfer rate constant for conversion of the anthracene S_1 state to the charge separated state, $k_{for;}$ the charge recombination rate constant for conversion of the charge separated state back to the anthracene S_1 state, $k_{back;}$ and the charge recombination rate constant that converts the charge separated state to the anthracene S_0 state, k_{rec}.[12] The free energy gap between the anthracene S_1 excited state and the charge separated state is evaluated experimentally from the first two of these rate constants.

The temperature dependence of the charge separation and charge recombination rate constants of **1** vary dramatically depending on the structure of the alkyl benzene solvent. In benzene, the charge separation rate constant, $k_{for,}$ decreases and the charge recombination rate constant, $k_{back,}$ increases as the temperature is

increased. By contrast, k_{for} and k_{back} in 1,3,5- triisopropylbenzene both increase as the temperature increases. The rate constants k_{for} and k_{back} for **1** in 1,3-diisopropylbenzene exhibit more complex behavior, first increasing and then decreasing as the temperature is raised. The nonmonotonic temperature dependence of k_{for} and k_{back}, along with the availability of $\Delta_r G(T)$ data, provide significant constraints on kinetic models used to interpret these rate data. In particular, two possible explanations for the observed rate constant behavior of **1** in 1,3-diisopropylbenzene can be identified. First, the temperature dependence can be explained by a decrease of the effective electronic coupling magnitude with increasing temperature. Second, the temperature dependence could result from a small and temperature-independent value of the solvent reorganization energy, which, in conjuction with the temperature dependence of $\Delta_r G$, moves the charge separation and recombination reactions, k_{for} and $k_{back,}$ between the Marcus normal and inverted regions. Both interpretations can quantitatively reproduce the observed data for **1** in 1,3-diisopropylbenzene and are consistent with the models used to predict electron transfer rate constants. As discussed later in the manuscript, the combination of these data with earlier data in alkylbenzene solvents argues strongly for the first explanation, a temperature dependence of the electronic coupling magnitude.

This manuscript describes the determination and analysis of the electron-transfer rate constant for **1** in 1,3-diisopropylbenzene solvent. Data collection, rate constant determinations, and determination of the reaction free energy are described in the next section. The two explanations for the temperature dependence of the rate constants are developed in the third section. They differ significantly in the magnitude

and temperature dependence of the solvent reorganization energy, $\lambda_s(T)$. The fourth section describes the evidence for and against the two explanations and discusses the implications of these findings for solvent and temperature- dependent rate constants observed earlier. Although it is not possible to reject unambiguously either explanation, the explanation based on a temperature dependence of the effective electronic coupling magnitude is more consistent with prior experimental and theoretical results.

6.2 Data, Rate Constant, and $\Delta_r G$ Determinations

The preparation of **1** was reported elsewhere.[13] Solutions of **1** were prepared with an optical density of ca. 0.05 at the laser excitation wavelength, 375 nm. The solvent 1,3-diisopropylbenzene (9 8%) was purchased from Aldrich. The solvent was dried with anhydrous magnesium sulfate, filtered, and then fractionally distilled using a vigreux column. The purified fraction was used immediately to prepare the sample. Each sample solution was freeze-pump-thawed a minimum of three times. The samples were back-filled with argon to reduce solvent evaporation at the higher temperatures.

Excitation of the sample was performed at 375 nm by the frequency-doubled cavity- dumped output of a Coherent CR-599-01 dye laser using LDS750 (Exciton) dye, which was pumped by a mode-locked Coherent Antares Nd:YAG laser. The dye laser pulse train had a repetition rate of ca. 300 kHz. Pulse energies were kept below 1 nJ, and the count rates were kept below 3 kHz. All fluorescence measurements were made at the magic angle. Other specifics of the apparatus have been reported elsewhere.[14] Instrument response functions were measured using a

sample of colloidal $BaSO_4$ in glycerol. Fluorescence decays were fit to a sum of two exponentials (the decay law was convolved with the measured instrument function) using the Marquardt-Levenberg nonlinear least squares algorithm. Figure 6.1 shows a fluorescence decay for **1** in 1,3-diisopropylbenzene at 290 K, the calculated best-fit, biexponential decay curve, the impulse response, and the fit residuals. For temperatures above 260 K, the sample cuvette was placed in an aluminum block

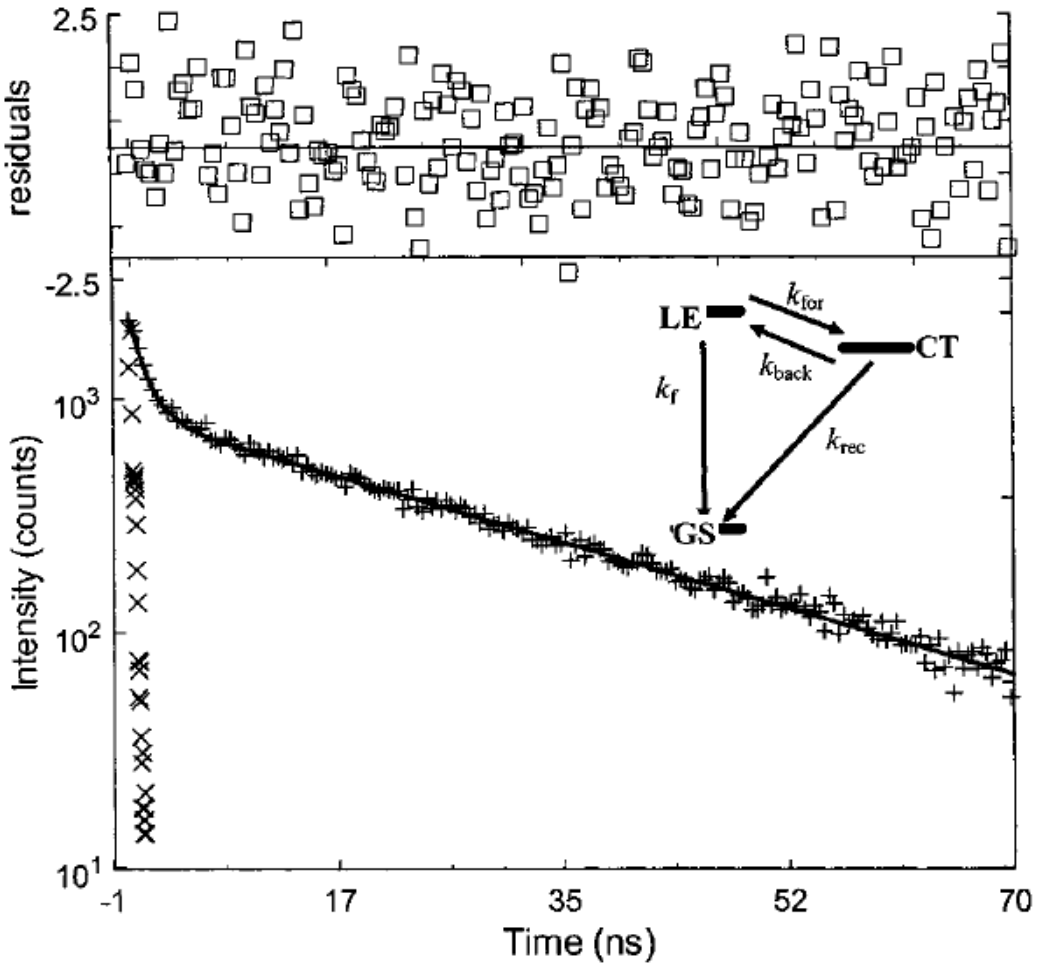

Figure 6.1 Fluorescence decay for 1 in 1,3-diisopropylbenzene at 290 K and the best fit to the data (solid line hidden by the raw data). The impulse response function (□) and the residuals (fl, at top) are also shown. The fitted curve gives rate constants of 814 ps (68%), 17.7 ns (32%), and a c^2 of 1.08. The inset shows an energy level diagram for the kinetics.

whose temperature was controlled by a NESLAB RTE-110 chiller. Temperatures were measured using a type-K thermocouple (Fisher-Scientific), accurate to within 0.1 °C. Slush baths were used for the lower temperature points: 247 K (*o*-xylene/liquid N_2), 240 K (chlorobenzene/liquid N_2), 235 K (acetonitrile/liquid N_2), and 218 K (chloroform/liquid N_2). The slush bath temperatures varied by ±2 K from the stated temperature.

6.2.1 Kinetic and Thermodynamic Analyses.

Photoexcitation of the anthracene donor moiety creates a locally excited state (S_1 or LE) whose energy is similar to that of the charge separated state in 1,3-diisopropylbenzene solvent. The inset to Figure 6.1 shows the kinetic scheme that is used to describe the kinetics following formation of the locally excited state by the light pulse. There are four unknown rate constants. The intrinsic decay rate constant of the locally excited state, k_f, is obtained from the LE decay kinetics of an analogue to molecule **1** that has no electron acceptor. Fitting the time-resolved fluorescence decay of **1**'s LE state to a biexponential form provides three additional parameters: a fast rate constant, a slow rate constant, and the amplitude fraction of the fast decay. The electron-transfer rate constants k_{for}, k_{back}, and k_{rec} are calculated using the fit parameters that reproduce the time-resolved fluorescence decay.[15] The Gibbs free energy of the charge separation reaction is determined at each temperature from the ratio of the forward and back rate constant, (eq 6.1)

$$\Delta_r G = -RT \ln(k_{for}/k_{back}) \tag{6.1}$$

The availability of experimental $\Delta_r G$, at each temperature, and of the internal reorganization energy parameters (vide infra) make it feasible to interpret the temperature-dependent rate constant data in terms of only two parameters: the solvent reorganization energy and the donor- acceptor electronic coupling.

6.3 Rate Constant Temperature Dependence and Possible Explanations

Figure 6.2 summarizes the temperature-dependent rate constant and $\Delta_r G$ data. Panel A displays the temperature dependence of the charge separation and charge recombination rate constants for molecule **1** in 1,3-diisopropylbenzene. Starting at 218 K, 8° above the solvent's melting point, both the charge separation and charge recombination rate constants increase upon increasing the temperature. The charge separation rate constant, $k_{for,}$ reaches a maximum near 270 K and then decreases sharply at higher temperatures, dropping more than 20-fold by 356 K. The charge recombination rate constant, $k_{back,}$ increases up to 320 K and then decreases 2-fold by 356 K. The maximum rate constants for the charge separation and charge recombination reactions are nearly equal, ~ 9 x 10^8 s^{-1}. Panel B presents the experimental $\Delta_r G$ for the charge separation reaction as a function of temperature. The free energy of charge separation varies nearly linearly from 280 to 350 K. However, as the temperature approaches the freezing point of the solvent, $\Delta_r G$ changes less steeply with temperature. The solid line shows a fit to the full temperature dependence of $\Delta_r G$ that is obtained with a quadratic expression. This fit is used later to aid in the analysis of the rate data.[16]

Semi-log plots of electron-transfer rate constant versus reaction free energy have been used to determine solvent reorganization energy and electronic coupling magnitudes. For **1**, the logarithms of k_{for} and k_{back} increase, plateau, and then decrease in a plot versus $\Delta_r G$ for the charge separation step (Figure 6.3). This shape suggests that k_{for} and k_{back} both span the Marcus normal and inverted regions and that the solvent reorganization energy is very small (vide infra). In a conventional Marcus plot, the temperature and solvent reorganization energy for all points are held as constant as possible. In Figure 6.3, however, the temperature for each data point varies from 218 (left side) to 356 K (right side). As a result, the variation of $\Delta_r G$ (abscissa) is attended by significant variation of $k_B T$ and, possibly, of the solvent reorganization energy and the electronic coupling. These variations must be considered in any interpretation of the rate constant plots in Figures 6.2 and 6.3 (vide infra).

The temperature dependence of the charge separation and recombination rate constants may be simulated using a semiclassical formulation[17] for the electron-transfer rate constant (eq 6.2). In this equation, |V| is the donor-acceptor electronic coupling, λ_S is the solvent reorganization energy, $h\nu$ is the quantized mode energy spacing, and *S* is the ratio of the internal reorganization energy, λ_v, to the quantized mode energy spacing, $S = \lambda_v / h\nu$. The quantity *S* is assumed to be temperature independent. Estimates of λ_v (0.39 eV) and $h\nu$ (0.175 eV) were previously determined using a combination of quantum chemistry calculations and CT emission spectra from related molecules.[18] Given these values for the internal reorganization parameters and the experimental values of $\Delta_r G$ at each temperature (Figure 6.2B), only the

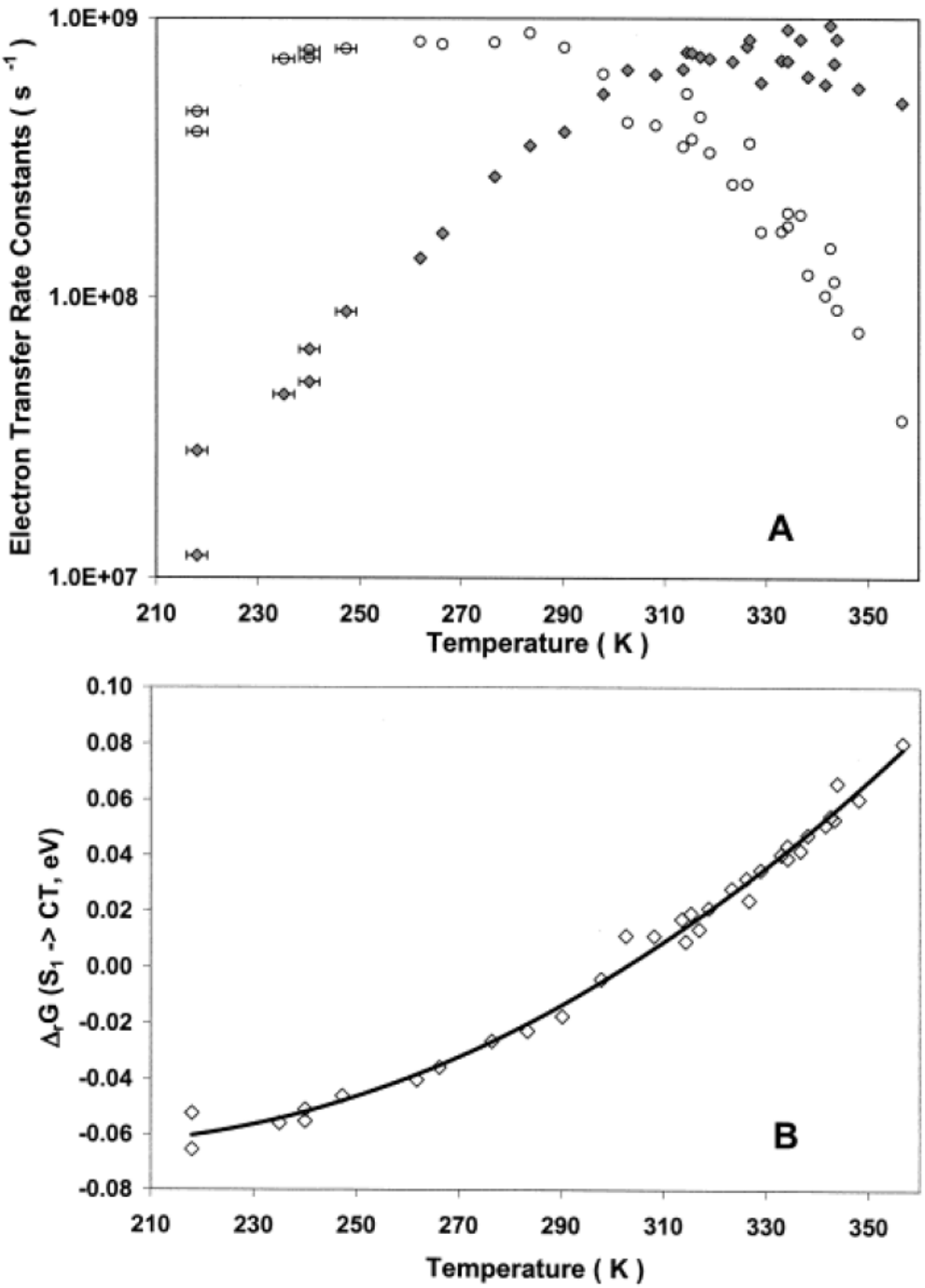

Figure 6.2 (Panel A) Charge separation (k_{for}, ○) and charge recombination (k_{back}, ♦) rate constants for molecule 1 as a function of temperature in 1,3-diisopropylbenzene. Panel B plots the free energy change for charge separation ($k_{for,}$ ◊) as a function of temperature for 1 in 1,3-diisopropylbenzene. The solid line represents a best fit of the data to a quadratic equation.

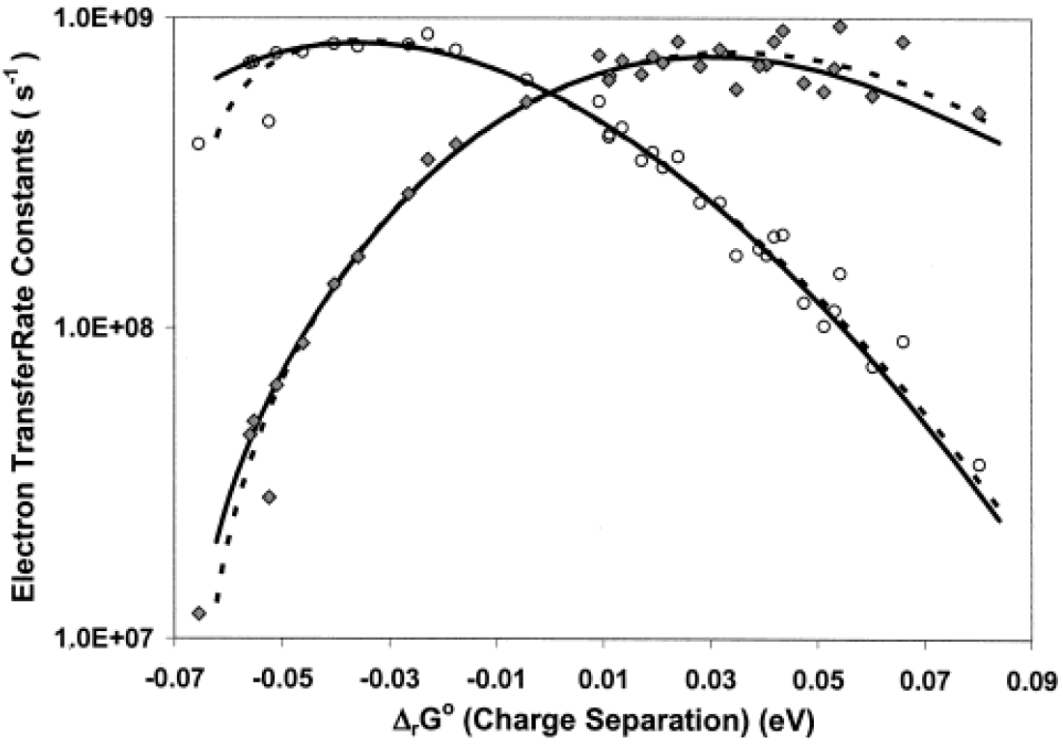

Figure 6.3 Plots of the charge separation (k_{for}, ○) and charge recombination (k_{back}, ♦) rate constants versus the free energy change for charge separation. To minimize overlap, both plots use the charge separation $\Delta_r G$ as the abcissa. The solid lines were calculated using eq 6.2 assuming $|V|$ = 2.25 cm^{-1} and λ_S = 0.033 eV. The dashed lines were calculated using the parametrized Matyushov model to predict $\lambda_S(T)$ and the regression estimates of $|V(T)|$ (see text).

magnitude and temperature dependence of λ_S and |V| may be "adjusted" to reproduce the experimental data. The extensive curvature of the k_{for} and k_{back} versus $\Delta_r G$ plots places significant constraints on the magnitude and temperature dependence of the solvent reorganization energy and/or of the electronic coupling. As discussed below, two possible explanations for the highly curved plots of k_{for} and k_{back} versus temperature (i.e., versus reaction free energy) have been identified.

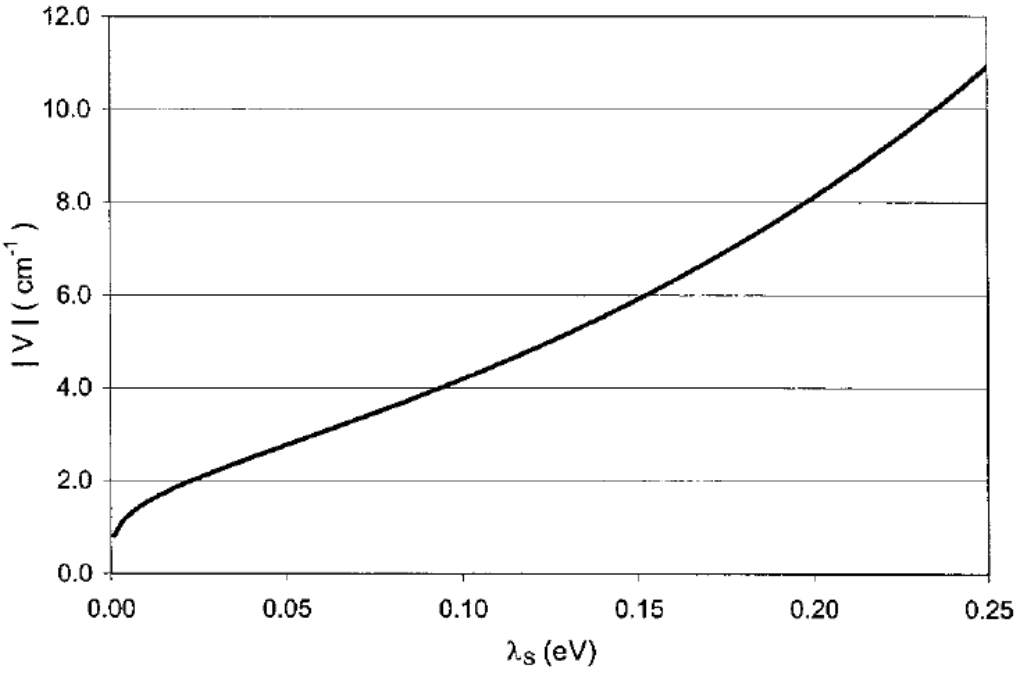

Figure 6.4 Correlation between |V| and λ_S for 1 derived from the experimental transfer rate constant at 297 K, where $\Delta_r G = 0$ eV.

The experimental k_{for} and k_{back} rate constants at each temperature establish a parametric relationship between the two unknown parameters in eq 6.2: the solvent reorganization energy and the electronic coupling. At 297 K, the temperature at which $\Delta_r G = 0$, the charge separation, and charge recombination rate constants are equal, and only the $n = 0$ term in eq 6.2 makes significant contributions to either rate constant.

The electronic coupling may be expressed as a simple function of the solvent reorganization energy, the temperature, and the rate constants by rearranging eq 6.2. Figure 6.4 displays this relationship between $|V|$ and λ_S for **1** in 1,3-diisopropylbenzene at 297K, with k_{for} and k_{back} ~ 5.8 x 10^8 s^{-1}, and shows that the electronic coupling increases monotonically as λ_S increases. A previous study of solvent-mediated, donor-acceptor electronic coupling for **1** determined that $|V|$ = 6 cm^{-1} in isopropylbenzene (cumene) and $|V|$ = 1 cm^{-1} in 1,3,5-triisopropylbenzene.[10] Furthermore, it was found that an increase in the alkyl substitution at the periphery of the benzene ring caused a systematic decrease of the magnitude of solvent-mediated coupling for **1**.[8c] Accordingly, the electronic coupling mediated by 1,3-diisopropylbenzene for **1** is expected to lie between the values in cumene and tri-isopropylbenzene, i.e. between 6 and 1 cm^{-1}, respectively. Using the range defined by these couplings, Figure 6.4 indicates that the solvent reorganization energy in 1,3-diisopropylbenzene at 297 K lies between 0.15 and 0.0 eV, respectively. The experimental values of $\Delta_r G$ for charge separation in 1,3-diisopropylbenzene vary, with temperature, between -0.07 and 0.08 eV. Thus, the charge separation reaction could lie in the Marcus normal region (if λ_S > 0.09 eV) or span the normal and inverted regions (λ_S < 0.06 eV).

By assuming a specific, *temperature independent* value of the electronic coupling, eq 6.2 may be used to determine the value of λ_S that is required at each temperature to reproduce the experimental rate constants. Figure 6.5 displays $\lambda_S(T)$, calculated in this manner, for two assumed values of the electronic coupling: 2.25 cm^{-1} (panel A) and 6.0 cm^{-1} (panel B). For the assumed value of $|V|$ = 2.25 cm^{-1}, the

extracted λ_S has a mean value of 0.033 ± 0.007 eV and exhibits a weak, positive temperature dependence, <0.1 meV/K. If λ_S for **1** in 1,3-diisopropylbenzene is this small and without significant temperature dependence, the charge separation reaction lies in the Marcus inverted region at temperatures below 270 K, and the charge recombination reaction lies in the Marcus inverted region at temperatures above 330 K. The solid lines in Figure 6.3 display the temperature dependence of k_{for} and k_{back} predicted using λ_S = 0.033 eV, |V| = 2.25 cm-1 and $\Delta_r G$ obtained from the data in Figure 6.2B. The calculated curves reproduce the data well. Using the larger assumed value of $|V|$ = 6.0 cm^{-1}, the λ_S values extracted with eq 6.2 (Figure 6.5B, circles) exhibit a U-shaped temperature dependence with a value at 297 K of 0.16 eV. Previous theoretical and experimental studies[19] of the solvent reorganization energy in liquids provide no evidence to substantiate such a U-shaped temperature dependence. Therefore, either the assumed coupling magnitude of 6 cm^{-1} is inappropriate or the assumption that the coupling magnitude is temperature independent is erroneous. From both these analyses it is clear that a meaningful determination of the coupling magnitude requires more information about the solvent reorganization energy.

As it is not possible to independently measure λ_S for **1**, theoretical estimates and experimental values from related systems need to be considered. Previously, a molecular solvation model, developed by Matyushov,[20] was calibrated[10] to reproduce the experimental values of the charge separation free energy for **1** in alkylated benzene solvents. This calibrated solvation model can be used to predict the magnitude and temperature dependence of the solvent reorganization energy. Table 6.1 presents these

predictions for the solvent reorganization energy and its temperature derivative at 295 K in seven alkylbenzene solvents and compares them to values of λ_S(265 K) that were obtained by fitting experimental rate constant data for **1**.[10,21] The model predicts a monotonic decrease of the solvent reorganization energy with increasing temperature and with increasing alkyl substitution of the solvent molecules. For the first five solvents in Table 6.1, the model predictions and the experimental values of λ_S(295 K) are in good agreement. Only the regression estimate of λ_S(295 K) in 1,3,5-tri-isopropylbenzene deviates significantly from the model's prediction (see below for an alternative analysis of the kinetic data for **1** in this solvent). The good agreement between the experimental and theoretical values of λ_S in five of the six solvents that are structurally related to 1 ,3-diisopropylbenzene suggests that the model's prediction of λ_S = 0.16 eV at 295 K for this solvent is reasonable. This value is much larger than the λ_S estimate required by assuming $|V|$ = 2.25 cm^{-1} but quite close to the value required by assuming $|V|$ = 6 cm^{-1}. The solid line in Figure 6.5B displays the parametrized solvation model prediction of λ_S versus temperature for **1** in 1,3-diisopropylbenzene.[22] Between 220 and 290 K, the theoretical predictions are slightly larger (by 0.02-0.03 eV) than the λ_S(T) values required to reproduce the rate data (circles) for the assumed value of $|V|$ = 6.0 cm^{-1}. These two sets of λ_S(T) deviate at higher temperatures.

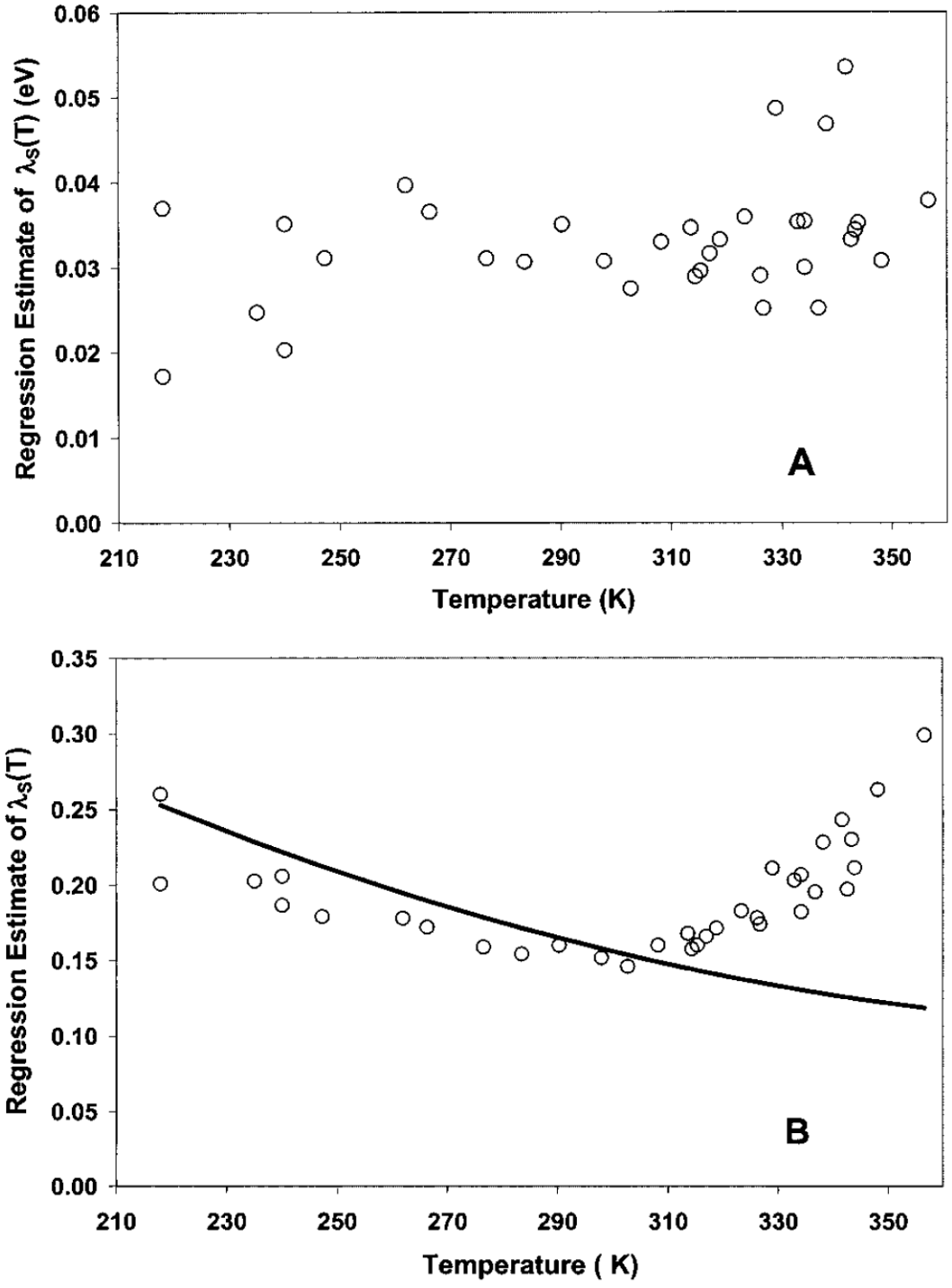

Figure 6.5 Values of $\lambda_S(T)$ obtained from the experimental rate constant data, eq 6.2 and an assumed value of $|V|$. The data in panel A were obtained with $|V|$ set to 2.25 cm^{-1}. The data in panel B were obtained by setting $|V|$ equal to 6.0 cm^{-1}. The solid line in panel B shows the $\lambda_S(T)$ prediction from the calibrated Matyushov model.

Table 6.1 Calibrated Solvation Model Predictions of λ_S (295 K), Its First Derivative, and Experimental Values of λ_S (295 K) Determined by Fitting $k_{for}(T)$ and $k_{back}(T)$ Data[a]

solvent	model: $d(\lambda_S(295K))/dT$ (eV/10^3 K)	model: $\lambda_S(295\ K)$[23] (eV)	expt: $\lambda_S(295\ K)$ (eV)
benzene	−1.1	0.27	0.26
toluene	−1.0	0.24	0.22
cumene	−0.83	0.19	0.17
mesitylene	−0.76	0.17	0.14
TMB	−0.75	0.20	0.16
13DIP	−0.63	0.16	
135TIP	−0.74	0.12	0.01

[a] TMB is 1,2,4-trimethylbenzene, 13DIP is 1,3-di-isopropylbenzene, and 135TIP is 1,3,5-tri-isopropylbenzene.

Both sets of $\lambda_S(T)$ values in Figure 6.5, panel B, are substantially larger than the experimental $-\Delta_rG$ values, suggesting that the charge separation and charge recombination processes lie in the Marcus normal region at all temperatures. In the Marcus normal region, larger λ_S values reduce the electron-transfer rate constant. The apparent increase of λ_S at temperatures above 310 K (circles, panel B) acts to decrease the transfer rate constant calculated using a temperature independent coupling of 6 cm^{-1}.

Given the mobility of solvent molecules and evidence that solvent placement influences coupling magnitude, it is possible that a decrease of the average, effective coupling, rather than an increase of λ_S, may be occurring at temperatures above 310 K. This proposal can be explored by assuming that the parametrized solvation model accurately predicts the magnitude and the temperature dependence of the solvent reorganization energy for **1**. With values for $\lambda_S(T)$, eq 6.2 may be used to determine

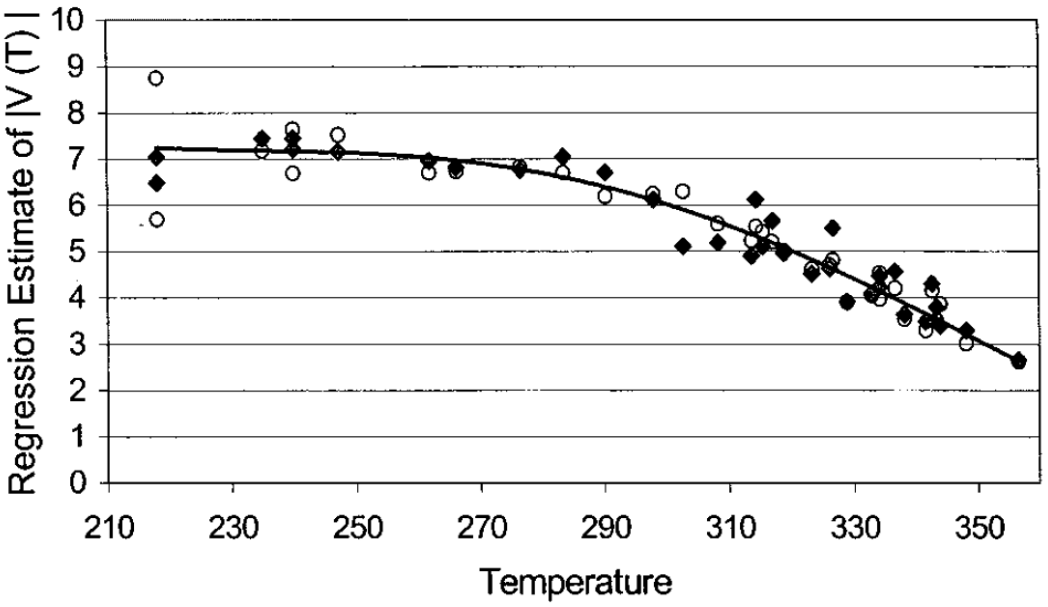

Figure 6.6 Values of the electronic coupling for 1 in 1,3-diisopropylbenzene, obtained by fitting the experimental rate constant data using the calibrated Matyushov model to calculate $\lambda_S(T)$, plotted as a function of temperature: (k_{back}, ○), (k_{for}, ♦).

the value of the electronic coupling required to reproduce the experimental rate constants at each temperature. The coupling magnitude obtained using this procedure (Figure 6.6) is relatively constant between 220 and 260 K, 7.2 ± 0.5 cm^{-1}, but decreases by more than 60% between 260 and 350 K.[24] The temperature dependence of k_{for} and k_{back} predicted by this analysis is in very good agreement with the experimental data (Figure 6.3, dashed lines).

At this point, two models have been advanced to explain the rate data from **1** in 1,3-di-isopropylbenzene. The two models reproduce the rate data using different values and temperature dependences of |V| and λ_S. In the next section, evidence is presented that confirms the validity of λ_S predictions from the calibrated molecular model and the validity of the |V(T)| explanation. Arguments that discount the accuracy of the "inverted" region model are also presented.

6.4 Pros, Cons, and Consequences of the Two Explanations

The temperature dependence of the charge separation and charge recombination rate constants for **1** in 1,3-diisopropylbenzene are well reproduced by both the "inverted region" and the "temperature-dependent electronic coupling" explanations. At low temperatures ($\Delta_r G(CS) < -0.05$ eV), the latter model fits the data slightly more accurately. For both explanations, the solvent reorganization energy is small, less than 0.3 eV. Determining which of the two proposed explanations is correct requires accurate information on the solvent reorganization energy magnitude and its temperature dependence, a task that is not experimentally feasible for **1**. As noted above, a molecular solvation model, which previously was parametrized[10] to reproduce the experimentally determined $\Delta_r G(T)$ data for **1** in a series of alkylbenzene solvents, predicts values of λ_S(295 K) for **1** (ranging from 0.12 to 0.27 eV) that are in good agreement with λ_S(295 K) determined by fitting experimental rate constant data. The model's prediction of λ_S(295 K) for **1** in 1,3-diisopropylbenzene, 0.16 eV, is significantly larger than the 0.033 eV value required by the "inverted region" explanation. In light of the model's predictive accuracy in the other alkylbenzene solvents, this discrepancy argues against the "inverted region" explanation.

Although **1** lacks detectable CT absorption and emission spectra, some qualitative information about λ_S can be obtained by studying the CT spectra of a related molecule. Compound **2** employs the same donor and acceptor as **1**, connected by an all-trans three-bond bridge, and exhibits CT emission.[25] The donor-acceptor separation in **2** is ~ 6 Å, roughly 1 Å smaller than that in **1**. At 295 K, the maximum of the CT emission, Franck-Condon lineshape from **2** appears at 2.19 eV

in 1,3-diisopropylbenzene, 2.12 eV in cumene, and 1.98 eV in benzene.[26] This energy is approximately equal to $\Delta_rG(S_0 \rightarrow CT) - \lambda_S - \lambda_V$ or, equivalently, to $\Delta_rG(S_0 \rightarrow S_1) + \Delta_rG(S_1 \rightarrow CT) - \lambda_S - \lambda_V$. The term $\Delta_rG(S_0 \rightarrow S_1)$ amounts to 3.00 eV for the anthracene chromophore in alkylbenzene solvents and the last term, λ_V, is 0.39 eV. Thus, $\lambda_S - \Delta_rG(S_1 \rightarrow CT)$ for **2** at 295 K is equal to 0.42, 0.49, and 0.63 eV in 1,3-di-isopropylbenzene, cumene, and benzene, respectively.[27] The same quantity, $\lambda_S - \Delta_rG(S_1 \rightarrow CT)$, calculated for **1** using the experimental $\Delta_rG(S_1 \rightarrow CT)$ data and the calibrated solvation model predictions of λ_S(Table 6.1) amounts to 0.16, 0.24 and 0.37 eV in 1,3-diisopropylbenzene, cumene and benzene, respectively. The variations of $\lambda_S - \Delta_rG(S_1 \rightarrow CT)$ with solvent are nearly identical for **1** and **2**. The offset of 0.26 eV between $\lambda_S - \Delta_rG(S_1 \rightarrow CT)$ for **1** and **2** is consistent with the different charge separation distances of **1** and **2**.[28] The similarity of the solvent dependencies of $\lambda_S - \Delta_rG(S_1 \rightarrow CT)$, for **1** and **2**, in conjunction with the accurate reproduction of the $\Delta_rG(T)$ data for **1** shows that the parametrized molecular model's treatment of solvation by weakly dipolar aromatic solvents and its treatment of solvent structural effects generate meaningful predictions for these anthracene donor, cyclobutenediester electron-transfer systems.[29] Although these arguments do not establish unambiguously the accuracy of the model's λ_S(295 K) predictions, they provide compelling evidence that λ_S for **1** in 1,3-diisopropylbenzene is larger than 0.033 eV. Accordingly, the "inverted region" explanation is not consistent with the available information on λ_S in 1,3-diisopropylbenzene.

Another problem with the "inverted region" explanation for **1** in 1,3-diisopropylbenzene lies in the calculated decrease of the transfer rate when $-\Delta_rG$ is greater than λ_S = 0.033 eV. This prediction may be an artifact of using a single quantum mode model. If λ_S is significantly smaller than the mode spacing, $h\nu$, eq 6.2 predicts a significant drop and recovery of the rate constant for $-\Delta_rG$ between λ_S and λ_S + hv (Figure 6.7; solid line). A modulation appears in a semilog plot of rate constant versus $-\Delta_rG$, with rate maxima at values of $-\Delta_rG$ that are close to $\lambda_S + nh\nu$.[30] This modulation extends from the "normal" region ($-\Delta_rG < \lambda_S + \lambda\nu$), through the peak of the Marcus curve and into the region *traditionally* referred to as inverted ($-\Delta_rG > \lambda_S + \lambda\nu$). If a

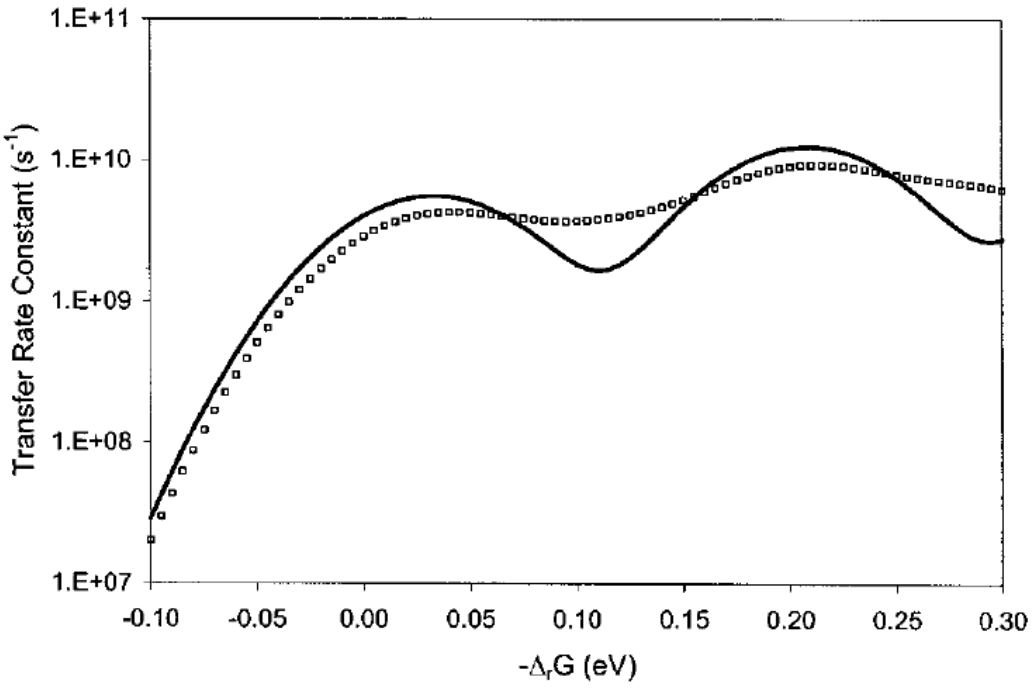

Figure 6.7 Examples of rate constant versus reaction free energy plots calculated using a one- quantized mode (—) and a two quantized mode (□) model. For both models, $|V|$ = 6 cm^{-1}, λ_S = 0.033 eV, $h\nu_1$ = 0.175 eV, $h\nu_2$ = 0.087 eV, and the total internal reorganization energy is 0.39 eV. For the two quantized mode calculation, the internal reorganization energies are λ_{v1} (0.175 eV mode) = 0.33 eV and λ_{v2} (0.087 eV mode) = 0.06 eV. For the one quantized mode calculation, λ_v(0.175 eV mode) = 0.39 eV.

small portion of the internal reorganization energy is associated with a second quantum mode of lower frequency, e.g., $h\nu$ ~ 700 cm^{-1}, a two quantum mode rate constant model predicts negligible modulation of the rate constant (Figure 6.7, squares).[31] Resonance Raman studies of intramolecular CT systems report significant reorganization associated with such intermediate frequency modes in other systems.[32] For **1**, modes involving the donor and acceptor rings likely fall in this range, whereas modes associated with reorganization of the donor methoxy and the acceptor ester groups likely occur at somewhat lower frequency. Thus, more realistic treatments of the internal reorganization within the rate constant calculation predict smaller or negligible reduction of the rate constant when $-\Delta_r G$ is greater than λ_S. This raises additional doubts about the validity of the "inverted region" explanation for the transfer rate data from **1** in 1,3-diisopropylbenzene.

If the molecular model prediction of λ_S for **1** in 1,3-diisopropylbenzene is correct, then 1,3,5-triisopropylbenzene is the only alkylbenzene solvent for which the molecular model prediction and the experimentally derived value of λ_S differ significantly. The solvent 1,3,5-triisopropylbenzene differs from the other alkylbenzenes in that the three bulky isopropyl groups spaced around the aromatic ring prevent facile entry of the solvent's aromatic core into the cleft between the donor and acceptor groups.[8c] Molecular mechanics calculations indicate that only the isopropyl groups from this solvent extend into the cleft. The absence of a "solvent aromatic ring" between the donor and acceptor groups might cause a larger reduction of λ_S, relative to the other solvents, than predicted by the molecular model. The solvation model treats

the CT molecule as a point dipole contained within a solvent free cavity. Thus, it does not include "cleft" solvent reorganization energy for any of the solvents.[33] If exclusion of the aromatic core of 1,3,5-triisopropylbenzene from the cleft interior is responsible for the 0.11 eV difference between the molecular model prediction and the experimental value (Table 6.1) of λ_S(295 K), then the molecular model must overestimate the "*extra-cavity*" solvent reorganization energy in all of these alkylbenzene solvents by a comparable amount. This line of reasoning suggests that the solvent reorganization energy attending motion of a single solvent molecule within the cleft, ~0.1 eV, is comparable to the solvent reorganization energy attending motions of all of the solvent molecules surrounding the donor and acceptor groups. Finite difference Poisson-Boltzmann calculations[34] that explicitly account for the shape and presence of a cleft in **1** generate similar values of λ_S whether the solvent is excluded or allowed into the cleft between the donor and acceptor.[35] Thus, exclusion of the aromatic core of 1,3,5-triisopropylbenzene from the cleft in **1** is not a likely source for the discrepancy between the calculated and experimental λ_S values.

An alternative explanation for the discrepancy between the molecular model and regression estimate of λ_S for **1** in 1,3,5-triisopropylbenzene is that the effective |V| in this solvent is also temperature-dependent. In analogy to the approach employed for **1** in 1,3-diisopropylbenzene, the magnitude and temperature dependence of the effective coupling for **1** in 1,3,5-triisopropylbenzene may be determined by assuming that the molecular model predictions of λ_S(T) are correct. The results of this analysis (Figure 6.8) suggest that the effective coupling for **1** in 1,3,5-triisopropylbenzene *increases* with temperature, from 2.9 cm^{-1} at 260 K to 3.5 cm^{-1}

at 283 K. A positive value of d|V|/dT provides a simple explanation for the experimental observation that both k_{for} and k_{back} increase with temperature in this solvent. The magnitude of the coupling obtained from this analysis is larger than the value of 1.0 cm^{-1} previously obtained with the assumption of a temperature independent coupling magnitude and a regression estimate of λ_S(295 K) = 0.01 eV. It is not surprising that a larger magnitude of |V| is obtained when larger values of λ_S are used in the analysis (Figure 6.4). Even with this increase, the effective coupling for **1** in 1,3-diisopropylbenzene is still more than 2-fold larger than in 1,3,5-triisopropylbenzene (260 K < *T* < 283 K). As was suggested previously, increased steric bulk about the periphery of the solvent's aromatic π system results in less effective solvent- mediated coupling.

Figure 6.8 shows the |V(T)| values that are obtained for the other alkylbenzene solvents when the solvation model's predictions for the temperature-dependent reorganization energy are assumed to be correct. The effective coupling magnitude, derived from the rate data and the molecular model λ_S(T), decreases with increasing temperature in the solvents benzene, cumene, and mesitylene. The diminution is greatest for mesitylene, for which the coupling magnitude and temperature dependence are similar to that for **1** in 1,3-diisopropylbenzene. The steep decrease of the coupling in mesitylene provides an explanation for the failure of the previous analysis,[10] which assumed temperature independent coupling magnitudes, to reproduce the experimentally observed steep decrease of k_{for} and k_{back} at temperatures above 315 K. The temperature derivative of the effective coupling in benzene and cumene, -0.04 cm^{-1} K^{-1}, is about half as large as that for mesitylene. For the five alkylbenzene solvents,

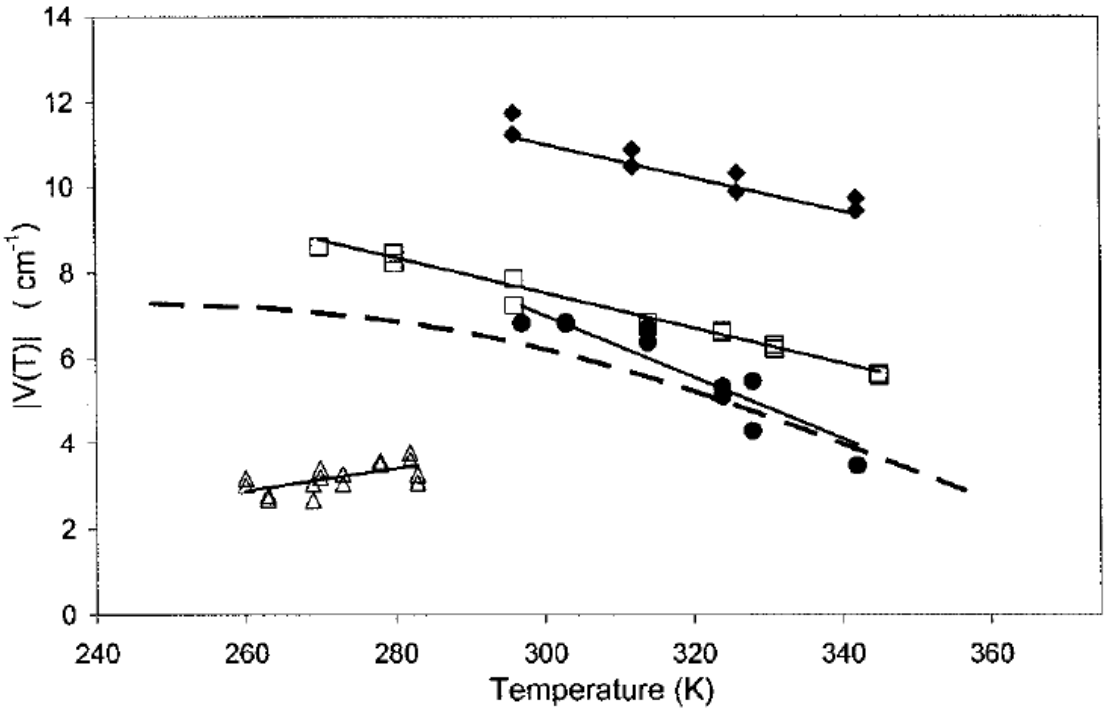

Figure 6.8 Temperature dependence of the electronic coupling for 1 in benzene (♦), cumene (□), mesitylene (•), and 1,3,5-tri-isopropylbenzene (△), obtained by fitting the experimental rate constant data and using the calibrated Matyushov model to calculate $\lambda_S(T)$. Regression lines are drawn through the data for each solvent. The best fit line to the 1,3-diisopropylbenzene |V(T)| data (— —) is reproduced from Figure 6.6.

the effective coupling magnitudes at 295 K are 12 cm^{-1} in benzene, 7.4 cm^{-1} in cumene, 6.8 cm^{-1} in mesitylene, 6.3 cm^{-1} in 1,3-diisopropylbenzene, and 3.9 cm^{-1} in 1,3,5-triisopropylbenzene.[36] With the exception of the last solvent, these magnitudes are within 20% of the values derived previously from analyses premised on temperature independent coupling.[10]

The structure and the number of alkyl groups on the periphery of the solvents' aromatic ring alter the electronic coupling magnitude for **1**. The alkyl groups have a minor effect on the aromatic π system's energy levels. They do influence the probabilities of locating the aromatic π system in positions that offer simultaneous overlap with the donor and the acceptor. Theoretical investigations confirm that such

simultaneous overlap is necessary for a coupling pathway constituted by a single solvent molecule to be effective.[5e] For a C-shaped molecule such as **1**, simultaneous overlap and significant coupling are realized by placement of the solvent's aromatic π system within the 7 Å wide cleft, directly between the donor and acceptor groups.[37] The observed dependence of **1**'s electronic coupling magnitude on the identity of the alkyl groups around the aromatic ring and on temperature can be explained in terms of solvent entry into this cleft. A benzene molecule readily accesses "in-cleft" solvent configurations that provide significant, simultaneous overlap of the solvent with the donor and the acceptor of **1**. For many of these "in-cleft" configurations of the benzene, substituting a peripheral H atom by an alkyl group introduces steric repulsion between the alkyl group and **1**. This repulsion disfavors solvent configurations with the aromatic core situated deeply within the cleft. Solvent configurations in which the (bulky) alkyl groups are farther from the cleft walls and edges are more probable. The latter configurations offer smaller simultaneous overlap of the donor and acceptor with the solvent π orbitals and, therefore, smaller electronic coupling. Larger and/or more numerous alkyl groups more severely reduce the probability of solvent configurations with large overlap and significant coupling. This explains the observed reduction of coupling magnitude with increasing alkyl substitution of the solvent.

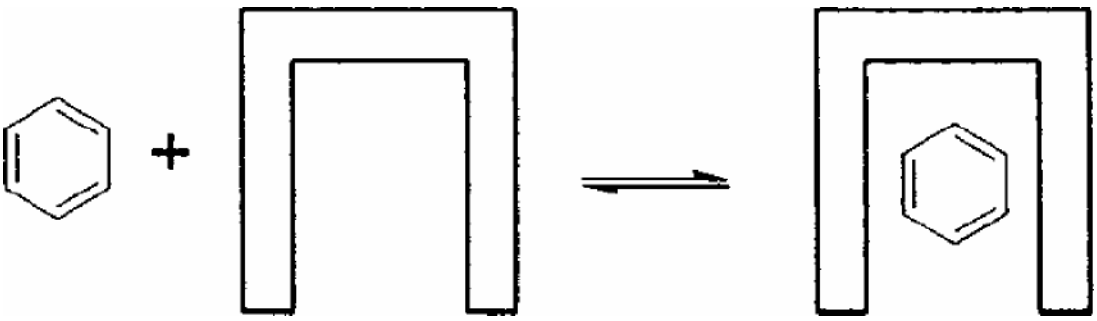

Scheme 6.1

Each “in-cleft” solvent configuration affords a unique coupling magnitude. As solvent molecules move within and out of the cleft, the donor-acceptor coupling magnitude fluctuates. The probability of an electron-transfer event is very small during any single initial state-final state level crossing (nonadiabatic transfer). As a result, each molecule of **1** samples a “large number” of solvent configurations before there is significant probability that the ensemble of excited states has undergone electron transfer. Rapid interconversion among solvent-**1** configurations, compared to the electron-transfer rate, generates experimental charge separation dynamics that are well reproduced by a single electron-transfer rate constant with an effective coupling magnitude that is a root-mean-square average of the individual coupling magnitude, $(V_j)^2$, in each possible configuration, $|V| = [\Sigma_j p_j (Vj)^2]^{1/2}$. The probability of each configuration, p_j, is determined by its free energy and by the temperature. The probability of each solvent-**1** configuration changes differently with temperature, thus altering the distribution of mediating configurations and the average value of the coupling. This provides an explanation for the temperature dependence of the observed electronic coupling.

The different signs of $d|V|/dT$ for **1** in benzene and 1,3,5-triisopropylbenzene may be attributed to the most prevalent “state” of the cleft in each solvent. For example, benzene readily fits within the cleft of **1**, and the equilibrium (see Scheme 6.1) should be characterized by a negative $\Delta H°$ and a negative $\Delta S°$.[38] Upon increasing the temperature, the equilibrium shifts toward “empty-cleft” configurations. Because the “in-cleft” solvent configurations provide larger electronic coupling than the “empty

cleft" configurations, the effective coupling magnitude in benzene decreases as the temperature increases. The rather shallow dependence of $|V|$ on temperature for **1** in benzene and cumene suggests that "in-cleft" configurations predominate throughout the investigated temperature ranges. The steeper dependence of $|V|$ on temperature for **1** in mesitylene and in 1,3-diisopropylbenzene indicate more significant conversion from predominantly "in-cleft" to "empty-cleft" configurations. The solvent 1,3,5-triisopropylbenzene presents a different situation. Steric repulsion between the isopropyl groups and **1** results in a positive enthalpy for formation of "in-cleft" solvent configurations in which the solvent's aromatic core is between the donor and acceptor. These configurations provide larger electronic coupling, but $\Delta G°$ for their formation is positive (i.e., the equilibrium constant for their formation is less than 1). Higher temperature increases the fraction of these higher free energy, larger coupling, "in-cleft" configurations, and enhances the effective coupling magnitude. Given the excellent correspondence between the experimental rate data for **1** and the rates calculated using the parametrized molecular model in a variety of alkylbenzene solvents, variation of the solvent mediated electronic coupling magnitude with temperature is a likely explanation for the unusual electron-transfer kinetics of **1** in 1,3-diisopropylbenzene.

6.5 Conclusion

The charge separation and charge recombination rate constants for **1** in 1,3-diisopropylbenzene increase, plateau, and then decrease when plotted against temperature or the experimentally determined reaction free energy change. Within

the framework of a single quantum-mode, semiclassical electron transfer rate expression, the origin of this rate behavior lies in the temperature dependence of the solvent reorganization energy and/or of the electronic coupling. Two explanations of the kinetic behavior have been advanced. The experimental data can be simulated using a small and temperature-independent solvent reorganization energy or a temperature-dependent electronic coupling magnitude. In the first scenario, the variation of the reaction driving force with temperature shifts the reactions between the Marcus normal and the Marcus inverted regions and is responsible for the highly curved rate plots. Between 210 and 360 K, $\Delta_r G$ for the charge separation and charge recombination reactions are insufficient to populate "products" with one or more quanta of vibrational energy.[39] Thus, the electron transfer rate constant in the normal and inverted regions decreases comparably as the reaction free energy shifts away from the optimum value. For this explanation to apply, there cannot be significant vibrational reorganization (energy) associated with modes in the 400-700 cm^{-1} range. The solvent reorganization energy would also need to be extremely small and unusually temperature-independent. Additionally, there are very few examples of charge separation reactions (neutral reactant - zwitterionic product) that exhibit rate versus $\Delta_r G$ profiles consistent with the Marcus inverted region.[40] Although many explanations have been advanced to justify the paucity of examples, invoking the inverted region to explain the rate constant data from **1** finds little if any precedent. This would also be the first example of a charge separation reaction in nonpolar solvents lying in the Marcus inverted region.

The alternative explanation for the kinetic data posits that the electronic coupling magnitude varies with temperature. Between 290 and 350 K, the effective coupling for **1** decreases 60% in 1,3-diisopropylbenzene, 50% in mesitylene, and 30% in cumene. The extensive curvature in the bridge of **1** requires an appropriately placed solvent molecule within the cleft between the donor and acceptor to mediate the electronic coupling. The probability of appropriate solvent placement and the efficacy of solvent-mediated coupling both vary with solvent structure and temperature. Although there are theoretical studies that support the feasibility of temperature-dependent, solvent mediated coupling magnitudes,[5,41] there is not yet *direct* evidence to confirm this explanation. The evidence in this manuscript is indirect, relying on a parametrized solvation model to provide accurate predictions of the solvent reorganization as a function of solvent structure and temperature. More direct investigation of the temperature dependence in solvent-mediated electronic coupling is clearly desirable. In summary, the experimental rate constant behavior for **1** in a number of alkylbenzene solvents is most reasonably explained by invoking a significant temperature dependence for the solvent-mediated, electronic coupling magnitude. Temperature-dependent electronic coupling may influence electron-transfer dynamics in any system where the composition or the structure of the coupling pathway fluctuates significantly.

6.6 References

(1) (a) Gould, I. R.; Young, R. H.; Moody, R. E.; Farid, S. *J. Phys. Chem.* **1991**, *95*, 2068. (b) Gould, I. R.; Young, R. H.; Mueller, L. J.; Albrecht, A. C.; Farid, S. *J. Am. Chem. Soc.* **1994**, *116*, 8188.

(2) (a) Winkler, J. R.; Di Bilio, A. J.; Farrow, N. A.; Richards, J. H.; Gray, H. B. *Pure Appl. Chem*. **1999**, *71*, 1753. (b) Casimiro, D. R.; Beratan, D. N.; Onuchic, J. N.; Winkler, J. R.; Gray, H. B *Adv. Chem. Ser.* **1995**, *246*, 471. (c) Miller, J. R.; Beitz, J. V.; Huddleston, R. K. *J. Am. Chem. Soc.* **1984**, *106*, 5057.

(3) (a) Hush, N. S. *Coord. Chem. Rev.* **1985**, *64*, 135. (b) Oliver, A. M.; Paddon-Row, M. N.; Kroon, J.; Verhoeven, J. W. *Chem. Phys. Lett*. **1992**, *191*, 371. (c) Morais, J.; Hung, R. R.; Grabowski, J. J.; Zimmt, M. B. *J. Phys. Chem.* **1993**, *97*, 13138. (c) Bixon, M.; Jortner, J.; Verhoeven, J. W. *J. Am. Chem. Soc.* **1994**, *116*, 7349.

(4) (a) Closs, G. L.; Miller, J. R. *Science* **1988**, *240*, 440. (b) Paddon-Row, M. N. *Acc. Chem. Res*. **1994**, *27*, 18. (c) Sachs, S. B.; Dudek, S. P.; Hsung, R. P.; Sita, L. R.; Smalley, J. F.; Newton, M. D.; Feldberg, S. W.; Chidsey, C. E. D. *J. Am. Chem. Soc.* **1997**, *119*, 10563. (d) Winkler, J. R.; Gray, H. B. *J. Biol. Inorg. Chem.* **1997**, *2*, 399. (e) Lewis, F. D.; Letsinger, R. L. *J. Biol. Inorg. Chem.* **1998**, *3*, 215. (f) Davis, W. B.; Svec, W. A.; Ratner, M. A.; Wasielewski, M. R *Nature* **1998**, *396*, 60.

(5) (a) Chohan, K. K.; Jones, M.; Grossmann, J. G.; Frerman, F. E.; Scrutton, N. S.; Sutcliffe, M. J. *J. Biol. Chem.* **2001**, 276, 34142. (b) Jones, G. A.; Carpenter, B. K.; Paddon-Row, M. N. *J. Am. Chem. Soc.* **1999**, *121*, 11171. (c) Xie, Q.; Archontis, G.; Skourtis, S. S. *Chem. Phys. Lett.* **1999**, *312*, 237. (d) Balabin, I. A.; Onuchic, J. N. *Science* **2000**, *290*, 114. (e) Cave, R. J.; Newton, M. D.; Kumar, K.; Zimmt, M. B. *J. Phys. Chem.* **1995**, *99*, 17501. (f) Castner, E. W., Jr.; Kennedy, D.; Cave, R. J. *J. Phys. Chem. A* **2000**, *104*, 2869.

(6) (a) Davis, W. B.; Ratner, M. A.; Wasielewski, M. R. *J. Am. Chem. Soc.* **2001**, *123*, 7877. (b) Graige, M. S.; Feher, G.; Okamura, M. Y. *Proc. Natl. Acad. Sci. U.S.A*. **1998**, *95*, 11679. (c) Hoffman, B. M.; Ratner, M. A. *J. Am. Chem. Soc.* **1987**, *109*, 6237. (d) Intermolecular electron- transfer reactions are influenced by the dependence of electronic coupling on donoracceptor separation and the nature of the intervening medium. See ref 5f.

(7) Fluctuations of rigid bridge mediated coupling magnitudes are small compared to the mean coupling matrix element in systems where the donor acceptor interaction is not symmetry forbidden (see the last column $_{(H\mathrm{CR})}$ of Table 9.1 for **1** in ref 5e. In systems where the donor- acceptor interaction is symmetry forbidden, the mean coupling value is small. Distortions of the molecular structure can generate coupling magnitudes that are larger than the mean value. See the sixth column $_{(H\mathrm{CS})}$ of Table 9.1 for **1** in ref 5e.

(8) (a) Lawson, J. M.; Paddon-Row, M. N.; Schuddeboom, W.; Warman, J. M.; Clayton, A. H. A.; Ghiggino, K. P. *J. Phys. Chem.* **1993**, *97*, 13099. (b) Kumar, K.; Lin, Z.; Waldeck, D. H.;

Zimmt, M. B. *J. Am. Chem. Soc*. **1996**, *118*, 243. (c) Read, I.; Napper, A.; Kaplan, R.; Zimmt, M. B.; Waldeck, D. H. *J. Am. Chem. Soc*. **1999**, *121*, 10976. (d) Lokan, N. R.; Paddon-Row, M. N.; Koeberg, M.; Verhoeven, J. W. *J. Am. Chem. Soc*. **2000**, *122*, 5075. (e) Kaplan, R. W.; Napper, A. M.; Waldeck, D. H.; Zimmt, M. B. *J. Am. Chem. Soc.* **2000**, *122*, 12039.

(9) The following citation describes the pressure dependence of electronic orbital overlap in hydrogen bonds: Li, H.; Yamada, H.; Akasaka, K.i; Gronenborn, A. M. *J. Biomol. NMR* **2000**, *18*, 207.

(10) Read, I.; Napper, A.; Zimmt, M. B.; Waldeck, D. H. *J. Phys. Chem. A* **2000**, *104*, 9385.

(11) Napper, A. M.; Read, I.; Kaplan, R.; Zimmt, M. B.; Waldeck, D. H. *J. Phys. Chem. A* **2002**, *106*, 5288-5296.

(12) The rate constant, $k_{rec,}$ comprises two distinct electron-transfer processes; conversion of the CT state to the molecule's ground singlet state and to the molecule's lowest energy triplet state. This is of no consequence to the current investigation.

(13) (a) Kumar, K.; Tepper, R. J.; Zeng, Y.; Zimmt, M. B*. J. Org. Chem.* **1995**, *60*, 4051. (b) Kaplan, R. Ph.D. Thesis, Brown University, Providence, RI, 2001.

(14) (a) Zeglinski, D. M.; Waldeck, D. H. *J. Phys. Chem.* **1988**, *92*, 692. (b) O'Connor, D. V.; Phillips, D. *Time Correlated Single Photon Counting*; Academic Press: New York, 1984.

(15) The fluorescence decay of **1** is fit to the biexponential form: $I(t) = a_+e^{-k_+ t} + (1-a_+)e^{-k-t}$. The forward electron-transfer rate constant k_{for} is obtained from $k_{for} = a_+(k_+ - k_-) - k_f + k_-$, and the reverse electron transfer rate constant k_{back} is obtained from $k_{back} = [(k_+ - k_-)^2 - (2k_f + 2k_{for} - k_+ - k_-)^2]/4k_{for}$. See the text for determination of k_f.

(16) The best fit equation is $\Delta_r G(\text{eV}) = 5.245\ 1 \times 10^{-6} T^2 - 2.0156 \times 10^{-3} T + 1.2979 \times 10^{-1}$. The temperature is in units of K.

(17) Jortner, J. *J. Chem. Phys.* **1976**, *64*, 4860.

(18) (a) Zeng, Y.; Zimmt, M. B. *J. Phys. Chem.* **1992**, *96*, 8395. (b) Kumar, K.; Kurnikov, I.; Beratan, D.; Waldeck, D.; Zimmt, M. B. *J. Phys. Chem. A* **1998**, *102*, 5529.

(19) (a) Vath, P.; Zimmt, M. B.; Matyushov, D. V.; Voth, G. A. *J. Phys. Chem. B* **1999**, *103*, 9130. (b) Vath, P.; Zimmt, M. B. *J. Phys. Chem. A* **2000***, 104*, 2626. (c) Derr, D. L.; Elliott, C. *J. Phys. Chem. A* **1999**, *103*, 7888. (d) Matyushov, D. V. *Chem. Phys*. **1993**, *174*, 199. (e) Corte´s, J.; Heitele, H.; Jortner, J. *J. Phys. Chem*. **1994**, *98*,

2527. (f) Evidence of increasing λ_S with decreasing temperature for bacterial reaction centers is presented in Ortega, J. M.; Mathis, P.; Williams, J. C.; Allen, J. P. *Biochemistry* **1996**, *35*, 3354.

(20) Matyushov, D. V.; Voth, G. A. *J. Chem. Phys*. **1999**, 111, 3630.

(21) The only other fitting parameter in these analyses was $|V|$, which was assumed to be temperature-independent.

(22) Over small temperature ranges, the predicted λ_S appear to vary linearly with temperature. Over larger temperature ranges (140 K for 13DIP), curvature in the $\lambda_S(T)$ plots are evident.

(23) The predicted values in column 3 of Table 9.1 are larger than previously reported in ref 10. A numerical error in a subroutine was responsible. The results of the corrected code have been checked with code kindly provided by Professor Matyushov.

(24) The line in Figure 9.6 is a polynomial fit to this derived $|V(T)|$ data. A polynomial fit yields $|V(T)| = 2.257 \times 10^{-8}T^4 - 2.630 \times 10T^3 + 1.106 \times 10^{-2}T^2 - 2.014 \times 10T + 1.423 \times 10^2$. The temperature is in units of K and $|V|$ is in cm^{-1}.

(25) Compound **2** in the current manuscript is the same as compound **8** in reference 18a.

(26) (a) The line shape of a CT emission band includes contributions from the frequency dependence of the transition moment in addition to the frequency dependence of the Franck- Condon factors.[26b] After correcting for the frequency dependence of the transition moment, the Franck-Condon line shape remains. The energy corresponding to the maximum of this line shape is reported in the text. (b) Marcus, R. A. *J. Phys. Chem.* **1989**, *93*, 3078. (c) It is not possible to extract unique values of λ_S and $\Delta_r G$ for compound **2** in alkylbenzene solvents. Impurity emissions obscure the blue side of these spectra, making a unique determination of $\Delta_r G$ impossible. The absence of detectable CT absorption bands eliminates a second route to unique $\Delta_r G$ determination. Consequently, there is substantial, correlated uncertainty in values of $\Delta_r G$ and λ_S obtained by fitting the CT emission line shape.

(27) Both λ_S and $-\Delta_r G$(S1→CT) are positive quantities that increase with increasing (nuclear) solvation. As a result, solvation differences provided by various alkylbenzene solvents reinforce, rather than cancel, in the term $\lambda_S - \Delta_r G$(S1→CT).

(28) In alkylbenzene solvents, the Coulomb interaction between the donor cation and acceptor ion amounts to 14.4 eV Å/(2.3 x 7.1 Å) = 0.88 eV for **1** and 14.4 eV Å/(2.3 x 5.7 Å) = 1.10 eV for **2**. The difference of these two values, 0.22 eV, is about the same as the 0.26 eV difference between the $\lambda_S - \Delta_r G$(S1→CT) values presented for **1** and **2**.

(29) Comparison of the magnitude and solvent dependence of λ_S for **1** and **2** would be particularly informative. It is not possible to extract accurate values of λ_S from the CT emission spectra.[26c]

(30) Ulstrup, J.; Jortner, J. *J. Chem. Phys.* **1975**, *63*, 4358.

(31) Figure 9.7 shows that the one quantum mode and two quantum mode models predict different rate constant dependence on reaction free energy for $-\Delta_r G > \lambda_S$. The two models predict comparable rate constant magnitudes and dependencies for $-\Delta_r G < \lambda_S$, however. Use of the two quantum model with $|V| = 7$ cm^{-1} and the parameters in Figure 9.7 yields rate constants that are indistinguishable from rate constants predicted using $|V| = 6$ cm^{-1} and the one quantum mode model in the range $-\Delta_r G < \lambda_S$. This demonstrates that electronic coupling magnitudes extracted from rate constant data in the Marcus normal region depend weakly on the model used to simulate the vibrational Franck-Condon factors. For further discussion of the influence of zero, one, and multi quantum mode models on Franck-Condon factors and extracted values of the electronic coupling, see refs 18b and 32d.

(32) (a) Hupp, J. T.; Williams, R. D. *Acc. Chem. Res.* **2001**, *34*, 808. (b) Hogiu, S.; Dreyer, J.; Pfeiffer, M.; Brzezinka, K. W.; Werncke, W. *J. Raman. Spectrosc.* **2000**, *31*, 797. (c) Godbout, J. T.; Zuilhof, H.; Heim, G.; Gould, I. R.; Goodman, J. L.; Dinnocenzo, J. P.; Kelley, A. M. *J. Raman Spectrosc*. **2000**, *31*, 233. (d) Lilichenko, M.; Tittelbach-Helmrich, D.; Verhoeven, J. W.; Gould, I. R.; Myers, A. B. *J. Chem. Phys.* **1998**, *109*, 10958.

(33) If reorganization of the cleft solvent makes significant contribution to λ_S, the agreement between the molecular model prediction and the experimental results (Table 9.1) is fortuitous and suggests that the parametrization of the molecular model overestimates the extra-cavity solvation of **1**.

(34) (a) Sharp, K.; Honig, B. *Annu. Rev. Biophys. Biophys. Chem.* **1990**, *19*, 301. (b) Sitkoff, D.; Sharp, K. A.; Honig, B. *J. Phys. Chem.* **1994**, *98*, 1978. (c) Zhang, L. Y.; Frieser, R. A. *J. Phys. Chem.* **1995**, *99*, 16479.

(35) The finite-difference Poisson-Boltzmann calculations indicate that exclusion of the solvent from the cleft of **1** reduces the solvent reorganization energy by less than 10%. See ref 18b.

(36) The value of $|V(295\ \text{K})|$ provided for 1,3,5-triisopropylbenzene is a linear extrapolation of the results obtained at lower temperatures.

(37) An alkyl group within the cleft provides smaller donor-acceptor electronic coupling than an aromatic ring in the cleft because the lowest energy superexchange state, D^+S^-A, has the “transferring” electron localized on the aromatic ring.

(38) (a) Dispersion and electrostatic interactions[38b] between the anthracene, benzene, and the alkene diester generate a negative enthalpy change for solvent entry. Solvent "complexation" with **1** results in a reduction of translational entropy relative to two, independently diffusing molecules. (b) Tsuzuki, S.; Honda, K.; Uchimaru, T.; Mikami, M.; Tanabe, K. *J. Am. Chem. Soc.* **2002**, *124*, 104.

(39) According to the best fit analysis, approximately 10% of the charge recombination products are formed with one quantum of vibrational energy when the temperature reaches 360 K.

(40) (a) Smitha, M. A.; Prasad, E.; Gopidas, K. R. *J. Am. Chem. Soc.* **2001**, *123*, 1159. (b) Prasad, E.; Gopidas, K. R. *J. Am. Chem. Soc.* **2000**, *122*, 3191.

(41) (a) Segal, D. A; Nitzan, A.; Davis, W. B.; Wasielewski, M. R.; Ratner, M. A. *J. Phys. Chem. B* **2000**, *104*, 3817. (b) Ashkenazi, G.; Kosloff, R.; Ratner, M. A. *J. Am. Chem. Soc*. **1999**, *121*, 3386. (c) Tang, J. *J. Chem. Phys.* **1993**, *98*, 6263.

Chapter 7 Use of U-shaped Donor-Bridge-Acceptor Molecules to Study Electron Tunneling Through Non-bonded Contacts

A systematic determination of electronic coupling matrix elements in U-shaped molecules is demonstrated. The unique architecture of these systems allows for the determination of the electronic coupling through a pendant molecular moiety that resides between the donor and acceptor groups, quantifying the efficiency of electron tunneling through non-bonded contacts. Experimental electron transfer rate constants and reaction free energies are used to calibrate a molecular based model that describes the solvation energy. This approach makes it possible to experimentally determine electronic couplings and compare them with computational values.[***]

7.1 Introduction

Electron transfer is a fundamental chemical process of immense scientific and technological importance. Consequently, it has received much attention.[1] This study evaluates the electron tunneling efficiency between electron donor and acceptor groups by way of non-covalent molecular contacts. The tunneling efficiency is quantified by the electronic coupling matrix element, |V|, which characterizes the electronic interaction between an electron donor (D) and acceptor (A). Donor-Bridge-Acceptor (DBA) molecules have been successfully used to address important issues in electron transfer because they provide systematic control over molecular properties such as bridge geometry,[2] electronic state symmetry,[3] reaction free energy,[4]

[***] This chapter was previously published as: Napper, A. M.; Head, N. J.; Oliver, A. M.; Shephard, M. J.; Paddon-Row, M. N.; Read, I.; Waldeck, D. H.; *J. Am. Chem. Soc.;* **2002**; 124(34); 10171- 10181.

and others. Electron transfer in DBA molecules can be viewed as a superexchange mechanism that occurs through the orbitals of the intervening medium along a path between the donor and acceptor groups.[5] Recent studies have demonstrated significant electronic couplings mediated through covalent bonds,[6] through hydrogen bonds,[7] and through solvent molecules.[8,9] This work quantifies the electronic coupling through molecular moieties in van der Waals contact.

The U-shaped DBA systems designed by the Zimmt[9,10] and Paddon-Row[8,13] groups provide insight into the nature of non-adiabatic electron transfer processes that involve electron tunneling through solvent molecules. These systems have the donor and acceptor groups connected by a highly curved, rigid, covalent bridging unit that holds them apart at a fixed distance and orientation. An increase in the electron transfer rate constant has been observed in such systems when solvents of appropriate sizes and orbital energetics are used. This increase has been ascribed to the occupation of the interior cavity by a solvent molecule(s), *e.g.* benzene or benzonitrile, that allows for an enhanced *line-of-sight* electron tunneling between the donor and acceptor groups, as opposed to a longer, through-bond, coupling pathway occurring via the U-shaped bridge. The electronic couplings determined in these systems can be correlated to the size of the solvent molecule[10b] and its electronic character.[11] However, these systems do not provide direct experimental evidence for the presence of a solvent molecule within the cleft.

More recently, Paddon-Row *et al.*[12] have constructed supramolecular systems in which a pendant group, covalently attached to the intervening bridge, occupies the interior of the cleft (Chart 7.1). Comparison of the electron transfer rates for three

different systems, **1**, **2**, and **3**[13], were measured as a function of solvent polarity. It was shown that when an aromatic moiety is positioned in the *line-of-sight* between the donor and acceptor pair, as in **1**, the observed rate constant is significantly higher than systems in which it is not present, as in **2,** or is not in the *line-of-sight*, as in **3.**[13] The current work quantitatively analyzes the electron transfer rate data for systems **1** and **2** in toluene and mesitylene solvents and combines it with earlier data[13] obtained in CH_2Cl_2, THF, and acetonitrile solvents. Electronic structure calculations and the experimental free energies of reaction in the aromatic solvent are used to calibrate a molecular solvation model and subsequently determine the values of the electronic coupling matrix element for **1** and **2**. The electronic couplings are then compared with those calculated for a model system.

A frequently applied analysis of the electron transfer rate constant relies upon a semi-classical version of the Marcus expression. In this treatment, the solute high frequency intramolecular degrees of freedom, which are coupled to the charge separation process, are treated as a single effective quantum vibrational mode and the low frequency intramolecular and solvent modes are treated classically, so that the rate constant can be expressed as

$$k_{eT} = \frac{2\pi |V|^2}{\hbar\sqrt{4\lambda_o \pi k_B T}} \sum_{n=0}^{\infty} e^{-S}\left(\frac{S^n}{n!}\right) \exp\left[\frac{-(\Delta_r G + \lambda_o + nh\nu)^2}{4\lambda_o k_B T}\right] \tag{7.1}$$

where $\Delta_r G$ is the reaction free-energy, λ_o is the outer-sphere (solvent) reorganization energy, ν is the frequency of the effective vibrational mode, and S is the Huang-Rhys factor given as the ratio of the inner-sphere reorganization energy, λi, to the

quantized mode energy spacing, ($\lambda i/h\nu$).[1b] The electron transfer rate constants predicted by eq. 7.1 are a strong function of the parameter set used, and an accurate determination of these parameters is necessary when drawing comparisons with experimental rate data. The quantities $h\nu$ and λi are typically evaluated using a combination of experimental charge transfer spectra and ab initio calculations. Usually, $\Delta_r G$ is estimated through experimental redox data and dielectric continuum corrections to the salvation energy. This approach is not appropriate in weakly polar and non-polar solvents, however. In this study $\Delta_r G$ is obtained in non-polar aromatic solvents from an analysis of the kinetic data using a two-state model. The model assumes that an equilibrium exists between the locally excited state and the charge-separated species and permits evaluation of the forward and backward electron transfer rate constants. These data are used to calibrate a molecular-based solvation model[14,15] that is able to reproduce the experimental $\Delta_r G(T)$ values. The same model is used to predict the temperature dependence of λ_o. The electronic coupling |V| and λ_o(295 K) are obtained by fitting the experimental rate constant data using the $\Delta_r G$ and $d\lambda_o/dT$ values from the model in conjunction with λi and ν values taken from charge transfer spectra.[10a,16]

7.2 Experimental and Computational Details

Time resolved fluorescence kinetics of **1** and **2** were measured in toluene and mesitylene as a function of temperature. Comparison of the fluorescence decay kinetics with that of the donor-only reference molecules (**1noA** and **2noA**) allowed the electron transfer rate constants to be obtained. In all cases the molecule's excited

decay law was found to be bi-exponential[17]. This finding is consistent with a small reaction free energy for charge separation, $\Delta_r G$. A previous study[13] measured the electron transfer kinetics for **1** and **2** in CH_2Cl_2, THF, and acetonitrile. In these three solvents, a single-exponential decay was observed, consistent with a larger reaction driving force. Simple continuum calculations suggest that the increased dipolar nature of these solvents leads to an increase in the magnitude of $-\Delta_r G$.

The preparation of the electron transfer molecules **1** and **2** were reported previously.[12] The solvents were purified in the manner described previously.[10] The ground and charge-separated (CS) states of the imido systems **4** - **7** were studied computationally. Ground state geometries of **4** - **7** were optimized at the RHF/3-21G level, whereas the excited singlet CS states were optimized at the UHF/3-21G level. It has been found that the UHF level of theory provides satisfactory optimized geometries of CS states,[18,19] provided that the CS state is the lowest energy state of that particular state symmetry and multiplicity. As the CS states of **4** - **7** possess ^{1}A" state symmetry, that criterion is satisfied in these molecules. All calculations were carried out using the Gaussian 98 program.[20]

Salient geometric features of the ground and CS states of **4 - 7** are summarized in Table 7.1. The ground state geometries for **4** - **7** are all very similar with the R group only having a small influence (< 2%) upon the distance between the DMN and DCV groups. The dipole moment varies little (5.3 - 6.0 D) and the total charges on the DMN, DCV, and imide chromophores show little change in going from **4** to **7**. It should be pointed out that the ground state optimized geometry of the N-phenyl system, **7**,

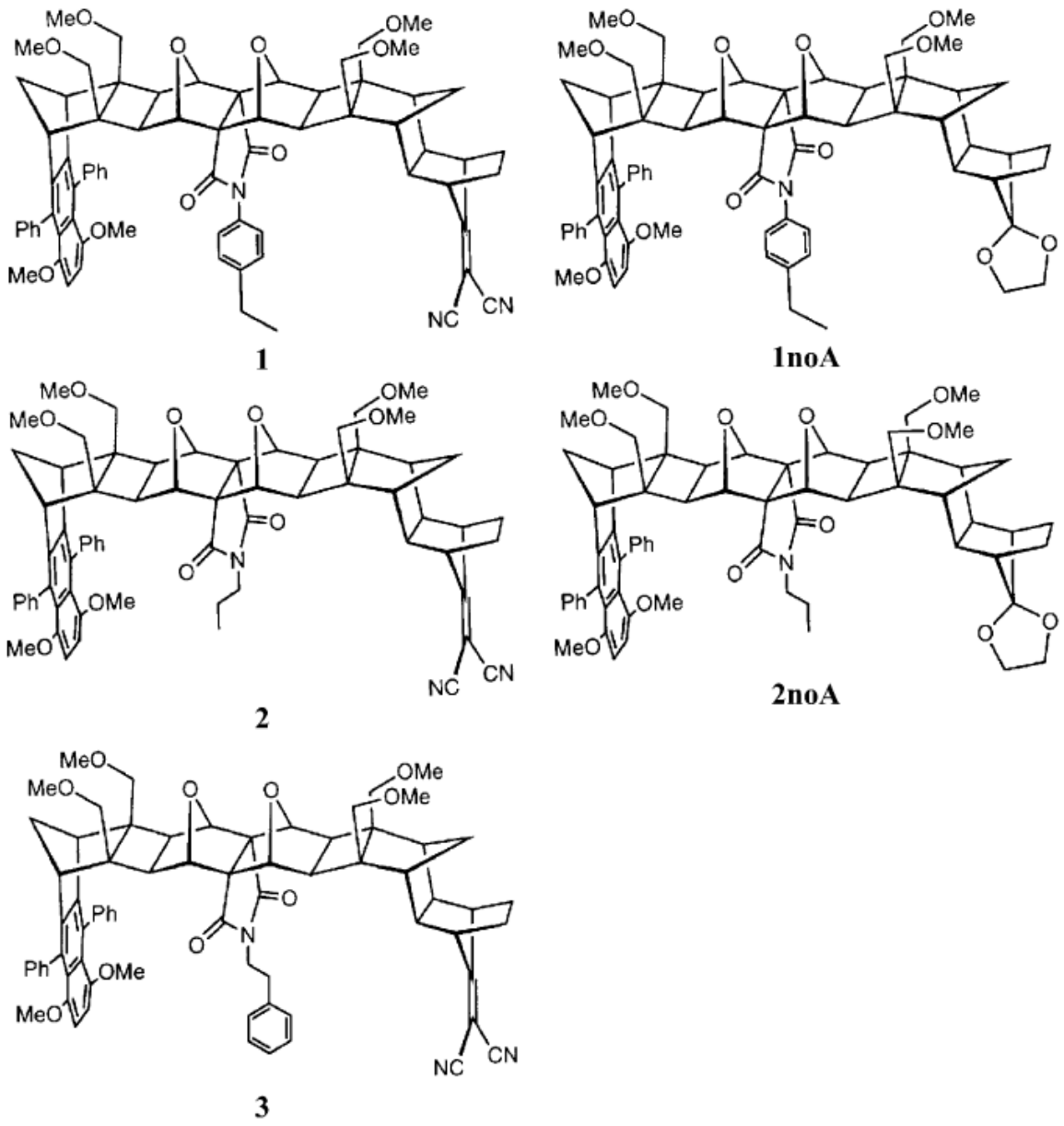

Chart 7.1 Electron Transfer Molecules Studied and their Donor Only Analogues.

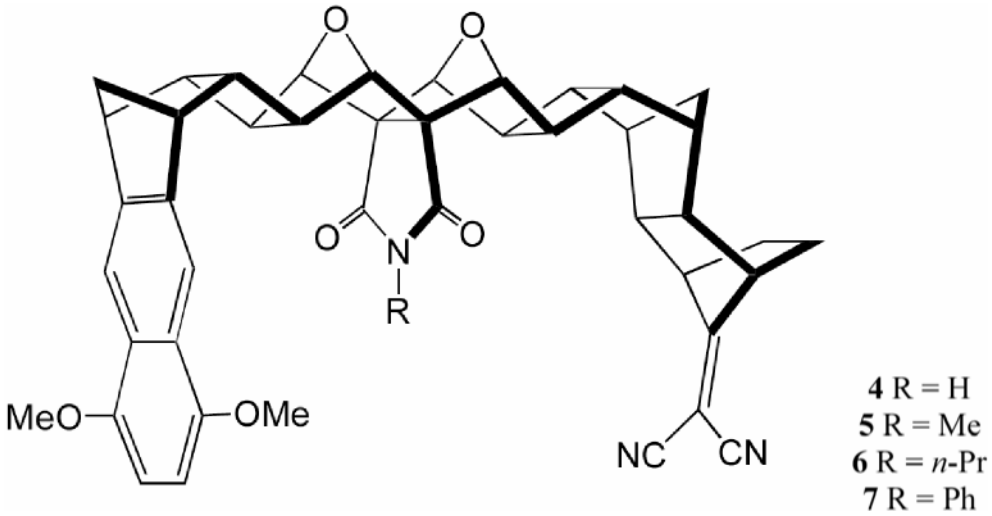

Chart 7.2 Chemical Structures of the Molecules Studied Computationally.

was constrained to have C_s symmetry, with the phenyl ring lying in the plane of the imide group, and hence parallel with the DMN and DCV groups. This is not the global minimum however; that structure corresponds to the configuration, 1.35 kcal/mol more stable than the C_s structure, where the phenyl ring is rotated 71º out of the imide plane. Similarly, the N-*n*-propyl system, **6**, possesses a global minimum structure similar to, but 0.23 kcal/mol lower in energy than, the C_s symmetric structure used in these calculations. However, since the UHF level geometry optimization calculation of the CS state required that the molecule possess some symmetry, the C_s symmetry structures were used rather than the global minima structures for **6** and **7**.

In general, there is much to criticize in using a single determinant UHF wavefunction to calculate excited states. Not only does it neglect electron correlation but it fails to give a qualitatively correct description of the open-shell singlet excited state wavefunction - the zeroth- order wavefunction of such states is biconfigurational. Consequently, the UHF wavefunction for singlet excited states is severely spin contaminated. Indeed, we find that

$<S^2>$ ~ 1 for the UHF CS singlet CS states of **4-7**, implying ca. 50:50 singlet-triplet mixing. The use of such a low level of theory (UHF) to calculate reliable relaxed geometries and dipole moments (but not energies) of CS states has been addressed and fully justified in earlier publications.[17,18] In particular, we have found that UHF/3-21G optimized geometries and dipole moments for giant CS singlet states related to those studied here are almost the same as those calculated using higher levels of theory, such as CIS which, being multideterminantal, does not lead to spin contamination of the singlet CS state wavefunction. We have also found that, at the UHF, CIS and DFT levels of theory, triplet CS state relaxed geometries and dipole moments of a variety of bichromophoric systems reported in ref 18 are practically identical to those calculated for the respective singlet CS

Table 7.1 Selected Data for the Ground and CS States of 4 - 7 and 7' Obtained from Geometry Optimizations at the (U)HF/3-21G Level

system	state	R_c[a] (Å)	R_e[b] (Å)	θ[c] (deg)	μ (D)	charge DMN	charge DCV	charge imide[d]
4	^{1}A′ ground	10.90	11.43		6.01	0.061	−0.191	−0.377
	^{1}A″ CS	6.50	9.56	38.9	12.84	0.830	−0.726	−0.340
5	^{1}A′ ground	10.78	11.38		5.59	0.059	−0.192	−0.358
	^{1}A″ CS	6.59	9.33	33.4	14.81	0.845	−0.718	−0.324
6	^{1}A′ ground	10.70	11.33		5.25	0.058	−0.192	−0.353
	^{1}A″ CS	9.03	11.02	36.5	30.81	0.906	−0.749	−0.382
7	^{1}A′ ground	10.97	11.45		5.75	0.069	−0.187	−0.394
	^{1}A″ CS	8.75	10.86	34.4	28.64	0.893	−0.751	−0.378
7′	^{1}A″ CS				30.53	0.904	−0.768	−0.381

[a] The center-to-center separation between the chromophores (see Fig. 7.1).
[b] The bridge edge-to-edge separation (see Fig. 7.1).
[c] The degree of pyramidalization of the DCV group (see Fig. 7.1).
[d] The charge on the *R* group is also included in the total charge on the imide group.

states. This finding is not unexpected, given that charge separation is practically complete in the CS states of these giant bichromophoric systems and that the two radical ion chromophores are only *weakly coupled*, *i.e.* the CS states may be regarded as two isolated radical ions interacting almost exclusively by coulombic attraction. Consequently, both singlet and triplet wavefunctions are expected to have nearly the same spatial distribution. This explains why - notwithstanding severe spin contamination, amounting to 50:50 singlet-triplet mixing - the UHF relaxed singlet CS state geometries and dipole moments should be of acceptable quality. Lastly, the geometry for **7** was optimized at the CIS/3-21G level and compared to that obtained at the UHF level. The geometry and dipole moments of the CS singlet state are nearly the same in the two calculations. The CIS dipole moment is 28.56D, compared to 28.64 D (reported in Table 7.1). The only noticeable geometric difference is in the pyramidalisation angle (9 in Table 7.1) about the DCV group; at the UHF level it is 34.4 degrees whereas at the CIS/3-21G level it is 28.2 degrees. This discrepancy is quite small and does not impact the conclusions.

7.3 Evaluation of Through-Bond Mediated Electron Transfer

Given the U-shaped architecture of molecules **1** and **2**, the intervening pendant group should mediate electron transfer between the donor and acceptor chromophores in preference to the two chromophores coupling via the orbitals of the connecting bridge in a *through-bond,* or superexchange, mechanism. The through-bond mechanism has been extensively studied in similar systems.[21] The importance of the through-bond coupling mechanism, which may be in operation in **1** and **2,** to the overall electronic coupling was assessed by comparing the electron transfer rate of **1** and **2** with that of a reference system, **8**. System **8** possesses a bridge with the same number of bonds linking the donor and

acceptor chromophores as in molecules **1** and **2**, however, it does not possess the U-shaped architecture, so that the most direct coupling of the donor and acceptor is via the bonds of the bridge and not through any solvent molecules. The electron transfer rate of **8** in toluene was found to be less than 2 x 10^8 s^{-1} at 293 K and 333 K. In contrast, the electron transfer rate of **1** in toluene was found to be 29 x 10^8 s^{-1} at 327 K, and the electron transfer rate of **2** in toluene was found to be 16 x 10^8 s^{-1} at 327 K. A comprehensive set of electron transfer rate constant data for **1** and **2** as a function of temperature is provided in the supplementary material. These data show that in the case of **1** and **2** the through-bond coupling mechanism is only weakly present, having only a minor influence upon the overall coupling.

7.4 Determination of λ_i and $h\nu$

Charge transfer absorption and emission band shape analysis provides an effective means of determining the internal reorganization energy associated with the electron donor and acceptor groups. For an electron transfer reaction that is coupled to a single, effective, high frequency vibrational mode, the emission band shape $L(\Delta E)$ is given by

$$L(\Delta E) = \exp(-S)\sum_{n=0}^{\infty}\frac{S^n}{n!}\exp\left[-\frac{(\Delta_r G + \Delta E + nh\nu + \lambda_o)^2}{4\lambda_o k_B T}\right] \quad (7.2)$$

where ΔE is the photon energy. In practice, the fitting treats $\Delta_r G$, $h\nu$, λ_i and λ_o as adjustable parameters and often gives several parameter sets that provide adequate fits.

By combining this analysis with quantum chemical calculations a suitable range of parameter values can be established. [10]

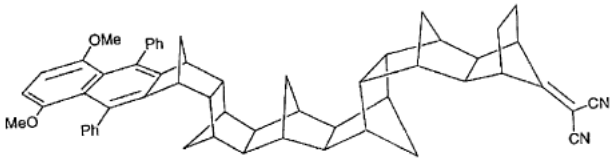

8

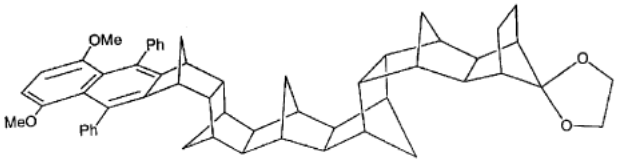

8noA

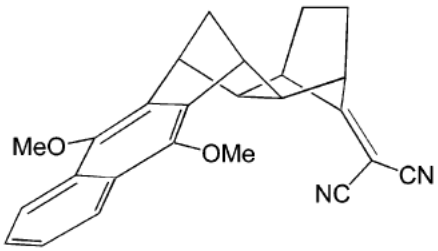

9

Chart 7.3

7.4.1 Charge Transfer Spectra

In the present work, the internal reorganization energy is determined using the charge transfer absorption and emission spectra for a related compound, **9**, in hexane[21d,22]. Although **9** has a different bridge structure than **1** and **2**, it has the same donor and acceptor groups and can reliably be used to quantify the internal reorganization parameters, since they are primarily associated with the geometry changes of the donor and acceptor upon electron transfer. The Stokes shift, *B*, is related to the total reorganization energy through

$$B = 2(\lambda_o + \lambda_i) \tag{7.3}$$

and the Stokes shift for **9** in hexane is 1.26 eV. Assuming that λ_o in this solvent is zero, a value of 0.63 eV is obtained for λ_i. The frequency of the effective quantum mode can be

determined from the charge-transfer emission bandwidth, $\Delta E_{1/2}$. When the mode frequency $h\nu >> k_BT$, the emission bandwidth can be written as,

$$(\Delta E_{1/2})^2 \cong 8(\ln 2)(2k_B T\lambda_o + \lambda_i h\langle \upsilon \rangle) \quad (7.4)$$

Assuming that the outer sphere reorganization energy is zero in hexane, one finds an average intramolecular mode frequency, $h<\nu>$, of 1100 cm^{-1} from the emission spectrum shown in Ref. 21 d.

7.4.2 Theoretical Calculations

Quantum chemical calculations indicate that electron transfer can result in dramatic geometrical changes between the ground and charge separated (CS) states for these U-shaped molecules, particularly in non-polar solvents.[18,19] The two major structural features present in the CS state geometries, compared to those calculated for the ground states, is the pyramidalization of the DCV radical anion group at C7 and the degree of distortion in the DMN radical cation group, as shown in Figure 7.1. Some distortion of the connecting bridge also occurs. While the pyramidalization is inherent in the DCV radical anion species[18,19], the direction of this pyramidalization and the general distortion of both the DMN group and the bridge arise from the strong Coulomb attraction between the two oppositely charged ends of the molecule. For example, the center-to-center chromophore separation, R_c, contracts, on average, by 3.6 Å, while the bridge's edge-to-edge separation, R_e, contracts by about 1.5 Å (Fig. 7.1 and Table 7.1). Unlike the ground state structures, the R_c and R_e values found for the CS state geometries of **4** - **7** depend upon the nature of the imide substituent group, R. For R_c, the range of values for the CS state geometries is 2.53 Å, whereas for the ground states it is only 0.21 Å. For R_e, the ranges are 1.69 Å in

the CS states and 0.11 Å in the ground state. Especially noticeable is the difference in the R_c distances between the molecules with small pendant groups **4** (6.50 Å) and **5** (6.59 Å) as compared to the molecules with more bulky pendant groups, **6** (9.03 Å) and **7** (8.75 Å). This difference arises from the size of the *n*-propyl and phenyl groups, which are fully interposed between the DMN and the DCV groups in **6** and **7**, respectively. The steric bulk of these groups forces the oppositely charged DMN^+ and DCV^- chromophores in the CS state to remain further apart despite the strong Coulomb attraction. In contrast, the H and methyl groups are small enough to allow significant distortion of the DMN and DCV chromophores to occur. Consequently, the charge-transfer state dipole moment that was calculated for molecule **7** was used in the calculations of the outer-sphere reorganization energy and Gibbs free energy of reaction, which are presented below.

We emphasize that all optimized geometries refer to gas phase structures. Consequently, the relaxed gas phase geometries of the CS states will be more distorted than those in solvent because the electrostatic interactions will be attenuated in solvent. Unfortunately, all attempts so far to calculate relaxed geometries by including solvent effects (using solvation continuum models) have failed, owing to lack of convergence in the SCF part of the calculation. Nevertheless, we did manage to calculate the relaxed geometry for the radical anion of 7- dicyanovinylnorbornane, **10**, in a solvent continuum having a dielectric of 37.5, equivalent to acetonitrile. As with the gas phase structure, **10** displayed a marked pyramidalization about the DCV group. We therefore believe that our relaxed gas phase geometries of CS states reveal structural features that are retained, perhaps to an attenuated degree, in solvents.

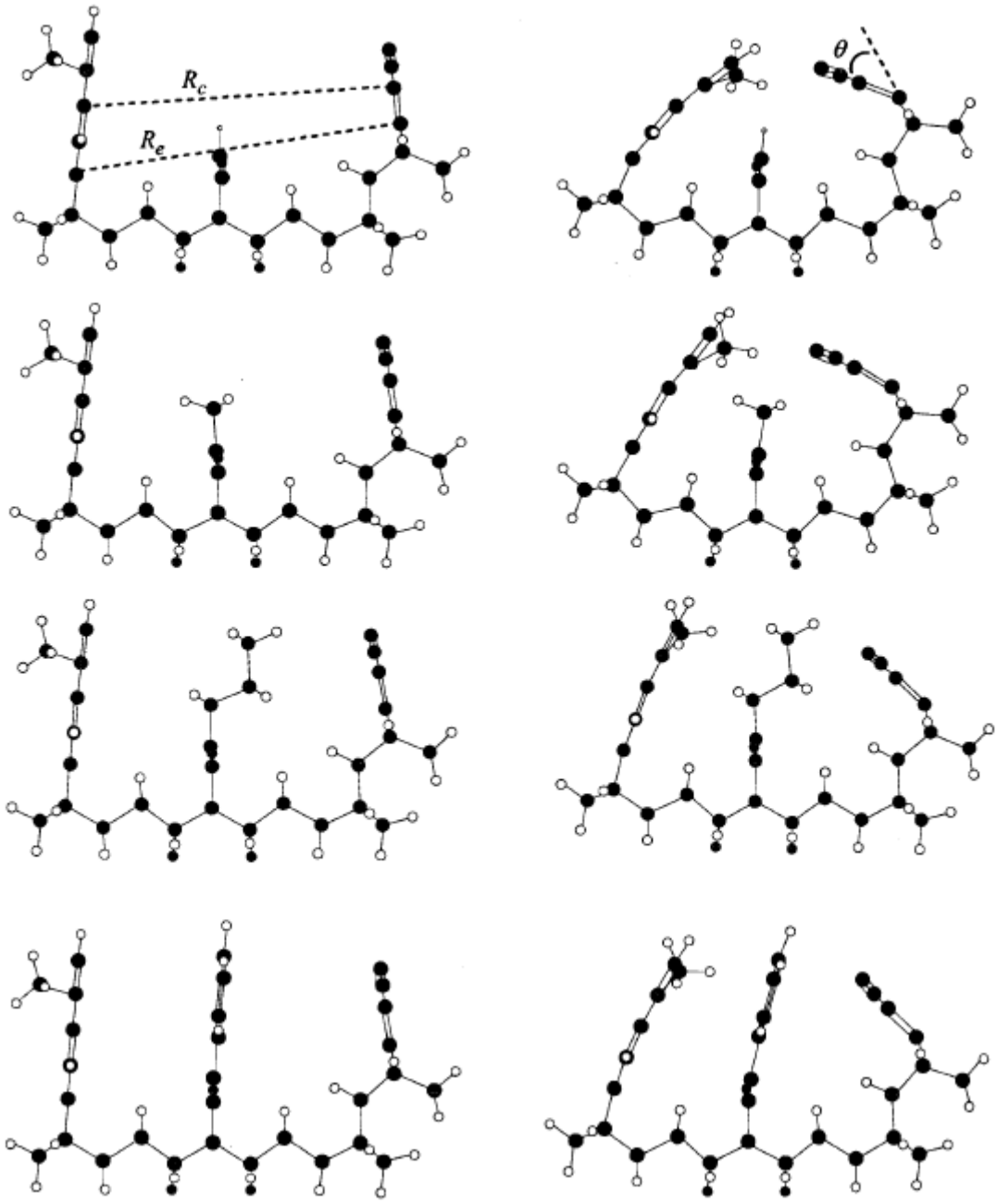

Figure 7.1 Profiles of the ground (left) and CS (right) optimized geometries for the systems 4 (top) - 7 (bottom) obtained at the (U)HF/3-21G level.

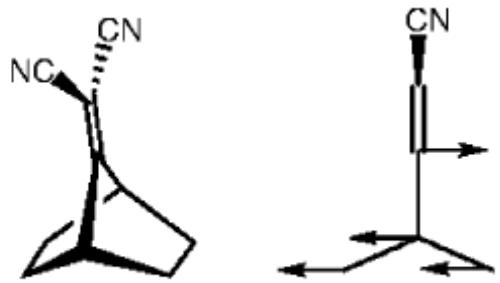

10 10a

Chart 7.4

Two vibrational modes appear to be coupled to the electron transfer in our systems. First, the formation of the anion involves a pyramidalization of the DCV acceptor group and an out-of-plane bending mode (see Chart 7.4). The frequency associated with out-of-plane bending of the DCV group, schematically depicted by 10a, is 1088 cm^{-1}.[23]

Second, the naphthalene ring undergoes a ring deformation upon formation of the cation that primarily involves stretching modes at ~ 1600 cm^{-1}. These frequencies bracket the 1100 cm^{-1} effective mode frequency found from the analysis of the charge transfer spectra. Both results are consistent with the large internal reorganization energy observed in these systems. With no information at this time as to the degree of partitioning of the internal reorganization energy with respect to the high-frequency modes, the analysis is largely limited to the case of a single high- frequency mode of 1600 cm^{-1}. This choice is consistent with prior attempts at analysis using the semi-classical equation in related systems with dicyanoethylene acceptors.[10a] The effect of independently partitioning the inner-sphere reorganization energy between two modes, taken to be 990 cm^{-1} and 1600 cm^{-1}, was

explored to examine its impact on the ratio of the electronic coupling matrix element for **1** and **2**. Calculations of the actual partitioning of the inner-sphere reorganization energy are underway and will be published later. Lastly, no matter what partitioning was used, the electronic coupling was always larger for **1** than **2**.

7.5 Determination of $\Delta_r G$

$\Delta_r G$ can be determined from experimental fluorescence lifetime data, provided the locally excited (LE) and charge separated (CS) states lie close in energy, so that an excited state equilibrium occurs.[10b,24,25] The analysis assumes that the absorption and emission of radiation arises from the LE state of the donor and allows the rate constants k_{for} (LE to CS) and k_{back} (CS to LE) to be determined. Their ratio is used to compute $\Delta_r G$. This behavior was observed for **1** in both toluene and mesitylene. In toluene and mesitylene the reaction free energy for **1** changes systematically with temperature from –0.12 eV and –0.05 eV (see Fig 7.2). At higher temperatures the same effect was observed for **2** in mesitylene. In toluene the fluorescence lifetime decay was clearly dominated by the short time component (*ca.* 99% or greater at all the temperatures) so that it was not possible to accurately determine the reaction free energy for this solvent. In the more polar solvents, THF, CH_2Cl_2, and CH_3CN, the CS state is sufficiently stabilized so that the back electron transfer is not observed.[13]

The measured $\Delta_r G$ values for **1** (in mesitylene and toluene) and **2** (in mesitylene only) were used to calibrate a molecular-based solvation model. The model was then used to predict the temperature dependence of λ_o and the reaction free energy in more polar solvents. The model treats the solute and solvent molecules as polarizable hard spheres

and accounts for dipole-dipole, dipole-quadrupole, induction, and dispersion interactions. $\Delta_r G$ is calculated as the sum of four components

$$\Delta_r G = \Delta_{vac} G + \Delta_{dq,i} G^{(1)} + \Delta_{disp} G + \Delta_i G^{(2)} \quad (7.5)$$

where $\Delta_{vac}G$ is the free energy of the process in vacuum, $\Delta_{dq,i}G^{(1)}$ is the contribution from first-order dipole, quadrupole, and induction interactions, $\Delta_{disp}G$ is the contribution from dispersion interactions and $\Delta_i G^{(2)}$ represents contributions from second-order induction interactions. Details about this model and its implementation are provided in Appendix A and elsewhere.[14]

Use of this model requires parameters for both the solute and the solvent. The toluene and mesitylene solvent parameters are the same as those described in earlier work[14]. The solute ground and excited state dipole moments were set equal to those calculated at the UHF/3-21G level for **7** (Table 7.1), namely 5.75 D for the ground state and 28.64D for the CS state. The polarizability was calculated to be ~ 128 Å^3 for **1** and 124 Å^3 for **2.**[26] Table 7.2 summarizes the other solute parameters. Calibration of the molecular model requires determination of the parameters $\Delta_{vac}G$, the solute radius R_o, and $\Delta\gamma'$ The temperature dependent $\Delta_r G$ values in toluene and mesitylene, measured for **1** and **2** (mesitylene only), were simultaneously fit to eq 7.5 by adjusting these three parameters.

The fit of the model to the experimental $\Delta_r G$ for **1** in toluene, **1** and **2** in mesitylene, and the predicted $\Delta_r G$ values for **2** in toluene are shown in Figure 7.2. Given the similarity between molecules **1** and **2**, the parameter set was taken to be the same for both solutes with the exception of $\Delta_{vac}G$. The $\Delta_{vac}G$ value was chosen independently for the two solutes, so that the $\Delta_r G$ value in **2** was more negative than in **1**, an observation

Table 7.2 Parameters used in the molecular solvation model.

Solute Radius (Å)	7.77
$\Delta_{vac}G$ (eV) for **1**	0.159
$\Delta_{vac}G$ (eV) for **2**	0.114
$\Delta\gamma'$ (Å^3)	6.2
m_{ex} (D)	28.64
m_{gs} (D)	5.75
Toluene polarizability (Å^3)	12.32
Mesitylene polarizability (Å^3)	16.14

consistent with the experimental data. The difference in $\Delta_{vac}G$ for **1** and **2** can be rationalized as the difference in the Coulomb stabilization energies for **1** and **2** in vacuum.

Using effective dielectric constants for benzene and hexane in the Coulomb's law expression, the Coulomb stabilization energy for **2** is estimated to be 0.066 eV lower than that for **1**.[27] The resulting $\Delta_r G$ values are in qualitative agreement with the experimental data. The difference in the value of $\Delta_{vac}G$ for solutes **1** and **2** was also estimated by treating $\Delta_{vac}G$ as an adjustable parameter, which was constrained by fitting the experimental Gibbs free energy data from predictions derived using the molecular solvation model. The best fit difference of 0.045 eV is quite close to the observed difference and that which is estimated. The table in Appendix A gives the predicted $\Delta_r G$ values and lists the contributions from the different terms in eq. 7.5.

With a parameterization of the internal reorganization energy parameters (λ_i and ν) and the reaction free energy ($\Delta_r G$) in hand, it is possible to fit the temperature dependent rate data to the form of eq 7.1 and obtain values for the electronic coupling parameter |V| and the solvent reorganization energy λ_o. This analysis would be straightforward if |V| and λ_o were known to be temperature independent. Although |V| is likely to satisfy this approximation, the solvent reorganization energy is expected to be temperature dependent since the solvation of the solute by the solvent is temperature dependent. For this reason the molecular model that is parameterized to the reaction free energy data is used to treat the temperature dependence of the solvent reorganization energy. The temperature dependent rate constant data can then be used to extract the best fit parameters for the electronic coupling parameter |V| and the solvent reorganization energy at 295K, λ_o(295 K).

7.6 Determination of λ_o

The outer sphere reorganization energy is also calculated using this molecular solvation model. The reorganization energy is written as a sum of three components

$$\lambda_o = \lambda_p + \lambda_{ind} + \lambda_{disp} \qquad (7.6)$$

where λ_p accounts for solvent reorganization arising from the solvent dipole and quadrupole moments, λ_{ind} is the contribution from induction forces, and λ_{disp} accounts for the dispersion interactions. The model treats the solute as a dipolar, polarizable sphere and finds the reorganization energy; see the Appendix and earlier work[14,15] for further details. The appendix also provides the values of the reaction free energy and the reorganization energy

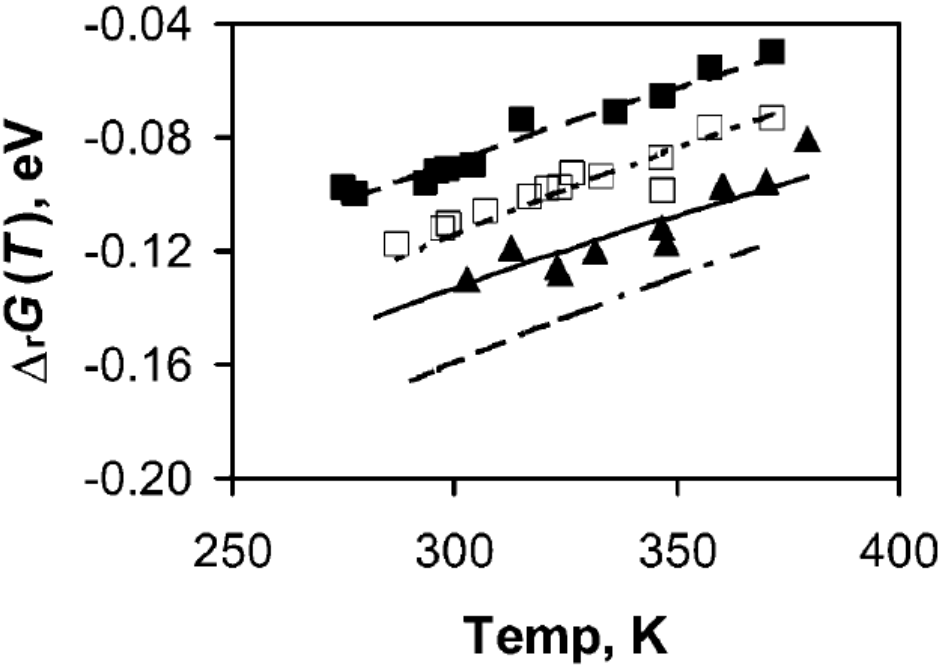

Figure 7.2 The experimental $\Delta_r G$ values are plotted for 1 in toluene (open square) and mesitylene (filled square). The experimental values for 2 in mesitylene are shown as filled triangles. The lines show the $\Delta_r G$ values predicted for all four aromatic systems by the molecular model with the parameters given in Table 7.2. The experimental values for 2 in toluene could not reliably be determined from the fluorescence lifetime data. The $\Delta_r G$ values predicted by the model for 2 in toluene are indicated by the bottom dot-dashed line. See text for details.

that are predicted by the model. It is well appreciated that continuum calculations are unreliable in non- polar solvents. More importantly, the continuum theory fails to predict the temperature dependence of λ_o, *i.e.,* the sign of $d\lambda_o/dT$, even in polar systems, whereas the molecular model predicts the correct temperature dependence.[10a] The continuum model incorporates only the temperature dependence of molecular rotation, whereas the molecular model includes both translational and rotational degrees of freedom so that the temperature dependence of the reorganization energy is more faithfully reproduced. For these reasons the molecular model is used to calculate $d\lambda_o/dT$

and an adjustable offset is used to fit the experimental data. The best fit λ_o(295 K) values are reported in Tables 7.3 and 7.4.

7.7 Determination of the Electronic Coupling, $|V|$

Using the values obtained for λ_i, ν, $\Delta_r G$, and $d\lambda_o/dT$, it is possible to fit the temperature dependent rate data to eq 7.1 and obtain electronic coupling $|V|$ and λ_o(295 K) values. For these systems, λ_i was taken to be 0.63 eV and v was taken to be 1600 cm^{-1}. The fitting was performed using $\Delta_r G(T)$ and $d\lambda_o/dT$ values predicted by the molecular model. Figures 7.3 and 7.4 show fits of the model to the rate data for **1** and **2** in toluene and mesitylene as well as three more polar solvents, namely CH_2Cl_2, THF, and acetonitrile. The rate data for **1** and **2** in the latter three solvents were reported earlier[13], but until now a quantitative analysis of the data has not been reported. The rate data were fit to eq 7.1 by adjusting λ_o(295 K) in each solute-solvent system and adjusting the electronic coupling of the solute. Clearly the fit quality is excellent. The values obtained for |V| and λ_o are reported in Tables 7.3 and 7.4. The electronic coupling is not dependent on the solvent and the value obtained for **1** is almost four times larger than the value obtained for **2,** namely 168 cm^{-1} *versus* 46 cm^{-1}.

Table 7.3 Best Fit |V| and λ_o(295 K) values for the aromatic systems.

System	$\|V\|$, cm^{-1}	λ_o(295 K) in toluene, eV	λ_o(295 K) in mesitylene, eV
1	168	0.73	0.69
2	46	0.59	0.56

Table 7.4 Free energy and reorganization energies for 1 and 2 in the more polar solvents.

Solvent	$\Delta_r G$ [a] (295 K), eV		λ_o(295 K), eV	
	1	**2**	**1**	**2**
THF	-0.37	-0.42	1.13	1.09
CH_2Cl_2	-0.37	-0.42	1.20	1.16
CH_3CN	-0.52	-0.57	1.50	1.50

a The reaction free energy was calculated using the molecular model for solvation. Details may be found in the text and in the appendix.

From eq 7.1, a three to fourfold increase in the electronic coupling should give rise to a nine to sixteen fold increase in the rate constants. However the magnitude of the *FCWDS* term, arising from the differing $\Delta_r G(T)$ data, also changes for **1** and **2** and this change partially counteracts the effect from the change in |V|. The best fit λ_o values, evaluated at 295 K, are also reported. From simple continuum arguments, the solvent reorganization energy is expected to be larger for the solvent with the more dipolar character, and this expectation is verified for both **1** and **2** (see Tables 7.3 and 7.4). In addition the reorganization energy for **1** is found to be a bit higher than that for **2** in most of the solvents, which may indicate a small difference in the effective molecular volume or dipole moment between the molecules. The dependence of the electronic coupling ratio (|*V*(**1**)| / |*V*(**2**)| on the value of the solvent reorganization energy was analyzed in a systematic manner and the electronic coupling of **1** was found to be larger than that of **2** for all reasonable reorganization energies. Details of this analysis are provided in the supplemental information, which contains contour plots of |*V*(**1**)| / |*V*(**2**)|

and χ^2 as a function of λ_o, and plots like that shown in Figure 7.3 under different fitting constraints.

Within the context of a two-state model, the electronic coupling matrix element $|V|$ may be taken to be one half of the energy gap at the avoided crossing of the two adiabatic electronic states, in this case being the locally excited and the CS states, (*i.e.*, $\Delta E = 2V$) as shown in Figure 7.5. To determine if the electronic coupling between the DMN

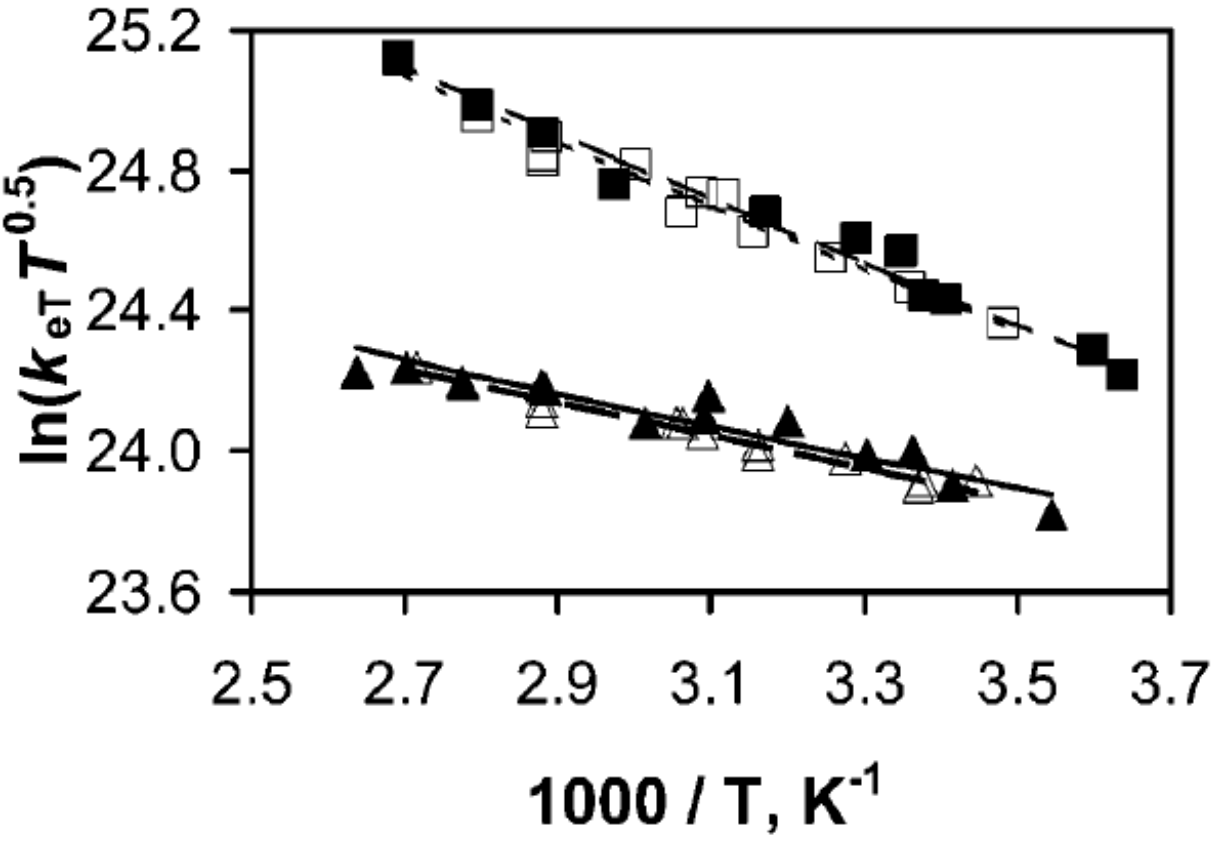

Figure 7.3 Experimental rate data (k_{for}) are plotted versus $1/T$, for 1 in toluene (open square), 1 in mesitylene (filled square), 2 in toluene (open triangle), and 2 in mesitylene (closed triangle). The lines represent the best fits to eq 7.1; see text for details.

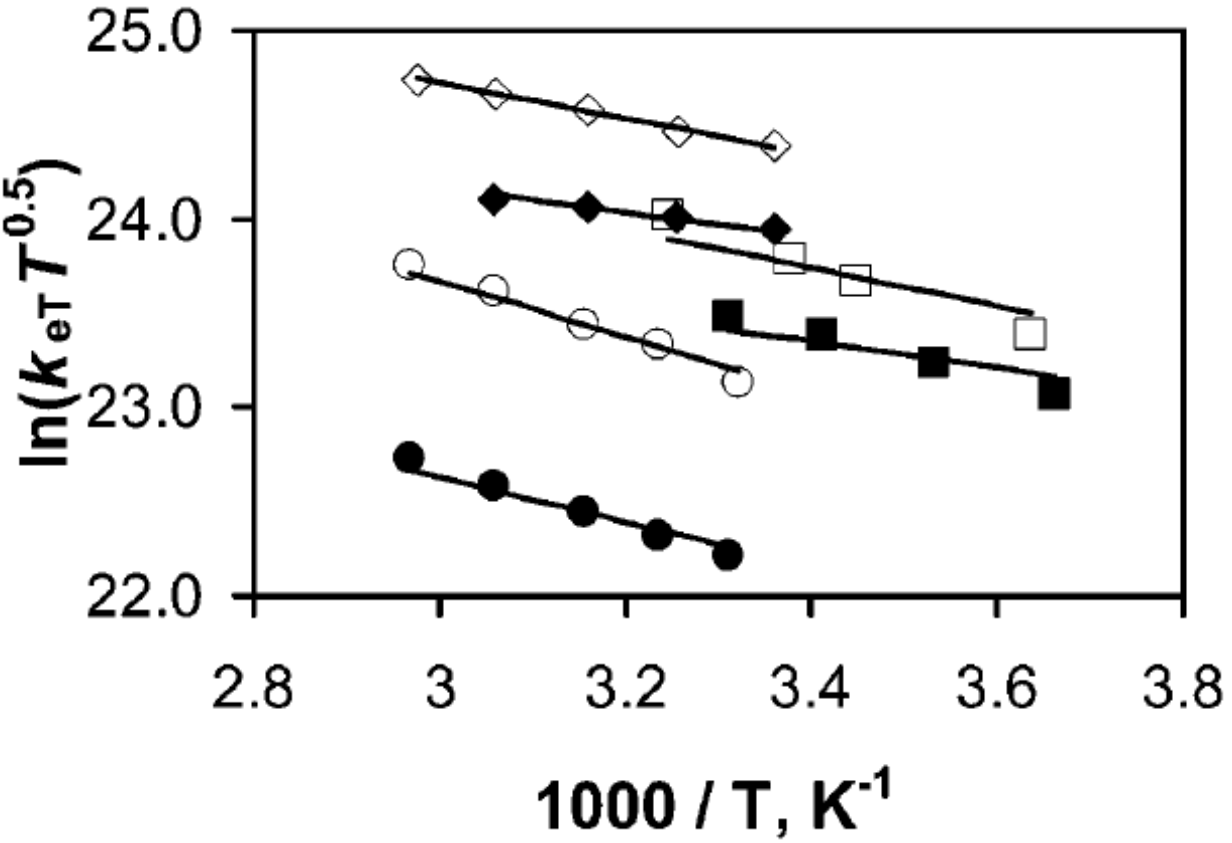

Figure 7.4 Experimental rate data (k_{for}) are plotted versus 1/*T*, for 1 in CH3CN (open circle), CH2Cl2 (open square) and THF (open diamond) and 2 in CH3CN (filled circle), CH2Cl2 (filled square), and THF (filled diamond). The lines represent the best fits to eq 7.1; see text for details.

and DCV groups is in fact mediated by the substituent on the central imide group, or whether the coupling proceeds mainly via a through-bond mechanism,[28] D*E* was calculated for model systems based on the N-phenyl system, **7**, using the CIS method. Given the size of these systems two approximations were made in order to make the analysis computationally feasible. First, the model system **7'** was created, which, while possessing the same geometry as the CS state of the N-phenyl imide, **7**, has a hydrogen atom in place of the phenyl group (with an N-H bond length of 1.01 A).[29] Second, it was assumed that the reaction coordinate for the electron transfer in **7** (and **7'**) is the DCV pyramidalization angle, θ, and that all other geometrical parameters are frozen. This assumption was deemed reasonable because exploratory calculations on **7** revealed that the electron transfer process is very sensitive to the magnitude of θ but not other geometrical features. Thus, for both **7** and **7**$^{\Phi}$, a series of CIS/3-21G single point energy calculations were carried out in which θ was varied until the energy gap between the locally excited state and the CS state reached a minimum value which was then equated to twice the value of the electronic coupling, |*V*|.

In the case of **7**, the avoided crossing is encountered when the DCV is only slightly pyramidalized, with θ = 12°. The electronic coupling, |*V*|, at this point is 16 cm^{-1}. In the case of **7'** the avoided crossing occurs at a slightly larger pyramidalization angle of θ = 17.5°, with |*V*| equal to 5 cm^{-1}. Thus, |*V*| for **7'** is significantly smaller, by a factor of three, than that calculated for **7**. While the predicted magnitude of |*V*| for **7** is substantially smaller than that estimated for **1**, from experimental data, the calculations correctly predict a three to fourfold enhancement of the electronic coupling that arises

from the presence of the aromatic ring in the molecular cavity of **7,** compared to **7'**. The enhancement in the magnitude of |*V*| is, no doubt, caused by a superexchange mechanism. These computational results indicate that the central R group is important

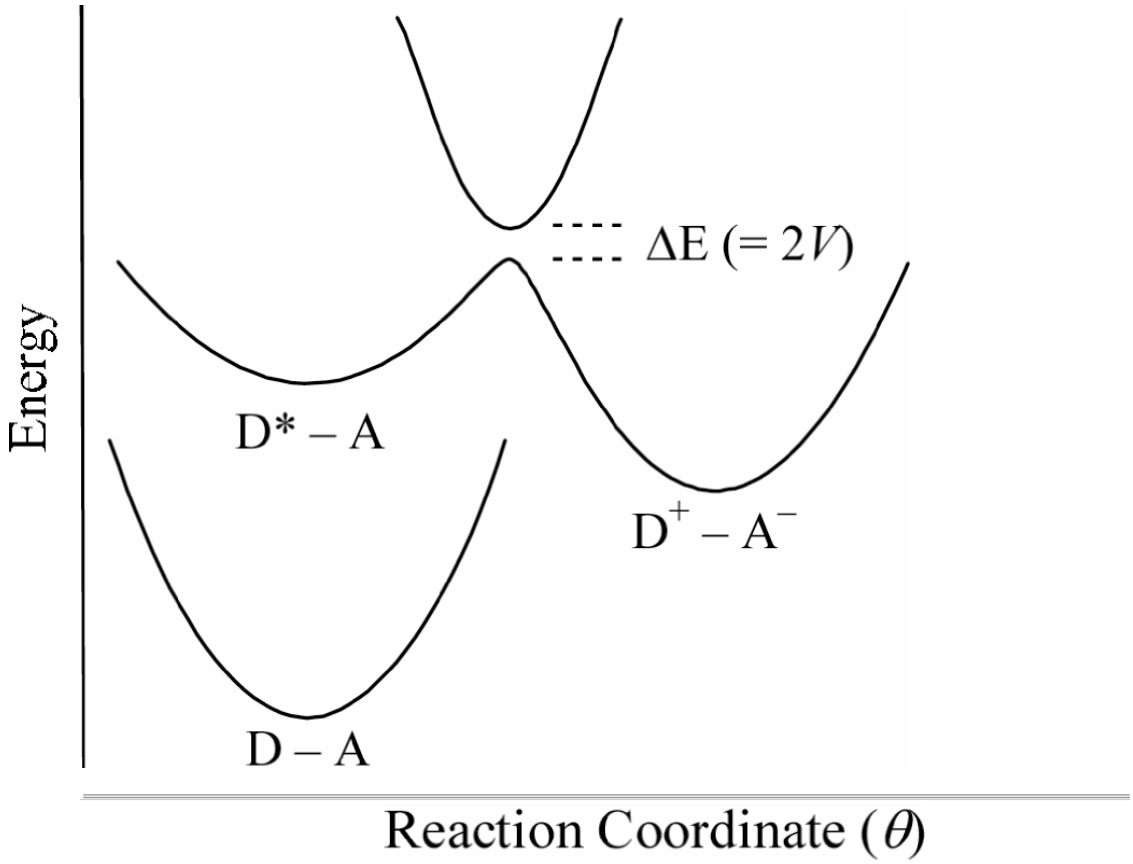

Figure 7.5 A schematic of the potential energy surface for photo-induced electron transfer is shown here. D-A is the ground state surface; D*-A is the locally excited state surface; and D^+-Ais the CS state surface. At the avoided crossing, the energy gap between the locally excited and CS states, ΔE, is twice the electronic coupling matrix element for electron transfer, |*V*|.

in mediating the coupling between the DMN and the DCV groups and that a U-shaped system provides a controlled way to analyze effects that different solvents may have upon inter- and intra-molecular electron transfer processes.

The magnitude of the electronic coupling that is extracted from experimental data depends strongly on the value of other parameters in eq 7.1, in particular the reorganization energies, the effective frequency and the free energy. The analysis in mesitylene and toluene uses the experimental free energy and adjusts the outer sphere reorganization energy along with the electronic coupling to fit the rate data. The impact of the modeling for the inner sphere reorganization energy with a single effective quantum mode was assessed by considering a two- mode model (*vide supra*). The use of a two mode model generated results that are consistent with that found from the single mode model; *i.e.,* the electronic coupling in **1** is significantly larger than that in **2**. Figure 7.6 shows how the ratio of electronic coupling magnitudes changes when the partitioning of the internal reorganization energy between the 1600 cm^{-1} mode and the 990 cm^{-1} mode is changed for each of the species **1** and **2**. This analysis shows that the ratio can change over the range of 2.5 to 5, depending on the details of the mode partitioning, but that the electronic coupling in **1** is always larger than that in **2**. In addition, when the partitioning of internal reorganization energy between the vibrational modes is similar in the two compounds (represented by the diagonal in the horizontal plane of the graph that goes from the origin of (0%,0% - a 900 cm^{-1} quantum mode in each compound) to the point at (100%,100% - a 1600 cm^{-1} quantum mode in each compound)), the ratio does not change dramatically. To the extent that the donor and acceptor groups rather than the pendant moiety controls the partitioning, this observation suggests that the ratio of ca.3.5 for the electronic coupling magnitudes is robust with respect to the modeling for the internal reorganization energy.

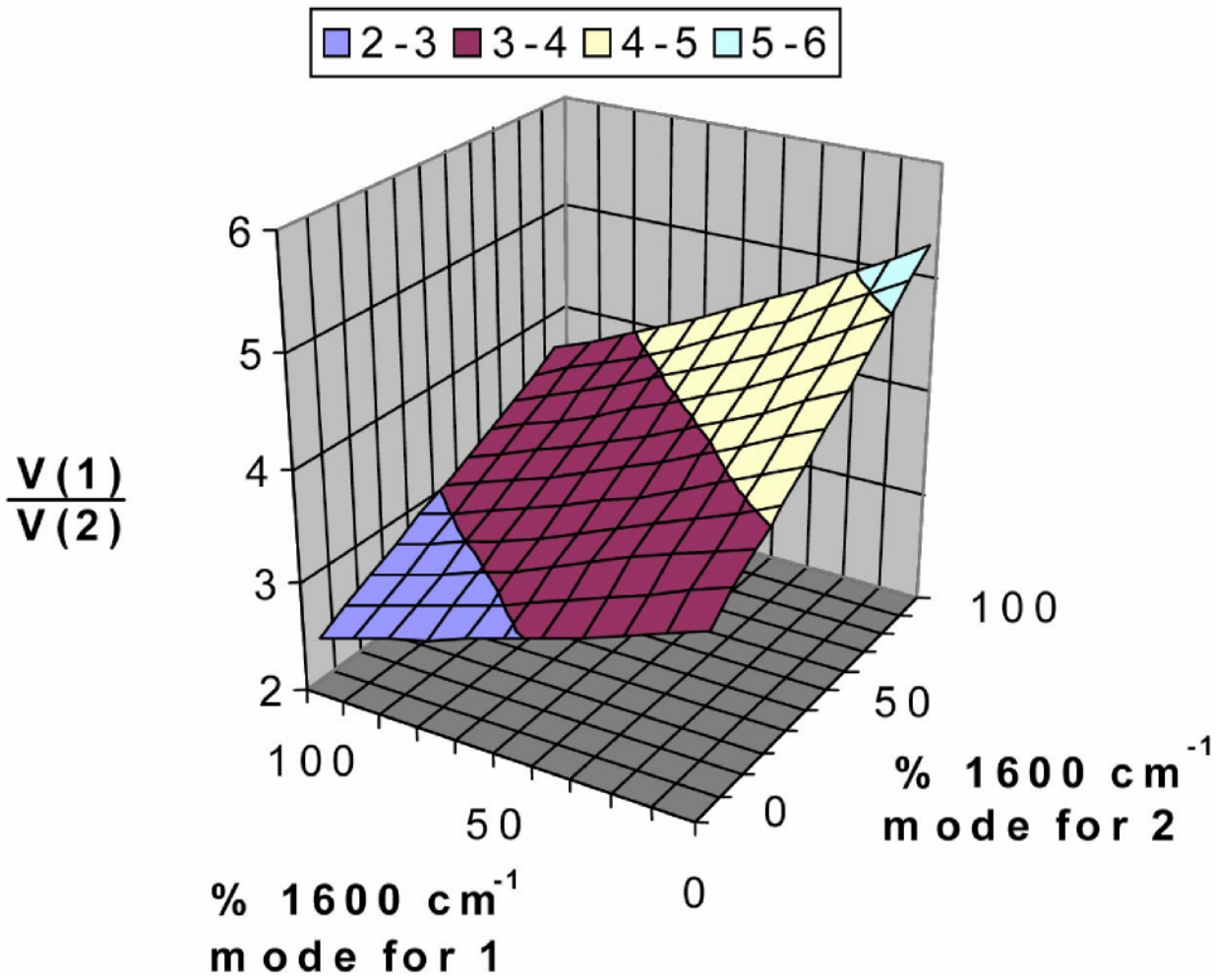

Figure 7.6 The internal reorganization energy is systematically partitioned between a 1600 cm^{-1} and a 990 cm^{-1} mode. The three-dimensional plot demonstrates the ratio of $|V|$ that is obtained between 1 and 2 for a given percentage of 1600 cm^{-1} mode. The lower frequency mode corresponds to a pyramidalization of the cyanoethylene acceptor group, whereas the higher frequency mode corresponds to a skeletal breathing mode of the naphthalene donor.

7.8 Conclusions

This work presents electron transfer rate data and computational results that demonstrate efficient electron tunneling through a pendant moiety located in the *line-of-sight* between electron donor and acceptor groups. The electron transfer rates for compounds **1** and **2** were compared with the control molecule **8** to demonstrate that the electron transfer proceeds through the pendant moiety, rather than the covalent bridge. The experimentally determined reaction free energy for **1** in toluene and mesitylene and **2** in mesitylene were used to calibrate a molecular based model for solvation. This model and charge transfer spectra were used to define the reorganization energy and free energy parameters for electron transfer of **1** and **2** in the five solvents studied. By combining the knowledge of these parameters with the temperature dependent rate data, it was possible to experimentally determine the electronic coupling for these two compounds in the solvents. Compound **1** was found to have an electronic coupling that is four times larger than that of compound **2**. The dependence of the empirically derived electronic coupling values on the reorganization energy parameters was evaluated in detail (see Discussion and Supplemental Information). Also, the electronic couplings for the compounds were found to be independent of the solvent. The difference in electronic coupling values reflects the more efficient tunneling through the aromatic moiety of **1** than the alkyl moiety of **2**. The absolute values of the experimentally derived electronic coupling values obtained for **1** and **2** were shown to be larger than those calculated by *ab initio* molecular orbital theory for analogues of **1** and **2**, but both agree that an aromatic group is better than a propyl group in mediating the electron transfer process.

Table 7.5 Individual Contributions to $\Delta_r G$ and λ_o for 1. All Values Listed in eV.

T (K)	$\Delta_{elp}G^{(1)}$	$\Delta_rG^{(2)}$	$\Delta_{disp}G$	Δ_rG	λ_p	λ_{ind}	λ_{disp}	λ_o
				Toluene				
287.15	-2.41×10^{-01}	-1.16×10^{-02}	-2.91×10^{-02}	-1.23×10^{-01}	5.60×10^{-02}	1.07×10^{-02}	4.75×10^{-04}	6.72×10^{-02}
297.55	-2.35×10^{-01}	-1.07×10^{-02}	-2.86×10^{-02}	-1.16×10^{-01}	5.37×10^{-02}	9.91×10^{-03}	4.48×10^{-04}	6.40×10^{-02}
298.75	-2.35×10^{-01}	-1.07×10^{-02}	-2.86×10^{-02}	-1.15×10^{-01}	5.34×10^{-02}	9.83×10^{-03}	4.45×10^{-04}	6.37×10^{-02}
307.15	-2.30×10^{-01}	-1.00×10^{-02}	-2.82×10^{-02}	-1.09×10^{-01}	5.16×10^{-02}	9.27×10^{-03}	4.25×10^{-04}	6.13×10^{-02}
316.95	-2.25×10^{-01}	-9.40×10^{-03}	-2.78×10^{-02}	-1.03×10^{-01}	4.96×10^{-02}	8.67×10^{-03}	4.03×10^{-04}	5.86×10^{-02}
320.85	-2.23×10^{-01}	-9.15×10^{-03}	-2.76×10^{-02}	-1.01×10^{-01}	4.88×10^{-02}	8.44×10^{-03}	3.95×10^{-04}	5.76×10^{-02}
323.85	-2.21×10^{-01}	-8.97×10^{-03}	-2.74×10^{-02}	-9.88×10^{-02}	4.82×10^{-02}	8.27×10^{-03}	3.88×10^{-04}	5.69×10^{-02}
326.65	-2.20×10^{-01}	-8.80×10^{-03}	-2.73×10^{-02}	-9.71×10^{-02}	4.77×10^{-02}	8.12×10^{-03}	3.83×10^{-04}	5.62×10^{-02}
333.15	-2.17×10^{-01}	-8.42×10^{-03}	-2.70×10^{-02}	-9.32×10^{-02}	4.64×10^{-02}	7.77×10^{-03}	3.70×10^{-04}	5.46×10^{-02}
346.55	-2.10×10^{-01}	-7.70×10^{-03}	-2.65×10^{-02}	-8.55×10^{-02}	4.40×10^{-02}	7.11×10^{-03}	3.45×10^{-04}	5.15×10^{-02}
346.95	-2.10×10^{-01}	-7.68×10^{-03}	-2.64×10^{-02}	-8.53×10^{-02}	4.39×10^{-02}	7.09×10^{-03}	3.44×10^{-04}	5.14×10^{-02}
347.05	-2.10×10^{-01}	-7.68×10^{-03}	-2.64×10^{-02}	-8.52×10^{-02}	4.39×10^{-02}	7.08×10^{-03}	3.44×10^{-04}	5.14×10^{-02}
357.75	-2.05×10^{-01}	-7.16×10^{-03}	-2.60×10^{-02}	-7.93×10^{-02}	4.21×10^{-02}	6.60×10^{-03}	3.26×10^{-04}	4.90×10^{-02}
371.45	-1.99×10^{-01}	-6.54×10^{-03}	-2.54×10^{-02}	-7.20×10^{-02}	3.99×10^{-02}	6.04×10^{-03}	3.05×10^{-04}	4.62×10^{-02}
371.55	-1.99×10^{-01}	-6.54×10^{-03}	-2.54×10^{-02}	-7.19×10^{-02}	3.99×10^{-02}	6.03×10^{-03}	3.04×10^{-04}	4.62×10^{-02}
				Mesitylene				
274.95	-2.07×10^{-01}	-1.40×10^{-02}	-4.09×10^{-02}	-1.03×10^{-01}	3.35×10^{-02}	1.29×10^{-02}	1.16×10^{-03}	4.75×10^{-02}
277.85	-2.06×10^{-01}	-1.37×10^{-02}	-4.07×10^{-02}	-1.01×10^{-01}	3.31×10^{-02}	1.26×10^{-02}	1.14×10^{-03}	4.68×10^{-02}
293.55	-1.99×10^{-01}	-1.23×10^{-02}	-3.98×10^{-02}	-9.19×10^{-02}	3.07×10^{-02}	1.14×10^{-02}	1.04×10^{-03}	4.31×10^{-02}
295.95	-1.98×10^{-01}	-1.21×10^{-02}	-3.96×10^{-02}	-9.05×10^{-02}	3.04×10^{-02}	1.12×10^{-02}	1.02×10^{-03}	4.26×10^{-02}
298.45	-1.97×10^{-01}	-1.19×10^{-02}	-3.95×10^{-02}	-8.91×10^{-02}	3.00×10^{-02}	1.10×10^{-02}	1.01×10^{-03}	4.21×10^{-02}
304	-1.94×10^{-01}	-1.15×10^{-02}	-3.91×10^{-02}	-8.60×10^{-02}	2.93×10^{-02}	1.06×10^{-02}	9.78×10^{-04}	4.09×10^{-02}
315.35	-1.90×10^{-01}	-1.07×10^{-02}	-3.84×10^{-02}	-7.99×10^{-02}	2.78×10^{-02}	9.85×10^{-03}	9.17×10^{-04}	3.86×10^{-02}
336.35	-1.82×10^{-01}	-9.35×10^{-03}	-3.72×10^{-02}	-6.92×10^{-02}	2.54×10^{-02}	8.63×10^{-03}	8.18×10^{-04}	3.48×10^{-02}
347.05	-1.78×10^{-01}	-8.75×10^{-03}	-3.65×10^{-02}	-6.40×10^{-02}	2.42×10^{-02}	8.07×10^{-03}	7.73×10^{-04}	3.30×10^{-02}
357.75	-1.74×10^{-01}	-8.20×10^{-03}	-3.59×10^{-02}	-5.89×10^{-02}	2.31×10^{-02}	7.56×10^{-03}	7.31×10^{-04}	3.14×10^{-02}
371.55	-1.69×10^{-01}	-7.54×10^{-03}	-3.51×10^{-02}	-5.27×10^{-02}	2.18×10^{-02}	6.96×10^{-03}	6.81×10^{-04}	2.94×10^{-02}
				THF				
297.5	-4.92×10^{-01}	-5.36×10^{-03}	-3.27×10^{-02}	-3.71×10^{-01}	2.21×10^{-01}	4.95×10^{-03}	4.88×10^{-04}	2.26×10^{-01}
307.1	-4.83×10^{-01}	-5.00×10^{-03}	-3.23×10^{-02}	-3.61×10^{-01}	2.16×10^{-01}	4.61×10^{-03}	4.63×10^{-04}	2.21×10^{-01}
316.4	-4.73×10^{-01}	-4.67×10^{-03}	-3.18×10^{-02}	-3.51×10^{-01}	2.11×10^{-01}	4.30×10^{-03}	4.41×10^{-04}	2.16×10^{-01}
326.7	-4.64×10^{-01}	-4.33×10^{-03}	-3.14×10^{-02}	-3.40×10^{-01}	2.06×10^{-01}	3.99×10^{-03}	4.18×10^{-04}	2.10×10^{-01}
336	-4.55×10^{-01}	-4.05×10^{-03}	-3.09×10^{-02}	-3.31×10^{-01}	2.01×10^{-01}	3.74×10^{-03}	3.99×10^{-04}	2.05×10^{-01}
				Acetonitrile				
301	-6.52×10^{-01}	-1.38×10^{-02}	-2.01×10^{-02}	-5.27×10^{-01}	3.49×10^{-01}	1.28×10^{-02}	1.38×10^{-04}	3.62×10^{-01}
309	-6.47×10^{-01}	-1.37×10^{-02}	-1.98×10^{-02}	-5.21×10^{-01}	3.47×10^{-01}	1.27×10^{-02}	1.32×10^{-04}	3.59×10^{-01}
317	-6.41×10^{-01}	-1.36×10^{-02}	-1.96×10^{-02}	-5.16×10^{-01}	3.44×10^{-01}	1.26×10^{-02}	1.26×10^{-04}	3.57×10^{-01}
327	-6.35×10^{-01}	-1.35×10^{-02}	-1.92×10^{-02}	-5.08×10^{-01}	3.41×10^{-01}	1.24×10^{-02}	1.19×10^{-04}	3.54×10^{-01}
337	-6.28×10^{-01}	-1.34×10^{-02}	-1.88×10^{-02}	-5.01×10^{-01}	3.38×10^{-01}	1.23×10^{-02}	1.13×10^{-04}	3.50×10^{-01}
				Dichloromethane				
275	-5.29×10^{-01}	-6.37×10^{-03}	-2.31×10^{-02}	-3.99×10^{-01}	2.51×10^{-01}	5.88×10^{-03}	2.18×10^{-04}	2.57×10^{-01}
290	-5.13×10^{-01}	-5.73×10^{-03}	-2.24×10^{-02}	-3.82×10^{-01}	2.43×10^{-01}	5.28×10^{-03}	1.98×10^{-04}	2.49×10^{-01}
296	-5.06×10^{-01}	-5.49×10^{-03}	-2.21×10^{-02}	-3.75×10^{-01}	2.40×10^{-01}	5.07×10^{-03}	1.91×10^{-04}	2.45×10^{-01}
308	-4.94×10^{-01}	-5.06×10^{-03}	-2.16×10^{-02}	-3.61×10^{-01}	2.33×10^{-01}	4.66×10^{-03}	1.78×10^{-04}	2.38×10^{-01}

Table 7.6 Individual Contributions to $\Delta_r G$ and λ_o for 2. All Values Listed in eV.

T (K)	$\Delta_{elec}G^{(1)}$	$\Delta_rG^{(2)}$	$\Delta_{disp}G$	Δ_rG	λ_p	λ_{ind}	λ_{disp}	λ_o
				Toluene				
290.25	-2.38×10^{-01}	-1.12×10^{-02}	-2.89×10^{-02}	-1.19×10^{-01}	5.49×10^{-02}	1.04×10^{-02}	4.67×10^{-04}	6.58×10^{-02}
296.15	-2.35×10^{-01}	-1.08×10^{-02}	-2.87×10^{-02}	-1.15×10^{-01}	5.36×10^{-02}	9.96×10^{-03}	4.52×10^{-04}	6.40×10^{-02}
296.65	-2.35×10^{-01}	-1.08×10^{-02}	-2.86×10^{-02}	-1.15×10^{-01}	5.35×10^{-02}	9.92×10^{-03}	4.50×10^{-04}	6.39×10^{-02}
305.35	-2.30×10^{-01}	-1.01×10^{-02}	-2.83×10^{-02}	-1.09×10^{-01}	5.17×10^{-02}	9.34×10^{-03}	4.29×10^{-04}	6.14×10^{-02}
316.3	-2.24×10^{-01}	-9.39×10^{-03}	-2.78×10^{-02}	-1.03×10^{-01}	4.94×10^{-02}	8.66×10^{-03}	4.04×10^{-04}	5.85×10^{-02}
316.45	-2.24×10^{-01}	-9.38×10^{-03}	-2.78×10^{-02}	-1.02×10^{-01}	4.94×10^{-02}	8.65×10^{-03}	4.04×10^{-04}	5.84×10^{-02}
323.75	-2.21×10^{-01}	-8.93×10^{-03}	-2.75×10^{-02}	-9.80×10^{-02}	4.79×10^{-02}	8.24×10^{-03}	3.89×10^{-04}	5.66×10^{-02}
326.65	-2.19×10^{-01}	-8.76×10^{-03}	-2.73×10^{-02}	-9.63×10^{-02}	4.74×10^{-02}	8.08×10^{-03}	3.83×10^{-04}	5.58×10^{-02}
327.5	-2.19×10^{-01}	-8.71×10^{-03}	-2.73×10^{-02}	-9.58×10^{-02}	4.72×10^{-02}	8.03×10^{-03}	3.81×10^{-04}	5.56×10^{-02}
347.55	-2.09×10^{-01}	-7.62×10^{-03}	-2.64×10^{-02}	-8.42×10^{-02}	4.36×10^{-02}	7.03×10^{-03}	3.43×10^{-04}	5.10×10^{-02}
347.55	-2.09×10^{-01}	-7.62×10^{-03}	-2.64×10^{-02}	-8.42×10^{-02}	4.36×10^{-02}	7.03×10^{-03}	3.43×10^{-04}	5.10×10^{-02}
368.3	-2.00×10^{-01}	-6.65×10^{-03}	-2.55×10^{-02}	-7.29×10^{-02}	4.02×10^{-02}	6.13×10^{-03}	3.09×10^{-04}	4.66×10^{-02}
				Mesitylene				
282.15	-2.03×10^{-01}	-1.32×10^{-02}	-4.05×10^{-02}	-9.78×10^{-02}	3.22×10^{-02}	1.22×10^{-02}	1.11×10^{-03}	4.55×10^{-02}
292.85	-1.99×10^{-01}	-1.23×10^{-02}	-3.98×10^{-02}	-9.16×10^{-02}	3.07×10^{-02}	1.14×10^{-02}	1.04×10^{-03}	4.31×10^{-02}
297.45	-1.97×10^{-01}	-1.19×10^{-02}	-3.95×10^{-02}	-8.90×10^{-02}	3.00×10^{-02}	1.10×10^{-02}	1.01×10^{-03}	4.20×10^{-02}
302.75	-1.94×10^{-01}	-1.15×10^{-02}	-3.92×10^{-02}	-8.60×10^{-02}	2.93×10^{-02}	1.06×10^{-02}	9.85×10^{-04}	4.09×10^{-02}
312.55	-1.90×10^{-01}	-1.08×10^{-02}	-3.86×10^{-02}	-8.07×10^{-02}	2.80×10^{-02}	9.98×10^{-03}	9.32×10^{-04}	3.89×10^{-02}
323.05	-1.86×10^{-01}	-1.01×10^{-02}	-3.80×10^{-02}	-7.52×10^{-02}	2.67×10^{-02}	9.34×10^{-03}	8.79×10^{-04}	3.70×10^{-02}
323.65	-1.86×10^{-01}	-1.01×10^{-02}	-3.79×10^{-02}	-7.49×10^{-02}	2.67×10^{-02}	9.30×10^{-03}	8.76×10^{-04}	3.68×10^{-02}
331.75	-1.83×10^{-01}	-9.58×10^{-03}	-3.74×10^{-02}	-7.09×10^{-02}	2.57×10^{-02}	8.84×10^{-03}	8.38×10^{-04}	3.54×10^{-02}
346.65	-1.77×10^{-01}	-8.73×10^{-03}	-3.66×10^{-02}	-6.36×10^{-02}	2.41×10^{-02}	8.06×10^{-03}	7.74×10^{-04}	3.29×10^{-02}
347.45	-1.77×10^{-01}	-8.69×10^{-03}	-3.65×10^{-02}	-6.32×10^{-02}	2.40×10^{-02}	8.02×10^{-03}	7.71×10^{-04}	3.28×10^{-02}
360.25	-1.73×10^{-01}	-8.04×10^{-03}	-3.58×10^{-02}	-5.73×10^{-02}	2.27×10^{-02}	7.41×10^{-03}	7.21×10^{-04}	3.09×10^{-02}
360.35	-1.73×10^{-01}	-8.03×10^{-03}	-3.58×10^{-02}	-5.72×10^{-02}	2.27×10^{-02}	7.41×10^{-03}	7.21×10^{-04}	3.09×10^{-02}
370.15	-1.69×10^{-01}	-7.57×10^{-03}	-3.52×10^{-02}	-5.28×10^{-02}	2.18×10^{-02}	6.98×10^{-03}	6.86×10^{-04}	2.95×10^{-02}
379.25	-1.66×10^{-01}	-7.17×10^{-03}	-3.47×10^{-02}	-4.88×10^{-02}	2.10×10^{-02}	6.61×10^{-03}	6.55×10^{-04}	2.82×10^{-02}
				THF				
297.5	-4.88×10^{-01}	-5.34×10^{-03}	-3.27×10^{-02}	-3.67×10^{-01}	2.18×10^{-01}	4.93×10^{-03}	4.88×10^{-04}	2.24×10^{-01}
307.2	-4.79×10^{-01}	-4.97×10^{-03}	-3.23×10^{-02}	-3.57×10^{-01}	2.14×10^{-01}	4.58×10^{-03}	4.63×10^{-04}	2.19×10^{-01}
316.4	-4.70×10^{-01}	-4.65×10^{-03}	-3.18×10^{-02}	-3.47×10^{-01}	2.09×10^{-01}	4.29×10^{-03}	4.41×10^{-04}	2.14×10^{-01}
326.9	-4.60×10^{-01}	-4.30×10^{-03}	-3.13×10^{-02}	-3.37×10^{-01}	2.04×10^{-01}	3.97×10^{-03}	4.18×10^{-04}	2.08×10^{-01}
				Acetonitrile				
302	-6.45×10^{-01}	-1.38×10^{-02}	-2.01×10^{-02}	-5.20×10^{-01}	3.44×10^{-01}	1.27×10^{-02}	1.37×10^{-04}	3.57×10^{-01}
309	-6.40×10^{-01}	-1.37×10^{-02}	-1.98×10^{-02}	-5.15×10^{-01}	3.42×10^{-01}	1.26×10^{-02}	1.32×10^{-04}	3.55×10^{-01}
317	-6.35×10^{-01}	-1.36×10^{-02}	-1.96×10^{-02}	-5.09×10^{-01}	3.40×10^{-01}	1.25×10^{-02}	1.26×10^{-04}	3.53×10^{-01}
327	-6.28×10^{-01}	-1.34×10^{-02}	-1.92×10^{-02}	-5.02×10^{-01}	3.37×10^{-01}	1.24×10^{-02}	1.19×10^{-04}	3.49×10^{-01}
337	-6.22×10^{-01}	-1.33×10^{-02}	-1.88×10^{-02}	-4.95×10^{-01}	3.34×10^{-01}	1.23×10^{-02}	1.13×10^{-04}	3.46×10^{-01}
				Dichloromethane				
273	-5.27×10^{-01}	-6.43×10^{-03}	-2.31×10^{-02}	-3.97×10^{-01}	2.50×10^{-01}	5.93×10^{-03}	2.21×10^{-04}	2.56×10^{-01}
283	-5.16×10^{-01}	-5.99×10^{-03}	-2.27×10^{-02}	-3.86×10^{-01}	2.44×10^{-01}	5.52×10^{-03}	2.07×10^{-04}	2.50×10^{-01}
293	-5.05×10^{-01}	-5.58×10^{-03}	-2.22×10^{-02}	-3.74×10^{-01}	2.39×10^{-01}	5.15×10^{-03}	1.95×10^{-04}	2.44×10^{-01}
302	-4.96×10^{-01}	-5.24×10^{-03}	-2.18×10^{-02}	-3.64×10^{-01}	2.34×10^{-01}	4.84×10^{-03}	1.84×10^{-04}	2.39×10^{-01}

7.9 Appendix A

The molecular model for solvation in these electron transfer systems has been discussed extensively in earlier work.[14] This model develops explicit expressions for the reaction free energy and the solvent reorganization energy.

The free energy of reaction is given by the sum of four terms in eq 7.5. The most significant contribution in these solvents comes from the $\Delta_{dq,i}G^{(1)}$ term given by

$$\Delta_{dq,i}G^{(1)} = -\frac{(m_e^2 - m_g^2)}{R_{eff}^3} f(y_d, y_q)\Psi^P(y_d, y_q) \tag{A1}$$

where m_i is the permanent dipole moment of the excited and ground electronic states, $f(y_i)$ renormalizes the solute dipole moment to account for its size and polarizability, R_{eff} is the effective solute radius, and $\Psi(y_i)$ is the polarity response function given by,

$$\Psi^P(y_d, y_q) = \frac{\dfrac{y_d I_{0s}^{(2)} + y_q I_6^{(2)}}{I_{0s}^{(2)}}}{1 + \dfrac{y_d^2 \kappa_d I_{0s}^{(3)} + y_d y_q \kappa_{dq} I_{DDQ}^{(3)} + y_q^2 \kappa_q I_{DQQ}^{(3)}}{y_d I_{0s}^{(2)} + y_q I_6^{(2)}}} \tag{A2}$$

In this equation the κ terms account for saturation of the dipolar response that arises from higher order interactions, and the I_{ij} are polynomial representations of the two and three particle perturbation integrals. Their explicit form can be found elsewhere.[14,30]

The solvent reorganization energy is given by a sum of three terms in eq 7.6. The major contribution in the aromatic solvents comes from λ^p and is given by

$$\lambda_p = \frac{(m_e - m_g)^2}{R_{eff}^3}\left[f(y_d,y_q)\Psi^P(y_d,y_q) - f(y_e)\Psi^P(y_e)\right] \tag{A3}$$

where y_e is the reduced polarizability density of the solvent. The induction term λ_{ind} makes a small but relatively significant contribution to the overall reorganization energy in these solvents (see Table A1) and is given by

$$\lambda_{ind} = \frac{(m_e^2 - m_g^2)^2 f(y_e)^2}{400\ kT\ \eta\sigma^6}\frac{(\epsilon_\infty - 1)^2}{(\epsilon_\infty + 2)^2}\left[3 + \frac{8}{3}(\epsilon_\infty - 1)^2\right]I_{0s}^{(4)} \tag{A4}$$

where η is the reduced packing density of the solvent molecules, σ is the solvent hard sphere diameter,[31] and ε_∞ is the solvent high frequency dielectric constant. Previous work[14] indicated that the absolute values of λ_o predicted from the model are too small. Therefore, only its temperature dependence is used.

7.10 References

(1) a) Balzani, V.; Ed. *Electron Transfer in Chemistry*; Wiley - VCH: Weinheim, 2001. b) Barbara, P. F.; Meyer, T. J.; Ratner, M.A., *J. Phys. Chem.* **1996**, *100*, 13148; c) Electron Transfer-From Isolated Molecules to Biomolecules, *Adv. Chem. Phys*. Jortner, J.; Bixon, M. eds. (Wiley, NY, **1999**).

(2) a) Hush, N. S.; Paddon-Row, M. N.; Cotsaris, E.; Oevering, H.; Verhoeven, J. W.; Heppener,*Chem. Phys. Lett.* **1985**, *117*, 8. b) Oliver, A. M.; Craig, D. C.; Paddon-Row, M. N.; Kroon, J.; Verhoeven, J. W. *Chem. Phys. Lett.* **1988**, *150*, 366. c) Johnson, M. D.; Miller, J. R.; Green, S.; Closs, G. L. *J. Phys. Chem.* 1989, 93, 1173. d) Paddon-Row, M. N. *Acc. Chem. Res.* **1994**, *27*, 18.

(3) a) Zeng, Y.; Zimmt; M. B., *J. Phys. Chem.* **1992**, *96*, 8395; b) Oliver, A. M.; Paddon-Row, M. N.; Kroon, J.; Verhoeven, J. W. *Chem. Phys. Lett.* **1992**, *191*, 371.

(4) Closs, G.L.; Miller, J.R. *Science* **1988**, *240*, 440.

(5) a) Newton, M. D. *Adv. Chem. Phys.* **1999**, *106*, 303; b) Jordan, K. D.; Paddon-Row, M. N. *Chem. Rev.* **1992**, *92*, 395.

(6) a) Paddon-Row, M. N.; Jordan, K. D. In *Modern Models of Bonding and Delocalization*; Liebman, J. F., Greenberg, A., Eds.; VCH Publishers: New York, 1988; Vol. 6; pp 115. b) Shephard, M. J.; Paddon-Row, M. N, K. D. *Chem. Phys.* **1993**, *176*, 289. c) Paddon-Row, M. N.; Shephard, M. J. *J. Am. Chem. Soc.* **1997**, *119*, 5355.

(7) a) Roberts, J. A.; Kirby, J. P.; Nocera, D.G. *J. Am. Chem. Soc.* **199**5, *117*, 8051. b) de Rege, P. J. F.; Williams, S. A.; Therien, M. J. *Science* 1995, *269*, 1409. c) LeCours, S. M.; Philips, C. M.;DePaula, J. C.; Therien, M. J.; *J. Am. Chem. Soc*. 1997, *119*, 12578. d) Arimura, T.; Brown, C. T.; Springs, S. L.; Sessler,J. L. *Chem. Commun*. **1996**, 2293.

(8) a) Lokan, N. R.; Craig, D. C.; Paddon-Row, M. N. *Synlett* **1999**, 397. b) Lokan, N. R.; Paddon-Row, M. N.; Koeberg, M.; Verhoeven, J. W. *J. Am. Chem. Soc.* **2000**, *122*, 5075. c) Koeberg, M.; de Groot, M.; Verhoeven, J. W.; Lokan, N. R.; Shephard, M. J.; Paddon-Row, M. N. *J. Phys. Chem.* **2001**, *105*, 3417. d) Jolliffe, K. A.; Bell, T. D. M.; Ghiggino, K. P.; Jordan, K..; Langford, S. J.; Paddon-Row, M. N. *Angew. Chem., Int. Ed.* **1998**, *37*, 916. e) Jolliffe, K. A.; Langford, S. J.; Oliver, A. M.; Shephard, M. J.; Paddon-Row, M. N. *Chem. Eur. J.* **1999**, *5*, 2518. f) Bell, T. D. M.; Jolliffe, K. A.; Ghiggino, K. P.; Oliver, A. M.; Shephard, M. J.; Langford, S. J.; Paddon-Row, M. N. *J. Am. Chem. Soc.* **2000**, *122*, 10661. g) Goes, M.; Groot, M. de; Koeberg, M.; Verhoeven, J. W.; Lokan, N. R.; Shephard, M. J.; Paddon-Row, M. N. *J. Phys. Chem. A* **2001**, *105*, 3417.

(9) Kumar, K.; Lin, Z.; Waldeck, D.H.; Zimmt, M. B*. J. Am. Chem. Soc.* **1996**, *118,* 243.

(10) a) Kumar,K.; Kurnikov, I.; Beratan, D. N.; Waldeck, D. H.; Zimmt, M. B. *J. Phys. Chem. A* **1998,** *102*, 5529; b) Read, I.; Napper, A.; Kaplan, R.; Zimmt, M. B.; Waldeck, D. H. *J. Am. Chem. Soc.* **1999,** *121*, 10976; c) Napper, A. M; Read, I.; Kaplan, R.; Zimmt, M.B.; Waldeck, D. H. *J. Phys. Chem. B* in press.

(11) a) Kaplan, R.; Napper, A. M.; Waldeck, D. H.; Zimmt, M. B. *J. Am. Chem. Soc.* **2001**, submitted. b) Kaplan, R.; Napper, A.; Waldeck, D. H.; Zimmt, M. B. *J. Am. Chem. Soc.* **2000,** *122,* 12039; c) Napper, A. M.; Read, I.; Waldeck, D. H.; Kaplan, R. W.; Zimmt, M. B. *J. Phys. Chem. B*, in press.

(12) Head, N. J.; Oliver, A. M.; Look, K.; Lokan, N. R.; Jones, G. A.;Paddon-Row, M. N. *Angew. Chem., Int. Ed.* **1999**, *3*8, 3219.

(13) Napper, A.M.; Read, I.; Waldeck, D. H.; Head, N. J.; Oliver, A. M.; Paddon-Row, M. N. *J. Am. Chem. Soc.* **2000,** *122,* 5220.

(14) Read, I.; Napper, A. M.; Zimmt, M. B.; Waldeck, D. H. *J. Phys. Chem. A* **2000,** *104,* 9385.

(15) Matyushov, D. V.; Voth, G. A. *J. Chem. Phys.* **1999**, *111*, 3630.

(16) a) Marcus, R. A. *J. Phys. Chem.* **1989**, *93*, 3078; b) Lilichenko, M.; Tittelbach-Helmrich, D.; Verhoeven, J. W.; Gould, I. R.; Myers, A. B. *J. Chem. Phys.* **1998**, *109*, 10958.

(17) As described in an earlier report[13], the fluorescence decay also shows a contribution from an impurity that corresponds to the donor only compound but this feature is accounted for in the data fitting.

(18) Shephard, M. J.; Paddon-Row, M. N. *J. Phys. Chem.* **1999**, *103*, 3347.

(19) Shephard, M. J.; Paddon-Row, M. N. *J. Phys. Chem.* **2000**, *104*, 11628.

(20) Frisch, M. J.; Trucks, G. W.; Schlegel, H. B.; Scuseria, G. E.; Robb, M. A.; Cheeseman, J. R.; Zakrzewski, V. G.; Montgomery Jr., J. A.; Stratmann, R. E.; Burant, J. C.; Dapprich, S.; Millam, J. M.; Daniels, A. D.; Kudin, K. N.; Strain, M. C.; Farkas, O.; Tomasi, J.; Barone, V.; Cossi, M.; Cammi, R.; Mennucci, B.; Pomelli, C.; Adamo, C.; Clifford, S.; Ochterski, J.; Petersson, G. A.; Ayala, P. Y.; Cui, Q.; Morokuma, K.; Malick, D. K.; Rabuck, A. D.; Raghavachari, K.; Foresman, J. B.; Cioslowski, J.; Ortiz, J. V.; Baboul, A. G.; Stefanov, B. B.; Liu, G.; Liashenko, A.; Piskorz, P.; Komaromi, I.; Gomperts, R.; Martin, R. L.; Fox, D. J.; Keith, T.; Al-Laham, M. A.; Peng, C. Y.; Nanayakkara, A.; Gonzalez, C.; Challacombe, M.; Gill, P. M. W.; Johnson, B.; Chen, W.; Wong, M. W.; Andres, J. L.; Gonzalez, C.; Head-Gordon, M.; Replogle, E. S.; Pople, J. A. *Gaussian 98*, Gaussian Inc: Pittsbugh, PA, **1998**.

(21) a) Warman, J. M.; de Haas, M. P.; Paddon-Row, M. N.; Cotsaris, E.; Hush, N. S.; Oevering, H.; Verhoeven, J. W. *Nature* **1986**, *320*, 615. b) Penfield, K. W.; Miller, J. R.; Paddon-Row, M. N.; Cotsaris, E.; Oliver, A. M.; Hush, N. S. *J. Am. Chem. Soc.* **1987**, *109*, 5061. c) Warman, J. M.; de Haas, M. P.; Verhoeven, J. W.; Paddon-Row, M. N. *Adv. Chem. Phys.* **1999**, *106*, 571. d) Oevering, H.; Verhoeven, J. W.; Paddon-Row, M. N.; Warman, J. M. *Tetrahedron* **1989**, *45*, 4751.

(22) Oevering, H.; Paddon-Row, M. N.; Heppener, H.; Oliver, A. M.; Cotsaris, E.; Verhoeven, J. W.; Hush, N. S. *J. Am. Chem. Soc.* **1987**, *109*, 3258.

(23) A harmonic frequency calculation was carried out on neutral 7-dicyanovinylnorbornane **10**. The level of theory used was B3LYP/6-3 1 1+G(d,p)//B3LYP/6-3 1 1+G(d,p), and the geometry optimization was carried out under *C2v* symmetry constraint. The frequency associated with outof-plane bending of the DCV group, schematically depicted by **10a**, is 1132 cm^{-1}. Applying the recommended scaling factor of 0.9613 gave a corrected frequency of 1088 cm^{-1}; see Wong, M. W. *Chem. Phys. Lett.* **1996**, *256*, 391.

(24) Gu, Y.;Kumar, K.; Lin, A.; Read, I.; Zimmt, M. B.; Waldeck, D. H. *J. Photochem. and Photobiol. A.* **1997,** *105,* 189.

(25) a) Paddon-Row, M. N.; Oliver, A. M.; Warman, J. M.; Smit, K. J.; de Haas, M. P.; Oevering, H.; Verhoeven, J. W. *J. Phys. Chem.* **1988**, *92*, 6958. b) Warman, J. M.; Smit, K. J.; de Haas, M. P.; Jonker, S. A.; Paddon-Row, M. N.; Oliver, A. M.; Kroon, J.; Oevering, H.; Verhoeven, J. W. *J. Phys. Chem.* **1991**, *95*, 1979.

(26) The polarizabilities of the molecules were obtained using the HF/3-21+G method and a 'divide and conquer' approach. Calculations were performed for analogues of **1** and **2** that did not contain the phenyl substituents on the naphthalene, nor the four CH2OCH3 groups on the bridge. This calculation yielded values of 73 $Å^3$ for the analogue of **1** and 70 $Å^3$ for the analogue of **2**. Independent calculations for the phenyl and ether substituents gave 9 $Å^3$ and 4 $Å^3$, respectively. The polarizability of **1** and **2** were obtained by assuming that the polarizabilities of these components were additive and yielded 107 $Å^3$ for **1** and 103 $Å^3$ for **2**. A comparison of calculated polarizabilities for a range of molecules whose polarizabilities are known indicated that the calculation systematically underestimated the polarizability by a factor of 0.83. Correction by this factor gives 128 $Å^3$ for **1** and 124 $Å^3$ for **2**.

(27) The molecular moiety's polarizability was used to estimate the effective dielectric constant of the molecular cleft through the Clausius-Mossatti relationship. The polarizability perpendicular to the propyl group's long axis was taken to be 5.7 $Å^3$, and the polarizability perpendicular to the phenyl axis was taken to be 7.4 $Å^3$. The polarizabilities were taken from Ma, B; Lii, J.-H.; and Allinger, N. L. *J. Comp. Chem.* **2000**, *21*, 813. The cleft volume was estimated to be 100 $Å^3$. This simple calculation predicts a shift in the reaction free energy between compounds **1** and **2** that is similar to the observed difference.

(28) a) Hoffmann, R. *Acc. Chem. Res.* **1971**, *4*, 1; b) Paddon-Row, M. N. *Acc. Chem. Res.* **1982**, *15*, 245; c) Paddon-Row, M. N. in *Electron Transfer In Chemistry*; Balzani, V., Ed.; WileyVCH: Weinheim, **2001**; Vol. 3, Part 2, Chapter 1, 179.

(29) The N-H system, **4**, was not used for these calculations because, given the approximations made, the modified system, **7'**, provides a better comparison to **7** for the influence that the phenyl group has upon the DMN - DCV coupling.

(30) a) Matyushov, D. V.; Schmid, R. *J. Chem. Phys.* **1996**, *105*, 4729; b) Matyushov, D. V.; Ladanyi, B. M. *J. Chem. Phys.* **1999**, *110*, 994.

(31) Ben-Amotz, D.; Willis, K. G. *J. Phys. Chem.* **1993**, *97*, 7736.

Chapter 8 Conclusions

The preceding chapters have outlined a general strategy for analyzing experimental electron transfer rate data. The molecular systems used were designed to allow for systematic control of the structure between the D-A pair. Studies focused on the model system, A9DCE, demonstrated how the solvent can mediate electronic coupling. These results show that solvation, albeit important, is not the only role played by the solvent in electron transfer reactions. Further, the enhancements in the electronic coupling observed for aromatic solvents reveal, quantitatively, the relevance of nonbonded interactions in electron transfer. Both conclusions highlight the importance of this work.

The analysis protocol used throughout this work was shown to be a general and robust approach for interpreting electron transfer rate data. Chapters 2 and 3 presented a systematic method for determining vital thermodynamic parameters. With this information, the solvation energetics and their temperature dependencies can be determined. According to the semiclassical rate expression several parameters must be known before the electronic coupling can be evaluated ($\Delta_r G$, λ, and $h\nu$). This work revealed that, in nonpolar solvents, a molecular based solvation model is necessary in the calculation of physically meaningful results for $\Delta_r G$ and λ_o. An important result from Chapter 2 was the ability to experimentally determine the reaction free energy. This allows for a careful comparison of results calculated using continuum theory with those produced using a molecular based model. In chapter 3, an extension of the molecular model which included higher order solute-solvent interactions (i.e. quadrupolar) was evaluated and shown to provide a reliable way to calculate the reaction free energy and

the solvent reorganization energy across a wider range of solvent polarity. The generality of results predicted by the model was tested in several model systems and in several different solvents.

According to the Marcus model, the reorganization energy also has contributions from the intermolecular solute reorganization. To date, there are no reliable methods for measuring the inner-sphere reorganization energy. For this work, the charge transfer emission spectra of relevant model systems were used to determine its value. Because the spectral fitting parameters are not unique, quantum chemical calculations provide a reliable method for determining the reorganization energy. Chapter 7 details this procedure. In addition, the vibrational mode frequency was also determined using a combination of charge transfer data and calculations.

Results from the calculations also showed that the electron transfer event primarily involves only a single vibrational mode which corroborates the single mode approximation. To further test its validity, rate data was analysed using an extended rate expression incorporating a second intramolecular vibration. The results showed little difference with those derived from the single mode description. Overall, the single mode approximation was shown to be a reliable and the inclusion of additional modes added unnecessary complexity.

In addition to defining a protocol for the analysis of electron transfer rate contants, many chemical conclusions can be drawn from this work. First, the electronic coupling, |V|, can be mediated by nonbonded contacts such as solvent molecules. The orbital energetics play an important role in determining the magnitude of the coupling. For instance, conjugated systems can more efficiently mediate electron transfer. This

observation is consistent with the superexchange model of electron transfer where the mediating electronic state lies close in energy to the relevant electronic orbitals of the D-A pair. The results are presented for A9DCE as a function of solvent electron affinity in chapter 5. The results are consistent with the eT reaction being 'electron mediated' since the electronic coupling is correlated to the solvents increasingly positive electron affinity and not its ionization potential. The results support the conclusion that the electronic coupling is correlated to both the solvent position (Chapter 2) and the solvent electronic structure. This explanation is consistent with superexchange theory.

Second, the solvent's position has a significant impact on the observed coupling. The experiments in Chapter 7, where the molecular size restricts the available conformations of the solvent inside the cleft, a temperature dependent electronic coupling was observed. The observation can be explained by considering the conformational freedom the solvent molecule has when 'bound' within the cleft of A9DCE. Because the association energy is relatively low, increasing the temperature increases the number of available configurations adopted by the intermolecular complex. The increased conformational space effectively decreases the coupling efficiency at higher temperatures in bulky solvents.

Overall, this work demonstrates the critical role that solvent plays in chemical transformations. Not only do solvent molecules provide thermodynamic stability but they can also modify the electronic structure of the reactants to facilitate a particular transformation.